

# **Synthesis and mechanochemical activation of copper(I)-bis(NHC) complexes with different architectures**

## **Dissertation**

zur Erlangung des Doktorgrades der Naturwissenschaften  
(Dr. rer. nat.)

der

Naturwissenschaftlichen Fakultät II  
Chemie, Physik und Mathematik

der Martin-Luther-Universität  
Halle-Wittenberg

vorgelegt von

Herrn Michel Biewend  
geb. am 24.06.1990 in Neindorf/ Beckendorf

Gutachter:

1. Prof. Dr. Wolfgang H. Binder
2. Prof. Dr. Michael Sommer

Verteidigung: 26.01.2021

## I. Danksagung

Ich möchte mich bei allen bedanken, die mir beim Erstellen dieser Arbeit sowohl fachlich als auch persönlich mit Rat und Tat zur Seite standen.

Insbesondere möchte ich mich bei Prof. Dr. Wolfgang H. Binder für die Bereitstellung dieses interessanten Themas und aller notwendigen Arbeitsmittel und Chemikalien, die zur Bearbeitung dieses Themas notwendig waren, bedanken.

Weiterhin möchte ich mich bei Dr. Philipp Michael und Dr. Diana Döhler für die zahlreichen Diskussionen fachlicher aber auch persönlicher Natur bedanken.

Zusätzlich möchte ich meinem ehemaligen und erneutem Kollegen Jan Freudenberg danken, der den Alltag im Labor auf eine stets freundliche und witzige Art und Weise geprägt hat.

Ich möchte mich bei dem Laborteam, Stefanie Deike, Sebastian Funtan, Alexander Funtan und Harald Rupp bedanken, die immer ein offenes Ohr für mich hatten und mich mit Spaß und Freude auch die schwierigen Zeiten aufmunterten.

Anke Hassi möchte ich für die Hilfe in Verwaltungsangelegenheiten danken, die zur Vereinfachung vieler, sonst umständlicher, Problemstellungen führten.

Frau Susanne Tanner und Frau Julia Weichhold danke ich für die GPC-, MALDI- und ESI-Messungen und die Bereitstellung von Chemikalien, Lösungsmitteln und Glasgeräten. Bei allen Mitarbeitern der analytischen Abteilung des Instituts für Organische Chemie bedanke ich mich für die Anfertigung der NMR-Spektren.

Natürlich gilt mein Dank auch allen weiteren Mitgliedern der Arbeitsgruppe Binder, die mir stets Vertrauen entgegenbrachten und eine herzliche Arbeitsatmosphäre ermöglichten.

Zuletzt, aber nicht im geringeren Maße, möchte ich meiner Familie, meiner Freundin Katharina Schulz und meinen Freunden für den stetigen Zuspruch und den nötigen Rückhalt in jeglichen Lebenssituationen danken, die wesentlich zum Gelingen dieser Arbeit beitrugen.

## II. Abstract

Triggering chemical reactions by mechanical stimuli has become important as it enables the direct transformation of destructive effects, like structural damage or leaking material properties, to productive applications. This is used for instance in the field of self-healing and stress-sensing materials. Several linear copper(I)-bis(*N*-heterocyclic carbene) (NHC) catalysts were developed which were attached by poly(isobutylene) and poly(styrene) backbones, establishing a stress-sensing approach in bulk by force induced triggering of a fluorogenic “click” reaction with conversions up to 8%.

In order to tune this approach in terms of catalytic activity, a series of chain-extended as well as network-based poly(styrene) mechanophores were designed containing copper(I)-bis(NHC) moieties, inactive in their initial state, but switched to an active state upon cleavage of one shielding NHC ligand solely by force. These catalysts were investigated within a fluorogenic copper(I) azide alkyne cycloaddition (CuAAC) of initially non-fluorescent substrates, which were embedded into the matrix material forming a highly fluorescent reporter dye. The quantification of fluorescence via fluorescence spectroscopy revealed different activation efficiencies by varying the architecture of the mechanophore. Enabling a higher overall chain length, which accompanies by the presence of multiple copper(I)-centers (chain extended approach) enhances the catalytic activity up to conversions of 44% but abolishes the completely latent state. The introduction of a three-dimensional structured catalyst (network concept) restored this latency due to the reduction of the critical chain length but did not influence the catalytic activity (conversions up to 44%). This emphasized the network-structured mechanophores as the most promising concept.

Furthermore, a series of copper(I)-bis(NHC) containing poly(urethane) networks with covalently incorporated mechanophores were designed to transmit the applied force most efficiently to the labile Cu-carbene bond. The mechanophoric catalysts could trigger a modified fluorogenic “click” reaction of 8-azido-2-naphtol and 3-hydroxy phenylacetylene resulting in a highly transparent material. Systematic studies of applied nominal stress, stress rates and crosslinking densities towards the mechanophore activation efficiency were accomplished by quantifying the fluorescence via fluorescence spectroscopy. The increase of the maximum stress improved the overall activation of mechanophores ( $\sigma_N = 1.45$  MPa, 5% to  $\sigma_N = 2.79$  MPa, 17%) whereas the increase in stress rate influences the activation per time ( $f = 0.25$  s<sup>-1</sup>, 10<sup>5</sup> cycles to  $f = 1.00$  s<sup>-1</sup>, 10<sup>4</sup> cycles for 12% conversion). The reduction of crosslinking density steadily improved the catalytic activity reaching a maximum at 24 mol m<sup>-3</sup> with conversion up to 25% (24 h,  $\sigma_N = 2.79$  MPa,  $f = 0.50$  s<sup>-1</sup>).

As a result, a completely transparent force responsive poly(urethane) material was designed, beneficial and easy to adapt, proving the potential for stress-sensing applications.

Additionally, single molecule force spectroscopy (SMFS) of cyclic low molecular weight copper(I)-bis(NHC) complexes were conducted via atomic force microscopy (AFM), precisely determine the bond rupture forces of copper carbene bond (1600 pN to 2600 pN) by utilization of a safety line concept. This allowed to transfer the mechanophore behavior from a microscopic scale to potential autonomous stress-sensing or self-healing applications.

### III. Kurzzusammenfassung

Das Auslösen chemischer Reaktionen durch mechanische Stimuli gewann innerhalb der Materialwissenschaften eine stetig wachsende Bedeutung, da es die direkte Transformation von destruktiven Effekten zu produktiven Anwendungen ermöglicht. Die strukturell hervorgerufenen Schäden und die damit einhergehenden Änderungen der chemischen Umgebung prädestinieren diese Art von Materialien wiederum für den Einsatz im Bereich der Selbstheilung bzw. Stress Sensorik. In vorhergehenden Arbeiten wurde dieses Konzept durch die kraftinduzierte Katalyse einer fluoreszenz erzeugenden CuAAC durch polymere Kupfer(I) Bis(*N*-Heterozyklische Carben)-Komplexe realisiert. Die dafür benötigte thermische Latenz der Katalysatoren wurde durch das Anbringen linearer Polyisobutylene- bzw. Polystyrolketten gewährleistet, die aufgrund der hohen Volumenausdehnung das aktive Kupfer(I)-Zentrum abschirmen und auf Basis der Flexibilitätseigenschaften eine mechanische Entschlafung ermöglichen. Innerhalb des entwickelten Stressdetektionssystems konnten Umsätze von bis zu 8% erreicht werden. Ziel dieser Arbeit war es; den Einfluss verschiedener Polymerarchitekturen auf die mechanochemische Aktivierbarkeit zu untersuchen und somit die katalytische Aktivität hinsichtlich der fluoreszenz erzeugenden CuAAC in festen Materialien zu optimieren. Dazu wurden einerseits kettenverlängerte, Polystyrol-basierte Kupfer(I)-Bis(NHC)-Komplexe hergestellt, die sowohl eine höhere Gesamtkettenlänge als auch mehrere Kupfer(I)-Zentren innerhalb einer Polymerkette aufweisen. Dabei konnten im Gegensatz zu den linearen Katalysatoren Umsätze von bis zu 44% innerhalb der fluorogenen Klick-Reaktion erzielt, jedoch die vollständige thermische Latenz nicht aufrechterhalten werden. Die Anwendung netzwerkbasierter Polystyrol-Komplexe unterschiedlicher Netzwerkdichte, ermöglichten wiederum eine dreidimensionale Kraftübertragung und erzielten gleichwertige Umsätze (44%), wobei die thermische Latenz durch das Unterschreiten der kritischen Kettenlänge erhalten blieb. Diese Eigenschaften prädestinierten die netzwerkbasierten Strukturen als vielversprechende Kandidaten zur mechanochemischen Aktivierung. Um aufwendige Synthese- und Verblendungsstrategien der Komplexe zu vermeiden; wurde ein „All-in-one“-Ansatz entwickelt bei dem ein niedermolekularer, hydroxyfunktionalisierter Kupfer(I)-Bis(NHC)-Komplex kovalent in eine Polyurethanmatrix eingebracht wurde und hinsichtlich der kraftinduzierten, fluorogenen Klick-Reaktion von 8-Azido-2-naphtol und 3-Hydroxyphenylacetylen untersucht wurde. Dabei wurden systematisch der Einfluss verschiedener Parameter, wie Maximalkraft, Frequenz und Netzwerkdichte auf die katalytische Aktivität und somit indirekt auf die mechanochemische Aktivierbarkeit getestet. Die Erhöhung der Maximalkraft induzierte eine Steigerung der Gesamtaktivität ( $\sigma_N = 1.45$  MPa, 5% zu  $\sigma_N = 2.79$  MPa, 17%), wohingegen die Erhöhung der Frequenz zu einer schnelleren Aktivierung führt, jedoch den Gesamtumsatz nicht beeinflusst ( $f = 0.25$  s<sup>-1</sup>, 10<sup>5</sup> Zyklen zu  $f = 1.00$  s<sup>-1</sup>, 10<sup>4</sup> Zyklen für das Erreichen des Maximalumsatzes von 12%). Weiterhin führt die Verringerung der Netzwerkdichte zu einer verbesserten katalytischen Aktivität, die ein Maximum bei 24 mol m<sup>-3</sup> mit Umsätzen von 25% (24 h,  $\sigma_N = 2.79$  MPa,  $f = 0.50$  s<sup>-1</sup>) erreicht. Diese transparenten und einfach zu adaptierenden Polyurethansysteme ermöglichten durch die Quantifizierung der stressinduzierten, auftretenden Fluoreszenz somit den Einsatz als potenzielle Materialien für den Bereich der Stresssensorik. Zusätzlich wurden die Kräfte der Kupfer-Carben-Bindungsspaltung auf mikroskopischer Ebene mittels Einzelmolekülspektroskopie untersucht. Hierbei wurden verschiedene zyklische und azyklische, niedermolekulare Kupfer(I) Bis(NHC)-Komplexe synthetisiert und die Bindungsenergien bzw. Elongationen durch Zuhilfenahme der Rasterkraftelektronenmikroskopie bestimmt. Dabei konnten Bindungskräfte von 1600 pN bis 2600 pN ermittelt und durch quantenchemische Rechnungen bestätigt werden.

# Table of contents

<b>I. Danksagung</b>	<b>1</b>
<b>II. Abstract</b>	<b>2</b>
<b>III. Kurzzusammenfassung</b>	<b>3</b>
<b>IV. List of abbreviations</b>	<b>7</b>
<b>1. Introduction</b>	<b>12</b>
1.1. Mechanophores	12
1.2. Activation of mechanophores	13
1.2.1. Activation on a microscopic scale	13
1.2.1.1. Multimechanophore concept (Method A)	14
1.2.1.2. Safety Line concept (Method B)	16
1.2.1.3. Reaction cascade concept (Method C)	16
1.2.2. Activation on a macroscopic scale	19
1.3. Polymer networks	21
1.3.1. Classification of polymer networks	21
1.3.1.1. Thermoplastics	21
1.3.1.2. Elastomers	21
1.3.1.3. Thermosets	22
1.3.1.4. Gels	22
1.3.2. Structure of polymer networks	22
1.3.3. Mechanical properties of polymer networks	23
1.3.3.1. Stress-strain curves	23
1.3.3.2. Rubber elasticity and network model	24
1.3.3.3. Rheology of polymer networks	24
1.3.3.4. Swelling behavior of polymer networks	25
1.3.4. Mechanophoric networks	26
1.3.4.1. Mechanochemically active spiropyrane	26
1.3.4.2. Mechanochemically active dioxetanes	27
1.3.4.3. Mechanochemically active benzofuranones	29
1.3.4.4. Mechanochemically active metal-ligand complexes	30
1.4. Mechanocatalysts	32
1.4.1. Metal-(NHC) complexes	33
1.4.2. Copper(I) (NHC) complexes	35
1.4.2.1. Copper(I)-(NHC) complexes in catalysis	36
<b>2. Aim of the Thesis</b>	<b>40</b>
2.1. Objective and motivation	40
2.2. Concept	41
<b>3. Result and discussion</b>	<b>44</b>
3.1. Synthesis and characterization of an acyclic and cyclic copper(I)-bis(NHC) complexes	44
3.1.1. Synthesis of acyclic copper(I)-bis(NHC) complexes	44
3.1.2. Synthesis of cyclic copper(I)-bis(NHC) complexes	46
3.2. Single molecule spectroscopy	47
3.3. Chain extended and network structured copper(I)-bis(NHC) complexes	49
3.3.1. Synthesis and characterization of chain extended copper(I)-bis(NHC) complexes	49
3.3.2. Synthesis and characterization of network structured copper(I)-bis(NHC) complexes	54
3.3.3. Mechanochemical activation of chain extended and network structured copper(I)-bis(NHC) complexes in bulk by compression	55
3.4. Fluorogenic “click” dyes	59
3.4.1. Anthracene-based system	59
3.4.1.1. Synthesis of anthracene-based azide	59
3.4.1.2. Optical properties of the anthracene-based dyes	60
3.4.2. Naphthalen based dyes	60

3.4.2.1.	Synthesis of naphthalene-based azide	60
3.4.2.2.	Optical properties of naphthalene-based dyes	61
3.5.	Mechanochemically active poly(urethane) networks	61
3.5.1.	Synthesis and chemical characterization of crosslinked poly(urethane)s ( <b>PUXX</b> )	61
3.5.2.	Determination of material properties	64
3.5.3.	Mechanochemical activation of copper(I)-bis(NHC) complex in poly(urethane) networks	67
3.5.3.1.	Quantification of fluorogenic “click” reaction during mechanochemical activation	67
3.5.4.	Self-healing ability	72
<b>4.</b>	<b>Experimental Part</b>	<b>74</b>
4.1.	Methods and materials	74
4.2.	Synthesis of low molecular weight copper(I)-bis(NHC) complexes	75
4.2.1.	Synthesis of 3-(11-hydroxyundecyl)-1-methylimidazolium bromide ( <b>1</b> )	75
4.2.2.	Synthesis of copper(I) mono(NHC) complex ( <b>2</b> )	76
4.2.3.	Synthesis of OH end-capped copper(I)-bis(NHC) complex ( <b>3</b> )	76
4.2.4.	Synthesis of 3-(11-hydroxyundecyl)-1-methylimidazolium bromide ( <b>4</b> )	77
4.2.5.	Synthesis of OH end-capped copper(I)-bis(NHC) complex ( <b>5</b> )	77
4.2.6.	Synthesis of 1,5-dibromododecane ( <b>6a</b> )	78
4.2.7.	Synthesis of 1,5-di(imidazolyl) alkane ( <b>7</b> )	78
4.2.8.	Synthesis of 1,1'-(alkane-1,5-diyl)bis(3-(hydroxyundecyl)imidazolium) bromide ( <b>8</b> )	79
4.2.9.	Synthesis of OH end-capped copper(I)-bis(NHC) complexes with safety line ( <b>9</b> )	80
4.2.10.	Synthesis of COOH end-capped copper(I)-bis(NHC) complexes with safety line ( <b>10</b> )	81
4.2.11.	Synthesis of 3-(11-hydroxyundecyl)-1-hexylimidazolium bromide ( <b>11</b> )	82
4.2.12.	Synthesis of 6,11 - OH end-capped copper(I)-bis(NHC) complex ( <b>12</b> )	83
4.3.	Synthesis of chain extended polymeric copper(I)-bis(NHC) complexes	83
4.3.1.	Synthesis of 1,4-bis(1-bromoethyl)benzene ( <b>13</b> )	83
4.3.2.	Synthesis of 1,4-phenylenebis(ethane-1,1-diyl) dibenzodithioate ( <b>14</b> )	84
4.3.3.	General RAFT polymerization for bivalent poly(styrene)s ( <b>15</b> )	84
4.3.4.	Synthesis of 3-(11-(2-bromopropionyloxy)undecyl)-methyl-1-imidazolium bis(trifluoromethane)sulfonimide ( <b>16</b> )	85
4.3.5.	Synthesis of bivalent imidazolium-telechelic poly(styrene) ( <b>17</b> )	86
4.3.6.	Synthesis of chain-extended copper(I)-bis(NHC) complexes ( <b>18</b> )	87
4.4.	Synthesis of network-based copper(I)-bis(NHC) complexes	88
4.4.1.	Synthesis of (bis(3-(vinylbenzyl)-1-methyl-imidazole-2-yl)copper(I)-hexafluorophosphate) ( <b>19</b> )	88
4.4.2.	Copolymerization of poly[(styrene)- <i>stat</i> -1-methyl-3-(4-vinylbenzyl)-1H-imidazol-3-ium hexafluorophosphate] ( <b>20</b> )	88
4.4.3.	Synthesis of poly(styrene) copper(I)-bis(NHC) networks ( <b>21</b> )	89
4.5.	Mechanochemical activation of copper(I)-bis(NHC) complexes in bulk via compression	90
4.5.1.	Synthesis of 3-azido-7-hydroxycoumarine ( <b>22</b> )	90
4.5.2.	Synthesis of 7-hydroxy-3-(4-phenyl-[1,2,3]triazol-1-yl)-coumarine ( <b>24</b> )	91
4.5.3.	Fluorescence calibration for fluorogenic “click” reaction	92
4.5.4.	Synthesis of 3-benzyl-1-methylimidazolium bromide ( <b>25</b> )	93
4.5.5.	Synthesis of low molecular weight copper(I)-bis(NHC) complex ( <b>26</b> )	93
4.5.6.	Mechanochemical activation	94
4.6.	Synthesis of poly(urethane) networks	94
4.6.1.	Synthesis of trans-dispiro[oxirane-2,9'[10 <sup>1</sup> H]-anthracene-10',2''-oxirane] ( <b>27</b> )	94
4.6.2.	Synthesis of 10-(hydroxymethyl) anthracene-9-carbaldehyde ( <b>28</b> )	95
4.6.3.	Synthesis of (10-Azidomethylanthracen-9-yl)methanol ( <b>29</b> )	95
4.6.4.	Synthesis of [10-(4-Phenyl-[1,2,3]triazol-1-ylmethyl)-anthracen-9-yl] methanol ( <b>30</b> )	96
4.6.5.	Synthesis of 8-azidonaphthalen-2-ol ( <b>31</b> )	97
4.6.6.	Synthesis of 8-(4-(3-hydroxyphenyl)-1,2,3-triazol-1-yl)naphthalen-2-ol ( <b>33</b> )	97
4.6.7.	Synthesis of 3-(1-(7-((hexylcarbamoyl)oxy)naphthalen-1-yl)-1H-1,2,3-triazol-4-yl)phenyl hexylcarbamate ( <b>34</b> )	98
4.6.8.	Fluorescence calibration for fluorogenic “click” reaction	99
4.6.9.	Synthesis of thermoplastic poly(urethane)s as prepolymers ( <b>Cu-PU</b> )	100
4.6.10.	Synthesis of PU networks ( <b>PUXX</b> )	101

4.7.	Mechanical properties of PU networks	101
4.7.1.	Determination of E-modulus	101
4.7.2.	Determination of crystallinity (DSC analysis)	102
4.7.3.	Swelling experiments	102
4.8.	Mechanochemical activation of copper(I)-bis(NHC) complex containing PU networks via uniaxial tensile rheology	102
4.8.1.	Fluorescence calibration	102
4.8.2.	Synthesis of OH end-capped copper(I)-bis(NHC) complex (35)	103
4.8.3.	Activation of PU networks	103
4.9.	Synthesis of multivalent fluorogenic dyes	105
4.9.1.	Synthesis of 2,4,6-tris((trimethylsilyl)ethynyl)phenol (36)	105
4.9.2.	Synthesis of 2,4,6-triethynylphenol (37)	105
4.9.3.	Synthesis of (4-azidophenyl)methanol (38)	106
4.9.4.	Synthesis of 4-azidobenzyl hexylcarbamate (39)	106
4.9.5.	Synthesis of trivalent conjugated dye (40)	107
4.9.6.	Synthesis of tris(4-bromophenyl)methanol (41)	108
4.9.7.	Synthesis of tris(4-azidophenyl)methanol (42)	108
4.9.8.	Synthesis of 3-ethynylphenyl hexylcarbamate (43)	109
4.9.9.	Synthesis of trivalent "click" dye (44)	109
4.9.10.	Synthesis of tris(4-((trimethylsilyl)ethynyl)phenyl)methanol (45)	110
4.9.11.	Synthesis of tris(4-(ethynyl)phenyl)methanol (46)	111
<b>5.</b>	<b>Summary</b>	<b>112</b>
<b>6.</b>	<b>References</b>	<b>116</b>
<b>7.</b>	<b>Appendix</b>	<b>132</b>
7.1.	Synthesis of cyclic and acyclic complexes	132
7.2.	Atomic force microscopy	140
7.3.	Synthesis of chain extended mechanophores	141
7.4.	Synthesis of network based mechanophores	144
7.5.	Synthesis of coumarine based fluorogenic system	145
7.6.	Synthesis of low molecular weight model complex	147
7.7.	Synthesis of anthracene based fluorogenic "click" system	148
7.8.	Synthesis of naphthalene based fluorogenic system	150
7.9.	Synthesis of urethane quenched copper(I)-bis(NHC) complex	152
7.10.	Synthesis of trivalent fluorogenic "click" systems	153
<b>8.</b>	<b>Curriculum Vitae</b>	<b>161</b>
<b>9.</b>	<b>Publikationen</b>	<b>162</b>
<b>10.</b>	<b>Eigenständigkeitserklärung</b>	<b>163</b>

**IV. List of abbreviations**

AAC	alkyne azide cycloaddition
ABF	arylbenzofuranone
AFM	atomic force microscopy
AIBN	azobis(isobutyronitril)
Asc	sodium ascorbate
ATRP	atom transfer radical polymerization
BAD	bis(adamantyl)-1,2-dioxetane
BCB	benzocyclobutene
BD	1,4-butane diol
BDE	bond dissociation energy
Binol	1,1'-bi-2-naphthol
BPB	(bromopropoxy)benzene
bpy	2,2'-bipyridine
CoGEF	Constrained Geometries simulate External Force
CTA	chain transfer agent
CuAAC	copper(I)-alkyne/azide cycloaddition
DA	Diels-Alder reaction
DABBF	diarylbibenzofuranone
DBU	1,8-diazabicyclo[5.4.0]undec-7-ene
DCM	dichloromethane
DCTB	<i>trans</i> -2-[3-(4- <i>tert</i> -butylphenyl)-2-methyl-2-propenylidene] malononitrile
De	dissociation energy
DFT	density functional theory
DHA	2,3-dihaloalkene
DIPEA	<i>N,N</i> -diisopropylethylamine
Dithranol	1,8-dihydroxy-9,10-dihydroanthracen-9-one
DMA	dynamic mechanical analysis
DMF	dimethylformamide
DMSO	dimethyl sulfoxide
DN	double network
DP	degree of polymerization
DS	damage-sensing

---

DSC	different-scanning-calorimetry
E	E-modulus (Young's modulus)
EA	ethylacrylate
EGDMA	ethylene glycol dimethacrylate
EPR	electron paramagnetic resonance
ESI	electron-spray-ionization
gDBC	<i>gem</i> -dibromocyclopropane
gDCC	<i>gem</i> -dichlorocyclopropane
gDFC	<i>gem</i> -difluorocyclopropane
gDHC	<i>gem</i> -dihalocyclopropane
GPC	gel permeation chromatography
HDI	hexamethylene diisocyanate
HOMO	highest occupied molecule orbital
IAd	1,3-bis(1-adamantyl)imidazol-2-ylidene
I <sup><i>t</i></sup> Bu	1,3-bis(1- <i>tert</i> -butyl)imidazol-2-ylidene
I <sup><i>n</i></sup> Bu	1,3-bis(1- <i>n</i> -butyl)imidazol-2-ylidene
ICy	1,3-bis(1-cyclohexyl)imidazol-2-ylidene
IMes	1,3-bis(2,4,6-trimethylphenyl)imidazol-2-
IPr	1,3-bis(2,6-diisopropylphenyl)imidazol-2-
IR	infrared
s	strong
m	middle
w	weak
KHMDS	potassium hexamethyldisilazide
LCCP	living carbocationic polymerization
LUMO	lowest unoccupied molecule orbital
MALDI	matrix-assisted-laser-desorption-ionization
Mebip	2,6-bis(1'-methylbenzimidazolyl)pyridine
Me6-TREN	tris[(2-dimethylamino)ethyl]amine
M <sub>n</sub>	number average molar mass
MR	merocyanine
MS	mass spectrometry
M <sub>w</sub>	weight average molar mass
NHC	<i>N</i> -heterocyclic carbene
NMR	nuclear magnetic resonance spectroscopy

---

s	singlet
bs	broad singlet
d	doublet
dd	double doublet
t	triplet
q	quartet
m	multiplet
NBS	<i>N</i> -bromo succine imide
NP	naphthopyrane
PBD	poly(1,4-butadiene)
PDI	polydispersity index ( $PDI = M_w/M_n$ )
PEG	poly(ethylene glycol)
PIB	poly(isobutylene)
PMA	poly(methylacrylate)
PMMA	poly(methylmethacrylate)
PNB	poly(norbornene)
PS	poly(styrene)
PDMS	poly(dimethylsiloxane)
PET	photo induced electron transfer
PTHF	poly(tetrahydrofuran)
PU	poly(urethane)
PVA	poly(vinyl alcohol)
RCM	ring-closing metathesis
RI	refractive index
ROMP	ring opening metathesis polymerization
SBR	styrene butadiene rubber
SH	self-healing
SMFS	single molecule force spectroscopy
SN	single network
SP	spiropyran
STP	spirothiopyran
TABS	Thermally Activated Barrier to Scission
$T_g$	glass transition temperature
THF	tetrahydrofuran
TLC	thin-layer-chromatography

---

TMC	thiomerocyanine
TMP	trimethylolpropane
TN	triple network
TOF	time-of-flight
tpy	2,2':6',2''-terpyridine
UPy	2-ureido-4-pyromidone
US	ultrasound
UV	ultraviolet
vis	visible
$\lambda_{em}$	emission wavelength
$\lambda_{ex}$	excitation wavelength

Parts of the Results and Discussion as well as of the Experimental Part were already published in

1. “*Mechanochemical activation of fluorogenic CuAAC "click" reactions for stress-sensing applications*” (Michael, P.; Biewend, M.; Binder, W. H), *Macromol. Rapid Commun.*, 2018, 1800376, DOI: 10.1002/marc.201800376;
2. “*Synthesis of Polymer-Linked Copper(I) Bis(N-Heterocyclic Carbene) Complexes of Linear and Chain Extended Architecture*” (Biewend, M.; Neumann, S.; Michael, P.; Binder, W. H.) *Polym. Chem.*, 2019,10, 1078-1088. DOI: 10.1039/c8py01751d
3. “*Detection of stress in polymers: mechanochemical activation of CuAAC click reactions in poly(urethane) networks*” (Biewend, M., Michael, P.; Binder, W. H) *Soft Matter.*, 2020, 5, 1137-1141. DOI: 10.1039/C9SM02185J

and were in parts adapted with permission from John Wiley and Sons. Inc. ©2018 and Royal Society of chemistry ©2020.

# 1. Introduction

## 1.1. Mechanophores

“Mechanophores are force sensitive molecular units, that respond to external mechanical fields by undergoing predicted chemical transformation.”<sup>1</sup> Mechanophores mostly contain a labile chemical bond, e.g. a strained ring<sup>2</sup> or an isomerizable functionality<sup>3</sup>, which are affected by mechanical pulses, thus causing a molecular transformation respectively a chemical reaction. First observations about the effect of mechanical forces on polymers has already been made by Staudinger<sup>4-6</sup> in the 1930s. He observes the decrease in molecular weight of a rubber material during rolling process in the presence of oxygen and thus prove the breakage of chemical bond due to external forces. These homolytic bond cleavage along the polymer chain could be later investigated by electron spin resonance spectroscopy<sup>7</sup> revealing a radical mechanism.

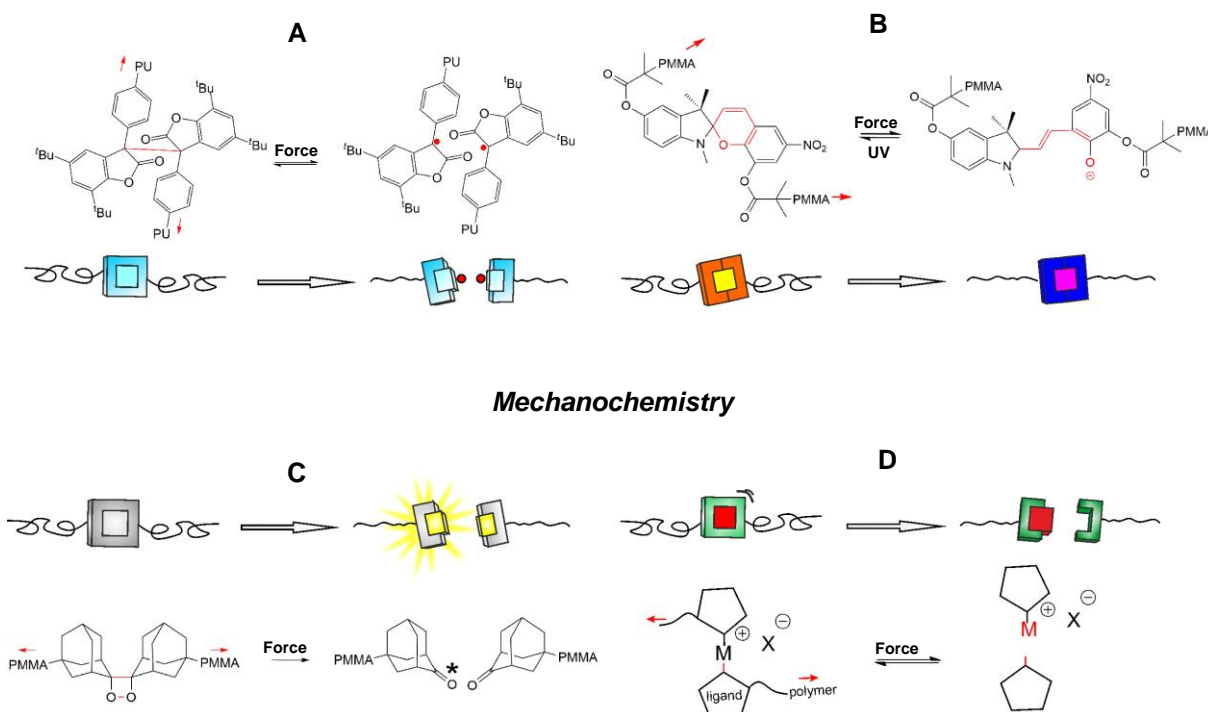


Figure 1. Schematic classification of polymeric mechanophores and their mechanochemical response to external forces: (A) cleavage of covalent bonds with the formation of radical species, (B) isomerization induced color change, (C) the appearance of fluorescence and chemiluminescence and (D) the creation of a catalytic active site.

There are several types of mechanophores (Figure 1), which can be divided by their response due to mechanical load. The selective cleavage of a labile bond, which accompanies by the formation of a reactive species, in turns enabling to trigger e.g., crosslinking reactions, represents the first category (A)<sup>8-19</sup>. Further, there are so called mechanochromophores (B) (e.g. spiropyranes<sup>1,3,11,20-46</sup>, spirothiopyranes<sup>47</sup>, naphthopyranes<sup>48,49</sup>, anthracenes<sup>50-55</sup>, coumarines<sup>56</sup> and rhodamines<sup>57-60</sup>) in which a mechanical stimulus triggers an isomerization reaction which leads to a temporary color change. The third category (C) is represented by molecules that respond with the appearance of light emission under mechanical stress. This can be realized either by the force triggered release of a molecule<sup>2,61-65</sup> or by the change in the spatial environment<sup>66-69</sup>. That goes along with the transient emission of light or by the formation of a UV-active molecule<sup>70-74</sup> that shows fluorescence after irradiation. If a metal center is

attached by several ligands in which at least one ligand could be cleaved off under mechanical stress and thus initiating a metal catalyzed reaction, these are called mechanocatalysts<sup>75-89</sup> (D). There are various other subgroups of mechanophores e.g. oxime sulfonates<sup>90</sup>, triarylsulfonium salts<sup>55</sup> or supramolecular mechanophores<sup>91</sup> that will not be discussed in this work. In order to improve the mechanochemically activation polymer chains can be attached. Due to the application of external force these polymer chains will continuously uncoiled up to a fully stretched state. Thus, the applied force is transmitted to the labile chemical bond, which is also been stretched and weakened and finally breaks<sup>80</sup>. This weakening of the labile bond is explained by the lowering of the dissociation energy barrier within the thermally activated barrier scission (TABS)-theory<sup>92-94</sup>. Herein the increasing of applied force led to a reduction of the dissociation barrier and thus facilitate the mechanochemical activation even at lower temperatures. This can also be improved by an increased chain length of attached polymer backbones<sup>95-97</sup>, due to the longer relaxation time to the initial random coil state. To ensure an optimal force transmission, the centered positioning of the labile bond is supportive<sup>95,98</sup> ( $\pm 15\%$ ) otherwise promoting the occurrence of radicals in the polymer backbone or prevent bond scission completely. Therefore, living polymerization techniques were often used to synthesize the polymer backbones, guaranteeing low molecular weight distribution and thus immobilize the labile bond close to the middle point. Furthermore, the nature of polymer backbone influencing the activation process reaching an optimal balance between stiffness and flexibility for efficient force transmission<sup>99-101</sup> which will be discussed in the next chapter.

## 1.2. Activation of mechanophores

### 1.2.1. Activation on a microscopic scale

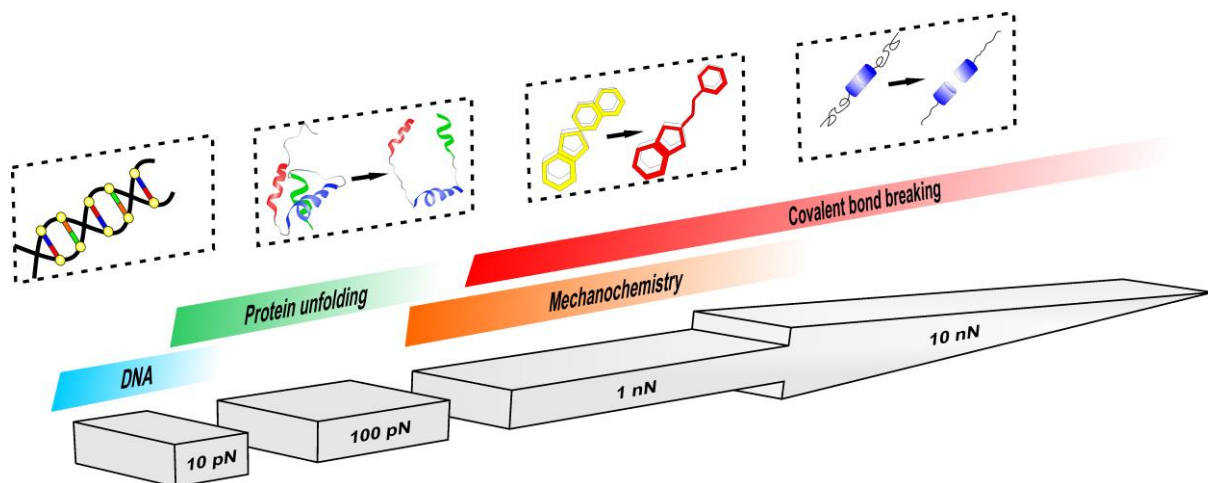


Figure 2. Scale bar of different molecular processes and the required forces.

In order to understand the mechanochemical activation within this large plethora of many mechanophores, the understanding of bond rupturing and its dependencies on polymer structure<sup>99</sup>, spatial influences<sup>102</sup> as well as anchoring points<sup>24</sup> on a microscopic scale plays a crucial role. For this purpose, single molecule force spectroscopy (SMFS) offers the possibilities to discover mechanosensitive moieties on a micro level and allows to transfer these observations to a “real life” application<sup>24,39</sup>.

To classify the mechanochemistry in terms of required forces and applicability, Figure 2 shows the comparison between the classic mechanophores and some other molecular processes ranging from mechanoenzymatics<sup>103,104</sup> or soft mechanochemistry (e.g. protein unfolding<sup>105,106</sup>)

in the low piconewton regime (10 – 100 pN) up to covalent bond breakage which, in turn, needs forces in the nanonewton regime (0.1 – 10 nN). Using atomic force microscopy for SFMS allows to comprise this broad range investigating bond rupture events as well as structural changes. For experimental realization a single polymer chain, which includes the mechanophore, is immobilized between a silicon substrate and the tip either by chemical reaction (e.g., peptide coupling) or solely by adsorption (Figure 3). Herein, the polymer chain allows to transmit the applied force to the labile chemical bond by minimizing the required dissociation energy as discussed in chapter 1.1. The retraction of the tip reveals the so-called force extension curve which allows to precisely determine characteristic molecular events, typically for the certain molecule.

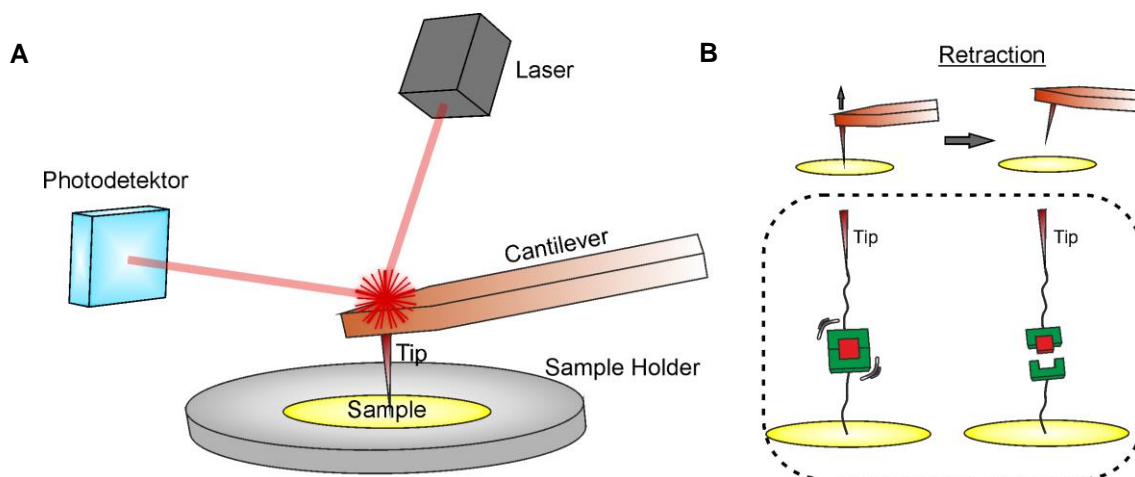


Figure 3: (A) Schematic representation of a typical AFM setup in which a mechanophore containing single polymer chain is immobilized between the surface and the tip. (B) Gradual retraction of the cantilever initiates the mechanophore rupture event.

#### 1.2.1.1. Multimechanophore concept (Method A)

The simple immobilization of single mechanophores between the surface and the AFM tip did not reveal reliable results due to the ambiguous assignments of rupture events. Contrary to the required mechanophore rupture events several side events could occur like polymer backbone rupture events or anchor-surface rupture events. In order to precisely determine the required mechanophore rupture event different methods were developed (Figure 4). For multimechanophores (Figure 4 A), which were embedded into one polymer chain, a plateau value in force-tension curve was reached indicating the bond breakage event. The high resolution of this method also allowed correlating the influence of conformation and structural changes with the previous determined rupture force. First reports on determination of rupture forces investigated the behavior of Z-alkene or E-alkene substituted *gem*-dichlorocyclopropanes (gDCC) allowed to determine the respective rupture forces of 770 pN for E-alkene as well as 1160 pN for the Z-alkene<sup>100</sup>(Table 1, Ent. 3). The extension lengths, which were calculated with differential functional theory (DFT) and the experimental values coincide, resulted in an extension length of 16 nm (E-alkene) respectively 12 nm (Z-alkene). The lower rupture force of the E-alkene correlated with its higher mechanical advantage in comparison to the Z-alkene, acting as a kind of “lever” which, in turn, induced a more efficient force transmission. Further investigations regarding the lever arm effect<sup>99</sup> used *gDCC* and *gem*-dibromocyclopropane (gDBC), which were immobilized in poly(butadiene) (PBD) as well as poly(norbornene) (PNB) matrix material. The influence of polymer backbone nature was studied for the first time contradicting the previous assumed chain length dependency as the

only influencing factor. Herein, the cyclopentyl rings of PNB backbones are mechanically advantageous acting as a lever arm which enhances the mechanical coupling to the force induced ring opening reaction.

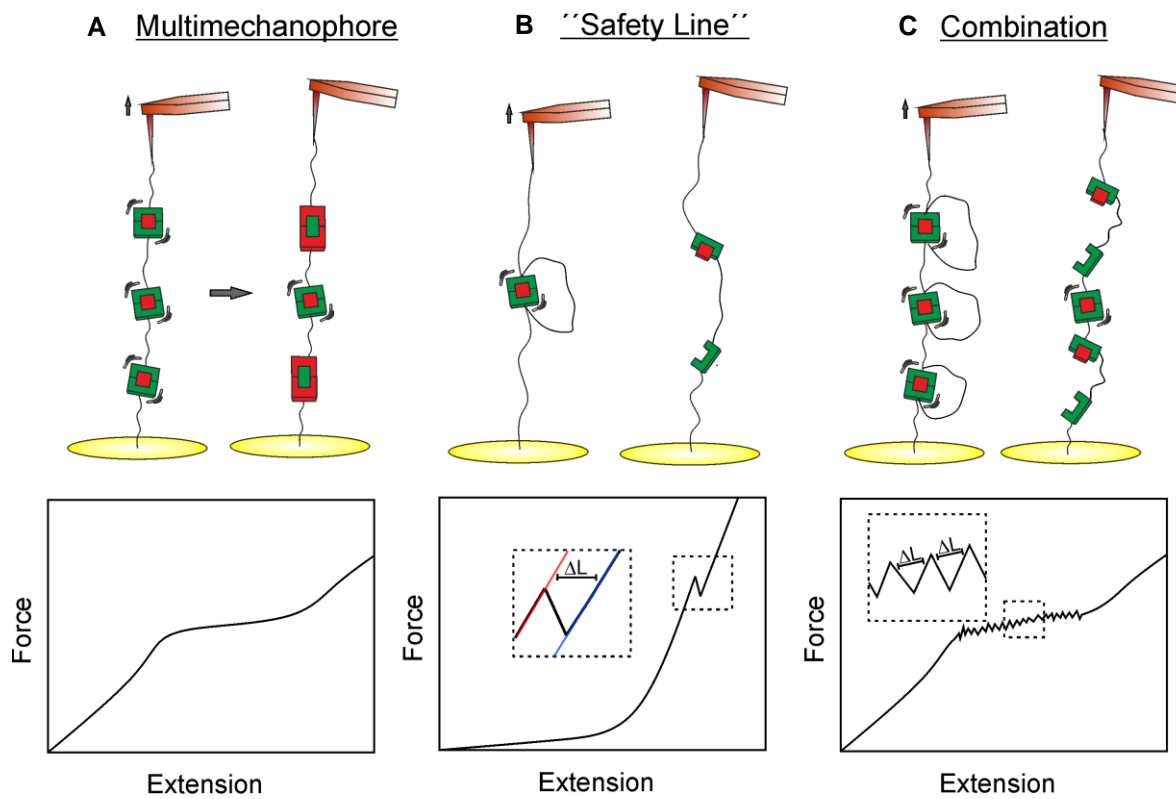


Figure 4. Several methods for identifying bond rupture events and their force-extension curves: (A) multiple mechanophores immobilized within a polymer chain, (B) a mechanophore is secured by a safety line and (C) multiple mechanophores each secured with safety line.

Furthermore the multimechanophore concept, in which mechanophores were located within one polymer chain, was used to determine rupture forces of spiropyranes<sup>24</sup>, triggering a force induced isomerization to merocyanine. Herein activity-affecting regiochemical effects were investigated on a single molecule scale, achieved by different connection of the anchored polymer chain on the spiropyran ring system. Both isomers, the external phenyl connected (Table 1, Ent. 5) and the nitrogen attached (Table 1, Ent. 6) reveal experimentally rupture forces of 260 pN and 240 pN, which are below the rupture forces of gDCC. The slight decrease was, in turn, explained by the occurring mechanical advantage due to favored regiochemical substitution. Further investigation on SMFS was done by Wang and coworkers<sup>107,108</sup>. They enabled the ring opening reactions of cyclopropanes as well as cyclobutanes which are prohibited according to the Woodward-Hoffman rules<sup>109</sup>. They found out, that symmetry allowed ring-opening reaction needs higher rupture forces in contrast to the symmetry forbidden. This was firstly determined by using gem-chlorofluorocyclopropanes (gDFC) observing a reduction of rupture forces from 1500 pN for disrotatory mechanism to 1290 pN for conrotatory mechanism. This was confirmed by further observation of gDCC and gDFC, heightened the rupture forces in favored disrotatory pulling from 1290 pN (gDFC) or rather 1300 pN (gDCC) (Table 1, Ent. 1) to 1840 pN (gDFC) and 2290 pN (gDCC) (Table 1, Ent. 2) for conrotatory pulling. In contrast, benzocyclobutanes (BCB) showed different preferences resulting in higher activation forces of the allowed conrotatory pulling (1500 pN) as for the forbidden disrotatory pulling (1370 pN). This was explained by higher mechanochemical coupling/ reactivity of the cis-BCB compared to trans-BCB. While the previous described lever

arm effect can be neglected here, further studies intentionally attached  $\alpha$ -alkene moieties and reduces the bond rupture forces of cis-BCB further from 1370 pN to 900 pN emphasizing the lever arm effect as an universal tool to realize actually forbidden reaction paths<sup>101</sup>.

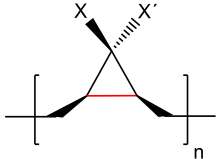
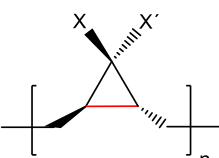
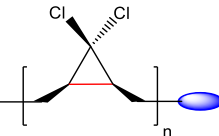
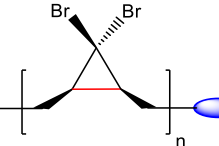
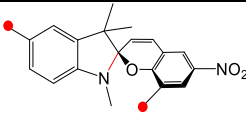
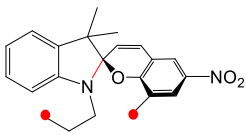
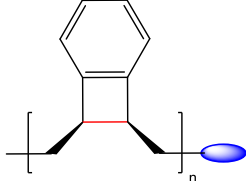
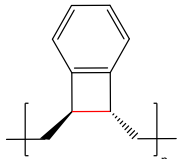
#### 1.2.1.2. Safety Line concept (Method B)

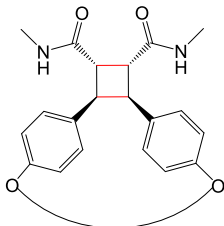
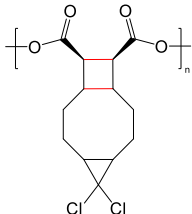
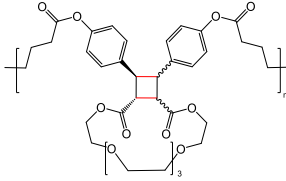
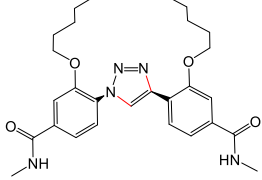
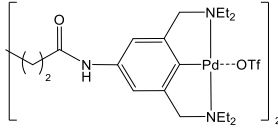
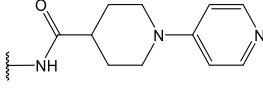
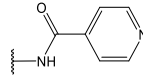
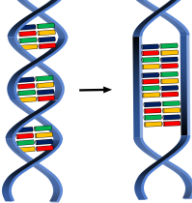
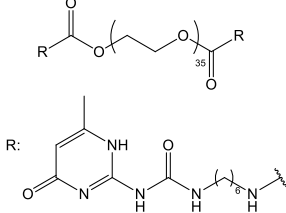
The concept of multimechanophore containing single polymer chains was substituted<sup>110</sup>, using a biochemical inspired template<sup>111-116</sup>, in which the mechanophore was bypassed with a safety line (Figure 4 B). Hence, rare mechanophore assigned bond rupture events can be precisely determined amidst a multitude of irrelevant ones (rupture of backbone, detachment from tip as well as multiple attachment of chains) detecting the defined length of the safety line. This allows to observe simple mechanochemical bond-breaking, which leads to a full polymer rupture instead of a determinable elongation of isomerizing mechanophores. First investigations were done using a macrocyclic triazole based mechanophore<sup>110</sup> (Table 1, Ent. 12), in which the force sensitive triazole ring was located in the shorter branch and the longer branch was constituted by the safety line. Afterwards, the synthesized macrocycle was covalently immobilized between glass substrate and AFM tip conducting the SMFS experiment in the fly-fishing mode<sup>117</sup> meaning the frequent immerse and retraction of the AFM Tip up to a binding event. Only 5% of all binding events were assigned to double rupture events, indicating the ring opening of a macrocycle or the detachment of two polymer chains. This can be defined more detailed by comparing the slopes in the force-extension curves. The revealed bond rupture forces for triazole ring opening reactions varying from 1100 pN to 2000 pN but due to the rare valuable events a quantitative statistical analysis did not occur. This concept was also transferred to cyclobutanes<sup>118</sup>, investigating the force induced cycloreversion, which was previously described by Moore<sup>14</sup> and Craig<sup>13</sup>. Herein cyclobutanes were embedded into macrocycles with different sizes. This has improved the assignment of rupture sites in contrast to the triazole mechanophore. Rupture forces ranging from 1700 pN to 3900 pN (Table 1, Ent. 9) could be observed, which, in turn, could precisely identified by proving the elongation of the safety line (2.4 nm (for  $n = 18$ ) and 3.4 nm (for  $n = 27$ )).

#### 1.2.1.3. Reaction cascade concept (Method C)

Further investigations revealed the combination of both previous discussed concepts. Herein a dual mechanophore (5,5-dichlorotricyclo(7.2.0.0)undecane) was used building up a reaction cascade (Figure 4 C), in which cis-gDCC was "protected" by a cyclobutene moiety. This resulted in higher activation energies of "protected" cyclopropane compared to the purely gDCC containing polymer<sup>119</sup>. The resulting force-extension curves showed a distinctive saw-tooth pattern, which is attributed to the ring-opening reasoned extension of cyclobutane. This was specified by observing force-extension curves of cinnamate ester containing macrocycles<sup>102</sup> yielding two different plateaus, which constitutes the different dissociation energy of syn-and anti-isomer. The resolution of each plateau indicates that each saw tooth corresponds to a single cycloreversion event with elongation of approximately 2.5 nm and rupture forces of 870 pN for syn dimer and 2000 pN for anti-dimer (Table 1, Ent. 11).

Table 1. Summary of different mechanophores and the determined forces via SMFS.

Ent.	Mechanophore	Substructure	Method	Rupture force
1	gDHC <sup>99,100,107</sup>		A	X, X' = F, F 1290 pN
2				X, X' = Cl, Cl 2290 pN
3	cis-gDCC		A	PB 1300 pN
4				PNB 900 pN E- $\alpha$ - alkene 770 pN Z- $\alpha$ - alkene 1160 pN
5	Spiropyrane <sup>24</sup>		A	260 pN
6				240 pN
7	BCB <sup>101,107</sup>		A	$\alpha$ - alkane 1370 pN E- $\alpha$ - alkene 920 pN Z- $\alpha$ - alkene 1250 pN
8				1500 pN

9			B	1700 pN – 3900 pN
10	Cyclobutane <sup>102,118,119</sup>		C	2200 pN
11			C	Syn: 870 pN Anti: 2000 pN
12	Triazole <sup>110</sup>		B	1100 pN – 2050 pN
13	Pincer complex <sup>120</sup>		-	 93 – 166 pN  54 – 102 pN
14	DNA <sup>121</sup>		-	65 pN
15	UPy <sup>122</sup>		-	180 pN

Another example is the simultaneous bivalent coordination of Pd-N bonds<sup>120</sup> (Table 1, Ent. 13). Herein the substrate surface as well as the AFM tip were functionalized via pyridine containing substituents, in which the simultaneous formation of several Pd-N bonds allows to determine the rupture forces. In contrast to the safety line concept potential side rupture events cannot be excluded. This technique was also used to investigate the force accelerating hydrolysis of

amide bonds<sup>123</sup>. As mentioned above SMFS can be also used to determine further supramolecular interactions by immobilization and withdrawn of (bio)macromolecules<sup>124</sup> (dsDNA stretching<sup>121</sup>(Table 1, Ent. 14), UPy-UPy interactions<sup>122</sup> (Table 1, Ent. 15)).

After all, SMFS turns out as a universal tool to investigate isolated single chains, studying covalent bond ruptures as well as unlock new fundamental insights in terms of structural, conformation and mechanistic influences on the mechanochemical behavior itself. However, the study of “real” material is invincible considering a variety of influences on activation behavior (e.g., polymer chain interactions), which are neglected on a microscopic scale but offers the potential for applicability of mechanochemistry even in industrial scale.

### 1.2.2. Activation on a macroscopic scale

The steadily growing of mechanoresponsive materials revealed a variety of activation methods, ranging from solution-based methods (e.g. pulsed ultrasound<sup>95,125-131</sup> or freeze-thaw cycles<sup>132-134</sup>) over methods in bulk (e.g. compression<sup>23,37,85,135-139</sup>, grinding/ball milling<sup>18,19,134,140-142</sup> or tensile testing<sup>3,11,21,22,40</sup>) up to interfacial activation methods<sup>39,73,143-145</sup>, accompanying by a comprehensive variety of different forces and strain rates.

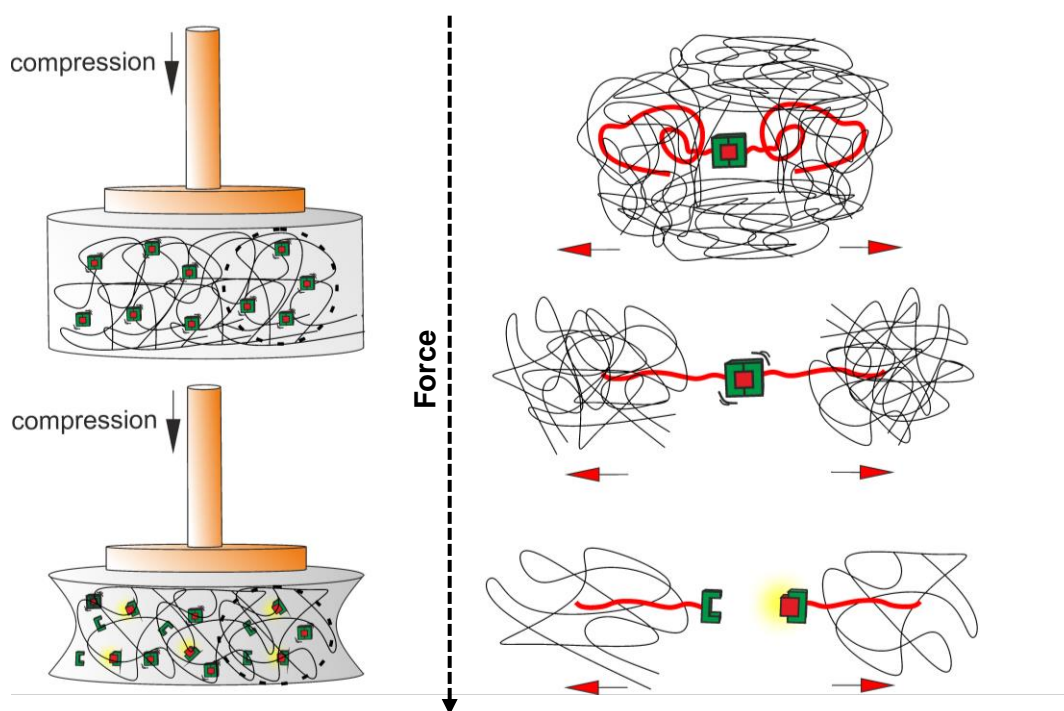


Figure 5. The application of compression load led to disentanglement of matrix polymer chain, in which the anchored polymeric handles will be stretched and transmit the force to the labile centered bond.

In solution, ultrasonication is the commonly activation method where the force is transferred by the formation of a void volume due to collapsing cavitation bubbles<sup>95,96,125-127,129,130</sup>. This stretches the polymer chain and transmit the force to the labile bond. Herein, higher strain rates are necessary for efficient mechanochemical activation because the molecular deformation must exceed the molecular vibration (strain rates  $> 10^4 \text{ s}^{-1}$ , maximum forces up to  $10^{-9} \text{ N}$ ). Several studies of mechanochemical activation were accomplished in solution by pulsed ultrasound (e.g. chain length dependency<sup>80,94-97,146-148</sup>), however, in polymeric mechanochemistry the most promising applications were realized in solid state material e.g. for stress-sensing applications<sup>91,149,150</sup>. Activation methods in bulk achieved higher maximum forces in contrast to the solution but often limited in accessible stress rates (strain rates  $> 1 \text{ s}^{-1}$ ).

<sup>1</sup>, maximum forces up to  $10^5$  N). For example, the activation by compression was realized by anchoring the polymeric backbone of the mechanophore within the matrix material (Figure 5), either by solely physical entanglements or by supramolecular<sup>26-29,151</sup> or covalent chemical crosslinks<sup>25,42,57</sup>. The activation process itself was started by force induced stretching of the matrix polymer chains, whereby the anchored polymer chains were also stretched until a critical disentanglement is reached. This transmits the force through the polymer chain to the labile centered bond and finally activates the mechanophore.

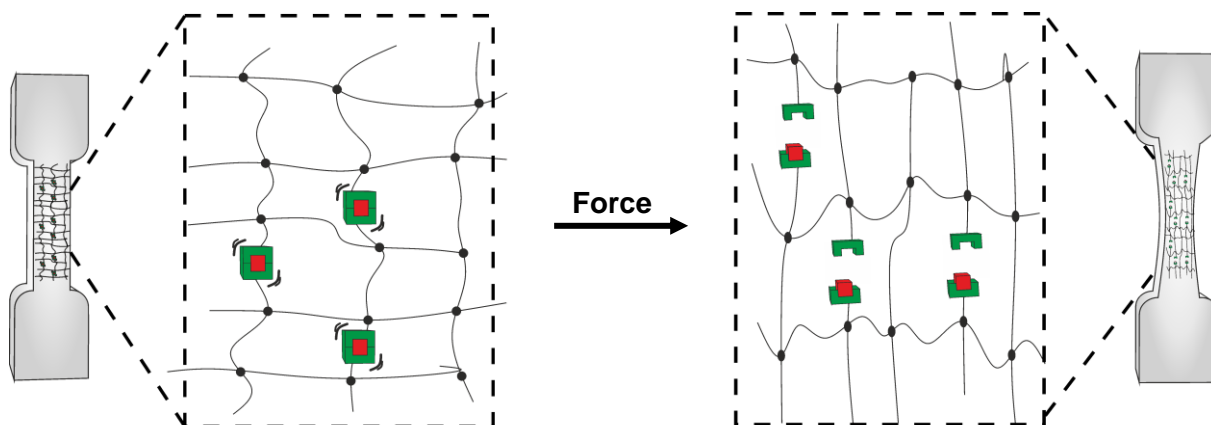


Figure 6. During tensile experiments, the matrix anchored mechanophore will be activated by stretching matrix polymer chains.

Another example is the activation via elongation either by tensile testing via DMA or via rheological instrumentation<sup>2,152</sup> (Figure 6). Herein, a defined shaped specimen (dog bone or precise rectangular shape) is fixed, and uniaxial stress is applied at the gauge region of the sample. The control and quantification of applied stress and strain are emphasized as the main advantages of tensile methods, contrary to the activation via compression. The group of Sijbesma triggered the cycloreversion of 1,2 dioxetanes, which were fixed as crosslinker within a PMMA matrix detecting the force induced chemiluminescence as a measure of activation<sup>2</sup>. Here, the force was applied via extension rheological instrumentation, in which the specimen was fixed between two rotating drums applying the uniaxial stress via elongating of the polymer film. The simultaneous optical detection allowed to quantify the mechanoresponsivity and facilitated the correlation between material properties and mechanochemical activation. Additionally, tensile testing experiments were done by incorporating diazobenzenes amide oligomers into poly(urethane) networks which were immobilized in a specific cis conformation. During the application of tensile stress with strains ranging from 100 – 300% the hydrogen bond interaction between the mechanophores was distorted, which leads to a cis-trans isomerization detectable via UV-spectroscopy<sup>152</sup>. In contrast to the purely physically entangled polymers, the efficiency of activation could be improved by cooperating the polymer backbone of the mechanophore into a network structure<sup>21,25,30,62,85,139,140,149,153</sup> or co-crystallize them within a matrix material<sup>85</sup>. This created more crosslinking points, which in turn, hindered the chain flexibility and the accompanying inhibition of entanglements. This led to a more efficient force transmission and thus enhanced the mechanochemical activation. In order to understand this context, deeper insights into the structure-property relationship of polymer networks are necessary.

### 1.3. Polymer networks

Polymer networks<sup>154-156</sup> are either covalently<sup>157</sup> or non-covalently<sup>158</sup> (ionic<sup>159,160</sup>, hydrogen bonds<sup>161</sup> etc.) crosslinked. They are of steadily growing interest for a wide range of applications reaching from drug delivery systems<sup>162</sup> over energy storage<sup>163</sup> up to catalyst and sorbents<sup>163-165</sup>. In order to ensure and expand this wide range of applicability, it is important to understand how structural factors influence the suitability for the respective usage.

#### 1.3.1. Classification of polymer networks

In contrast to linear polymers, the manufacturing of polymer networks requires molecules containing at least three functionalities, which enable the formation of three-dimensional structures with high molecular weight. This leads to a multiaxial expansion, in which the crosslinking point connects several polymer strands like linear polymer chains or short molecules. Considering the type of linkage, two different categories can be derived from this: supramolecular as well as chemical polymer networks. While structural features of chemical networks are mostly described by covalent connections, supramolecular networks based on physical interactions like Van-der-Waals interactions, hydrogen bonding<sup>166</sup> or metal-ligand interactions<sup>167</sup>. Referring to different structure and properties, polymer networks can be divided into four different categories: thermoplastics, elastomers, thermosets and gels (Table 2).

Table 2. Classification of polymer networks with typical representatives.

Thermoplastics	Elastomers	Thermosets	Gels
TPU	SBS	MPF	Gelatin
Acrylates	SBR	Phenol resin	Polyacrylamide hydrogel
UPy terminated PIB	PU	Epoxy	PHEMA
PA	NR	Polyester resin	PVA

##### 1.3.1.1. Thermoplastics

Thermoplastic polymer networks<sup>168</sup> are linear polymer chains, which are connected by supramolecular interactions, and thus, are not irreversible crosslinked. Herein, the recyclability is guaranteed due to the transition of solid material to viscoelastic fluids above a certain temperature, in which the dissociation energy of supramolecular interactions is exceeded. However, the material properties of thermoplastic polymer networks (e.g., polyamide 6,6) are mostly similar to thermosets whereas the introduction of segmented block structured copolymers can also induce elastic properties (e.g., thermoplastic poly(urethane)s).

##### 1.3.1.2. Elastomers

Slightly covalent crosslinked polymer networks which have soft and elastic properties (Young modulus  $E \sim 1$  MPa) are called elastomers<sup>169</sup>. In contrast to other polymer network classes, elastomers withstand high deformation (500 – 1000%) without rupture and are capable to restore their initial form after removal of stress. This elasticity based on the high chain length of polymer strands (soft domain) between crosslinking points, which normally have a low glass transition temperature ensuring the flexibility of the chain. This, in turn, induces physical

interactions (e.g., entanglements of polymer chains), which additionally allows to compensate the applied force. Prominent examples of elastomers are natural rubber<sup>170</sup>, crosslinked poly(urethane)s<sup>171</sup> or styrene-butadiene-rubber<sup>172</sup> (SBR).

#### 1.3.1.3. Thermosets

Varying the ratio of strands and covalent crosslinking points to lower values accompanying with the reduction of the chain length in between leads to a dense material which is called thermoset<sup>173,174</sup>. In contrast to elastomers, thermosets are applied at temperatures below the glass transition temperature that classifies them to rigid and stiff material (Young modulus  $E \sim 1000$  MPa). They are normally insoluble in any solvent and not further processable after manufacturing (except e.g. vitrimers<sup>175</sup>). Formaldehyde resins<sup>176</sup> or epoxide resins<sup>177</sup> can be assigned to this group, applicable due to their insensitivity and resistance of high temperatures.

#### 1.3.1.4. Gels

Gels are physical or covalent polymer networks used in the swollen state, in which the solvent (water or any other organic solvent) is enclosed within elastic network structure leading to a wet and soft material (Young modulus  $E \sim 0.001 - 0.01$  MPa), capable of endure large deformation<sup>178</sup>. Gels can be further classified according to the source (e.g. natural or synthetic), to the liquid medium (e.g. hydrogels<sup>179</sup>/ organogel<sup>180</sup>) as well as to their type of cross-linkage (physical or chemical). Typical examples of gels are gelatin or poly(acrylamide) hydrogels.

### 1.3.2. Structure of polymer networks

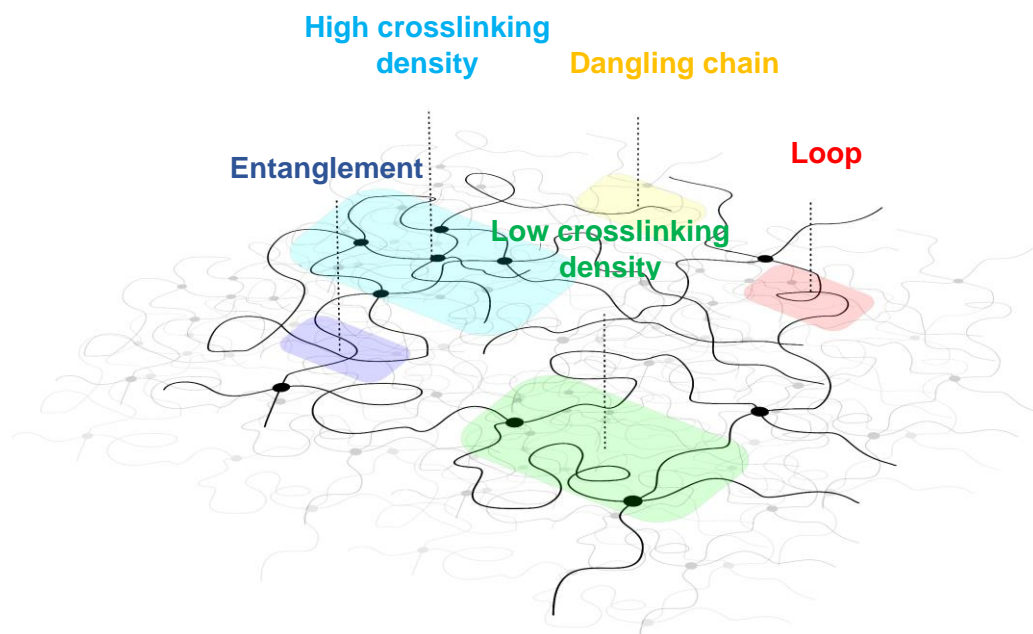


Figure 7. Structural elements within a polymer network indicating different chemical as well as physical interactions.

Topological investigations of polymer networks become major importance in polymer science estimating information about material properties like elasticity<sup>181</sup> or porosity<sup>182</sup> by understanding structural relationships (e.g. crosslinking density). Since the most polymer networks are amorphous or semi-crystalline in nature, a variety of structural features can be identified. In Figure 7, different structural characteristics are shown, in which the strands are connected by network points with inhomogeneities in crosslinking density due to fluctuations

during manufacturing. Besides the fully integrated chains, there are dangling chains, which remains after polymerization process, entanglements, emerging by interpenetration of random coil chains and finally loops, occurring by the reaction two chain ends of one strand with the same crosslinker. Although these topological characteristics are well known, only indirect methods are available for characterization (swelling, tension, rheology) allow predicting some structural properties like crosslinking density or critical entanglement.

### 1.3.3. Mechanical properties of polymer networks

#### 1.3.3.1. Stress-strain curves

The mechanical behavior of polymer networks having an outstanding significance for the activation of network-based mechanophores. It describes the stress, deformation as well as flow characteristics of matrix materials during the application of stress and thus provides information about force transmission processes. The probably most used method to investigate such material properties is represented by tensile testing. Herein, the stress-strain properties were determined by observing the tension stress during elongation of a polymer network up to its rupture<sup>183</sup>. The resulting stress strain curves offer structural features, which can unambiguously indicate the properties of a material.

In Figure 8 A, the black plot describes schematically the behavior of a strong but not tough material, in which high forces but low energy (area below the curve) must apply on the material to break the sample. These brittle materials show very high stresses at very low deformations. The blue curve describes a flexible plastic material which does not resist deformation as strong as rigid plastics<sup>184,185</sup>.

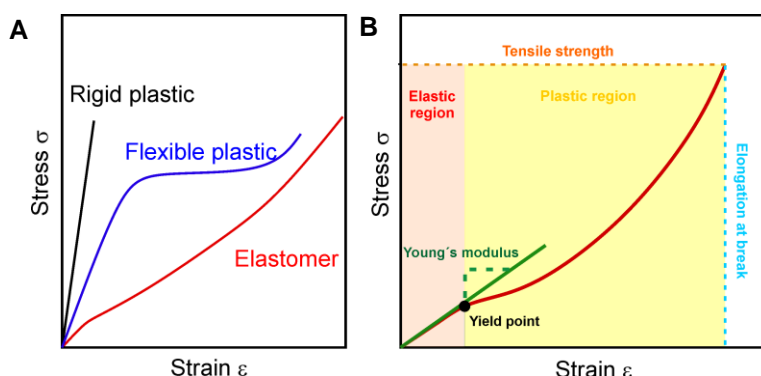


Figure 8. (A) Schematic stress-strain curves of rigid plastic (black), flexible plastic (blue) and elastomers (red) as well as (B) typical characteristics of an elastomeric stress-strain curve.

Applying stress to those plastic materials leads to an initially large slope but merge finally into a deformation regime, which in turn, suggests an approaching break. The red curve describes an elastic material, which behaves like a rubber material finally enabling a recovering of its original shape when stress is released. The main topic of this work deals with elastomer materials, therefore a closer look on the stress strain curve is necessary (Figure 8 B). The plot of an elastomer is divided into the elastic and plastic region which is kept apart by the so-called yield point. While in the plastic region permanent deformations remains after stress relaxation, a recovery of initial structure can be observed within the elastic region due to its entropic elasticity. An explanation can be given by Hook's law, which describes the consistent proportionality of the applied stress with strain. It based on the compensation of force by flexible entanglements, which are brought to higher entropic state during deformation

subsequently returning to an entropy favorable state after stress release. The proportionality factor is the Young's modulus  $E$ , which in turn, is a measure for the stiffness of a material.

### 1.3.3.2. Rubber elasticity and network model

In order to describe the rubber elasticity<sup>156</sup> more detailed theoretical considerations reveals three different simplified network models: the affine networks<sup>186</sup>, the phantom networks<sup>187</sup> and the real elastic networks.

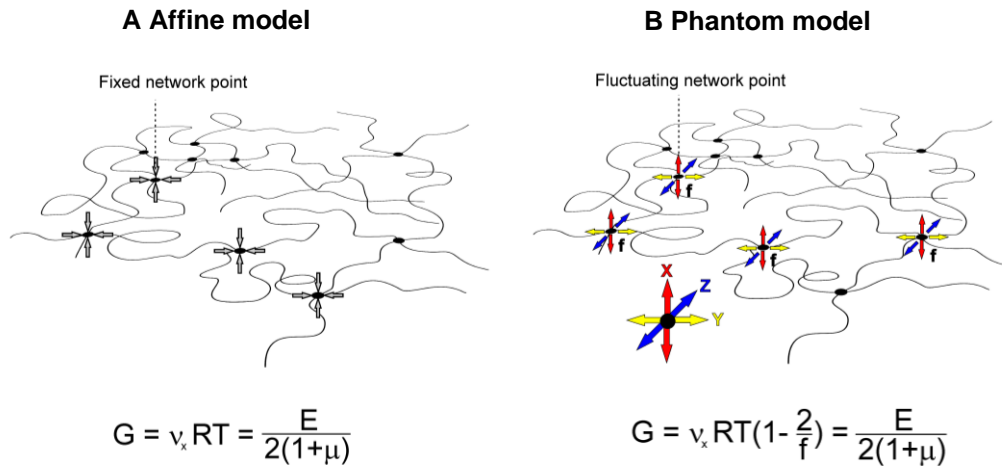


Figure 9. Schematic description of simplified network models as well as the connection of crosslinking density and storage modulus: (A) affine model with fixed network points as well as (B) phantom model with fluctuation network points considering the network branch functionality  $f$ .

Within the affine networks model (Figure 9 A) it is assumed that macroscopic deformations, equally acting on a network strands on microscopic scale, considering network strands as Gauß shaped chains and neglecting intermolecular interaction as well as incompressibility. Contrary, the phantom network model (Figure 9 B) describes polymer networks with fluctuating crosslinking groups around their middle position, which leads to a reduction of free energy due to the increasing degrees of freedom.

The intensity of these fluctuations correlates with the relationship of microscopic and macroscopic deformation, however, assuming the penetrability of individual network chains<sup>188</sup>. The real elastic network model<sup>189-191</sup> includes the influence of formed loops within the network structure and allows determining unambiguous values of shear modulus of certain gels. These three models give a good overview of rubber elasticity but neglect essential influences factors like topological restrictions (entanglements) which additionally acts as supramolecular crosslinkers and influence significantly the mechanical behavior. Therefore, many other advanced models complement these simplifications that describe intermolecular interactions as a basis of different assumptions (e.g. constrained-junction model<sup>192</sup>).

### 1.3.3.3. Rheology of polymer networks

Polymer networks often exhibit properties, which correspond equally to solid and liquid materials, named viscoelasticity<sup>193</sup>. Here, shear induced deformation occurs, in which the respective parts can be assigned to either viscous or elastic behavior. The viscous behavior causes irreversible time dependent deformations of material whereas the elastic behavior leads to spontaneous, reversible deformation. The elastic part is described as storage modulus  $G'$  whereas the loss modulus  $G''$  includes the viscous part. If the scenario  $G' > G''$  occurs, the

material behaves like a “solid” material, in which the opposite ratio  $G'' > G'$  leads to liquid like behavior. Contrary to dynamic polymer networks, which often show complex rheological behavior, within covalent crosslinked polymer networks  $G'$  significantly exceeds  $G''$  resulting in a frequency independent value at a certain deformation (shear modulus). Fluctuating behavior of loss modulus is attributed to relaxation behavior of soluble fractions as well as to imperfections within the network structure, which also leads to higher  $G''$  values. Experimentally, oscillatory shear experiments allow following network forming reactions observing the transition of a viscous solution to an elastic solid material, which is indicated by the crossing point of  $G'$  and  $G''$ , also named gel point<sup>194</sup>. Temperature dependent measurements offer information about dynamic properties (e.g. hydrogen bond) within polymer networks or reveal information about temperature dependent material properties (e.g. E-modulus) or melting/ glass transition temperatures<sup>195</sup>.

#### 1.3.3.4. Swelling behavior of polymer networks

In contrast to linear polymers, polymer networks, which are crosslinked via sufficiently strong covalent bonds are generally insoluble in any solvent. However, there are specific interactions which accompanies by an equilibrated volume increase due to the absorption of solvent (Figure 10)<sup>196,197</sup>.

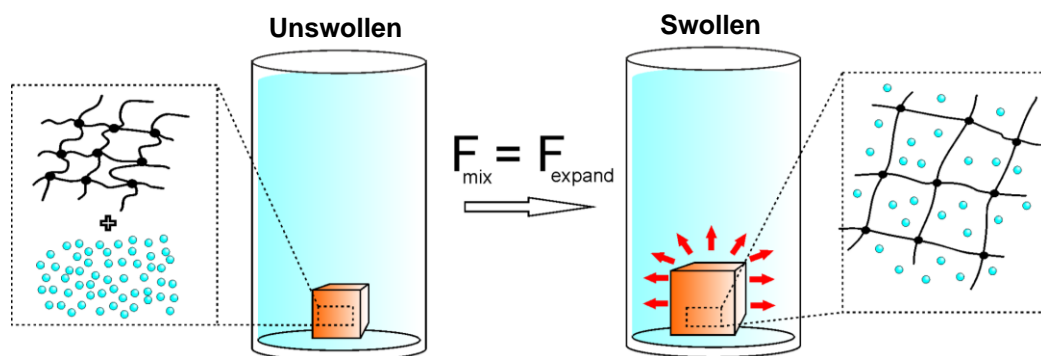


Figure 10. Schematic representation of a swollen polymer network with a good solvent establishing an equilibrium ( $F_{\text{mix}} = F_{\text{expand}}$ ).

This could be described by the interplay of two driving forces. On the one hand, there is the free energy of mixing (polymer – solvent), in which the solvent infuses and thus dilute the polymer leading to an entropic increase. This dilution process depends on the number of solvent molecules as well as the volume fractions of polymer and solvent, and thus, likewise on the polymer-solvent interaction parameter also called Flory-Huggins parameter  $\chi$ <sup>198</sup>. Opposed to this, the elongation of crosslinked polymer chain during swelling causes an inward elastic retractive force, which favors a decrease in entropy. The interplay of both opposing forces lead to a steady-state behavior ( $F_{\text{mix}} = F_{\text{expand}}$ ), which causes an equilibrium swelling. The Flory-Rhener equation<sup>199-201</sup> describes the swelling process theoretically offering a simple estimation of material properties of polymer networks.

The swelling behavior can be influenced by temperature, the nature of solvent and polymer as well as the amount of crosslinking. The higher the crosslinking density of a polymer network the higher the retractive forces and thus the lower the swelling degree. Considerations about swelling with this equation have some limitations, on the one hand the application on exclusively solvent free synthesized polymers, the assumption of Gauß distribution, as well as the neglect of monomer correlation along the chain. Over the years, several terms were

added<sup>202-204</sup> (e.g. osmotic pressure<sup>205</sup>) considering intra- and intermolecular interactions, which complement the theory.

### 1.3.4. Mechanophoric networks

As already mentioned above, embedding mechanophore into polymer networks leads to a more efficient activation due to the enhanced force transmission, which is caused mainly by covalent crosslinking points. Experimental considerations reveal that mechanophores which are parallel orientated to the vector of the applying force are preferably activated than the randomly distributed ones. However, within a polymer network the crosslinking points can redirect the applied force which in turn reach also the perpendicular orientated parts and lead to a more efficient mechanochemical activation<sup>3,20,21</sup>.

#### 1.3.4.1. Mechanochemically active spiropyrane

Spiroyrans are force sensitive molecules, in which an applied force can induce a  $6\pi$  electrocyclic ring opening reaction to a merocyanine unit accompanying by a specific color change (yellow to purple) in the visible spectrum (Figure 11).

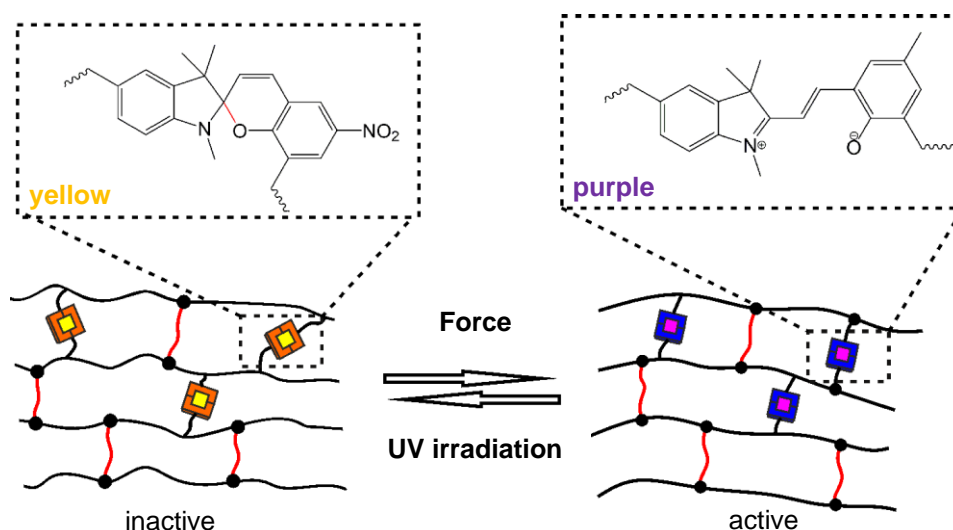


Figure 11. Force induced activation of covalently crosslinked spiropyrane isomerizing in a  $6\pi$  electrocyclic ring opening reaction to merocyanine which leads to a color change from yellow to purple.

First linkage of spiropyranes within a polymer network was realized by crosslinking the divinyl attached spiropyrane into a glassy PMMA matrix by free radical polymerization and investigated their mechanical response towards compression force. In this connection, the stress induced color change raised centrally of the investigated bead, in which the maximum of simultaneous measured fluorescence intensity correlated with the predicted stress distribution. In order to enhance the load transfer to the mechanophore, the crosslinked PMMA matrix was modified with respect to the architecture<sup>31</sup>. Therefore, three different primary crosslinker with varying lengths were additionally introduced which are either similar or disparate to the length of spiropyrane (EGDMA, PEG550 and PEG750). Performed torsion testing revealed information about threshold of stress and strain values which are required for mechanochemical activation. However, the activation of mechanophores purely occurred after yield, thus, indicating the necessity of plastic flow, which could be influenced by varying several parameters (e.g., temperature, solvent). Overall, with growing crosslinker length (PEG550, PEG750) the needed stress became lower suggesting an enhanced load transfer to the mechanophore whereas the extension of PEG550 to PEG750 did not influence the

mechanochemical activation. Additionally, several parameters like temperature, loading rate or loading mode could intervene in the activation process, investigated precisely by tension or compression experiments<sup>206</sup>. Further studies also enabled to interrelate the fracture induced mechanochemical activation and the locally acting stress/strain within a propagating crack<sup>33</sup>. The author observes that the most efficient SP activation can be assigned to regions with the highest stress and strain. The determination of the force threshold as well as the spatially resolved activation of SP within this model system allows estimating field distribution of mechanophore containing specimen, in which no direct stress measurement took place.

As discussed in Chapter 1.3, covalent crosslinked polymer networks can interact with solvents exclusively, absorbing the solvent which leads to a simultaneous increase in volume fraction. The acting force ( $F_{\text{expand}}$ ) within the expansion process could be applied for mechanochemical activation, in which the swelling induced stretch of polymer strands causes forces on molecular level, which in turn, drove the electrocyclic ring opening of covalently embedded SP<sup>30</sup>. More detailed observations indicate the influence of solvent as well as crosslinking density enhancing the swelling induced activation either by the reduction of crosslinking points or by usage of solvents of intermediate polarity. Overall, the tunability of SP containing, crosslinked PMMA matrix facilitates the capture of material fatigue within glassy matrices by monitoring the mechanically induced optical response.

Furthermore, SP were incorporated into segmented poly(urethane)s<sup>23,26-29</sup>, which included soft domains often represented by poly(ether)s respectively poly(ester)s, as well as hard domains usually represented by isocyanates. This enabled supramolecular crosslinks due to the hydrogen bond interaction between the poly(urethane) groups which can further improved by using either chain extender (e.g., butanediol) or 2-ureido-4-pyromidone (UPy) units. This formed a doubled crosslinked network<sup>26</sup>, which improved the mechanochemical activation of SP units due to the phase separation. On the one hand, strong hydrogen bond interaction of UPy moieties generated additional crosslinking points, which could redirect the applied forces due to the three-dimensional structure. Additionally, the soft domain segments were responsible for strain-induced crystallization processes, which in turns led to a more efficient force transmission.

The identification of a two-color transition state during mechanochemical activation caused by ring opening of SP at a strained state as well as isomerization of MC at a relaxed state allowed to realize a SP based stress mapping application. This could in turn reveal information about the rupture mechanism of a propagating crack<sup>34</sup>. The main advantage of this elastomeric systems dealt with the recyclability of the mechanochemical activation in which the applied irradiation with light after relaxing the sample led to the initial color and thus “renewed” the potential stress-sensing ability. This was also investigated by embedding SP into a poly(dimethyl siloxane) (PDMS) network<sup>40,207,208</sup> confirming the fully shape recovery behavior over multiple activation cycles up to ten times in which the total activation of SP depends on electronic and geometric parameters.

Among the large plethora of polymer classes, spiropyrane containing mechanophore networks play a crucial role in the development of applicable stress-sensing systems. Beyond glassy matrices and reloadable elastomers up to hydrogels<sup>209</sup>, polymer dispersions<sup>210</sup> (LATEX), composites<sup>211,212</sup> and self-healing polymers<sup>29</sup>, SP turns out as an universal tool in material science.

#### 1.3.4.2. Mechanochemically active dioxetanes

Dioxetanes are pre-strained four-membered ring units, in which an applied force can induce a cycloreversion reaction that goes along with the formation of a singlet excited moiety. The

subsequent relaxation to the triplet state leads to an emission of blue light<sup>62</sup>. Due to the short timescale of the chemiluminescence, *in situ* crack propagations can be facilitated, and thus, enables to investigate polymer materials in terms of damage occurring and damage transfer. This was realized by embedding the dioxetane into an ethyl acrylate (EA) elastomeric network (Figure 12) and investigated their mechanical response during uniaxial stress loading, in which the chemiluminescence was detected by photocounting. Additionally, the mechanophore containing network was swollen with monomer and subsequently polymerized to form a double (DN) and triple network (TN). Realizing initial notch test revealed that swelling of the mechanophore containing network pre-stretched the network strands, which in turn pre-stressed the mechanophore itself. This achieved a more efficient activation with increasing swelling degree and thus allowed to tune mechanochemical activation by the tuning of material properties, for the first time.

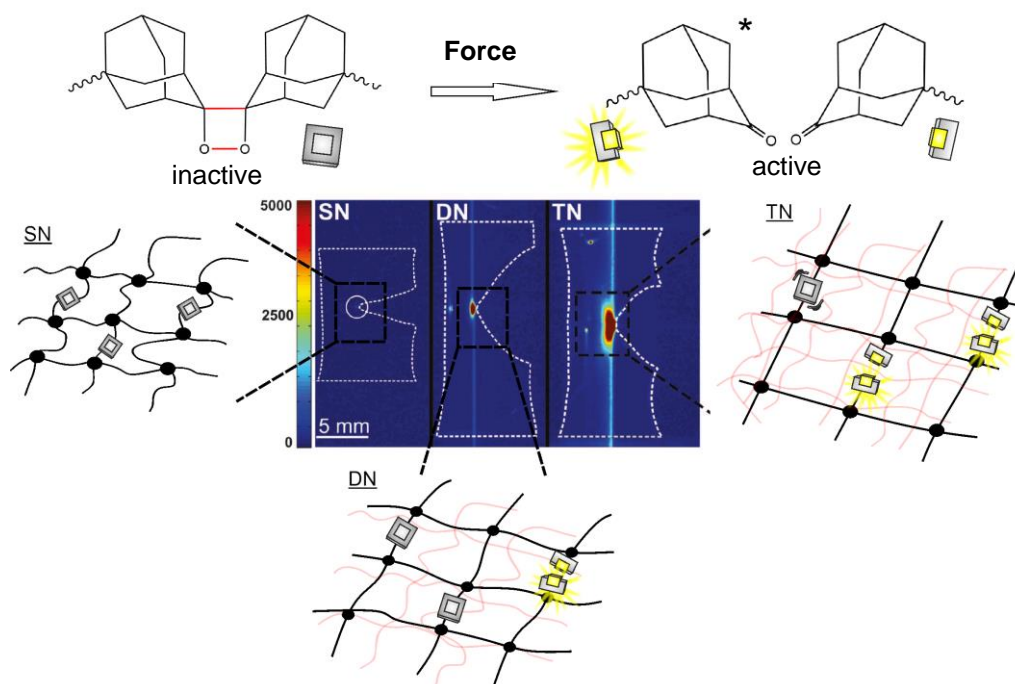


Figure 12. Mechanochemical activation of adamantly substituted 1,2 dioxetane incorporated within a single (SN), double (DN) and triple network (TN). The accompanying formation of an excited moiety leads to the emission of light (chemiluminescence) and allows to monitor *in situ* a crack propagation. Image was adapted with permission from AAAS.

In order to tune the material properties in terms of mechanical strength and high elasticity<sup>74</sup>, dioxetane mechanophores were incorporated within poly(urethane)/ siloxane hybrid polymers by polycondensation and subsequent sol-gel hydrolysis process. Different crosslinking densities were adjusted revealing a direct proportionality. The higher the crosslinking density the higher the cumulative light intensity at certain stress with consistent strain rate due to the improved force transmission.

In contrast to the uniaxial stress activated dioxetanes, swelling induced mechanoluminescence within glassy PMMA networks were investigated by ingress with chloroform, which acted as plasticizer<sup>64</sup>. This allowed to monitor *in situ* the progress of acting osmotic pressure which led to a cascade of bond rupture events quantifying the scissions of dioxetanes to  $10^9$  to  $10^{11}$  per event. Contrary to other crack monitoring applications<sup>213</sup>, the direct visualization, the microscopic level quantification as well as temporal resolution was accessible.

In addition, dioxetane containing covalent crosslinked networks were expanded by simultaneous introduction of dynamic (supramolecular) groups investigating the influence of metal-ligand<sup>63</sup> or hydrogen bonding interactions to the chain scission behavior. The growing hydrogen bond strength supported the chain entanglement, which provided additional crosslinks and thus promote the efficiency of force transmission.

The sensitivity of force induced luminescent probes could further improve by incorporating additional fluorescent dyes, accomplishing an energy transfer, which led to a yellow/green fluorescence<sup>63,214</sup>. Additionally, the sensitivity of dioxetane approaches could be improved by a shift of the white chemiluminescence to an intense red emission by inducing a controlled energy-transfer due to europium(III). Herein, transparent dioxetane crosslinked poly(methylacrylate) (PMA) films can be formed without mechanical shrinkage enabling the mapping of sensitive bond-breaking events within elastomeric materials.

### 1.3.4.3. Mechanochemically active benzofuranones

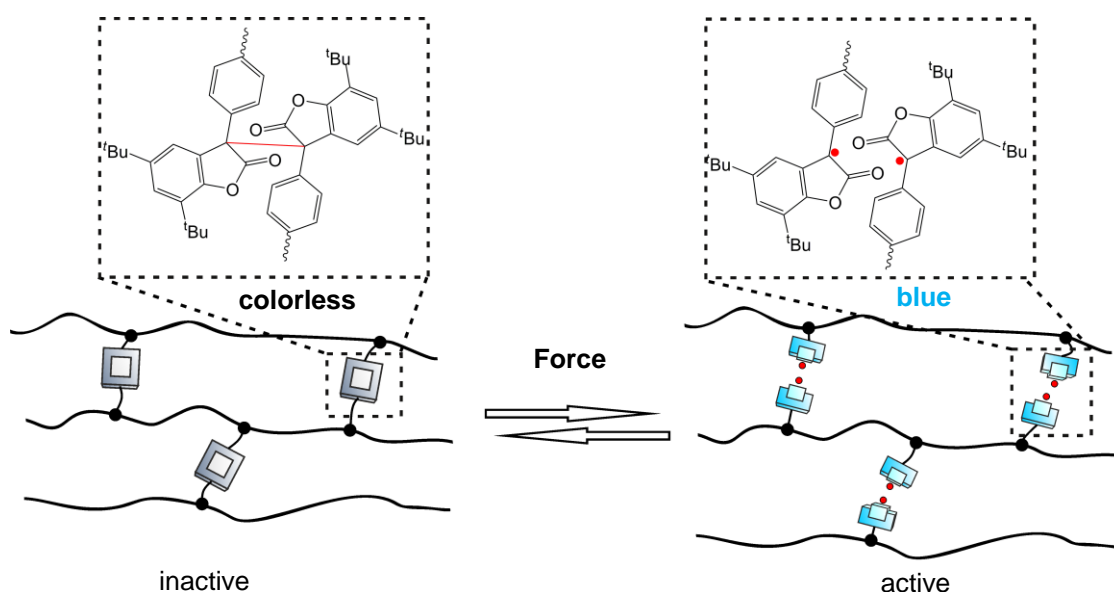


Figure 13. Mechanochemical activation of crosslinked diarylbibenzofurane (DABBF) leading to the formation of radicals accompanying with a color change from colorless to blue.

Diarylbibenzofurane (DABBF) exhibits a dynamic covalent bond behavior due to the fully reversible bond scission of the dimeric arylbenzofuranone (ABF) structure (Figure 13). This homolytic bond cleavage leads to the formation of blue colored radicals which are equilibrated with the colorless initial structure at RT. This enabled potential self-healing properties as well as an application as mechanchromophore for stress-sensing due to the force induced color change. In contrast to other systems, in which the quantification accompanies by difficulties, the main advantage of DABBF is the direct grasp of bond scission by electron paramagnetic spectroscopy. This enables a spatial and time resolved quantification e.g., during the freeze induced mechanochemical activation.

According to the literature<sup>215,216</sup>, the freeze induced cleavage of the labile bond is attributed to adhesion interactions of generated solvent crystallites with the polymer strands as well as morphological and conformation changes which induced mechanical forces along the polymer chain. This was exploited to study the mechanochemical activation of linear and crosslinked poly(urethane) matrices<sup>134</sup>, which contains DABBF-diol or -tetraol linkages. EPR measurements in a temperature range from 50 to -100 °C reveals that within the linear system the activation energy threshold for homolytic bond cleavage of DABBF was not exceeded

during freezing while the crosslinking approach allows activating mechanophore efficiently. Thus, crosslinking systems allowed to improve the propagating molecular forces, in which the transmission could be further enhanced by increasing number of crosslinker arms. Additionally, the force induced dynamic behavior of DABBF, which was incorporated in the soft segment of thermoplastic elastomers (poly(urethane)s)<sup>217</sup> allowed to enable the combination of repeatable activation and autonomous regeneration (self-healing) accompanying by an equilibrated color change.

In order to realize an applicable DABBF system with improved material properties, polymer composites<sup>145</sup> were developed in which DABBF was embedded into rigid silica networks. These networks were embedded into crosslinked poly(butyl acrylates) to realize the inhibited recombination of radicals due to the slight chain mobility of rigid silica particles. The precise interplay of rigid hard domains and mobile soft domains allows to tune the mechanoresponsivity of this polymer composites on hetero interfaces. Herein, the hard domains guarantee an efficient mechanochemical activation whereas soft domains were responsible for the recyclability process.

Adding a mechanochromophore to the existing DABBF containing polymer/silica composite allows to create a multicolor mechanochemical active system. The distinct mechanochromophore caused force dependent color changes from blue over green up to orange<sup>143</sup>. Therefore, DABBF was immobilized within the silica rich domains, whereas the naphthopyrane (NP) was located in poly(*n*-butyl acrylate) rich domain monitoring the subsequent mechanochemical activation UV-spectroscopy. Kneading at different strengths caused different color changes, contributed to the premature activation of DABBF. This leads to a blue color shift followed by the higher force induced isomerization of NP accompanying by a mixed green color shift. Adding of solvent favors the recombination of ABF radicals enabling an orange-colored material in which the initial pale-yellow color can be restored by irradiation with UV-light. This emphasizes the multimechanophore containing polymer/silica composite as a recyclable force sensitive stress-sensing material.

#### 1.3.4.4. Mechanochemically active metal-ligand complexes

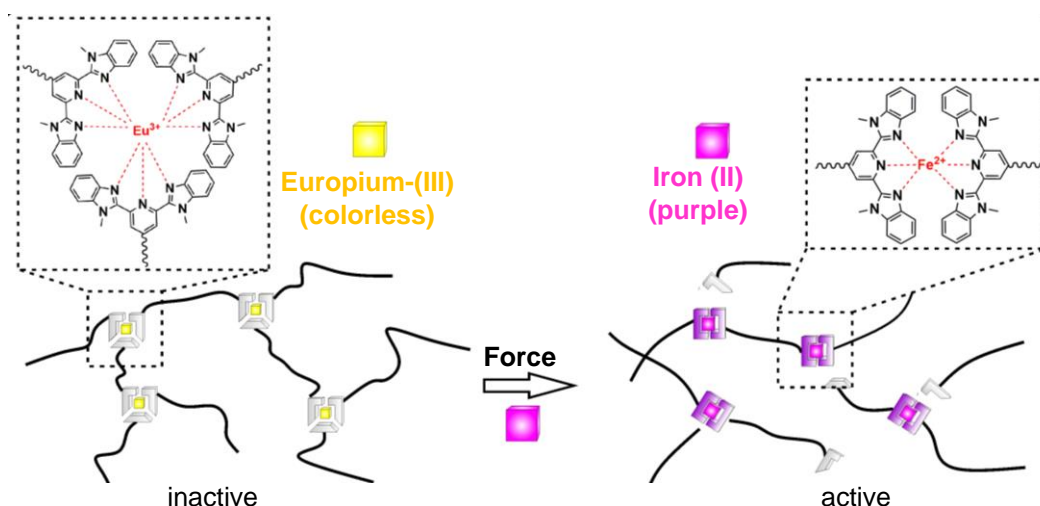


Figure 14. Mechanochemical activation of europium(III) crosslinked polymer network accompanying with a color change from colorless to deep purple due to the ion iron(II) promoted ion exchange.

Among a variety of different mechanophore networks, whose mechanoresponsivity based on isomerization, ring opening or homolytic bond cleavage, a new class was developed based on

metal-ligand decoupling. First examples of metal based mechanophores were reported by Balkende *et al.*, accomplishing the mechanochemical activation of europium(III)-2,6-bis(1'-methyl-benzimidazolyl)pyridine (Eu(Mebip)) within a metallosupramolecular network by ultrasonication and needle puncture of swollen films (Figure 14)<sup>218</sup>. In addition to the force induced healable character of this supramolecular network, simultaneous provision of iron(II) ion allows the formation of a more stable Fe(Mebip) complex accompanying with an irreversible color change from colorless to deep purple, which offer the usage as mechanically healable mechanochromic material. Similarly, the complexation of Eu(III) and Tb(III) ions by terpyridyl end-capped four arm PEG enabled a force induced gel-sol phase transition leading to a color change from white (gel) to blue (liquid) in which the transition can be reversed without external trigger<sup>219</sup>.

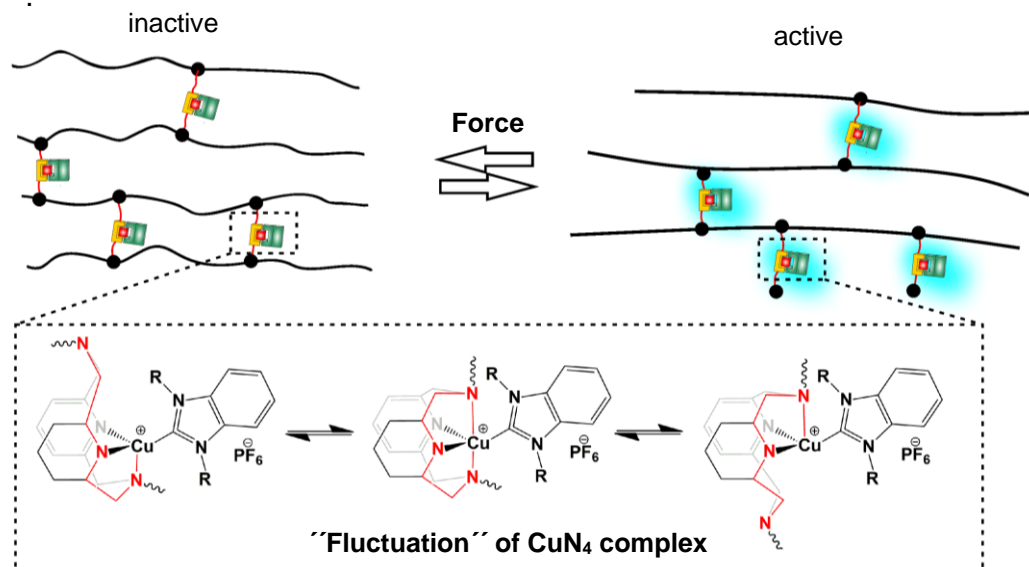


Figure 15. Mechanochemical activation of a copper(I) pincer complex crosslinked within a polymer structure in which the force induced suppression of isomerization leads to the appearance of light emission.

Newest reports investigate the mechanoresponsive behavior of  $\text{CuN}_4$  complexes which were built up from a macrocyclic pyridinophane ligand (Figure 15)<sup>66</sup> incorporated within a polymer structure and subsequently coordinating copper(I)-iodide. During tensile loading of mechanophore containing linear polymer films, the isomerization dynamic of  $\text{CuN}_4$  was suppressed, which in turn, restricted the non-radiative PL decay pathway and thus led to an increase in relative emission intensity. The additional coordination of an *N*-heterocyclic carbene (NHC) ligand allowed to induce an extension dependent blue shift of the relative emission which is attributed to the increase cation-anion separation during deformation<sup>67</sup>. In order to improve the stress or strain threshold,  $\text{CuN}_4$  complexes were introduced as crosslinker into a poly(*n*-butyl acrylate) backbone achieving mechanochemical activation at small strain and stress values (<50%, 0.1 MPa), and thus, confirmed the improved force transmission within network structured mechanophoric systems<sup>68</sup>. Preventing covalent bond breaking improved the recovery of the mechanophore initial state and guarantee a fully reversible response.

Deeper insights into structural features of the metal based mechanophoric systems agree on one common point: the usage of NHC ligands.

## 1.4. Mechanocatalysts

In contrast to the previous discussed metal-ligand mechanophores the field of mechanocatalyst uses polymeric structured substituents, blocking an active coordination site and thus prevent a thermal catalytic initiation. The application of external mechanical fields allows generating the catalytic active site by controlled cleavage of one ligand, and thus, trigger a catalytic process, solely by force.

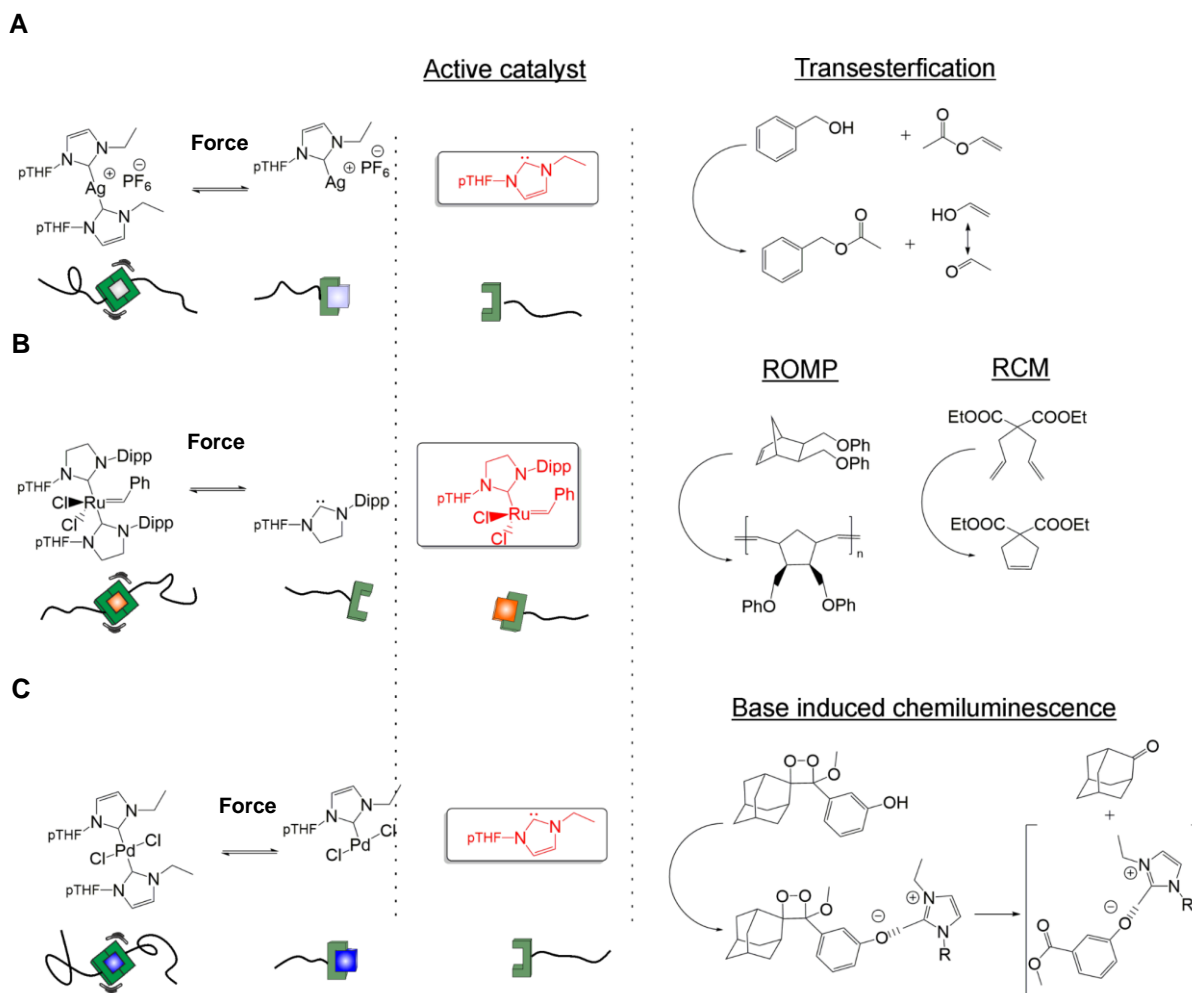


Figure 16. Force induced cleavage of polymeric metal-bis(NHC)-complexes initiating (A) transesterification by silver(I), (B) ROMP, RCM by Ru(II) and (C) dioxetane decomposition by Pd(II).

The first potential mechanocatalysts were reported by Paulusse and coworkers<sup>75-78</sup> who successfully investigated the selective bond scission of Pd- and Pt-P bonds in solution due to ultrasound induced shear forces. Herein, the attached pTHF chains could transmit the generated forces and led to selective bond rupture events of the labile M-P bonds, whereas the Pd-P bonds preferably broke three times faster after applying ultrasound for one hour (indicated by NMR-spectroscopy). This was the first time in which a metal coordination bond was reversibly ruptured solely by mechanical force, and thus, creates the basic requirements for the field of mechanocatalysis.

This concept was extended to polymeric silver(I)-bis(NHC) complexes<sup>80-84</sup>, in which one ligand was cleaved off due to the application of ultrasound and catalyzed a transesterification reaction (Figure 16 A) between benzyl alcohol and vinyl acetate. Hereby, conversions up to 65% could be reached confirming the almost complete latency of catalysts by thermal control experiments as well as the usage of a non-polymeric catalyst. The exchange of the central metal atom to

Ru offered the possibility to mechanochemically trigger an RCM as well as ROMP (Figure 16 B)<sup>84,86</sup> with conversions up to 84%. In both cases, the catalytic performance could be increased by preventing thermal side effects through the usage of an inert gas with a high heat capacity (methane), which in turn, increase the recyclability of the respective catalyst. This was also transferred to solid state investigations where the mechanically induced ROMP was triggered within a pTHF matrix material by applying compression force. The polymerization of monofunctional norbornene in bulk, that occurred in this way, revealed conversions up to 25% whereas the functionalization of norbornene also enabled a force induced crosslinking reaction<sup>85</sup>. Additionally, a polymeric NHC based palladium catalyst<sup>220</sup> was developed in which the ultrasound induced cleavage of one ligand led to the occurrence of chemiluminescence by a base catalyzed decomposition of dioxetane either by directly providing the dioxetane or *in situ* formation and subsequent decomposition in the presence of oxygen (Figure 16 C). There are series of other mechanocatalysts<sup>87,88,137,221-224</sup>, transition metal containing or metal free, which were developed to catalyze reactions like Heck- or Suzuki coupling or even could initiate an anionic polymerization. But one is common within the structure of these mechanocatalysts: The N-heterocyclic carbene.

#### 1.4.1. Metal-(NHC) complexes

The first report of NHC complexes was done by Wanzlick and Oefele, who synthesized chromium(0)<sup>225</sup> as well as mercury(II) NHC complexes<sup>226</sup>. From this, metal (NHC) complexes became more and more interesting applicable in several fields of chemistry, like homogenous catalysis<sup>227</sup>, coordination polymers<sup>228,229</sup> or in the synthesis of metal organic frameworks<sup>230</sup> (MOF). Comparing the electronic features with Fischer<sup>231,232</sup> and Schrock carbenes<sup>233-235</sup> revealed the main advantages of metal (NHC) complexes. Fischer carbene complexes<sup>236</sup> exhibit a positive charged carbene-carbon which is coordinated by midst or late transition metals (e.g. Mo(0), W(0)) which coordinates further  $\pi$ -acceptor ligands (e.g. CO). The additional substitution of  $\pi$ -donors (e.g. -OMe) on the carbene-carbon leads to an electrophilic character which is attributed to the overcome of acting  $\sigma$ - donation (from occupied  $sp^2$  hybrid orbital to empty metal orbital) in comparison with the slightly acting  $\pi$ -backdonation. This leads to an electron excess on the carbon atom in which the HOMO is formally metal-centered whereas the LUMO is localized near to the carbene-carbon<sup>237</sup>. Fischer carbenes represent the so-called singlet carbenes due to the paired electronic character and allows catalyzing reactions like cyclopropanation<sup>238</sup>-, Hegedus<sup>239-241</sup>- as well as Dötz-reaction<sup>242-244</sup>. While Fischer carbenes often reacts under nucleophilic attachment, Schrock carbenes have a negatively polarized carbene carbon, and thus, displays reactions with electrophilic partners within methylenation reactions<sup>245</sup> (Tebbe reagent) or olefin metathesis<sup>246</sup> (Grubbs catalyst). The nucleophilic character based on the missing donor ligands on the carbene fragment as well as the absence of acceptor ligands on the metal center, which results in a favored back donation, and thus, increase the electron density on the carbene-carbon. Herein, the polar double bond character is more pronounced due to the interaction of two single occupied orbitals ( $sp^2$  and p) with the metal (e.g. Ta(V), W(VI)) in which the HOMO is located on the carbon atom and the LUMO on the metal (triplet carbene)<sup>247</sup>.

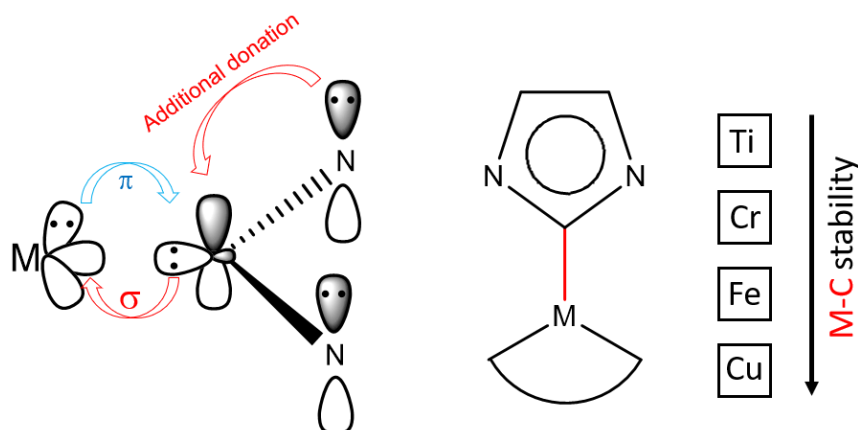


Figure 17. Electronic features within *N*-heterocyclic carbene metal complexes and their stability<sup>248</sup>.

In the case of metal-(NHC) complexes, many single-crystal X-ray diffraction studies of main group metal (NHC) complexes (Li, Be, Th) revealed the presence of a single M-C bond which is attributed to the assumption of a pure  $\sigma$ -donating NHC ligand. However, the synthesized complexes are often temperature, moisture and air sensitive. Only at the transition to metals with filled d-electrons the resulting complexes became more stable due to their ability of forming a  $\pi^*$  backdonation into the p- $\pi$  orbitals of the carbene (Figure 17).

Table 3. Average percent contributions of  $\Delta E_{oi}^{\sigma}$  and  $\Delta E_{oi}^{\pi}$  to the orbital interaction energy as well as the amount of  $\pi^*$ -backdonation and  $\pi$ -donation, respectively.

	d-electrons				
	0	4	6	8	10
$\Delta E_{oi}^{\sigma}$	90	88	86	85	80
$\Delta E_{oi}^{\pi}$	10	12	12	15	20
$\Delta E_{oi}^{\pi}$ ( $\pi^*$ - backdonation)	65	70	70	82	90
$\Delta E_{oi}^{\pi}$ ( $\pi$ - donation)	35	30	30	18	10

Within the alkali metal NHC complexes there was no  $\pi$  interaction possible, whereas the group 4 M-(NHC)'s already shown small but negligible parts. Along the transition metals ( $d^0 - d^{10}$ ) the calculated orbital interaction revealed that with increasing d-electron count the metal to ligand  $\pi$ -interaction also increased (Table 3). While for formal  $d^{10}$  systems percent contributions of up to 20% were determined within formal  $d^0$  systems the values decrease to negligible 10%.

Quantum chemical calculations of transition metal-(imidazol-2-ylidene) (TM-NHC) complexes demonstrated general trends in bond dissociation energy (BDE) with increasing d electrons. Normally, the higher the transition metal group number for each row the higher the bond dissociation energy, indicating a higher stable M-(NHC) bond with increasing  $\pi^*$  backdonation ability.

In comparison with phosphine ligands the donor abilities of NHC complexes often exceeded the most trialkyl phosphines whereas the electronic rangeability of phosphines were generally more comprehensive due to the direct tuneability of donor atom (P) with varying ligands instead of exclusively peripheral ligand tuning<sup>249</sup>.

Nevertheless, electronic features of NHC complexes could also be varied by changing the nature of azole ring ranging from low donating (benzimidazole) to high donating ability (imidazoline) or by changing the adjacent ligands from *n*-alkyl (low donation) over cyclic alkyl to aromatic structures (high donation)<sup>250-257</sup>. This allowed to tune the NHC complexes in terms

of thermal stability and catalytic function<sup>251</sup>. Influencing the electronic and steric features of metal(NHC) complexes also allow using these complexes to fulfill catalytic requirements among a large plethora of chemical reactions for example hydrosilylation reaction<sup>258</sup> by using Ag(NHC), conducting cycloisomerization reaction<sup>259</sup> with (Au(NHC)) and catalyze the CuAAC with Cu(NHC) complexes.

#### 1.4.2. Copper(I) (NHC) complexes

In 1993, Arduengo<sup>260</sup> and coworkers firstly isolate a stable homoleptic *N*-heterocyclic carbene complex containing copper(I). The field of copper(I) catalysis grows steadily due to some major advantages in terms of sustainable applicability, cost efficiency as well as the use in fields of biology and medicine. Especially in the field catalysis, the combination of copper(I) with advantageous NHC ligands takes a crucial role offering air, moisture and temperature stable catalysts which are easily tunable by simple variation of steric and electronic modification. There are mainly two different kinds of Cu(NHC) catalyst: the neutral [Cu(NHC)X] species as well as the cationic [Cu(NHC)<sub>2</sub>]X species in which several methods, direct or indirect, enable an efficient production of both complexes (Figure 18).

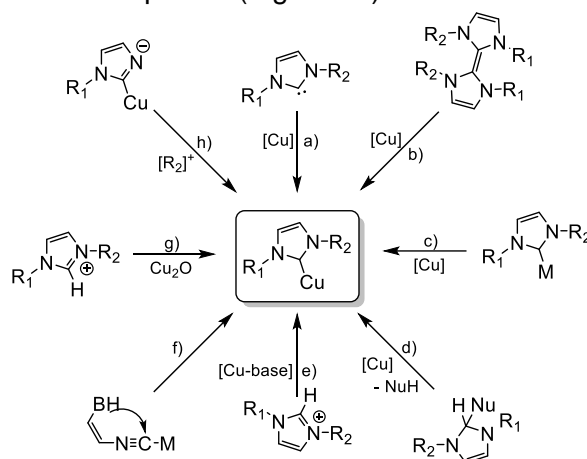


Figure 18. Synthetic routes to copper(I)-NHC complexes: a) coordination of free NHCs; b) cleavage of electron-rich ene-tetramines by transition metals; c) transmetalation routes; d) small molecule elimination; e) *in situ* deprotonation and complexation; f) metal template synthesis; g) oxidative addition to a low valent metal complex<sup>261</sup>.

The most common method is the direct deprotonation of azolium salts with a strong bases (e.g. KO<sup>t</sup>Bu<sup>262,263</sup>, KN(SiMe<sub>3</sub>)<sub>2</sub><sup>264,265</sup> which forms an *in situ* generated NHC subsequently reacting with a copper(I) salt (e.g. CuBr, [Cu(MeCN)<sub>4</sub>]PF<sub>6</sub> to form the respective complex<sup>257</sup> (Figure 18 e)). Another possibility is the reaction of the NHC precursor ligands with a copper(I) moiety which already bear a strong base at high temperature, deprotonating and complexing simultaneously. For the air stable and moisture insensitive copper(I)-oxide the high yielding complex formation<sup>266,267</sup> accompanies with the elimination of water in which the easy purifiable side products as well as the simple stoichiometric control consolidates this method as universal and clean<sup>268</sup> (Figure 18 g)). An additional method is the previous formation of a silver(I)-(NHC) complex by using azolium salt and Ag<sub>2</sub>O that subsequently allows to form the copper(I) pendant in a transmetalation reaction<sup>269-271</sup> due to the increased stability of Cu-NHC bond (Figure 18 c)). Despite the wide coverage of the described methods, there are many specific methods like electrochemical based techniques<sup>272</sup>, salt metathesis<sup>273</sup> or *N*-alkylation reaction<sup>274</sup> which also reveal NHC complexes but are rarely used. As mentioned above the diverse and simple synthesis as well as the outstanding electronic properties manifest these

complexes as an integral part of today's catalysis. Some insights of the applicability will be discussed in the next section.

#### 1.4.2.1. Copper(I)-(NHC) complexes in catalysis

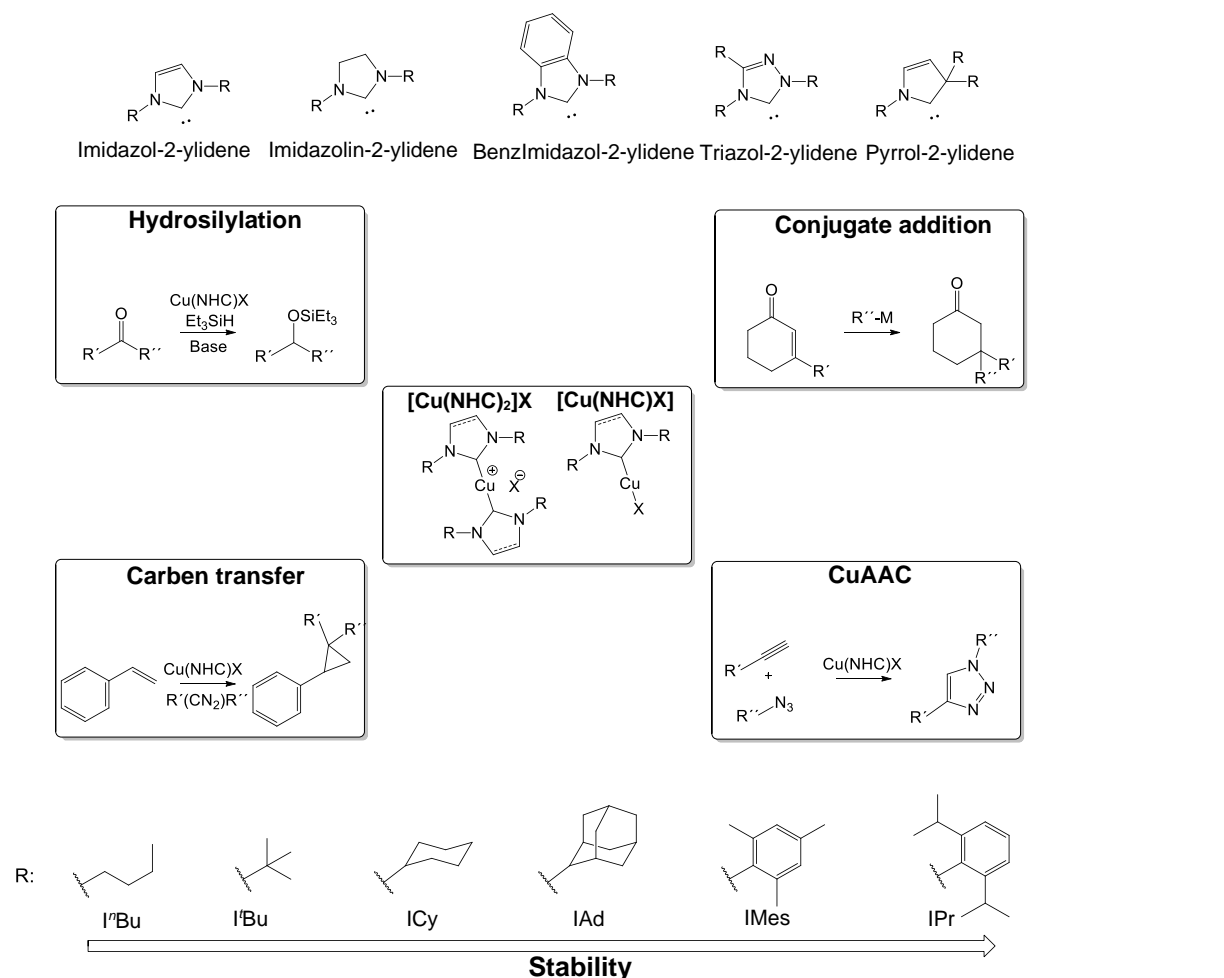


Figure 19. Cu(I)-NHC-based catalysts subdivided into neutral complexes  $[Cu(NHC)X]$  and cationic complexes  $[Cu(NHC)_2]X$  with a selection of five-membered -ylidene moieties employing different reaction types.

First reports on catalytic utilization of copper(I)-(NHC) complexes deals with the ethylation of enones<sup>275</sup> in 2001 as well as the reduction of  $\alpha,\beta$  unsaturated carbonyl compounds<sup>276</sup> in 2003, which were the counter stone for many other reactions like hydrosilylation, further conjugate addition reaction, carbene transfer reactions or the CuAAC (Figure 19)<sup>277</sup>.

Hydrosilylation reactions in the presence of  $[Cu(IPr)Cl]$  were conducted by Nolan *et al.* for the first time<sup>278</sup>. They found out that the actual reaction is attributed to the *in situ* formed hydride complex whereas the systematic carbene ligand tuning emphasized the cyclohexyl based NHC ligands (ICy) as catalyst with the highest performance (3 mol%, 80 °C, 1 h, quant.)<sup>279</sup>. The additional introduction of a second NHC ligand as well as a precise counter ion tuning improved the catalytic performance, even under mild conditions<sup>253</sup> (50 °C). Within conjugate addition reactions the introduction of enantiopure complexes could be realized by using either ligand-Cu-salts mixtures or predefined copper (NHC) complexes in which the chirality transfer was realized by using chiral NHC ligands, tunable by the increasing bulkiness of adjacent substituents<sup>280,281</sup>. The required functionalities were transferred by an organometallic compound, which allows forming quaternary centers enantioselectivity. The first step was the usage of zinc organometallic compounds, which were, however, limited by the marginal

availability of sufficiently different functionalities. The development of Grignard reagents enabled to omit an additional base and provided a higher availability of the implemented functionalities. For special applications further organometallic compounds like aluminum or boron could be used emphasizing the enormous versatility of copper (NHC) complexes<sup>277</sup>. Furthermore, carbene transfer reactions could be conducted by using copper (NHC) complexes, in which the catalyst is capable of abstracting a carbene from a diazo compound and subsequently transferred it to a double bond<sup>282</sup>. The regioselectivity of cyclopropane product can be influenced by using different metals (Au, Cu) reacting with  $[\text{Cu}(\text{IPr})\text{Cl}]/\text{NH}_4\text{PF}_6$  an almost pure tertiary substituted compound<sup>283</sup>. In this work, the main focus is on a reaction which was firstly described by Meldal<sup>284-286</sup> and Sharpless<sup>287-289</sup>: the CuAAC<sup>290</sup>.

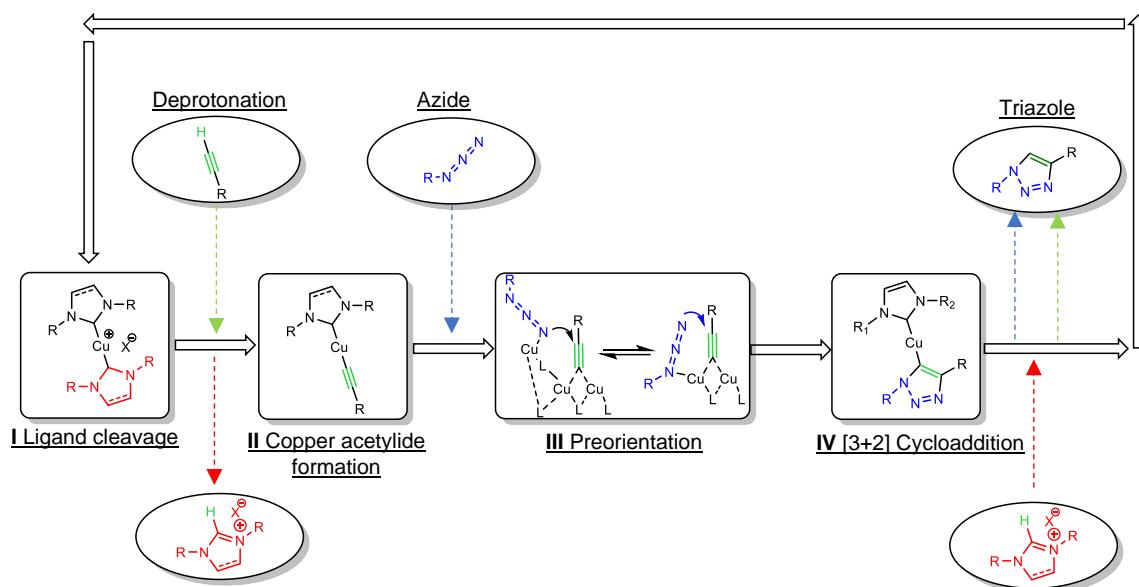


Figure 20. Mechanistic insights of copper(I) catalyzed alkyne azide cycloaddition (CuAAC).

The CuAAC was based on the thermal initiated Huisgen reaction<sup>291</sup>, where a substituted azide and an alkyne react in a [3+2] cycloaddition reaction revealing a triazole compound. The high activation energy as well as the missing regioselectivity within the reaction management could be passed over by the addition of copper(I). This led to an efficient catalytic system which acts under mild conditions and simply produces pure 1,4-triazoles compounds. Sharpless indicates this reaction as “click” reaction that fulfills special features. The main advantage of “click” reactions are the thermodynamic driving force of more than 20 kcal/mol which often led to quantitative yields. Furthermore, the reaction is stereoselective, solvent independent and simple purification steps are necessary. The CuAAC itself could be tuned by varying the substrates, the ligands or the catalyst itself, which allows to accomplish this reaction in diluted and bulk systems as well as for homogeneous and heterogeneous catalysis. This offers the use for many application in biological systems, for self-healing approaches as well as for stress-sensing materials (fluorogenic “click” reaction)<sup>290</sup>.

Both species of copper (NHC) complexes, the neutral and the cationic could catalyze the CuAAC emphasizing that the binding affinity of carbene ligand, which is influenced by electronic and steric properties, plays a crucial role<sup>292</sup> (Table 4). In the case of neutral complexes, the saturated SIMes based catalyst are more efficient than their unsaturated (IMes) and bulkier (DIPP) analogues<sup>255,293</sup>, whereas a *N*-aliphatic substitution (IAd/ICy) facilitate the CuAAC compared to their *N*-aromatic (IMes) analogues. In addition to this, the counterion as well as the solvent<sup>294,295</sup> also influences the catalytic behavior highlighting the

combination of IAd substitution with iodine counterion<sup>293-297</sup> as the most promising candidate among the neutral complexes. Adding one additional NHC ligand and thus creating the cationic (NHC) complex led to a gain in catalytic efficiency within the CuAAC (Figure 20) in which the second ligand supported the deprotonation of the acetylene moiety after cleavage (I)<sup>254</sup> accompanied by the formation of copper(I)-acetylide (II). Mechanistically<sup>285,298-305</sup>, the subsequent coordination of the azide (III) on the copper(I)-acetylide pre-orientate the triazole moiety by forming a binuclear/trinuclear complex and thus creates within the [3+2] cycloaddition (IV) a stereospecific product which can be obtained after protonation and decoordination (V). Typical conversion of copper(I)-bis(NHC) complexes within a CuAAC are shown in Table 4.

Table 4. Catalyst screening of benzyl azide and phenylacetylene with different Cu(NHC) complexes in water<sup>252,293</sup>.

Ent.	[(NHC) <sub>x</sub> Cu]X	Temperature [°C]	Time [h]	Conversion [%]
1	[(IPr)Cu(Cl)]		18	18
2	[(IPr) <sub>2</sub> Cu]PF <sub>6</sub>		18	71
3	[(IPr) <sub>2</sub> Cu]BF <sub>4</sub>	RT	8	100
4	[(IMes) <sub>2</sub> Cu]BF <sub>4</sub>		6	100
5	[(IAd) <sub>2</sub> Cu]BF <sub>4</sub>		3	100

Combining the previous discussed mechanophore approach with the copper(I)-bis(NHC) concept should allow to induce the CuAAC solely by force. Therefore, several linear mechanochemical active copper(I)-bis(NHC) complexes were developed and their catalytic activity towards the CuAAC were investigated. Activation experiments were accomplished either in solution by activation via ultrasound or in bulk material by applying compression force (Figure 21)<sup>306,307</sup>. In solution, the impact of ultrasound led to the detachment of one shielding ligand creating a free, catalytic active site. This, in turn, allowed to trigger the required formation of copper(I)-acetylide species which further initiated the catalytic process, as mentioned above. Hence, the mechanochemical activation of several complexes could be studied in terms of nature as well as chain length of polymer backbone by simple monitoring the conversion between benzylazide and phenylacetylene within a CuAAC via NMR spectroscopy. First experiments of PIB based mechanophore revealed the enhanced mechanochemical activation with the steadily increase of DP (degree of polymerization) (0%, model cat.; 11%, M<sub>n</sub> = 4750 g mol<sup>-1</sup>, DP = 72; 28%, M<sub>n</sub> = 17200 g mol<sup>-1</sup>, DP = 294). The same trend was observable by using poly(styrene) (PS) backbone in which the enhanced DP led to higher conversion ranging from 23% (M<sub>n</sub> = 6800 g mol<sup>-1</sup>, DP = 62) to 52% (M<sub>n</sub> = 13600 g mol<sup>-1</sup> DP = 126). Herein, the initially stiffer poly(styrene) (T<sub>g</sub> ≈ 100 °C in comparison with poly(isobutylene) (T<sub>g</sub> ≈ -80 °C) led to an almost doubling of conversion within the CuAAC which indicated a higher cleavage efficiency due to a better polymer solvent interaction, which, in turn, improved the force transmission. The attachment of pTHF polymeric handles led to a nearly quantitatively “click” conversion (97%, M<sub>n</sub> = 15600 g mol<sup>-1</sup>) whereas the fully latent state was not guaranteed due to a significant conversion of 24% without applying ultrasound.

This concept was further extended, and the catalysts were probed triggering a solvent free CuAAC within a high molecular weight pTHF matrix, which was able to achieve an optimal force transmission due to the included crystalline parts. In order to monitor the compression induced activation of mechanocatalysts, the so called fluorogenic “click” reaction was conducted, in which the CuAAC of non-fluorescent substrates (azido-coumarin and phenylacetylene) yielded a highly fluorescent product.

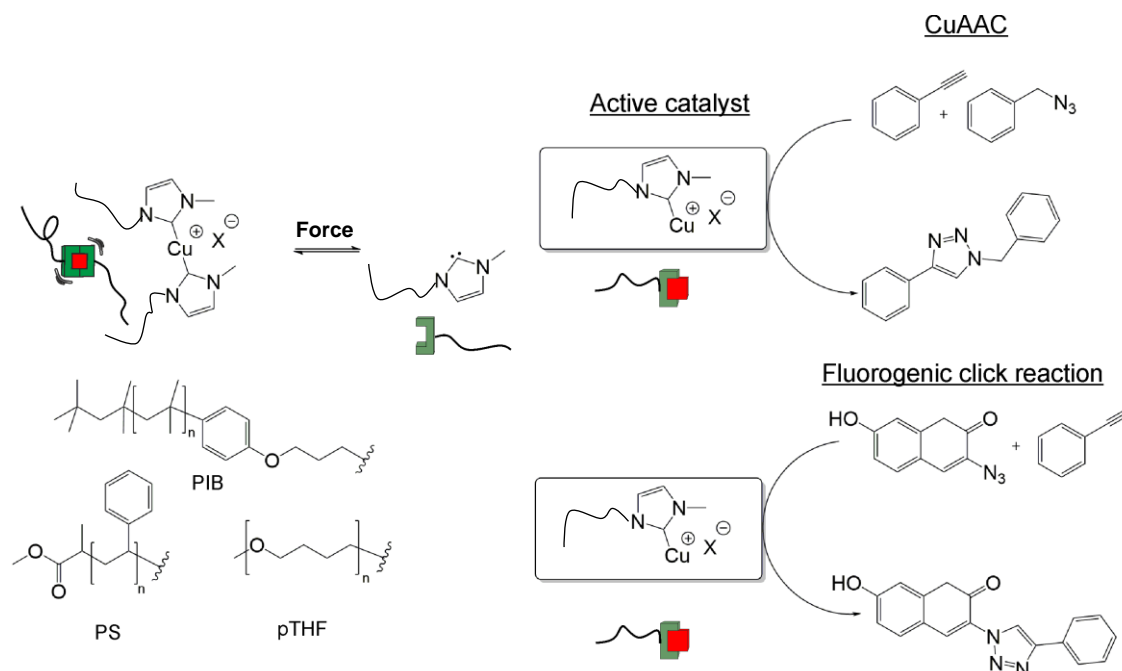


Figure 21. Force induced cleavage of polymeric copper(I)-bis(NHC)-complexes initiating the force induced CuAAC of benzylazide and phenylacetylene by ultrasound in solution as well as the fluorogenic CuAAC of 3-azido-7-hydroxy-coumarin and phenylacetylene by compression in bulk.

Hence, an optical signal was generated which correlated the increase of fluorescence intensity with mechanochemical activation. After calibration, this signal allowed to indirectly quantify the mechanochemical response. Herein, a stepwise increase of fluorescence intensity with higher number of compression cycle was valid for all linear mechanophores, which tended to a flattening due to catalyst decomposition. With increasing chain length of the attached polymer handles the mechanochemical activation was also enhanced, which is attributed to the better entanglement of catalyst and matrix polymer leading to a more efficient force transmission. However, due to synthetic hurdles this linear approach was limited in reaching up molecular weights over  $15000 \text{ g mol}^{-1}$  accompanied with maximum conversions up to 8 within the fluorogenic "Click" reaction.

The created optical response due to mechanical stress highlights this approach to real life polymeric materials as potential self-reporting system for damage sensing applications.

## 2. Aim of the Thesis

### 2.1. Objective and motivation

The aim of this thesis was to investigate the mechanochemical activation of polymeric copper(I)-bis(NHC) complexes with different architectures. Due to the application of force, one shielding ligand can be detached, and thus, the generated catalytic active site will be able to trigger a copper(I) alkyne azide cycloaddition (CuAAC) (Figure 22 A). Previous investigations revealed that the catalytic activity increased with increasing chain length of the attached polymer backbone. Since the elongation of the chain length is limited due to the rising decomposition for longer polymer handles, a chain extended architecture should be developed. Herein, the bivalent functionalization should enable a chain-extended mechanophoric system with a higher overall chain length and an increased number of cleavable mechanophores. In order to further improve the force transmission to the mechanochemically labile bond, a network-structured mechanophore should be developed (Figure 22 B).

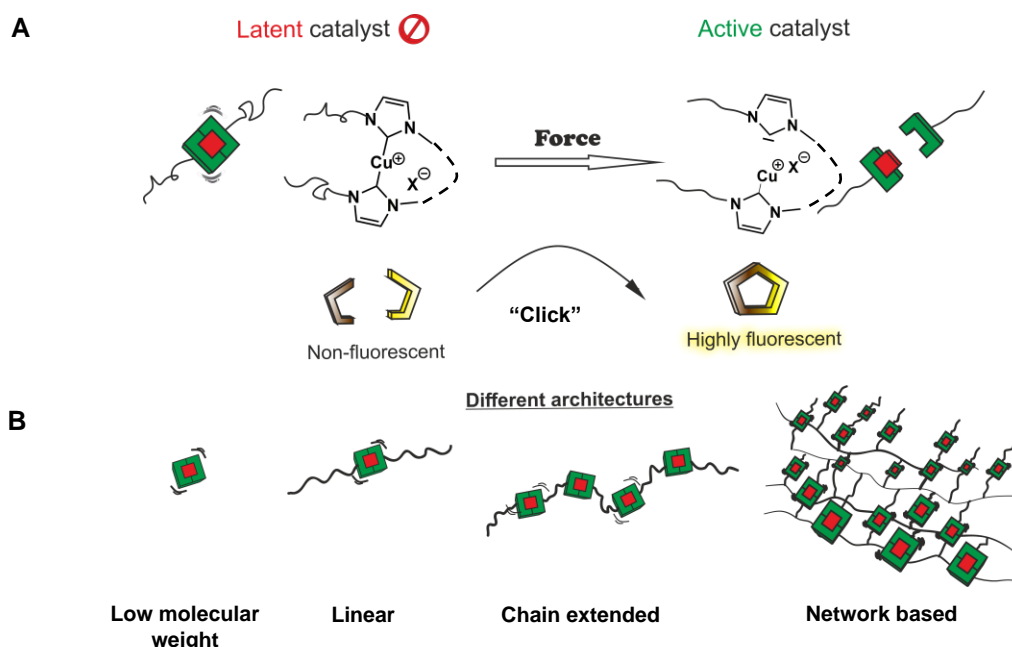


Figure 22. The mechanochemical activation of copper(I)-bis(NHC) complexes of different polymeric architectures yielding the catalytic active mono(NHC) species, which is able to trigger the fluorogenic “click” reaction applicable for stress-sensing applications.

In order to fulfil the requirements for potential stress-sensing applications, a transparent dye should be developed guaranteeing a much broader applicability compared to the previously dark-brown colored coumarins. Moreover, an all-in-one mechanochemical approach should be established, in which the copper(I)-bis(NHC) mechanocatalyst as well as the fluorogenic dye precursors should covalently be incorporated within the matrix material. This allows to neglect matrix blending effects that cause inhomogeneous catalyst distribution as well as time-consuming adaptations of the catalyst-polymer linkage. This system should enable an easy tunability of material properties in terms of stiffness and elasticity by varying, e.g., the crosslinking density, which also influences the activation of single mechanophore.

Additionally, the mechanophoric behavior of the copper-carbon bond within a copper(I)-bis(NHC) complex should be investigated via SFMS to get precise information about rupture forces on a microscopic scale that can be transferred to further potential macroscopic applications.

## 2.2. Concept

In order to realize SFMS, different acyclic (**5**) and cyclic (**10**) copper(I)-bis(NHC) complexes should be synthesized by complexation of previously modified bis imidazolium moieties (**4**, **8**) within a highly diluted copper(I)-oxide method. These cyclic complexes should be further modified and finally investigated via AFM in order to detect the necessary rupture forces for cleavage of copper(I)-(NHC) bond.

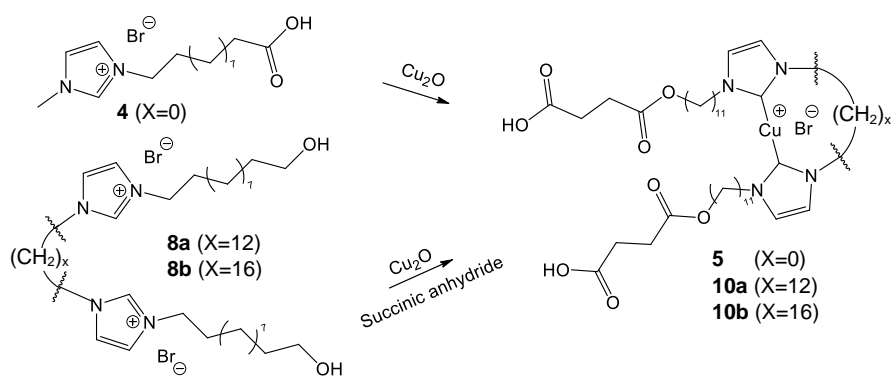


Figure 23. Synthetic route towards acyclic and cyclic low molecular weight copper(I)-bis(NHC) complexes (**5**, **10**).

The chain extended copper(I) bis(NHC)-complexes should be realized by increasing the overall number of copper(I)-bis(NHC) complexes per chain which in turn elongates the effective chain length, and thus, enhances the activation behavior.

Poly(styrene) backbones should be used due the improved force transmission ability according to previous works. The use of living polymerization technique (RAFT) (Figure 24 A) should guarantee the required positioning of labile mechanochemically active bond, close to the middle of polymer chain, which is necessary for an optimal activation process. By using the highly efficient thio bromo “click” reaction to introduce the imidazolium moieties intends to yield after subsequent complexation the chain extended copper(I)-bis(NHC) complexes (**18**). Afterwards, the effect of chain length, degree of polymerization as well as the amount of copper(I) moieties should be investigated towards mechanochemical activation. Therefore, the catalysts should be embedded in a high molecular weight pTHF matrix triggering a compression force induced fluorogenic “click” reaction in which non fluorescent 3-azido-7-hydroxy-coumarin (**22**) and phenylacetylene (**23**) generating a highly fluorescent 7-hydroxy-3-(4-phenyl-1H-[1,2,3]triazole-1-yl)-coumarin (**24**). The progress of this reaction should be monitored and subsequently quantified via fluorescence spectroscopy.

For realizing the network-based concept, two different strategies will be selected: Firstly, a statistic copolymer (**20**) bearing functional imidazolium groups will be prepared via ATRP (Figure 24 B). The amount of copper-carbene precursor should be simply varied adapting the monomer ratio of functional to non-functional component. Thus, the number of the crosslinking points can easily be tuned and varied in a broad range. A subsequent deprotonation and coordination step to a copper(I)-salt will establish the mechanophoric network (**21**) with different crosslinking densities. The influences towards the mechanochemical activation should also be investigated via the previous discussed, compression force induced fluorogenic “click” reaction.

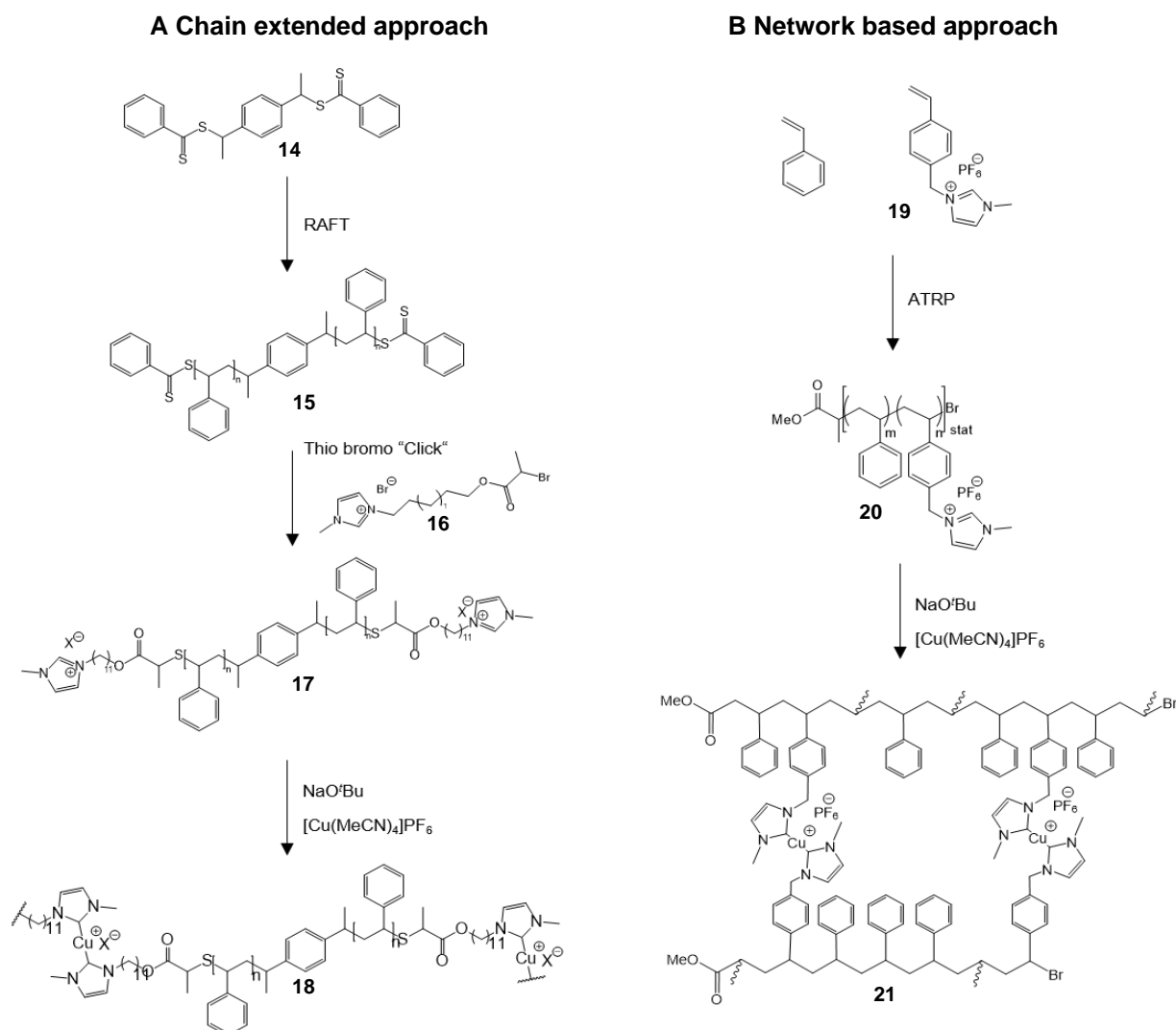


Figure 24. Synthetic routes toward poly(styrene) based chain extended (**18**) or rather network based copper(I)-bis(NHC) complexes (**21**). (A) The synthesis of chain extended mechanocatalysts will be started from the bivalent dithiobenzoate end-capped initiator (**14**) which polymerize styrene in a RAFT polymerization. The subsequent functionalization via thio bromo "click" reaction will introduce the imidazolium moieties (**17**) and the final deprotonation and complexation with a NaO<sup>t</sup>Bu and copper(I)-salt will yield the corresponding copper(I)-bis(NHC) complex (**18**). (B) The copolymerization of **19** with styrene via ATRP will lead to a side chain functionalized statistical copolymer (**20**) which will be able to form after deprotonation with NaO<sup>t</sup>Bu and complexation with copper(I)-salt the resulting network-based copper(I)-bis(NHC) mechanocatalyst (**21**).

Furthermore, an all-in-one approach (Figure 25) with a bifunctional hydroxy-end-capped low molecular weight copper(I)-bis(NHC) complex (**3**) should be developed, which enables a direct covalent linkage into the poly(urethane) matrix material by polyaddition reaction. A new fluorogenic system (**31**, **32**), which can also be covalently linked directly in the poly(urethane) matrix should be developed avoiding the dark brown color, the fluorescence quenching effects as well as potential leaching of components within the coumarin based system (**22**, **23**). Thus, a colorless elastomeric PU film can be achieved in which the transparency enables the reduction of copper(I) due to the higher sensitivity. The mechanochemical activation of the obtained material should also be tested via tensile oscillatory rheology with regard to material properties e.g., stiffness or crosslinking density as well as the variation of experimental parameters.

The synthesis of an OH-functionalized copper(I)-bis(NHC) complex (**3**) had to be established in which copper(I)-oxide should act as an internal base, which deprotonate the OH-

functionalized imidazolium precursor (**1**), subsequently coordinated by copper(I). The so achieved copper(I)-bis(NHC) complex (**3**) should take part within a multicomponent polyaddition reaction using pTHF as soft segment, HDI as hard segment, 1,1,1-trimethylolpropane (TMP) as trivalent crosslinker and **31** as well as **32** as fluorogenic dye precursor. The obtained elastomeric poly(urethane)s should be fabricated into foils and the mechanochemical response should be indirectly correlated with the increase in the fluorescence intensity by yielding the highly fluorescent **33**.

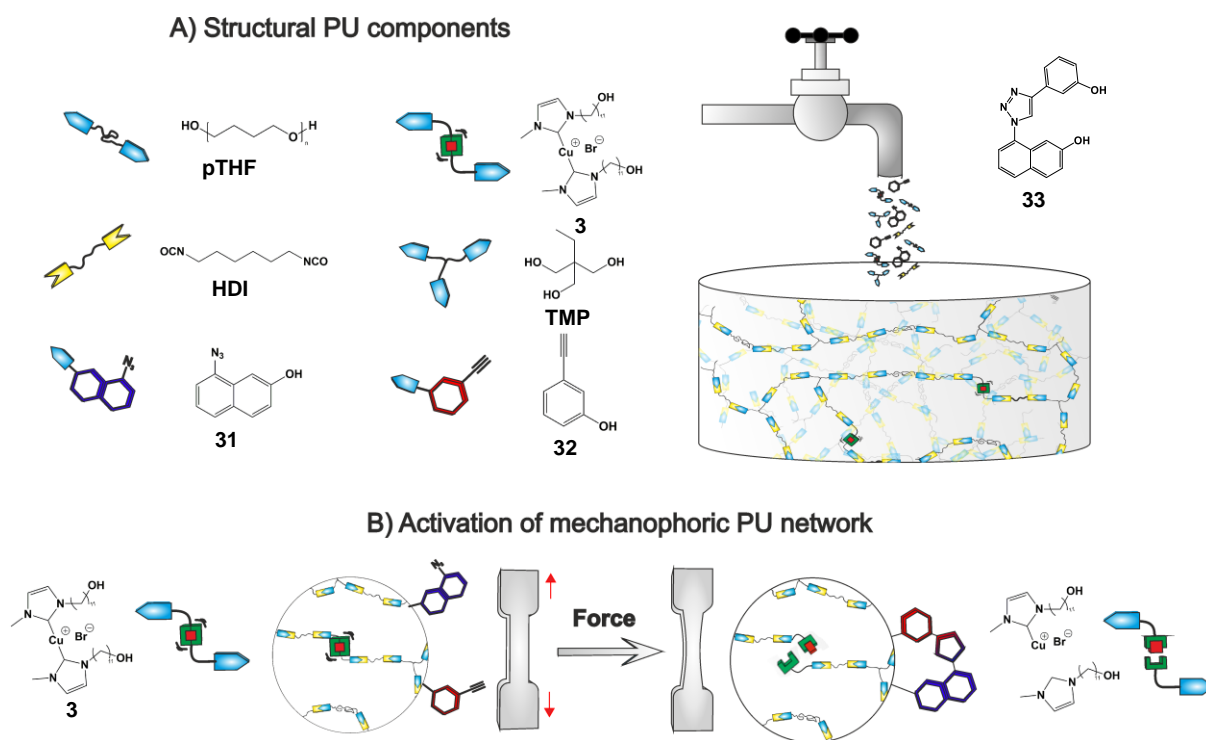


Figure 25. All-in-one stress-sensing approach based on a transparent poly(urethane) network film.

### 3. Result and discussion

Parts of the Results and Discussion as well as of the Experimental Part were already published in

1. "Mechanochemical activation of fluorogenic CuAAC "click" reactions for stress-sensing applications" (Michael, P.; Biewend, M.; Binder, W. H), *Macromol. Rapid Commun.*, 2018, 1800376, DOI: 10.1002/marc.201800376;
2. "Synthesis of Polymer-Linked Copper(I) Bis(*N*-Heterocyclic Carbene) Complexes of Linear and Chain Extended Architecture" (Biewend, M.; Neumann, S.; Michael, P.; Binder, W. H.) *Polym. Chem.*, 2019,10, 1078-1088. DOI: 10.1039/c8py01751d
3. "Detection of stress in polymers: mechanochemical activation of CuAAC click reactions in poly(urethane) networks" (Biewend, M., Michael, P.; Binder, W. H) *Soft Matter.*, 2020, 5, 1137-1141. DOI: 10.1039/C9SM02185J

and were in parts adapted with permission from John Wiley and Sons. Inc. ©2018 and Royal Society of chemistry ©2020.

#### 3.1. Synthesis and characterization of an acyclic and cyclic copper(I)-bis(NHC) complexes

##### 3.1.1. Synthesis of acyclic copper(I)-bis(NHC) complexes

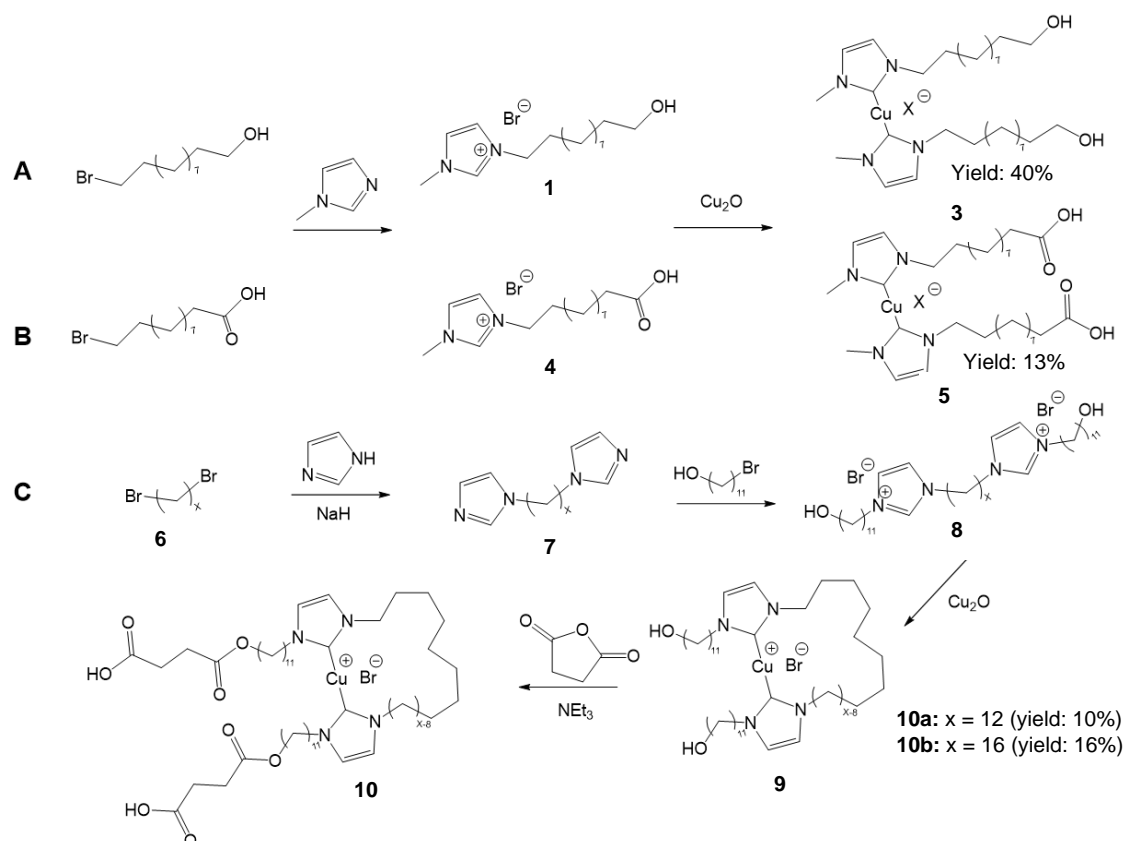


Figure 26. Two step synthesis of acyclic copper(I)-bis(NHC) complexes by direct quaternization with subsequent complexation reaction towards (A) *OH*- (**3**) and (B) *COOH*-functionalized (**5**) copper(I)-bis(NHC) complexes applying copper(I)-oxide. (C) Synthetic route for cyclic complexes with different chain length (**10a** for  $x=12$  and **10b** for  $x=16$ ).

The synthesis of acyclic low molecular weight copper(I)-bis(NHC) complexes (**3**, **5**) was accomplished within a two-step synthesis starting from with the direct quaternization of *OH*-(**1**) as well as *COOH*- $\omega$  (**4**) functionalized bromoalkane with 1-methylimidazole followed by complexation reaction with copper(I)-oxide (Figure 26 A and B). Herein, the copper(I)-oxide acts as an internal base at high temperature (100 °C) deprotonating the NCHN proton of imidazolium moiety forming the free carbene which was *in situ* complexed by copper(I)<sup>254,267</sup>. Varying the reaction conditions by using copper(I)-oxide in different amounts resulted either in the monocarbene species by using 0.65 eq. or the biscarbene species by using 5.00 eq. due to an internal condensation reaction. The obtained complexes were successfully synthesized and characterized by <sup>1</sup>H-NMR and <sup>13</sup>C-NMR spectroscopy as well as ESI-TOF-MS investigations proving the required copper(I)-bis(NHC) functionalization.

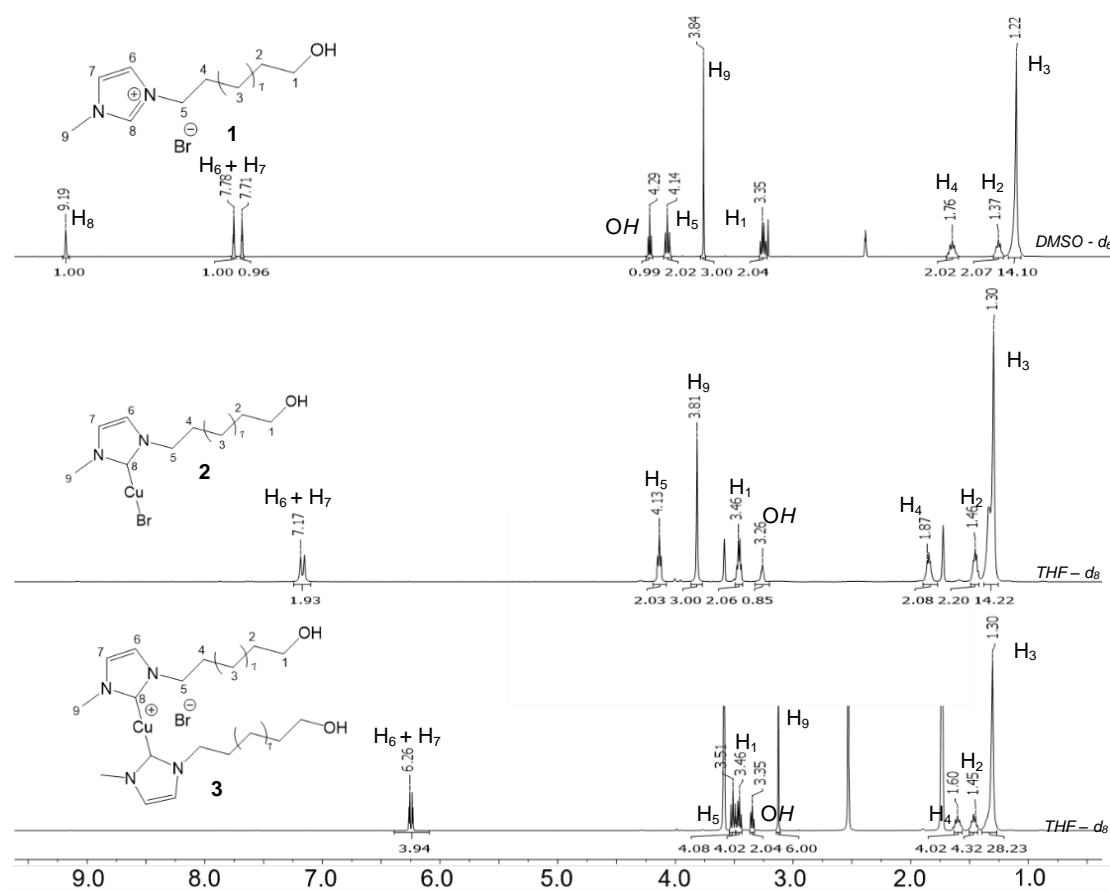


Figure 27: <sup>1</sup>H-NMR spectra of **1** (above), **2** (middle) and **3** (below) shows the disappearance of NCHN ( $H_8$ ) proton during complexation reaction as well as the shift of NCHCHN proton ( $H_6 + H_7$ ).

Comparing the <sup>1</sup>H-NMR spectra of the *OH*-functionalized copper(I)-bis(NHC) complex (**3**) to the monocarbene species (**2**) and the initial imidazolium ligand (**1**), the disappearance of NCHN resonance at 9.19 ppm is clearly visible. Furthermore, a clear shift of the NCHCHN resonances from 7.78 and 7.71 for **1** to 7.17 ppm for **2** and 6.26 ppm for **3** could be observed depending on the change in the electronic structure of the aromatic functionality. Additionally, a noticeably shift of the resonances for the CH<sub>2</sub> moieties ( $H_5$ ) as well as for the NCH<sub>3</sub> resonance ( $H_9$ ) confirm the complex formation as assigned in Figure 27. In <sup>13</sup>C-NMR spectroscopy a significant shift of the NCHN resonance from 136.5 ppm (**1**) to 171.3 ppm (**2**) to 152.8 ppm (**3**) is visible accompanied by a decreasing signal intensity due to the quadrupole coupling of Cu-C spins. A final undeniable proof of the predicted structure was accomplished by ESI-TOF-MS revealing the exact masses of 253.228 g mol<sup>-1</sup> (simulated 253.227 C<sub>15</sub>H<sub>29</sub>N<sub>2</sub>O<sup>+</sup>) for **1**, 474.982

g mol<sup>-1</sup> (simulated 474.984 C<sub>15</sub>H<sub>28</sub>Br<sub>2</sub>CuN<sub>2</sub>O<sup>-</sup>) for **2** as well as 567.362 g mol<sup>-1</sup> for **(3)** (simulated 567.369 C<sub>30</sub>H<sub>56</sub>CuN<sub>4</sub>O<sub>2</sub><sup>+</sup>). The synthesis and characterization of the COOH-functionalized complex **(5)** (Figure 26 B) was done likewise to the OH-functionalized catalyst **(3)**. However, the formation of monocarbene by using 0.65 eq. species could not be observed. Comparing the resonances in <sup>1</sup>H-NMR and <sup>13</sup>C-NMR spectroscopy as well as the measured and simulated pattern in ESI-TOF mass spectrometry confirm the required structure.

### 3.1.2. Synthesis of cyclic copper(I)-bis(NHC) complexes

For the synthesis of cyclic complexes (see Figure 26 C) with different cycle sizes (**10a**: x=12, **10b**: x=16), bivalent  $\alpha,\omega$ -dibromo alkanes act as starting point which had to be synthesized in the case of **6b** by bromination of 1,16-dihydroxyhexadecane. The attachment of imidazole moieties was accomplished by using sodium hydride (NaH) in a nucleophilic substitution and the purified **7** was subsequently quaternized with 11-bromo-undenanol. The complexation reaction of the thus obtained compound **8**, which acted, in turn, as a precursor for cyclic complexes was conducted by using copper(I)-oxide in highly diluted solutions to enable the formation of the intramolecular copper(I)-bis(NHC) complex **(9)**. The required COOH end groups were introduced by a post-modification reaction of **9** with succinic anhydride. The direct usage of COOH imidazolium moieties during complexation reaction accompanied by an complete coordination of copper(I) by the carboxylic groups which, in turn, led to very low conversions.

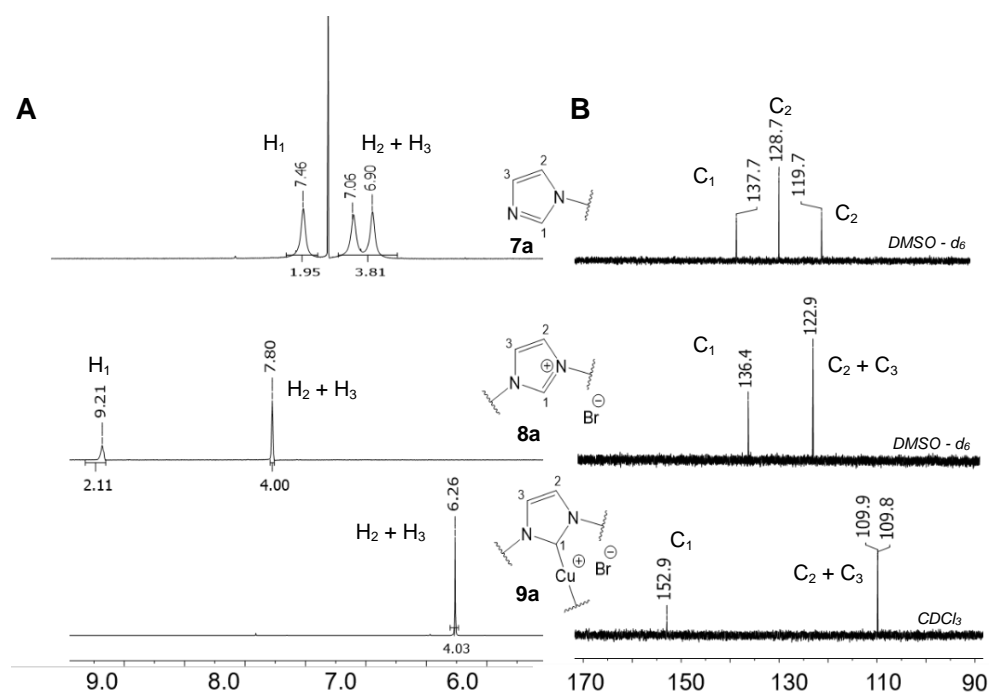


Figure 28. Partial cut of (A) <sup>1</sup>H-NMR spectra and (B) <sup>13</sup>C-NMR spectra for **7a** (above), **8a** (middle) and **9a** (below), indicating a significant shift of NCHN (H<sub>1</sub>) respectively NCHCHN proton (H<sub>2</sub> + H<sub>3</sub>) and of NCHN (C<sub>1</sub>) as well as NCHCHN (C<sub>2</sub> + C<sub>3</sub>) carbon resonances during functionalization.

The structural proof of cyclic complex **9a** (x=12) was accomplished by <sup>1</sup>H-NMR (Figure 28 A) and <sup>13</sup>C-NMR spectroscopy (Figure 28 B) analyzing the shift of NCHN proton resonances (H<sub>1</sub>) from 7.46 ppm for **7a** to 9.21 ppm for **8a** and the subsequent disappearance during complex formation.

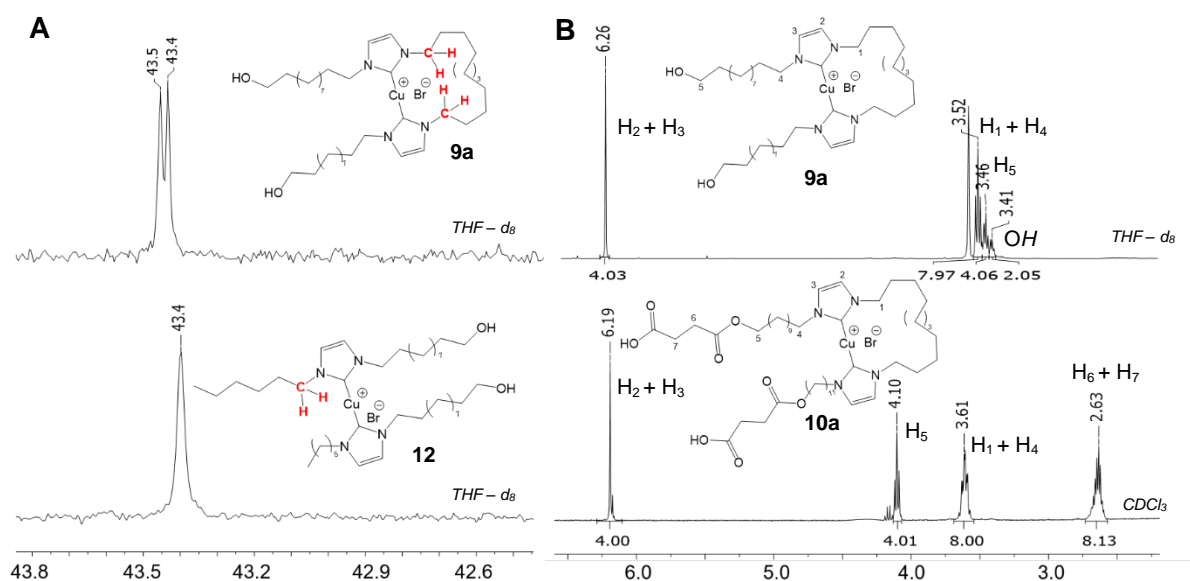


Figure 29. (A) Partial cut of  $^{13}\text{C}$ -NMR spectra for **9a** (above) and **12** (below), showed the doubling of  $\text{NCH}_2$  resonances comparing the cyclic and acyclic model complex. (B) Partial cut of  $^1\text{H}$ -NMR spectra for **9a** (above) and **10a** (below) revealing the appearance of  $\text{O}=\text{CCH}_2\text{CH}_2\text{C}=\text{O}$  resonances at 2.63 ppm and the shifted of  $\text{OCH}_2$  resonances from 3.46 ppm to 4.10 ppm confirming the successful functionalization.

The shift of  $\text{NCH}_2\text{CHN}$  resonances ( $\text{H}_2 + \text{H}_3$ ) from 7.06 ppm and 6.90 ppm for **7a** to 7.80 ppm for **8a** and 6.26 ppm for **9a** as well as the carbon shift of  $\text{NCH}_2$  resonances ( $\text{C}_1$ ) from 137.7 ppm over 136.4 ppm to 152.9 ppm prove the change in electronic structure during synthesis. In order to verify the cyclic structure, a model complex (**12**) was synthesized according to the copper(I)-oxide method. Comparing the resonances of  $\text{NCH}_2$  group of **9** and **12** (Figure 29) showed a doubled carbon signal for the cyclic complex which is caused due to the fixed conformation and the accompanied loss of rotational degree of freedom. Contrary, the acyclic model complex showed a single carbon signal due to the lack of hindrance guaranteed the fully freedom of movement. ESI-TOF-MS analysis showed a good match of measured and simulated pattern  $737.138 \text{ g mol}^{-1}$  (simulated  $737.538 \text{ C}_{41}\text{H}_{77}\text{CuN}_4\text{O}_3^+$ ) for (**9a**:  $x = 12$ ) as well as  $797.605 \text{ g mol}^{-1}$  (simulated  $797.549 \text{ C}_{44}\text{H}_{83}\text{CuN}_4\text{O}_2\text{Cl}^+$ ) (**9b**:  $x = 12$ ) prove the structural conformation. After post modification reaction,  $^1\text{H}$ -NMR spectroscopy showed a typical shift of  $\text{CH}_2$  protons in the direct neighborhood of the oxygen atom from 3.46 ppm for **9a** to 4.10 ppm for **10a** as well as the appearance of the  $\text{CH}_2\text{CH}_2$  resonances of the attached end group at 2.63 ppm. ESI-TOF-MS revealed no signal due to decomposition during ionization process. Complex **10b** ( $x=16$ ) was synthesized and fully characterized in the same manner (for more details see Appendix).

### 3.2. Single molecule spectroscopy

The mechanophoric behavior of copper-carbon bond within a copper(I)-bis(NHC) complex was investigated via single molecule force spectroscopy, in order to get precise information about rupture forces on a microscopic scale, that in turns can be transferred to potential macroscopic applications. Therefore, the acyclic and cyclic complexes were synthesized using the  $\text{COOH}$  functionalization as an anchor for immobilization of complexes between a modified AFM tip and a wetted substrate surface (for details see chapter 1.2.1). The AFM measurements were accomplished with special thanks by Matthew Sammon who is part of the working group of Martin Beyer from university of Innsbruck according to a published protocol<sup>110,118</sup>. For this purpose, the synthesized  $\text{COOH}$  end-capped cyclic and acyclic complexes were fixed between

the AFM tip and the glass substrate, coated with silane functionalized poly(ethylene glycol). 1-Ethyl-3-(3-dimethylaminopropyl)-carbodiimide (EDC) and N-hydroxy succinimide (NHS) were used as coupling agents to attach the copper(I)-bis(NHC) complex on the coated surfaces. The AFM tip was repeatedly dipped to the glass substrate, which is wetted by the DMSO diluted coupling agents enabling to get force-extension curves and reveal information about bond strength and maximal extension of copper-carbon bond (Figure 30 A).

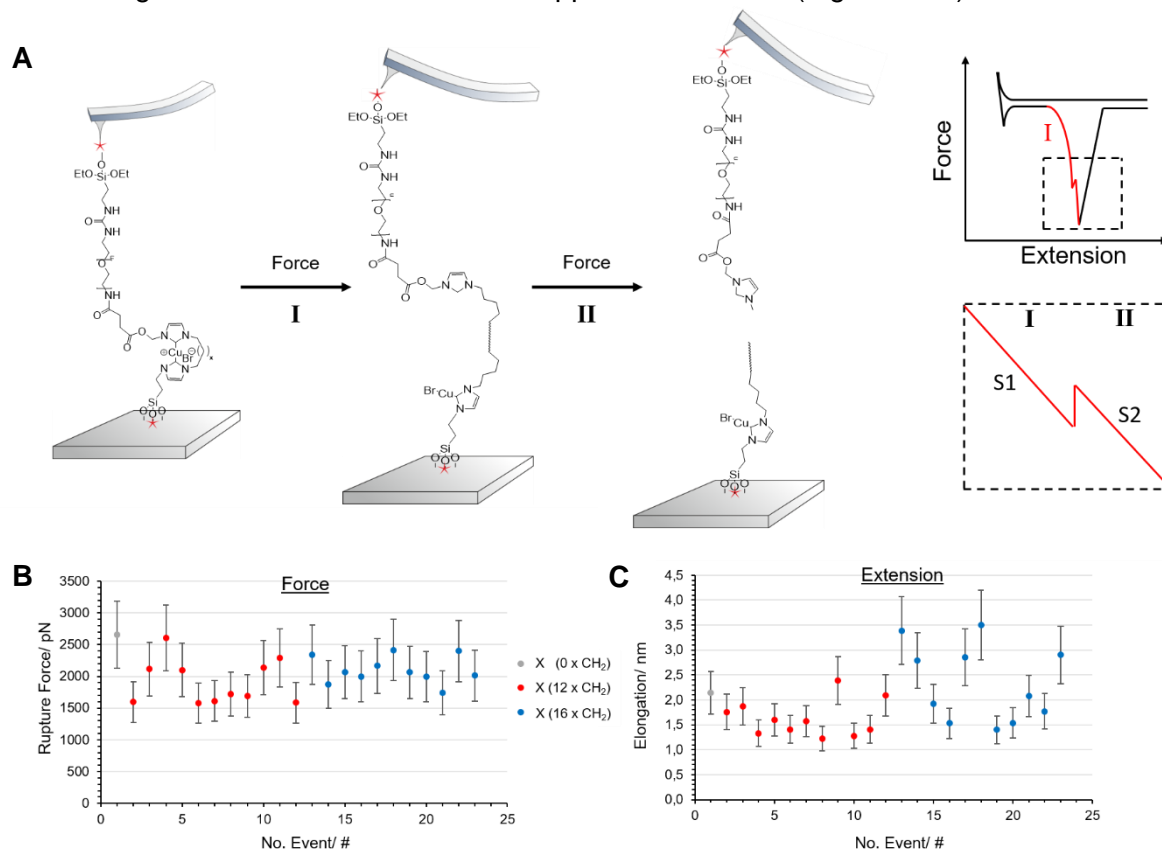


Figure 30. (A) Applying of force leads to a double rupture event of the most labile Cu-C bond of an anchored copper(I)-bis(NHC) complex subsequently followed by a second covalent bond. This allows to calculate force-distance curves which reveal information about (B) rupture forces and (C) elongation, offering the possibility to clearly identify the ruptured bond.

The introduction of a safety line allowed to clearly identify the nature of the ruptured bond evaluated by the comparison of the slope in a double rupture event. The recorded single rupture events for the acyclic complex (**5**) and double rupture events for the cyclic complexes (**10**) showed rupture forces from 1600 to 2600 pN which was significant below the calculated values for the C-C (6900 pN) and C-O bonds (7600 pN) of the polymer chain (Figure 30 B). As expected, the comparison of the maximum elongation in double rupture events for the cyclic structure revealed an increasing elongation with the increasing cycle number ( $1.63 \pm 0.6$  nm for **10a** to  $2.33 \pm 0.9$  nm for **10b**) (Figure 30 C).

There is a good agreement with the simulated values of the copper carbene bond rupture determined by CoGEF calculation that offers forces of  $\sim 1500$  pN. Thus, the bond strength within the copper(I)-bis(NHC) complex is comparable to other previous discussed mechanophores (Chapter 1.2.1) e.g., prestressed rings, but significantly exceed the forces of spiropyran isomerization.

### 3.3. Chain extended and network structured copper(I)-bis(NHC) complexes

#### 3.3.1. Synthesis and characterization of chain extended copper(I)-bis(NHC) complexes

Previous investigations of polymeric copper(I)-bis(NHC) complexes which were attached by poly(isobutylene) (PIB) or poly(styrene) (PS) “handles” showed an increased activity towards fluorogenic “click” reactions either by changing the backbone from flexible PIB to rigid PS or varying the chain length to a higher degree of polymerization<sup>306</sup>. Unfortunately, the direct quaternization of bromo telechelic polymers with 1-methylimidazole turned out as an unsuitable method for modifying longer polymer chains with molecular weight above 15000 g mol<sup>-1</sup>. The bulky polymer chains hamper the quaternization or the subsequent formation of the Cu(I) (bis)NHC complexes sterically, resulting in uneconomically low yields. Accordingly, the previously used combination of either LCCP or ATRP followed by post-functionalization chemistry led to an inefficient attachment of the *N*-alkyl imidazolium moieties, especially as these kinds of linkages displayed a Hofmann-type elimination reaction during the copper(I)-carbene formation<sup>307</sup>.

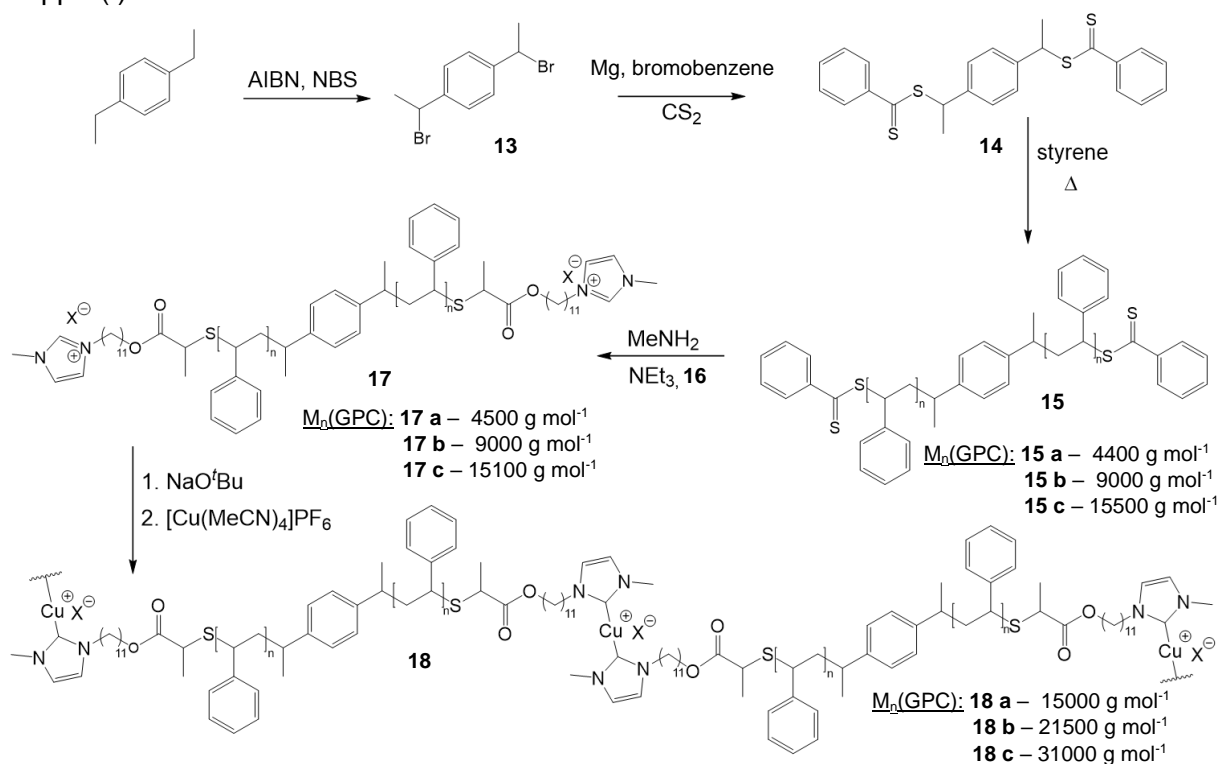


Figure 31. Synthetic route for chain extended mechanophores (**18**), starting with radical bromation subsequently followed by Grignard reaction to form the chain transfer agent (**14**). Subsequently, the RAFT polymerization of styrene revealed dithiobenzoate end-capped PS (**15**) followed by a thio bromo click reaction yielding the imidazolium precursor (**17**). The final complexation reaction generated the chain extended mechanophores (**18**).

In order to achieve an increase in chain length and ensure a more stable linkage of the copper(I)-(NHC) complex, a new synthetic strategy was developed. Figure 31 shows the synthetic route starting with the radical side chain bromination of diethylbenzene with *N*-bromo succinic imide (NBS) and (azobisisobutyronitril) AIBN to obtain the dibromated **13**. The introduction of the dithiobenzoate end groups via Grignard reaction was achieved by using dibromo benzene and magnesium. A subsequent reaction with carbon disulfide formed the dithiobenzoate anion, which can further react in a nucleophilic substitution with **13**. Afterwards, styrene was polymerized in a reversible addition fragmentation chain transfer (RAFT) polymerization which was thermally activated by auto initiation of styrene at 120°C<sup>308</sup> using **14**

as chain transfer agent (CTA). Three different molecular weights of **15** were achieved (Table 5) ranging from 5000 g mol<sup>-1</sup> 15000 g mol<sup>-1</sup> with low PDI around 1.2. This underlines the living character of this polymerization technique, which ensure the required centrally embedding of the mechanochemical active copper-carbon bond.

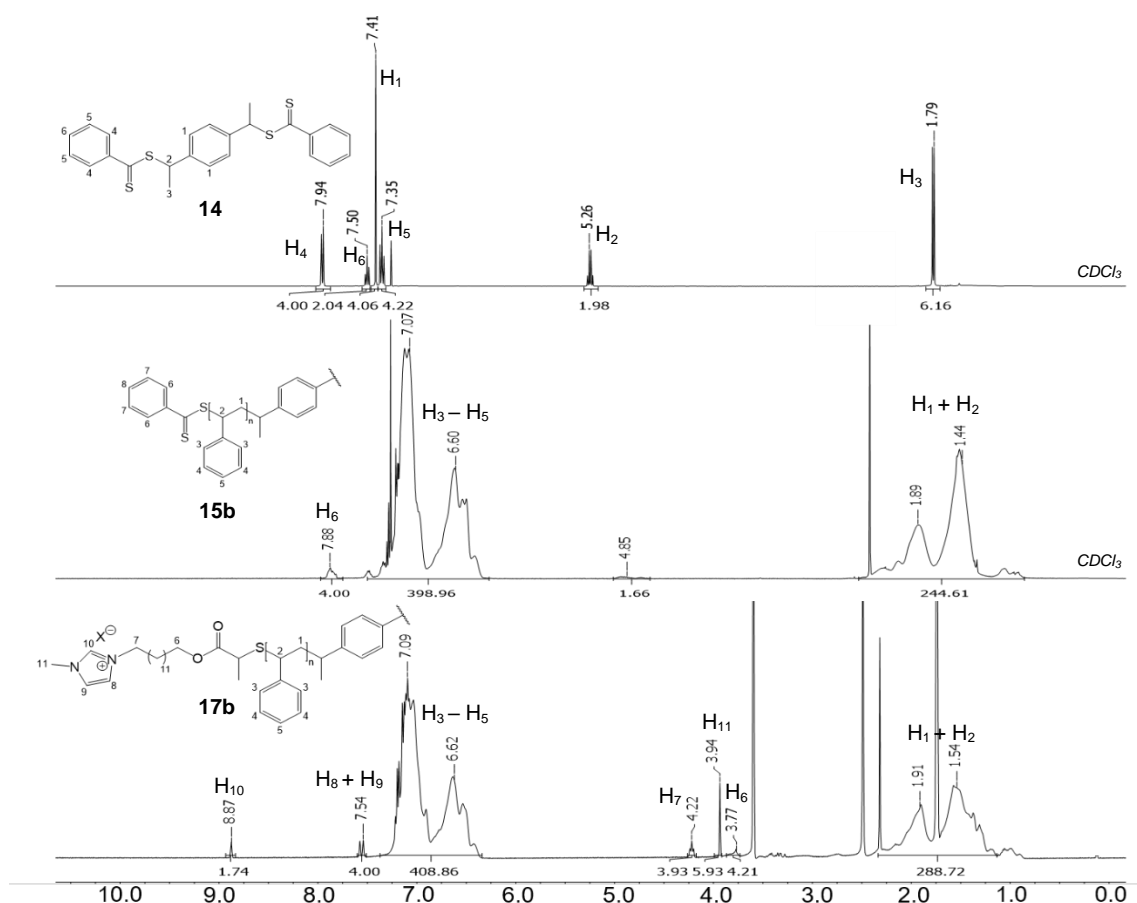


Figure 32. <sup>1</sup>H-NMR spectra **14** (above), **15b** (middle) and **17b** (below), indicating the successful polymerization via RAFT by the resonances of dithiobenzoate end group (*ortho* Ar-H) and the fully functionalization with imidazolium moieties by the signals of NCHN and NCHCHN.

In order to obtain the bivalent imidazolium PS (**17**), the bis-thiol end-capped PS was formed by an *in situ* reduction reaction with tributyl phosphine/methylamine and subsequently linked to the previous synthesized 3-(11-(2-bromopropionyloxy)undecyl)-methyl-1-imidazolium bis(trifluoromethane)sulfonimide (**16**) in a thio bromo “click” reaction with high yields<sup>308</sup>. The structural proof of the prepared  $\alpha$ ,  $\omega$ -bis imidazolium functionalized precursors (**17**) was accomplished via <sup>1</sup>H-NMR spectroscopy (Figure 32) by comparing the spectra of **14**, **15** and **17** showing the characteristic resonances of the imidazolium end group around 8.97 ppm (NCHN) and 7.54 ppm (NCHCHN) as well as the absence of dithiobenzoate group at 7.88 ppm. ESI-TOF-MS (Figure 33) revealed only one double charged series with the maximum at 2645.338 g mol<sup>-1</sup> which matched well with the simulated isotopic pattern for [M]<sup>2+</sup> (C<sub>390</sub>H<sub>420</sub>N<sub>4</sub>O<sub>4</sub>S<sub>2</sub><sup>2+</sup>) 2645.321 g mol<sup>-1</sup> and correspond to a molecular weight of 5290.679 g mol<sup>-1</sup> proving the successful attachment of both *N*-methylimidazolium end groups. The molecular weights as well as PDIs of (**15**) stayed unaffected during the modification compared to (**17**) (see Table 5).

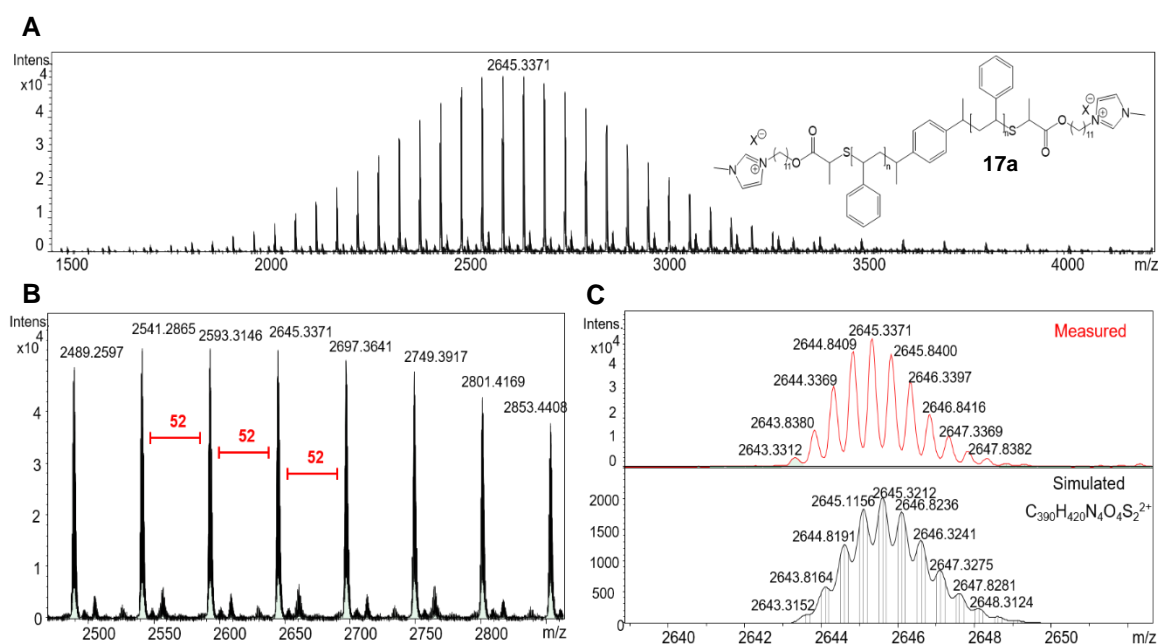


Figure 33. (A) Full ESI-TOF-mass spectrum of bisimidazolium functionalized poly(styrene) (**17a**) using THF as solvent showing one series with a distance of 52 g mol<sup>-1</sup> (B) which depends on the double charged character as well as (C) the measured and simulated isotopic pattern assigned to the C<sub>390</sub>H<sub>420</sub>N<sub>4</sub>O<sub>4</sub>S<sub>2</sub><sup>2+</sup>.

Table 5. Reaction conditions and characterization data of bifunctional PS (**15**, **17**) via RAFT.

Ent.	Comp.	CTA:M	n(CTA) [mmol]	n(M) [mmol]	T [°C]	M <sub>n</sub> (GPC) [g mol <sup>-1</sup> ]	M <sub>n</sub> (NMR) <sup>a</sup> [g mol <sup>-1</sup> ]	Đ	yield [%]
RAFT polymerization									
<b>1</b>	<b>15 a</b>	10: 500	1.75			4400	5000	1.10	37
<b>2</b>	<b>15 b</b>	10: 750	1.16	87.4	120	9000	8300	1.18	25
<b>3</b>	<b>15 c</b>	10:1000	0.87			15500	14800	1.17	13
Thio bromo "click" reaction									
<b>4</b>	<b>17 a</b>					4500	4800	1.12	98
<b>5</b>	<b>17 b</b>	-	-	-	RT	9000	8500	1.15	89
<b>6</b>	<b>17 c</b>					15100	18200	1.17	53

a) Determined via <sup>1</sup>H-NMR spectroscopy by ratio of resonance at 7.54 ppm and the polymer backbone.

The chain-extended copper(I)-bis(NHC) complexes (**18**) bearing more than one copper(I)-bis(NHC) moiety in the linear polymer chain were prepared by a condensation reaction. The *N*-methylimidazolium functionalized precursor polymers (**17**) were deprotonated by NaO<sup>t</sup>Bu in order to obtain the free *N*-heterocyclic carbene, which was subsequently complexed with the well soluble tetrakis(acetonitrile)copper(I) hexafluorophosphate [Cu(MeCN)<sub>4</sub>]PF<sub>6</sub>. As expected for condensation chemistry, the concentration of the reaction partners played a crucial role. Higher concentration (0.15 mmol mL<sup>-1</sup>) of the precursor polymer (**17a**) (4500 g mol<sup>-1</sup>) preferred intermolecular condensation, in turn leading to higher molecular weights (e.g., 15000 g mol<sup>-1</sup> for (**18a**)) (see Table 6) by combining several individual chains into one condensate resulting in conversions up to 87%. Lower concentrations (0.02 to 0.08 mmol mL<sup>-1</sup>) decreased the conversion as well as the obtained molecular weights indicating a ring formation of only a few (1-2) chains.

Table 6. Concentration effects in complexation reaction of **17a**.

Ent.	c <sup>a)</sup> [mmol mL <sup>-1</sup> ]	M <sub>n</sub> (GPC) ( <b>17a</b> ) [g mol <sup>-1</sup> ]	M <sub>n</sub> (GPC) mixture of ( <b>18a</b> ) [g mol <sup>-1</sup> ]	Conversion <sup>b)</sup> [%]
<b>1</b>	0.02	4500	5000	5
<b>2</b>	0.04		7400	8
<b>3</b>	0.08		9100	15
<b>4</b>	0.15		15000	87

a) Initial concentration of **17a** before NHC-formation.

b) Determined via <sup>1</sup>H-NMR spectroscopy of the crude reaction mixture by integration of precursor signals at 7.54 ppm and the resonances at 6.25 ppm assigned to the copper(I)-bis(NHC) complex.

<sup>1</sup>H-NMR spectroscopy was performed to prove the formation of the desired chain-extended copper(I)-bis(NHC) complexes (**18**) by a disappearance of the -NCHN- signal at 8.97 ppm and the shift of the -NCH<sub>2</sub>CH<sub>2</sub>N- signals from 7.54 ppm to 6.25 ppm as discussed in chapter 3.1.1. Analytic GPC measurements of the unseparated complexes revealed chromatograms with several maxima (see Figure 34 A) proving the formation of higher condensation products. In case of **18a**, at least 3 – 4 individual copper(I)-bis(NHC) functionalized polymer chains could be obtained; additionally, indicated by a clear increase in the average molecular weight from e.g., 4500 g mol<sup>-1</sup> for **17a** to 15100 g mol<sup>-1</sup> for the complex **18a** (see Table 6). In case of the higher molecular weight precursor polymer **17c** (15100 g mol<sup>-1</sup>) the formation of the poly-copper(I)-bis(NHC) complex is suppressed, which resulted in only a single condensation process with two chains obtaining **18c** in an average molecular weight of 31000 g mol<sup>-1</sup>. In order to separate the individual condensates, preparative GPC were performed: in case of e.g., **17a** (see Figure 34 B) four fractions (F1 – F4) could be identified, containing different copper(I)-bis(NHC) complex condensates ranging from 4200 g mol<sup>-1</sup> (F1) up to 17200 g mol<sup>-1</sup> (F4). Comparison with <sup>1</sup>H-NMR spectroscopy (Figure 34 C) of the isolated fractions supported the formation of different condensate species. For fraction F1 the molecular weight in GPC remained unaffected when compared to the precursor (**17a**), and the <sup>1</sup>H-NMR spectrum proved the presence of the neat *N*-methylimidazolium-telechelic macro ligand (**17a**) by the resonances H<sub>1</sub> of the -NCHN- group as well as the protons H<sub>2</sub> of the -NCH<sub>2</sub>CH<sub>2</sub>N- groups. Fraction F2 showed a clear shift in GPC compared to the neat ligand in F1 and in comparison, to the <sup>1</sup>H-NMR spectrum of F2 the clear formation of a copper(I)-bis(NHC) condensate by the presence of the signals at 6.25 ppm corresponding to the -NCH<sub>2</sub>CH<sub>2</sub>N- of the Cu(I) complex. However, also some signals of the free *N*-methylimidazolium around 7.54 ppm and the -NCHN- group were visible but shifted in comparison to the neat ligand. Together with the absence of the neat ligand (**17a**) around 4200 g mol<sup>-1</sup> of F1 in the GPC, a physical mixture of the desired Copper(I)-bis(NHC) complex and the initial *N*-methylimidazolium-telechelic macro ligand can be excluded. This indicates the presence of a copper(I)-bis(NHC) complex with two dangling *N*-methylimidazolium end groups, which match with the integration values of 1:1 of both signals H<sub>2</sub> and H<sub>3</sub>. GPC also revealed two maxima (shifted to lower retention times and thus higher molecular weights) indicating the presence of two copper(I)-bis(NHC) condensates which could be identified as a condensate of 2 respectively 3 chains into one chain-extended complex. A similar behavior could also be observed for the fractions F3 and F4, revealing mixtures of mainly 3 (and minor 2) chains per chain-extended complex for fraction F3 and 3 primarily 4 chains for F4. This indicates also the formation of macrocyclic structures by the absence of the dangling, unreacted imidazolium end groups H<sub>2</sub> at 7.54 ppm in the <sup>1</sup>H-NMR spectrum.

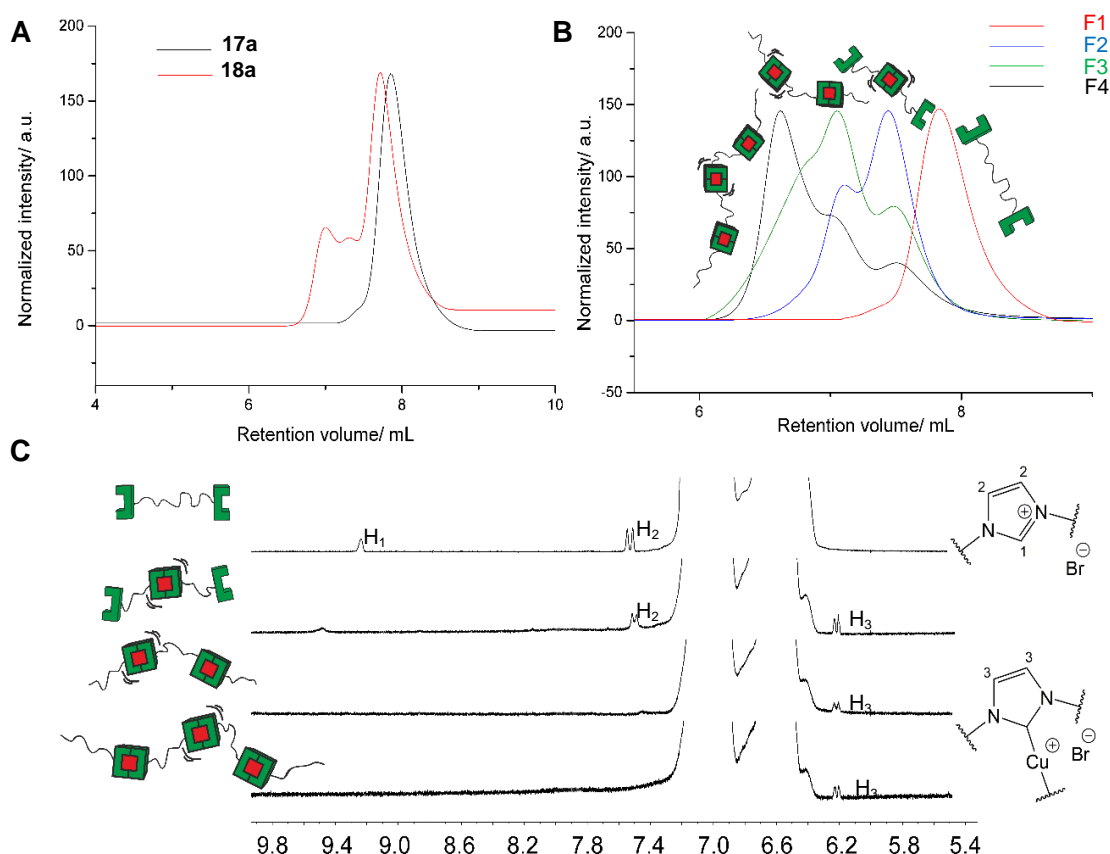


Figure 34. GPC traces of non-separated (A) and separated (B) copper(I)-bis(NHC) condensates (**18a**) formed during complexation reaction ( $F1 = 17200 \text{ g mol}^{-1}$ ,  $F2 = 12800 \text{ g mol}^{-1}$ ,  $F3 = 8500 \text{ g mol}^{-1}$ ,  $F4 = 4200 \text{ g mol}^{-1}$ ) as well as (C)  $^1\text{H-NMR}$  spectra from individual fractions (F1 – F4) of **18a** after separation via preparative GPC.

While the condensation for **17a** and **17b** yielded several condensates as described above, the condensation of **17c** formed only the linear copper(I)-bis(NHC) complex containing two polymer chains as proven by GPC measurements, indicating a molecular weight increase from  $15100 \text{ g mol}^{-1}$  to  $31000 \text{ g mol}^{-1}$  (see Table 7).

Table 7. Characterization data of unfractionated Chain-extended copper(I)-bis(NHC) complexes (**18**)

Ent.	Precursor	$M_n(\text{GPC})$ ( <b>17</b> ) [ $\text{g mol}^{-1}$ ]	Complex	$M_n(\text{GPC})^a$ ( <b>18</b> ) [ $\text{g mol}^{-1}$ ]	$\bar{D}$
1	<b>17a</b>	4500	<b>18a</b>	15000	1.6
2	<b>17b</b>	9000	<b>18b</b>	21500	1.5
3	<b>17c</b>	15100	<b>18c</b>	31000	1.5

a) average molecular weight of complex mixtures.

## 3.3.2. Synthesis and characterization of network structured copper(I)-bis(NHC) complexes

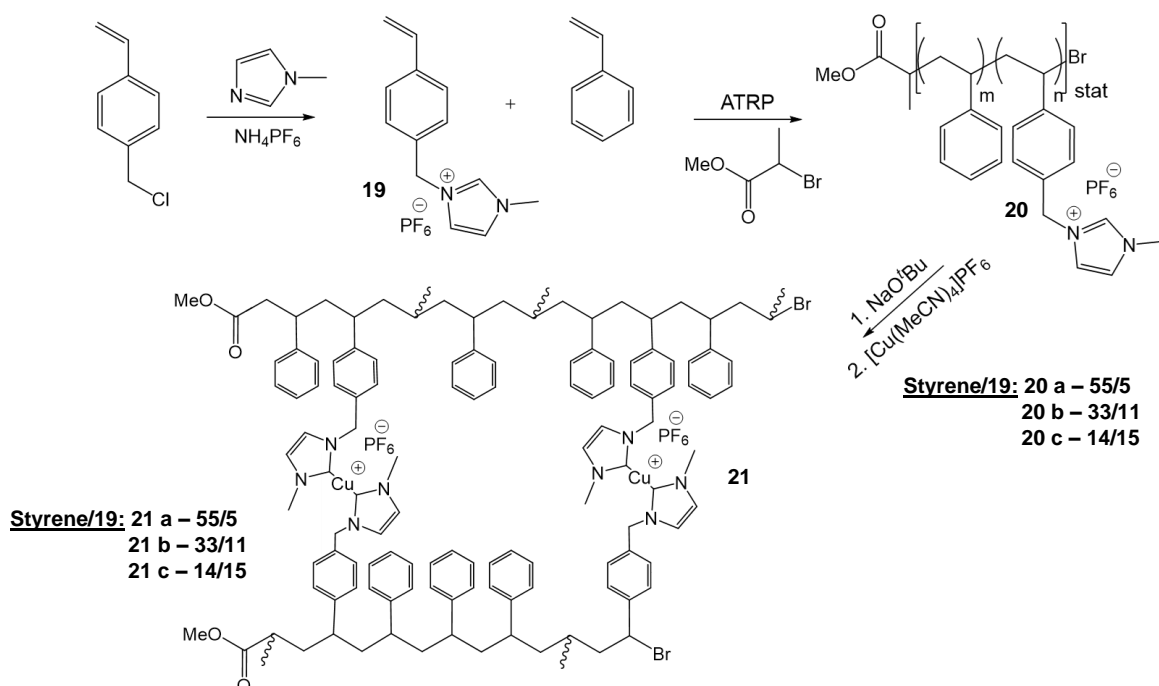


Figure 35. Synthetic route for network based mechanophores (**21**), starting with the synthesis of the imidazolium containing monomer (**19**) which was subsequently polymerized via ATRP. The deprotonation of the imidazolium moieties of the statistical copolymers (**20**) and subsequent complexation of the resulting free carbenes formed the network-based copper(I)-bis(NHC) mechanophores (**21**).

The synthesis of network based mechanophores (**21**) (Figure 35) was accomplished using statistic copolymers (**20**) consisting of styrene and an imidazolium functional monomer (**19**), which was synthesized by quaternization reaction of chloromethyl vinylbenzene and 1-methylimidazol. This was followed by a counterion exchange to increase the hydrophobicity of ionic liquid and thus the solubility for further application. Using methyl-2-bromopropionate (MBP) as initiator an ATRP was performed with different ratios of styrene and **19** ranging from 10/1 to 1/1 to create statistical copolymers which include a variety of cross linkable carbene precursor points. The imidazolium moieties of precursor polymer (**20**) were deprotonated by NaO<sup>t</sup>Bu and complexed with [Cu(MeCN)<sub>4</sub>]PF<sub>6</sub>, which finally generate the required mechanophoric networks (**21**).

Table 8 Overview of synthesized copolymers (**20**) as well as their monomer feed and polymer composition.

Ent.	Copolymer	Feed styr./19	Polymer styr./19	M <sub>n</sub> (NMR) [g mol <sup>-1</sup> ] <sup>a</sup>	M <sub>n</sub> (GPC) [g mol <sup>-1</sup> ]	Đ	Funct. groups
1	20a	10:1	11:1	7500	6300	1.4	5
2	20b	3:1	3:1	7200	5900	1.4	11
3	20c	1:1	1:1	6000	5700	1.4	15

a) Determined via <sup>1</sup>H-NMR spectroscopy using the resonances at 0.88 ppm (CH<sub>3</sub>OC(O)CH(CH<sub>3</sub>) of initiator) and the aromatic protons of the repetitive units 6.52 – 7.02 ppm or the resonances of the ionic species at 5.25 ppm (NCH<sub>2</sub>C<sub>6</sub>H<sub>4</sub>).

b) Heating rate 10 K min<sup>-1</sup>.

The individual compositions of **20** were calculated according to <sup>1</sup>H-NMR spectra by means of the resonances at 5.25 ppm of the NCH<sub>2</sub>C<sub>6</sub>H<sub>4</sub> group of the ionic species and the signals of the aromatic part from the polymer backbone at 6.52 – 7.02 ppm. The ratios were determined to 55/5 for (**20a**), 33/11 for (**20b**) and 14/15 for (**20c**) indicating a similar reaction rate for both monomers within the ATRP (see Table 8).

The carbene formation for the network-based mechanophores was done similarly by deprotonating the methylimidazolium moieties of the statistic copolymers (**20**) using NaO<sup>t</sup>Bu followed by the coordination to the copper(I)-salt. The thus formed copper(I)-bis(NHC) complexes are able to act as crosslinker between the individual polymer chains forming thus the covalent networks (**21**), which getting insoluble and start to precipitate over time. To determine the overall amount of copper inside the sample, FAAS measurements were performed figuring out copper contents of 0.055 mmol<sub>Cu</sub> for **21a**, 0.142 mmol<sub>Cu</sub> for **21b** and 0.178 mmol<sub>Cu</sub> for **21c** per 100 mg<sub>sample</sub> corresponding to a conversion of 83%, 93% and 79% of the theoretical value for full consumption of the imidazolium precursor moieties (Table 9).

Moreover, *in situ* melt rheology of toluene swollen networks was conducted to determine the network densities. The observed storage moduli ( $G'$ ) of the swollen networks were used to calculate the crosslinking density from plateau value in accordance to **equation 1** obtaining higher crosslinking density with increasing amount of functional groups in the copolymer from 120 mol m<sup>-3</sup> for (**21a**) (11/1 ratio of incorporated styrene/(**19**)) to 2360 mol m<sup>-3</sup> (**21b**) (1/1 styrene/(**19**)) (see Table 9).

$$v_x = \frac{G'}{RT} \quad (1)$$

Table 9 Characterization data for copper(I)-bis(NHC) based networks (**21**).

Ent.	Ratio Copolym. (Styrene/ <b>19</b> ) <sup>a)</sup>	$G'$ [MPa]	$\nu_{exp}$ [mol m <sup>-3</sup> ] <sup>b)</sup>	Amount Cu <sub>FAAS</sub> [mmol <sub>Cu</sub> /100 mg <sub>sample</sub> ] <sup>c)</sup>	Amount Cu <sub>Theo</sub> [mmol <sub>Cu</sub> /100 mg <sub>sample</sub> ] <sup>d)</sup>	Conv. [%]	
1	<b>21a</b>	11/1	0.30	120	0.055	0.072	83
2	<b>21b</b>	3/1	1.76	710	0.142	0.152	93
3	<b>21c</b>	1/1	5.85	2360	0.178	0.225	79

a) Determined via <sup>1</sup>H-NMR spectroscopy see Table 8.

b) Crosslinking density  $\nu_{exp}$  calculated according to equation (1) in swollen state.

c) Determined by FAAS; d) theoretical value for full conversion of imidazole moieties of **20**.

### 3.3.3. Mechanochemical activation of chain extended and network structured copper(I)-bis(NHC) complexes in bulk by compression

In order to get information about the catalytic activity of the successfully synthesized chain extended (**18**) and network-based copper(I)-bis(NHC) complexes (**21**), the mechanochemical activation should be accomplished in a solid matrix material. Due to the application of external force one shielding ligand should be cleaved, thus generating a free coordination side (see Figure 36) which enables to catalyzed e.g., CuAAC. Herein the placement of several mechanoresponsive groups into one polymer backbone is expected to increase the effective chain length and led to a larger amount of potentially activated mechanophores.

Mechanophore containing networks should similarly enhance the activation behavior due to the three-dimensional structure in which the crosslinking points were able to redirect the applied force and allowed to activate also the perpendicular parts, additionally to the parallel orientated parts.

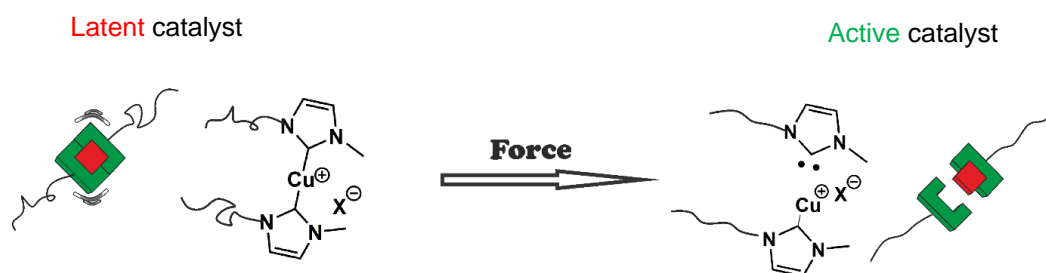


Figure 36. Mechanochemical activation of copper(I)-bis(NHC) complex attached by polymeric handles, transmitting the force through the polymer chain to the labile copper carbon bond, thus creating an active coordination site.

By using high molecular weight pTHF as matrix material ( $M_n = 112\,000\text{ g mol}^{-1}$ ; crystallinity 68%) the optimal transmittance of the applied force due to the crystalline regions<sup>306</sup> was guaranteed. Therefore, the synthesized mechanocatalyst (**18**, **21**) and the initially non-fluorescent components 3-hydroxy-7-azidocoumarin (**22**) and phenylacetylene (**23**) were embedded, in which the mechanochemical response of these catalysts triggers a force induced CuAAC and thus generating the highly fluorescent 7-hydroxy-3-(4-phenyl-1H-[1,2,3]triazole-1-yl)-coumarin (Figure 37). Hence, the increase in fluorescence intensity can indirectly correlate with the catalytic activity of the activated mechanocatalyst.

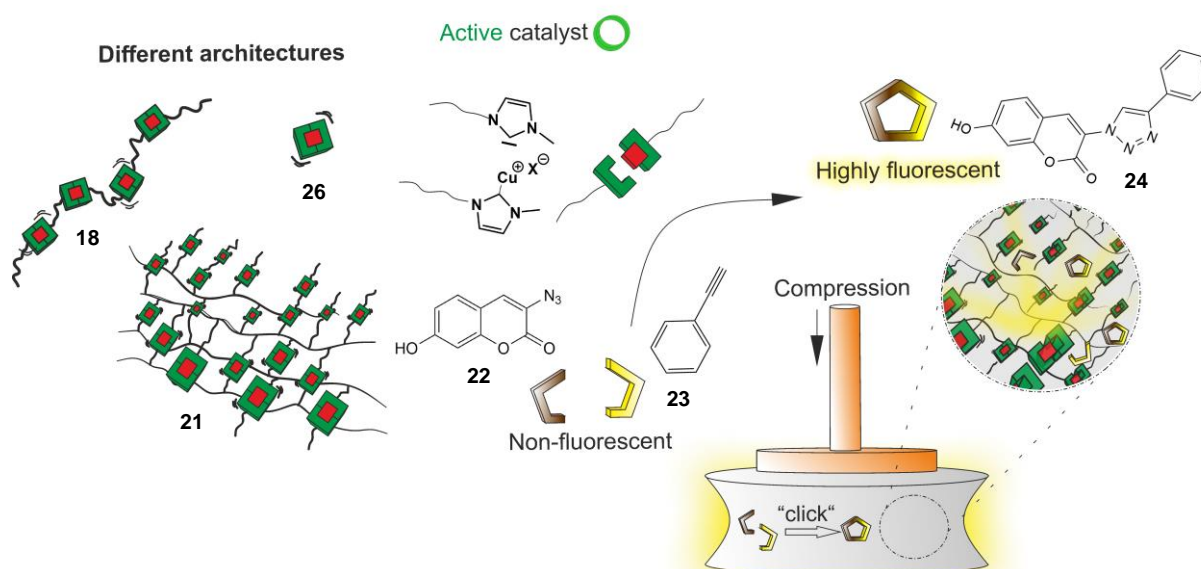


Figure 37. Fluorogenic “click” reaction of initially non fluorescent 3-azido-7-hydroxycoumarin (**22**) with phenylacetylene (**23**) triggered by the activation of a mechanocatalyst (**18**, **21**, **26**) solely by external applied force (compression) resulting in the formation of a highly fluorescent 7-hydroxy-3-(4-phenyl-1H-[1,2,3]triazole-1-yl)-coumarin (**24**).

In order to quantify the efficiency of the mechanochemical activation of different catalyst, fluorescence spectroscopy was performed, based on a calibration of the obtained fluorescence intensity as described in Chapter 4.5.3. The mechanochemical performance was investigated embedding 0.033 equivalents of the bis(NHC) complexes (**18**, **21**) together with **22** and **23** in 200 mg matrix material, achieving an overall mechanophore concentration of  $5.4 \cdot 10^{-6}\text{ mmol mg}_{\text{sample}}^{-1}$ . Subsequently, a compression force of ten tons (corresponding to 0.74 GPa) was applied via a hydraulic press into several compression cycles and the

fluorescence was measured after the 1<sup>st</sup>, 2<sup>nd</sup>, 3<sup>rd</sup>, 10<sup>th</sup>, and 20<sup>th</sup> compression cycle at an emission wavelength of 427 nm after excitation at 360 nm.

The obtained results are shown in Figure 38 and are summed up in Table 10. In comparison with the linear polymer mechanophores, which were investigated<sup>306</sup> the chain extended mechanophores (**18**) consisting of  $\alpha,\omega$ -NHC telechelic PSs linked to multiple Cu(I)-centers per polymer chain, showed a stepwise increase in fluorescence intensity at 427 nm with an increasing number of compression cycles (Figure 38 A). As expected, when the overall chain length of the attached polymer handles was heightened the catalytic efficiency was enhanced. This results in conversions up to 16.1% for (**18a**) ( $M_n = 15\,000\text{ g mol}^{-1}$ ,  $DP \approx 190$ ) and up to 44.2% for (**18b**) ( $M_n = 21\,500\text{ g mol}^{-1}$ ,  $DP \approx 190$ ).

An additional model complex was also synthesized performing a control experiment which underline the necessity of polymer chains for mechanochemical activation (for details see 1.1). The investigation of a low molecular weight copper(I)-bis(NHC) complex (**26**) in compression experiments show no significant increase in fluorescence intensity.

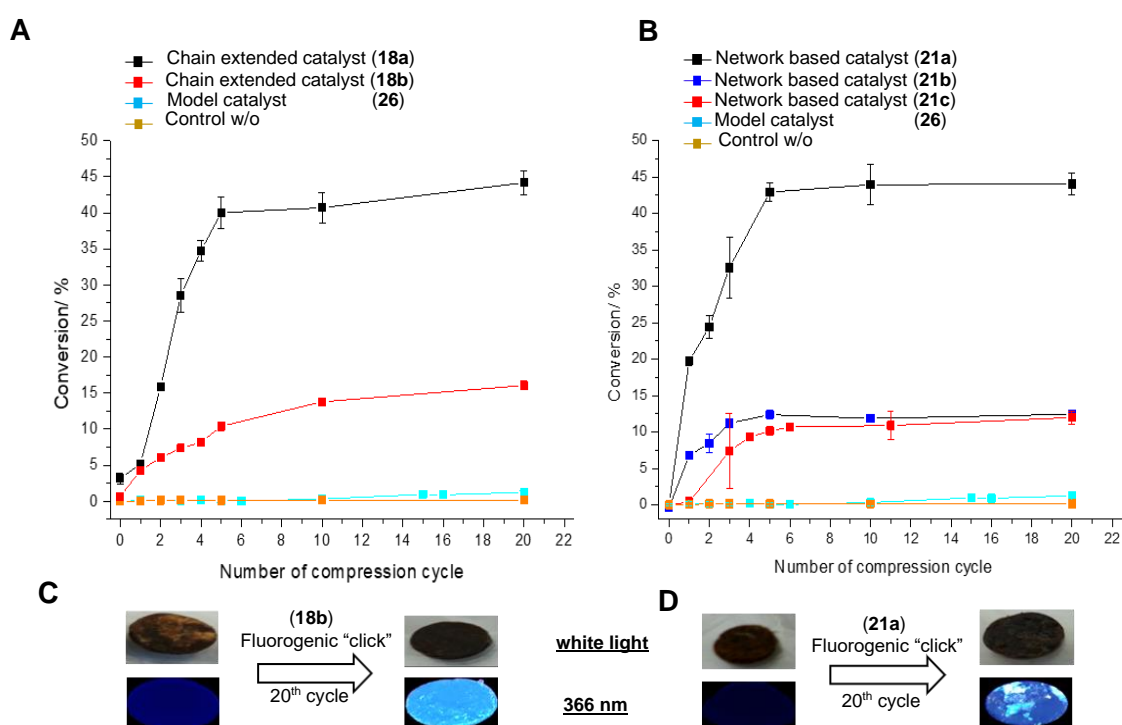
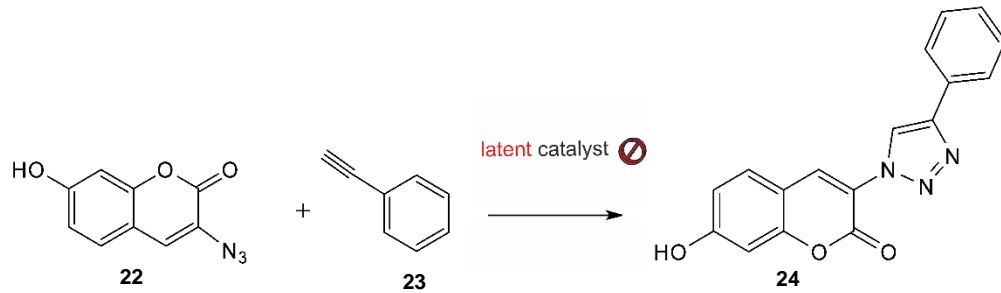


Figure 38. Mechanochemical activation of (A) chain extended (**18**) and (B) networks based mechanocatalysts (**21**) triggering a fluorogenic "click" reaction which results in the increase of the fluorescence activity due to the formation of highly fluorescent **24**. Pictures of **18b** (C) and **21a** (D) before and after compression experiments under white light as well as UV-light (366 nm).

Control experiments were performed in order to investigate thermal influences or the influence of the compression itself. For this purpose, control experiments without mechanocatalyst were conducted which did not show any catalytic activity thus excluding an occurring force induced cycloaddition. Furthermore, the prepared samples, which were also stored at room temperature for at least one week did not show a significant increase in fluorescence intensity for **18a**. The heightening of catalytic activity for higher molecular weight chain extended catalyst **18b** accompanied by an interruption of the fully latent state. This based on the reduced activation energy of ligand detachment due to the increased chain length which resulted in an initial value up to 3%. To improve the latency of mechanocatalysts and to shorten the effective length of the polymer chains between the copper(I)-bis(NHC) species, the network-based

copper(I)-bis(NHC) complexes (**21**) were tested (Figure 38 B). Herein, the active chain-length between the copper(I)-bis(NHC) centers was smaller (~11 repetitive units compared to more than 100 for the chain-extended complexes) and thus the complexes (**21**) were latent for the CuAAC until activated by external force. Thus, these complexes can still be activated very efficiently as can be seen by the high conversions for the fluorogenic “click” reaction of up to 44.1% for (**21a**, copolymer composition 11:1 styrene/**19**). Increasing the amount of ionic monomer (**19**) to 3:1 (**21b**) or 1:1 (**21c**) led to a decrease in their mechanochemical activation, presumably due to the lower flexibility and higher  $T_g$  preventing an efficient force transmission.

Table 10. Experimental conversions in the fluorogenic “click” reaction of initially non-fluorescent 3-azido-7-hydroxycoumarin (**22**) with phenylacetylene (**23**) forming the highly fluorescent 7-hydroxy-3-(4-phenyl-1H-[1,2,3]triazole-1-yl)-coumarin (**24**) after 20<sup>th</sup> compression cycle



Ent		copper(I)-bis(NHC) complex		“click” conversion [%] <sup>a)</sup>
		Nr.	$M_n$ (GPC) [g mol <sup>-1</sup> ]	
1	Control experiment	-	without	0.3
2		26	low MW	0.9
3	Mechanochemical activation of chain extended mechanocatalyst	18a	15000	16.1
4		18b	21500	44.2
5	Mechanochemical activation of network based mechanocatalyst	21a	11:1 network	44.1
6		21b	3:1 network	12.0
7		21c	1:1 network	13.0

a) Determined after 20 compression cycles as average value of at least three different measurements determined by fluorescence spectroscopy at 427 nm and calculated according to calibration. Deviation of measurements from  $\pm 0.2$  to  $\pm 1.6\%$ .

For the chain extended as well as network-based copper(I)-bis(NHC) complexes a catalytic activity towards the fluorogenic “click” reaction of the initially non-fluorescent of 3-azido-7-hydroxy-coumarin and phenylacetylene could be proven yielding the highly fluorescent dye after activating the complexes by compression force. However, the potential to use this system for stress-sensing applications is limited by some major drawbacks indicated e.g., the missing latency of chain extended mechanocatalyst. Within the most effective network-based approach, miscibility problems between the insoluble network and the matrix material limits the applicability due to the appearance of inhomogeneities. These causes an uneven distribution of catalysts, which limits the spatial availability for dye molecules hindering, in turn, the CuAAC. In addition, the dark brown colored properties of the sensing system lead to fluorescence quenching effects at higher dye concentrations<sup>306</sup>. Furthermore, potential leaching effects due to missing chemical anchoring into the matrix material reduce the practical use. To circumvent these problems a new all-in-one approach should be developed thus excluding matrix blending effects as well as a time-consuming adaption of the catalyst-polymer linkage. For this purpose,

new potential anthracene- and naphthalene-based fluorogenic systems were synthesized and investigated with respect to their application for stress-sensing system in respect to their optical properties (Figure 39).

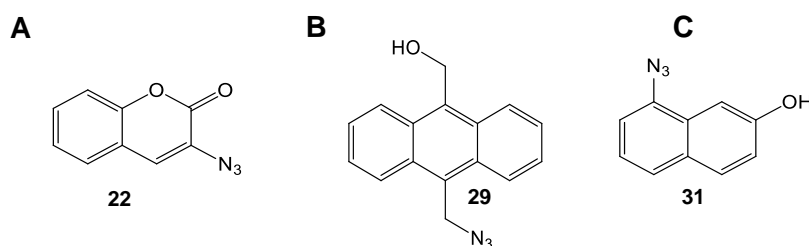


Figure 39. Fluorogenic dyes (A) coumarin-based system, (B) anthracene-based system as well as (C) naphthalene-based system.

### 3.4. Fluorogenic “click” dyes

#### 3.4.1. Anthracene-based system

##### 3.4.1.1. Synthesis of anthracene-based azide

In order to ensure the transparency of our material, a new fluorogenic dye was developed based on a bifunctionalized anthracene in which the azide group suppressed the actual fluorescence due to the photo induced electron transfer (PET)<sup>309</sup>.

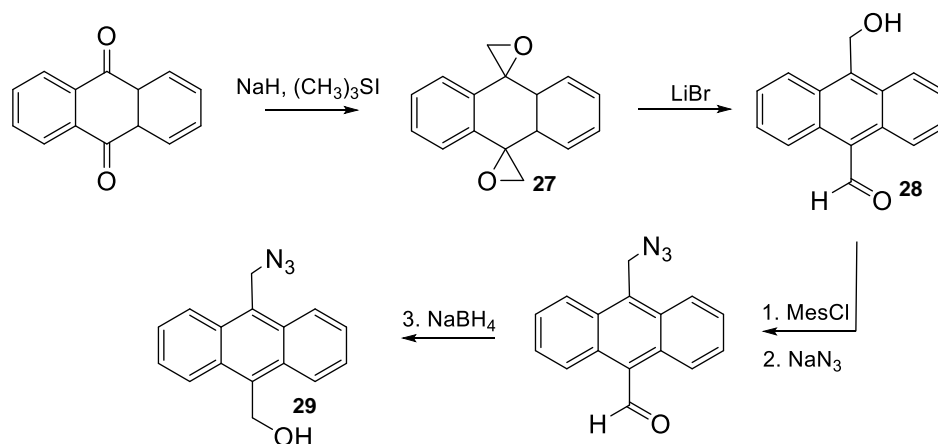


Figure 40. Synthetic route to (10-azidomethylantracene-9-yl)methanol (**29**).

The additional OH moiety acts as potential chemical anchoring point, which allowed to covalently embed the non-fluorescent dye within the polymer matrix. The synthesis (see Figure 40) was accomplished by performing a Johnson-Corey-Chaykovsky reaction of anthraquinone to get the epoxide substituted moiety that was further subjected to an intramolecular disproportionation. The thus obtained hydroxyl functionality was substituted by methane sulfonyl chloride (MesCl) subsequently followed by sodium azide to introduce the required azide functionality. The reduction of the aldehyde functionality with sodium borohydride generated finally the required OH as anchoring point and yielded **29** as slight yellow colored powder. The subsequent CuAAC with phenylacetylene yielded in a triazole formation (**30**) which theoretically interrupted the azide induced PET and thus generates a highly fluorescent compound.

### 3.4.1.2. Optical properties of the anthracene-based dyes

In order to realize the application of the synthesized components as an fluorogenic “click” system for the mechanochemical activation experiments the fluorogenic dye (**29**) should not exhibit an initial fluorescence, but exclusively be generated by fluorogenic CuAAC. According to literature<sup>310</sup> the excitation wavelength at 370 nm was used to determine the fluorescence behavior of **29** and **30** in THF as well as in a PU matrix (Figure 41). After excitation the fluorescence intensity at an emission wavelength of 420 nm increased but also revealed that the azide induced PET of **29** did not completely suppress the initial fluorescence. Therefore, this system turned out as unsuitable for potential stress detection.

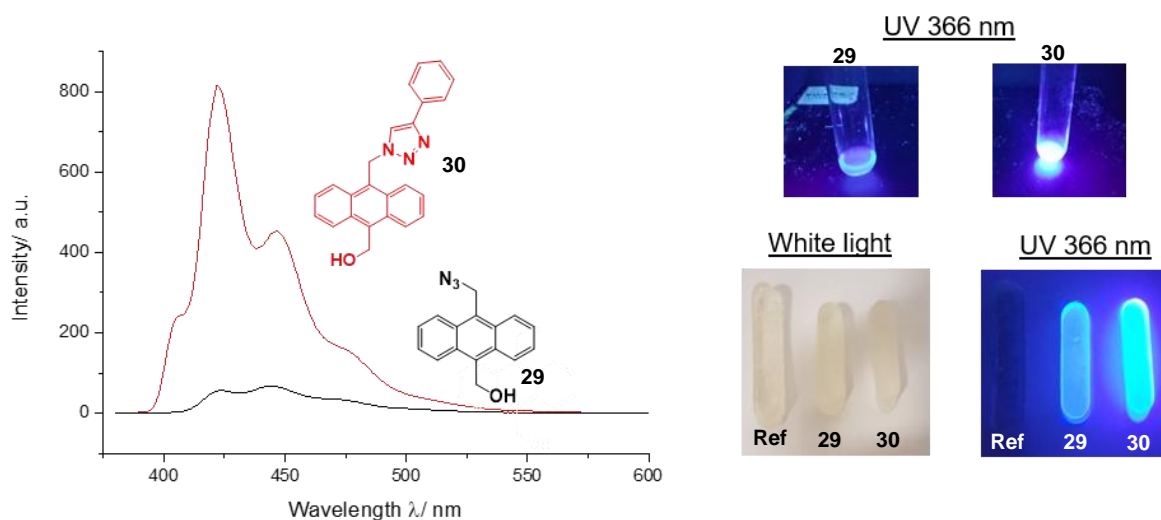


Figure 41. Fluorescence spectrum of **29** (black) and **30** (red) in THF after excitation at  $\lambda_{\text{ex}} \cong 370$  nm and images of **30** and **31** in THF in UV-light (366 nm) as well as images of **29** and **30** within PU matrix in white and UV-light (366 nm).

### 3.4.2. Naphthalen based dyes

#### 3.4.2.1. Synthesis of naphthalene-based azide

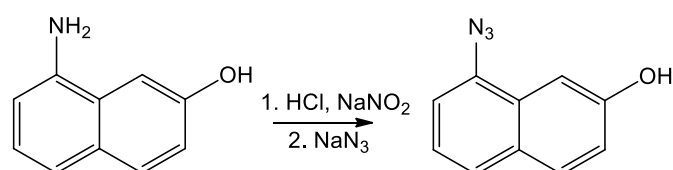


Figure 42. Synthetic route to 8-azidonaphthalen-2-ol (**31**).

In order to prevent the appearance of initial fluorescence, the anthracene-based approach was substituted by a system, which consists of non-fluorescent 8-azidonaphthalen-2-ol (**31**) and commercial 3-hydroxyphenylacetylene (**32**) forming the highly fluorescent 8-(4-(3-hydroxyphenyl)-1,2,3-triazol-1-yl)naphthalen-2-ol (**33**). The synthesis of **31** was accomplished by diazotization of 8-aminonaphthalen-2-ol forming in situ a diazonium salt which were substituted by sodium azide (Figure 42). The resulting product **31** contained additionally a hydroxyl functionality, which can act as a potential reaction partner for isocyanates enabling the covalently integration into e.g., poly(urethane) network. Furthermore, a CuAAC of **31** and **32** were conducted to obtain the required “click” dye (**33**) for the calibration of our system, which will be discussed in chapter 4.8.1.

## 3.4.2.2. Optical properties of naphthalene-based dyes

UV-experiments were done to determine the optical properties of **31** and **33** and revealed an absorption wavelength ( $\lambda_{\text{ex}}$ ) for 8-azido-naphthalene-2-ol (**31**) as well as 8-(4-(3-hydroxyphenyl)-1,2,3-triazol-1-yl)naphthalen-2-ol (**33**) at 340 nm, which did not compete with matrix signals (Figure 43).

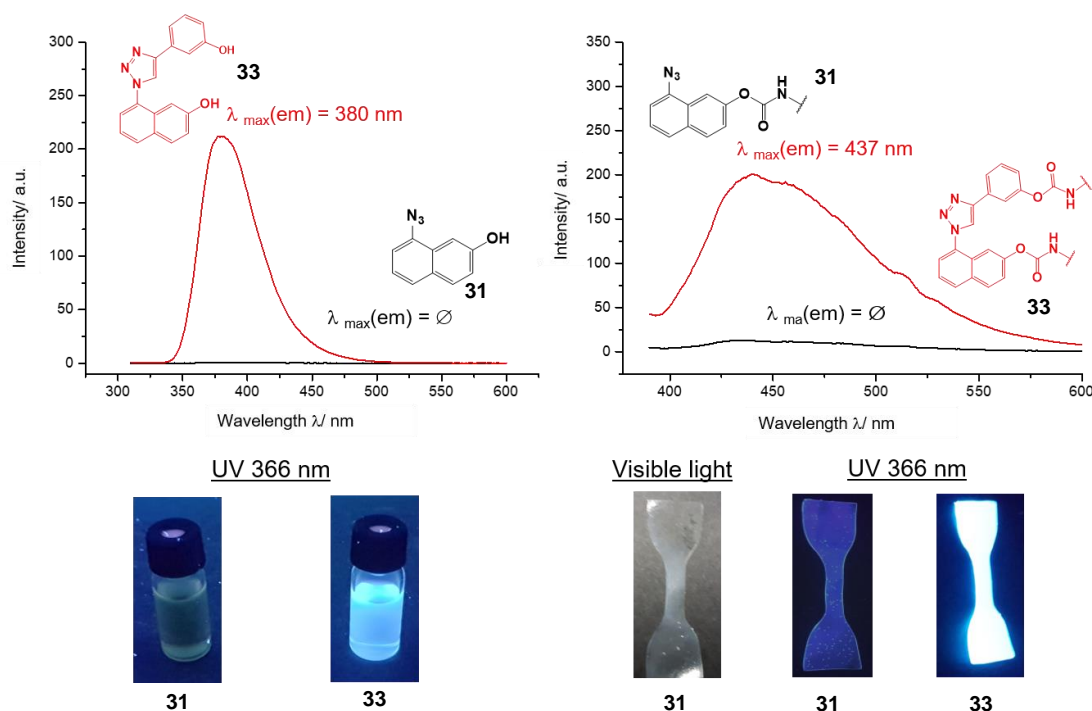


Figure 43. (A) Fluorescence spectrum of **31** (black) and **33** (red) in THF after excitation at  $\lambda_{\text{ex}} \approx 342$  nm and B) in PU matrix after excitation at  $\lambda_{\text{ex}} \approx 377$  nm as well as (C) images of **31** and **33** in THF in UV-light (366 nm) and (D) images of **31** and **33** within PU matrix in white and UV-light (366 nm).

After excitation at 340 nm, fluorescence occurred at 380 nm in the case of **33** while **31** showed no fluorescence (Figure 43 A). This is a result of the strong donation properties of the azide functionalization, which restrained the emission of light after excitation. This is annulled by the extension of the conjugated system during “click” reaction (**33**). The covalent embedding of compound **31** and **33** in a poly(urethane) matrix showed a slight shift in excitation and emission wavelength due to the change in the electronic properties of the conjugated system, while the absence of the initial fluorescence remained. Hence, the naphthalene approach was selected for further mechanochemical investigations, which were accompanied after external calibration, necessary for quantifying the occurred stress.

## 3.5. Mechanochemically active poly(urethane) networks

3.5.1. Synthesis and chemical characterization of crosslinked poly(urethane)s (**PUXX**)

The chemical design of the material is shown in Figure 44, depicting the novel copper(I)-bis(NHC) mechanophore (**3**) which were synthesized as previous discussed in chapter 3.1.1.. The thus obtained bivalent OH-end-capped copper(I)-bis(NHC) complex can be used in a post functionalization reaction e.g., with isocyanates to form a urethane group. For this purpose, a base initiated addition reaction with 1,8-diazabicyclo[5.4.0]undec-7-en (DBU) as catalyst was accomplished to activate the OH group and neglecting the potential redox reactions between copper(I) and tin(IV) which is commonly used as catalyst.

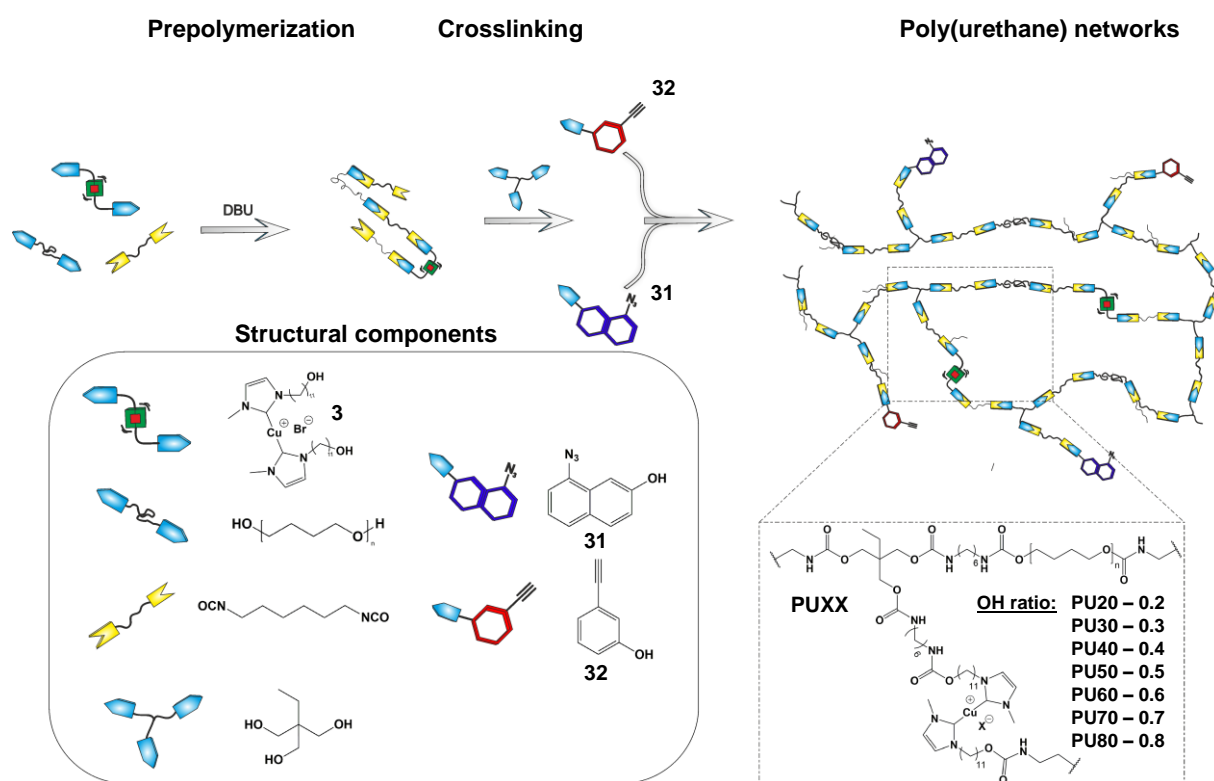


Figure 44. Schematic procedure for the synthesis of poly(urethane) based mechanophores (**PUXX**), consisting of pTHF as soft segment, HDI as hard segment, TMP as trivalent crosslinker, **3** as mechanochemical active component as well as **31** and **32** as fluorogenic system.

Thus, the mechanophore (**3**) was integrated into a multicomponent polyaddition reaction of  $\alpha$ ,  $\omega$ -telechelic bis(hydroxy) poly(tetrahydrofuran) (pTHF) ( $M_n = 2900$  g/mol), 1,6-hexamethylenediisocyanate (HDI) trimethylolpropane (TMP), resulting in an elastomeric poly(urethane) material which fulfills all requirements for the application as stress-sensing material (Figure 44). The synthesis was accomplished under inert conditions to prevent water and obtaining transparent foils.

Within this material, pTHF acts as a soft segment which introduce the required elasticity and enabling in turn an optimal force transmission due to the interplay of a low  $T_g$  and an existing crystallinity. Furthermore, the combination of HDI, which acted as a hard segment and TMP, which was applied as a trivalent crosslinker a robust, but highly transparent material was obtained fulfilling all requirements for an efficient mechanochemical activation. On the one hand, a sufficient stiffness for mechanochemical activation, which acts as a kind of lever and on the other hand the network offered the necessary mobility for the subsequent mechanical activation process without backbone fragmentation. The optimal placement of the mechanophores is crucial for the final activation as a positioning close to the midpoint of the polymer handles ensured a more efficient cleaving.

Prepolymerization reaction of **3** with HDI and pTHF was performed leading to an *in situ* generated  $\alpha$ ,  $\omega$ -isocyanate-telechelic pTHF chain extended copper(I)-bis(NHC) complexes (**Cu-PU**), which can further react with the  $\alpha$ ,  $\omega$ -telechelic bis(hydroxy) pTHF and finally crosslinked by the trivalent TMP crosslinker.

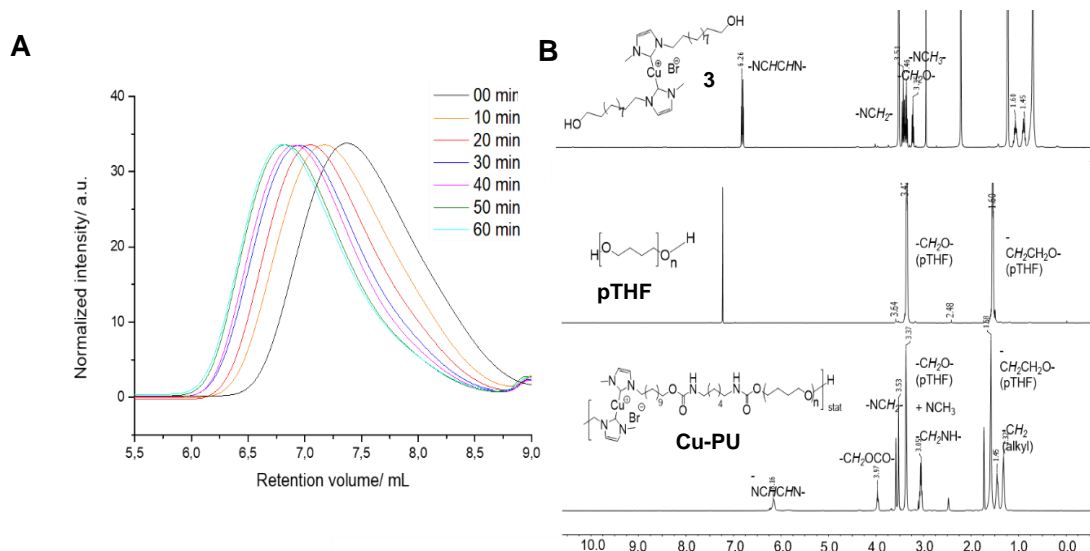


Figure 45. (A) GPC traces of Cu-PU monitoring the progress of the prepolymerization (measured in THF after precipitation in MeOH) as well as (B) Comparison of  $^1\text{H-NMR}$  spectra of copper(I)-bis(NHC) complex (**3**) and pTHF and the resulting prepolymer (**Cu-PU**) (ratio **3**/pTHF of 1/0.6) indicating the successfully introduction of **3** into the polymer.

Figure 45 A shows the increase in molecular weight during prepolymerization resulted in molecular weights up to  $6\,000\text{ g mol}^{-1}$  in 60 min whereas the correct linkage is proved by comparing the  $^1\text{H-NMR}$  spectra of a model prepolymer containing 0.6 eq. of TMP (regarding the amount of pTHF) the pure **3** and pTHF (Figure 45 B). It is visible that the  $\text{NCHNCH}$  protons of copper(I)-bis(NHC) complex remains during prepolymerization process as well as the disappearance of  $\text{CH}_2\text{OH}$  which indicates the successfully introduction of the low molecular weight complex into the polymer chain. Conducting the crosslinking process after 10 min by adding TMP and thus forming the required network structure turns out to be the best condition for mechanochemical activation, which will be further discussed in chapter 3.5.3.1

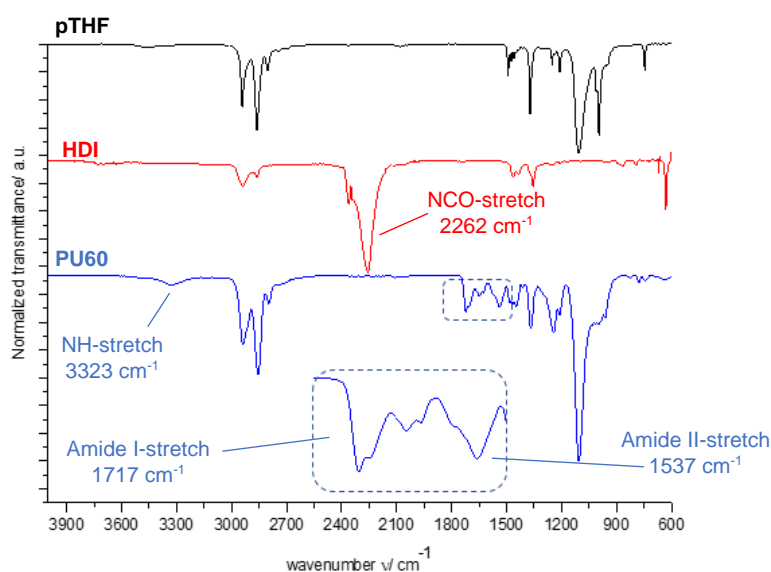


Figure 46. FT-IR spectrum of **PU 60** indicating fully crosslinking by the absence of NCO stretching band at  $\sim 2262\text{ cm}^{-1}$  as well as the forming of urethane groups at  $3323\text{ cm}^{-1}$  (NH-stretch),  $1717\text{ cm}^{-1}$  (amide I) and  $1537\text{ cm}^{-1}$  (amide II).

In order to prove the successful crosslinking of prepolymers IR spectroscopy was performed (Figure 46) pointing out the absence of the NCO stretching band, which is normally located at 2200 to 2300  $\text{cm}^{-1}$ . Furthermore, the appearance of NH stretches at  $\sim 3300 \text{ cm}^{-1}$  as well as amide I and amide II band at  $\sim 1700 \text{ cm}^{-1}$  and  $\sim 1550 \text{ cm}^{-1}$  prove the required urethane formation. DSC experiments (for more details see experimental part) showed a significant melting peak at 24  $^{\circ}\text{C}$  with a melting enthalpy of  $\Delta H_m = 41.4 \text{ J g}^{-1}$  allowing to calculate the degree of crystallization to 24% ( $\Delta H_{m0}(\text{pTHF}) = 172 \text{ J g}^{-1}$ ).<sup>311</sup>

### 3.5.2. Determination of material properties

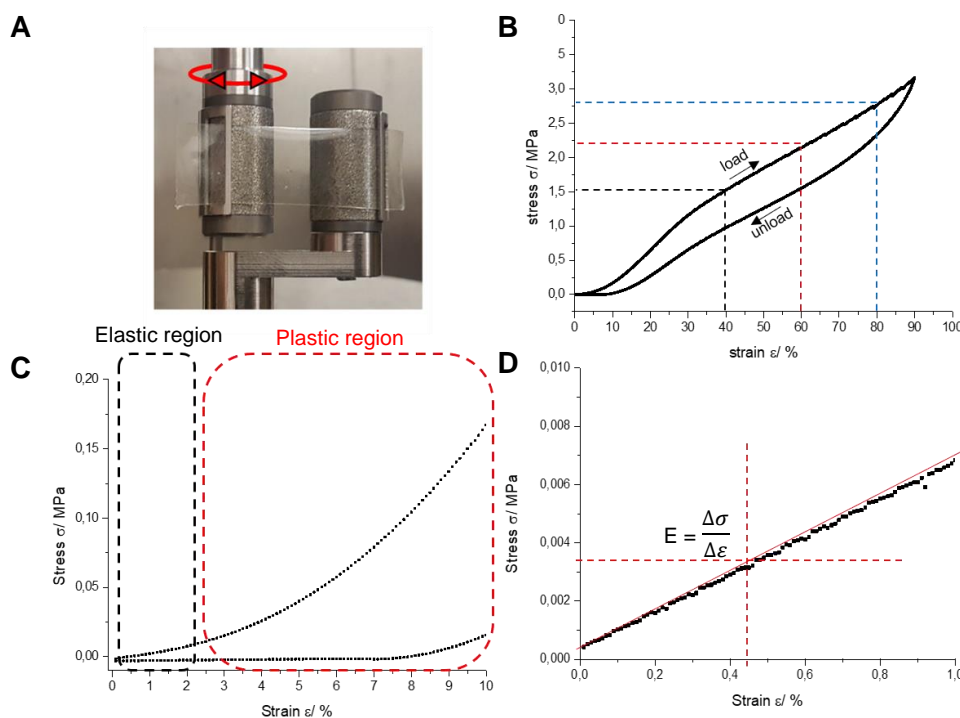


Figure 47. (A) Experimental setup of extensional rotational rheology experiments (B) Loading and unloading stress strain curve of **PU60** with strain rate 0.1% per second offering (C) the classification of the linear elastic and plastic regime as well as (D) the determination of Young's modulus.

The material properties of the synthesized poly(urethane) elastomers were determined via extensional rotational rheology to enable a subsequent correlation with the mechanochemical activation. PU foils with a rectangular shape of 40 x 10 x 0.1 mm were fixed in the UXF sample holder and were subjected to oscillating stress-strain experiments (Figure 47 A). The strain controlled rotational experiment of **PU 60** showed the dependence of stress with increasing strain up to 90% (Figure 47 B). Directly after starting the experiment, the poly(urethane) elastomer showed only a slightly linear increase in stress with increasing strain (Figure 47 C). This offered the possibility to determine the Young's modulus (E modulus), which describe the stiffness of a material and can be calculated by the slope of a stress-strain curve in the linear elastic region (Figure 47 D).

For **PU 60**, an E modulus of 0.7 MPa was determined which classified the material as a "rubber like" material. Further elongation of the **PU60** caused a higher increase in the resulting stress reaching the plastic region. This inelastic deformation of the material enabled the activation of the included mechanophores due to the uniaxial tension. For the later discussed activation of mechanophores, three different strain values (40%, 60% and 80%) were chosen leading to

stress values of 1.6 MPa, 2.2 MPa as well as 2.8 MPa. However, strain values over 90% could not reach due to the limitation of the device (full turn of the sample holding drum), which prevented the determination of the maximum elongation as well as the tensile strength at break. Unloading the stretched materials resulted in stress values below the initial values, due to loss of energy by structural and morphological changes (plastic deformation) as well as the permanent disruption of the sample.

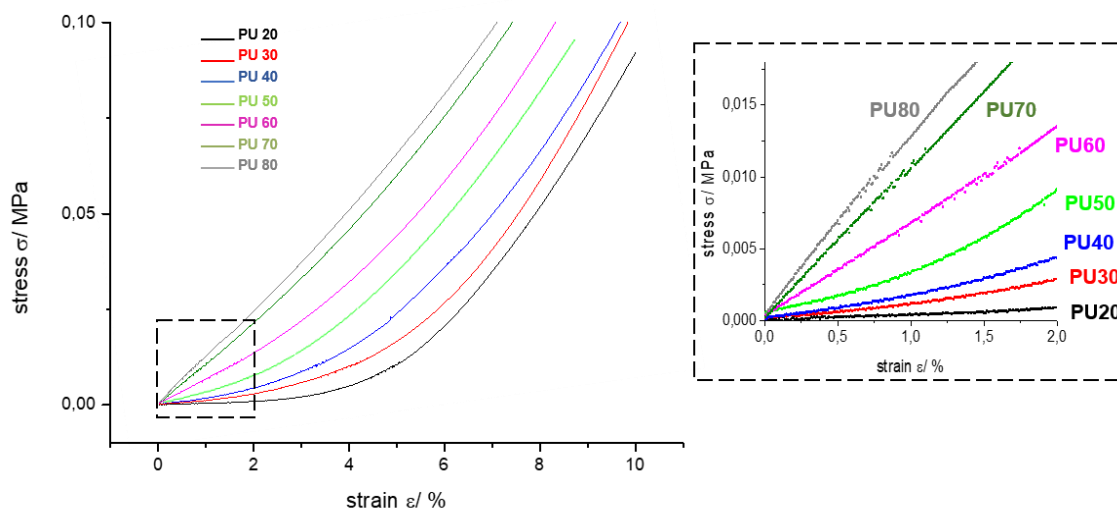


Figure 48. Determination of Young's moduli via linear regression within the elastic regime for poly(urethane) networks varying the OH ratio (tri/bivalent) from 0.2 (**PU20**) to 0.8 (**PU80**).

The experimental Young's modulus, which can be obtained from the previous discussed stress-strain plots, revealed an estimated crosslinking density as average number of networks stands per volume which based on the discussed rubbery elasticity theory (see chapter 1.3.3.2). Within this theory, the Young's modulus is correlated to the tensile storage modulus  $G'$  (equation (2)) including the Poisson coefficient as material parameter (ratio of transverse strain to axial strain during elongation). Subsequently, the required crosslinking density  $\nu_x$  can be calculated, with the assumptions of affine network model, according to equation (3).

$$G' = \frac{E}{2(1 + \mu)} \quad (2)$$

$$G' = \nu_x RT \quad (3)$$

Referring to these equations the Young's modulus of several poly(urethane) networks were determined varying the ratio of bivalent OH functionalities (pTHF + **3**) to trivalent OH functionalities (TMP) from 20/100 (tri/bivalent) (**PU20**) to 80/100 (**PU80**) as shown in Figure 48 and summarized in Table 11. The correlating crosslinking densities range from 0.4 (**PU20**) to 168 mol m<sup>-3</sup> (**PU80**) which allows to tune the material properties and correlate that with the mechanochemical activation that will be discussed later.

Additionally, the swelling ratios  $S$  of the resulting poly(urethane) networks were calculated with equation (4) in which  $W_w$  and  $W_d$  describes the weight of the polymer in the swollen state respectively in the native, dry form. THF was used as a good solvent for the soft domain of the poly(urethane) elastomers to ensure a maximum absorbance of solvent by the polymer until the retractive forces (opposed to the volume increase) overcompensate the forces of swelling<sup>196</sup>.

$$S = \frac{W_w - W_d}{W_d} * 100\% \quad (4)$$

$$Q = \frac{\frac{m_p}{d_p} + \frac{m_s}{d_s}}{\frac{m_p}{d_p}} \quad (5)$$

$$\phi = \frac{1}{1 + Q} \quad (6)$$

$$\frac{\rho}{v_x} = M_c = - \frac{\rho V_m (\phi^{\frac{1}{3}} - \frac{\phi}{2})}{\ln(1 - \phi) + \phi + (\chi \phi^2)} \quad (7)$$

Density polymer  $\rho$  (PU) = 1.101 g cm<sup>-3</sup>

$\phi$  - volume fraction

Density solvent  $\rho$  (THF) = 0.889 g cm<sup>-3</sup>

$m_{p/s}$  - mass of polymer/ solvent

Flory Huggins parameter  $\chi$  (PU) = 0.39

$v_x$  - crosslinking density

Molar volume:  $V_m = 81.09$  cm<sup>3</sup> mol

The absolute values (Table 11) of crosslinking density, which were determined by swelling using the Flory Rehner equation (equation (7)) parameters used from polymer handbook<sup>312</sup>, comparable with the mechanical calculated values, differ. The deviation occurs due to some inaccurate assumptions with respect to the Flory Huggins parameter as well as the affine network theory. Nevertheless, this allows to emerge a trend: The higher the crosslinking feed, the higher the crosslinking density of the material accompanies with an increasing stiffness and a reduced elasticity.

Table 11. Experimental results for the determination of material properties.

Ent.	Comp.	OH Ratio)	E <sup>a)</sup> [MPa]	$\mu^{312}$ [#]	G <sup>b)</sup> [MPa]	$v_x^{c)}$ [mol m <sup>-3</sup> ]	S <sup>d)</sup> [%]	$v_x^{e)}$ [mol m <sup>-3</sup> ]
1	PU20	0.2	0.04		0.01	4	1160	10
2	PU30	0.3	0.10		0.03	12	-	
3	PU40	0.4	0.19		0.06	24	820	37
4	PU50	0.5	0.32	0.49	0.11	45	-	
5	PU60	0.6	0.68		0.23	90	510	86
6	PU70	0.7	1.00		0.34	139	-	
7	PU80	0.8	1.20		0.40	168	420	130

a) Determined via linear regression within the elastic regime of extensional rotational rheology.

b) Calculated according to equation (2).

c) Calculated according to equation (3).

d) Calculated according to equation (4).

e) Calculated according to equation (7)

### 3.5.3. Mechanochemical activation of copper(I)-bis(NHC) complex in poly(urethane) networks

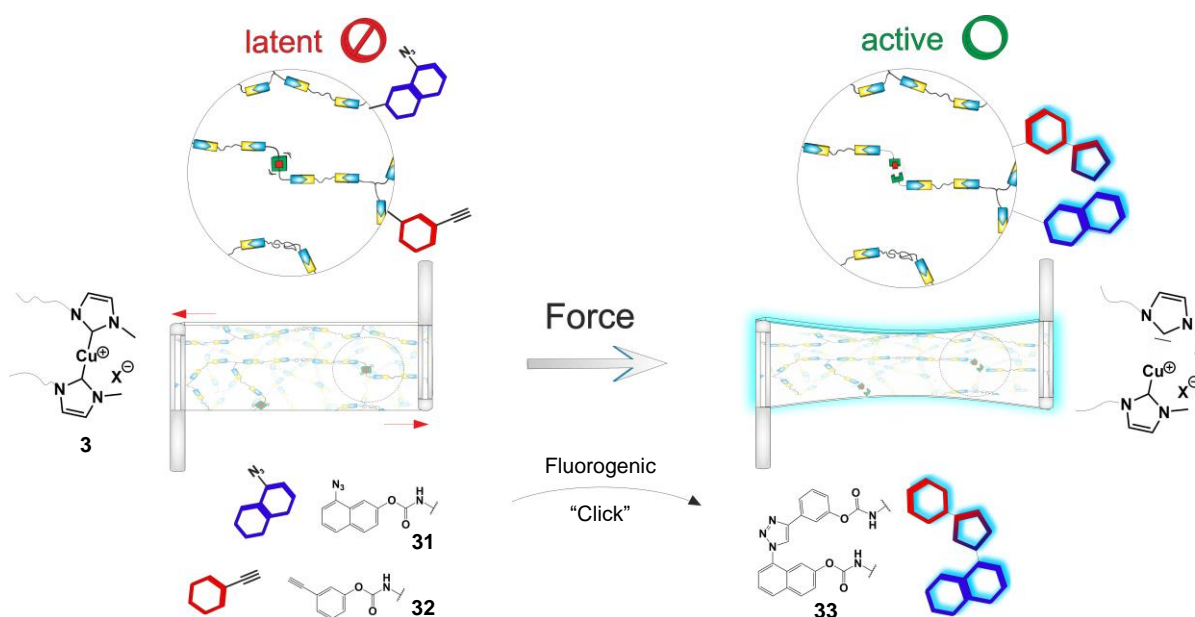


Figure 49. Mechanochemical activation of copper(I)-bis(NHC) complex covalently embedded within poly(urethane) matrix. Extensional oscillating rheology triggers the fluorogenic “click” reaction of initially non-fluorescent 8-azidonaphthalene-2-ol (**31**) with 3-hydroxyphenylacetylene (**32**) resulting in the formation of a highly fluorescent 8-(4-(3-hydroxyphenyl)-1,2,3-triazol-1-yl)naphthalen-2-ol (**33**).

In order to study the mechanochemical response of the copper(I)-bis(NHC) complex (**3**) which was covalently linked into the poly(urethane) network, extensional oscillatory rheology was conducted (Figure 49). This allowed applying defined stress values to the system and also offered to correlate the catalytic activity and thus the mechanochemical response to the previous determined material properties. In contrast to our previous developed mechanophoric system, the new all-in-one PU approach did not require an additional matrix material as it formed the matrix by the PU scaffold itself, which allows to direct the force to the labile copper carbene bond. This circumvents potential miscibility problems of the mechanophore and the matrix material itself and enable to tune precisely the mechanochemical activation without time-consuming adaption of the catalyst polymer linkage. Furthermore, a simple tunability of material properties in terms of strength and stiffness is possible by varying the number of crosslinking points, the nature of the soft- as well as hard domain and the defined amount of low molecular weight copper(I)-bis(NHC) complex (**3**). Thus, the so obtained, highly transparent material displayed a sufficient stiffness for mechanochemical activation to act as a kind of lever as well as guarantee the necessary mobility for the subsequent mechanical activation process without backbone fragmentation.

#### 3.5.3.1. Quantification of fluorogenic “click” reaction during mechanochemical activation

The mechanochemical activation was accomplished via oscillating tensile rheology applying defined stress rates and deformations to mechanophore containing poly(urethane) films (**PU20** – **PU80**) with rectangular shape (40 x 10 x 0.1 mm) (containing  $0.85 \mu\text{mol}_{(\text{Cu})} \text{g}^{-1}_{(\text{sample})}$ ), which were fixed in the UXF sample holder and subjected to oscillating stretch experiments for 24 h (Figure 50 A). Afterwards, the increase in fluorescence was measured three times at three

different positions at an emission wavelength of 437 nm (excitation wavelength 377 nm). During one cycle experiment (24 h) the material was deformed plastically which activate the incorporated mechanophores and led to a loss of the peak stress as well as the plateau value of the storage modulus (Figure 50 B). Subsequently, the procedure was repeated until a plateau value of fluorescence intensity was reached. Several control experiments were conducted at room temperature to neglect the premature activation of mechanophores during preparation (Figure 50 C). The samples were stored at room temperature for 96 h in total, in which the fluorescence intensity was measured every 24 h observing no significant increase at room temperature. Heating up the sample for 96 h to 60°C the intensity increases with time, which is attributed to the thermal activation of included copper(I)-bis(NHC) complex. Furthermore, oscillation experiments (80%, 0.5 s<sup>-1</sup>) were conducted in which the catalyst was excluded, proving thus the essential of copper(I)-bis(NHC) complex and also neglect a potential stress induced AAC. Finally, a model complex bearing low molecular weight urethane side chains was synthesized, by converting **3** with hexyl isocyanate. This prevents the covalently integration of the mechanophore into the poly(urethane) network to prove the force transmission via the polymeric handles.

The actual activation experiment was realized with the poly(urethane) foil **PU 60** including the fluorogenic “click” system as well as the covalently embedded catalyst which were tested under the same conditions (80%, 0.5 s<sup>-1</sup>). An increase of fluorescence intensity with time was observable reaching a plateau value after 96 h with conversion up to 16% (Figure 50 C and D). This plateau value turned out as a characteristic feature of the fluorogenic “click” reaction in bulk, independently of experimental or structural parameters. This is ascribable on the one hand to the oxidation of included Cu(I) to Cu(II) over time which retards the CuAAC as well as the limited spatial proximity of the covalently anchored dyes ((**31**) and (**32**)) to the catalyst.

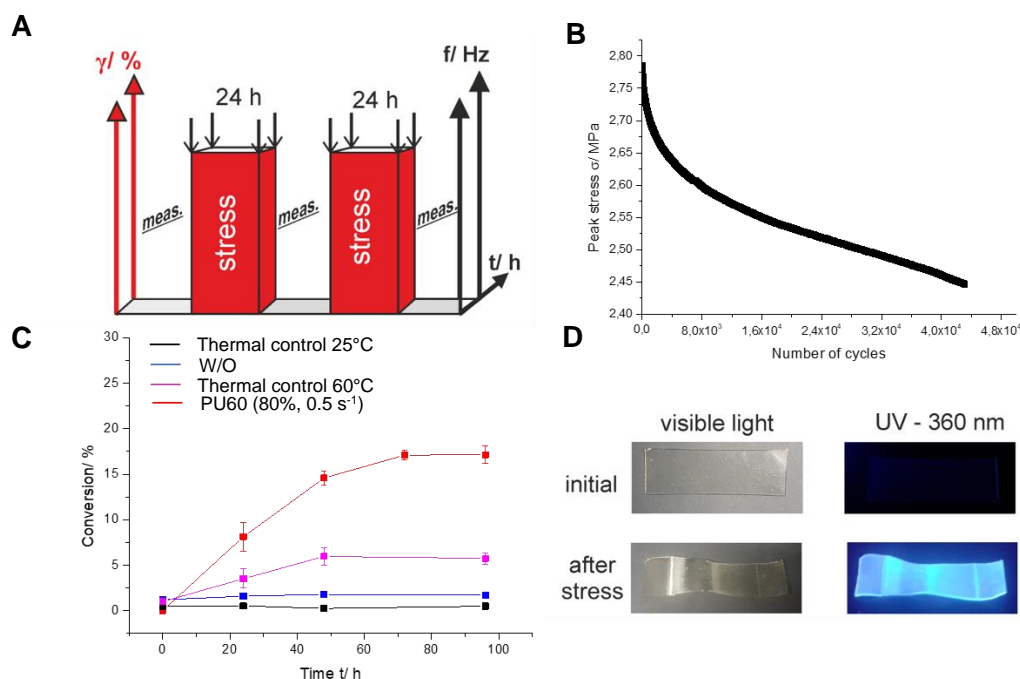


Figure 50. (A) Schematic protocol of rheological and fluorescence measurements of 24 h tensile rheological treatment interrupted by fluorescence spectroscopic measurements. (B) Peak stress behavior during one cycle experiment (24 h) (C) Thermal and pure control experiments in comparison with activation experiment of **PU 60** D: Images of PU networks before and after activation in white and UV-light (366 nm).

In order to enable an optimal force transmission within the network and thus activate the embedded mechanophore efficiently the correct placement of the mechanophores turned out to be crucial for the final results.

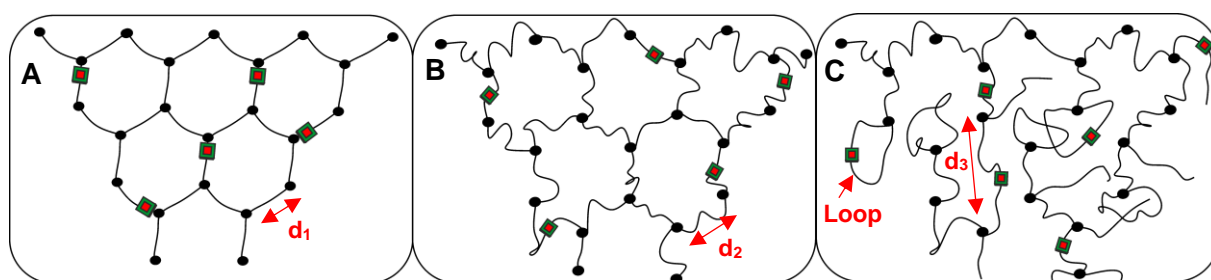


Figure 51. Schematic representation of **PUXX** (A) without (B) with 10 min as well as (C) with 30 min prepolymerization time in which the distance between crosslinking points ( $d_x$ ) increase with increasing time ( $d_1 < d_2 < d_3$ ).

Pre-experiments revealed that the simultaneous addition of linear components and crosslinker resulted in an inefficient activation of formed mechanophoric network (10% conversion in CuAAC of **31** and **32**) (Figure 52 A). This can be explained by the non-optimal positioning of the Cu-mechanophores close to the midpoint of a polymer strand due to the differing reactivity of low molecular weight components and pTHF, which in turns led to lower chain lengths between the respective crosslinking points (Figure 51 A).

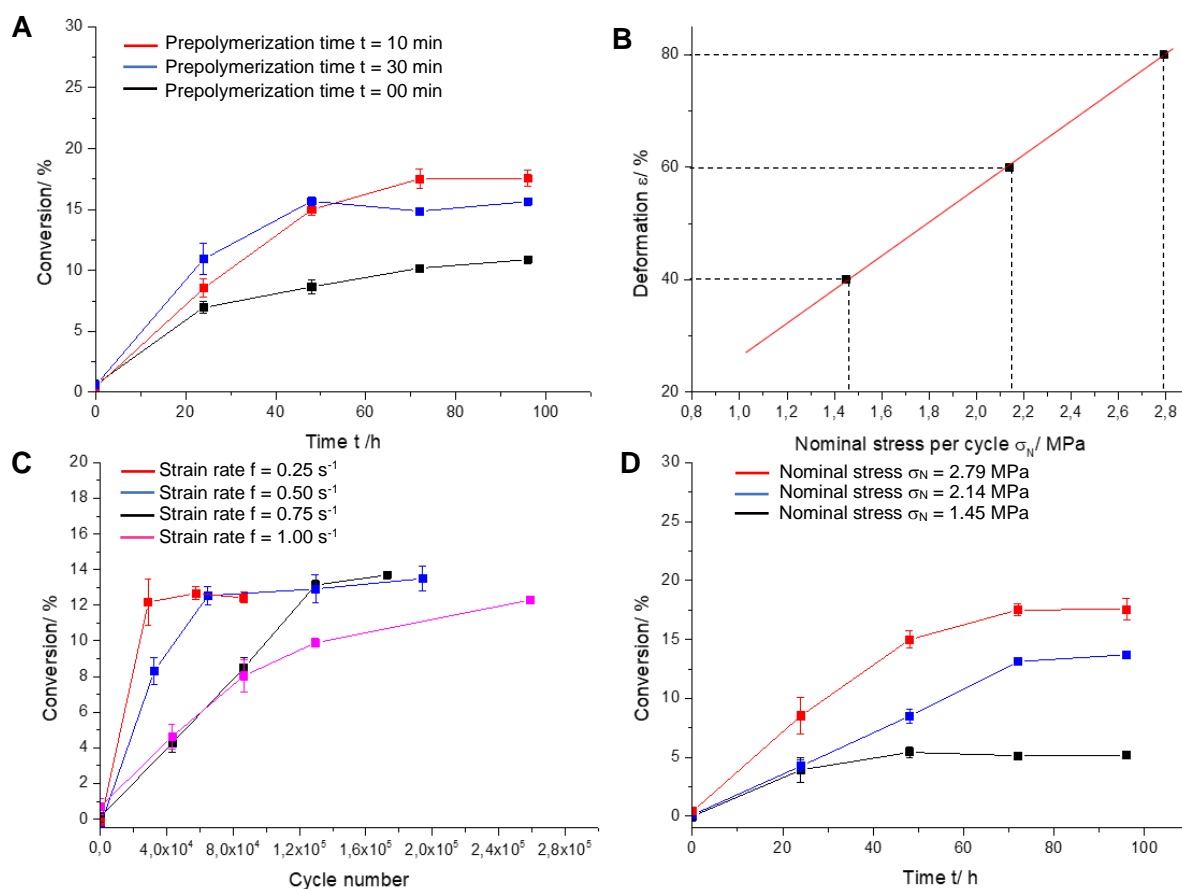


Figure 52. (A) Prepolymerization time dependence of **PU60** during mechanochemical activation. (B) Correlation of adjusted deformation and resulting nominal stress  $\sigma_N$ . (C) Stress rate dependence of **PU60** during mechanochemical activation. (D) Deformation dependence of **PU60** during mechanochemical activation.

Prepolymerization reactions of **3** with HDI and pTHF were performed leading to an *in situ* generated  $\alpha$ ,  $\omega$ -isocyanate-telechelic pTHF chain extended copper(I)-bis(NHC) which can further react with the  $\alpha$ ,  $\omega$ -telechelic bis(hydroxy) pTHF and finally crosslinked by the trivalent TMP crosslinker. This offered longer chain lengths of polymer strands (Figure 51 B) which enhanced the force transmission and resulted in higher mechanochemical activation (18% conversion). Further increase of prepolymerization time (30 min) revealed an extension of respective polymer strands ( $M_n = 6000 \text{ g mol}^{-1}$ ) and resulted in a lower mechanochemical response (15% conversion) presumably due to increased loops during the network formation (Figure 51 C). These loops impair the force transmission in all direction and prevent an optimal force yield, which is guaranteed by the central positioning of the copper(I)-bis(NHC) moiety. Further activation experiments were done with a prepolymerization time of 10 min. In order to investigate the stress rate dependency of the CuAAC in bulk, **PU60** with a ratio of 60/100 (tri/bivalent alcohols) was used, chosen by the optimal balance between toughness, elasticity and activation. The forces which act at different deformations, are shown in Figure 52 B, revealing the increase in nominal stress with increasing deformation. At a strain of  $\gamma = 60\%$  (correlates to nominal stress  $\sigma_N = 2.14 \text{ MPa}$ ) and a variable stress rate, a stepwise increase in fluorescence intensity with increasing time was visible in all cases. With increasing stress rate an accelerated mechanophore activation (determined again by the increasing fluorescence of formed **33** due to the triggered CuAAC) could be observed, represented by a larger slope (Figure 52 C).

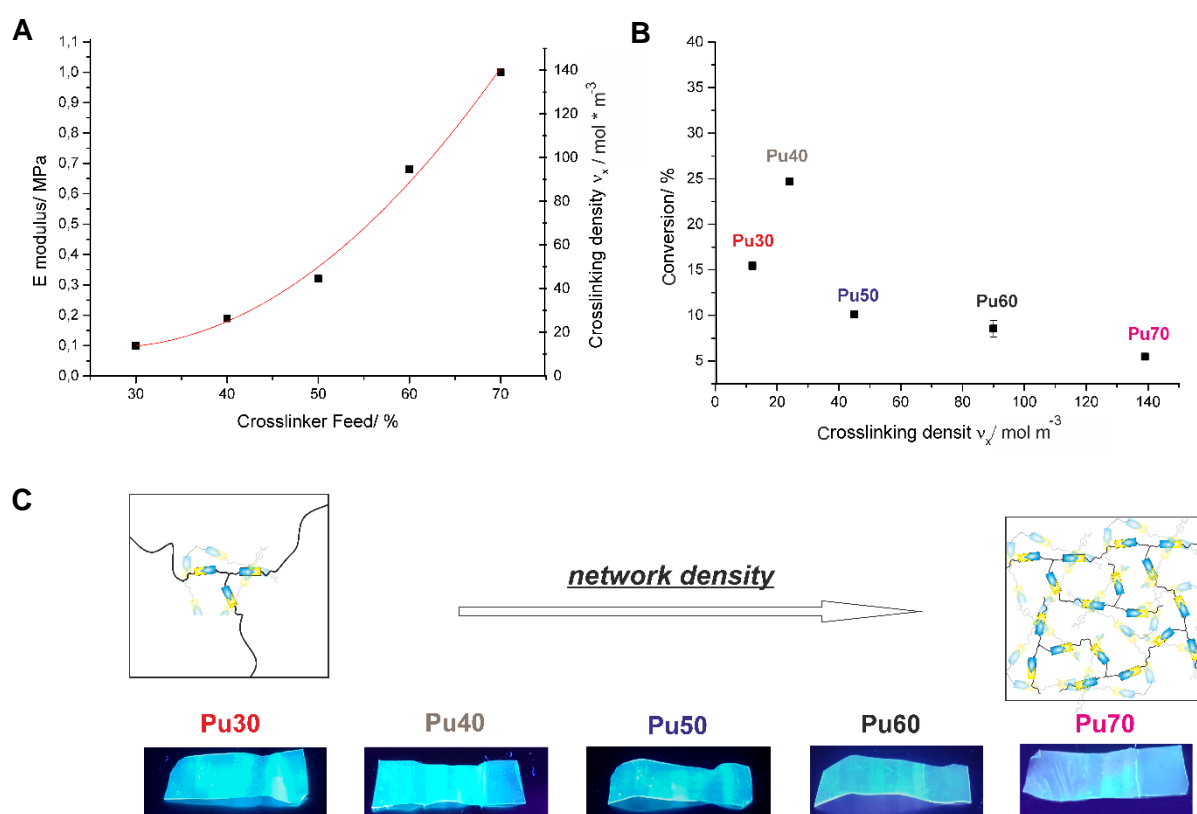


Figure 53. (A) Correlation of Young's modulus and calculated crosslinking densities to crosslinker feed. (B) crosslinking density correlated with conversion in a force induced CuAAC and (C) images of different PU networks (**PU30 – PU70**) after activation process ( $t = 24\text{h}$ ,  $f = 0.5 \text{ s}^{-1}$ ,  $\gamma = 80\%$ ) in UV light (360 nm).

However, the overall activation is stress rate independent, which was revealed by a constant conversion of 12% in CuAAC for  $0.25 \text{ s}^{-1}$ ,  $0.50 \text{ s}^{-1}$ ,  $0.75 \text{ s}^{-1}$  as well as  $1.00 \text{ s}^{-1}$ . Therefore, the stress rate was fixed to  $0.50 \text{ s}^{-1}$  and 96 h for further investigations to prevent a premature

rupture of the sample by fatigue failure. The deformation dependency was investigated by a stepwise increase in deformation, and thus, the acting nominal stress, observing an enhancement of overall mechanochemical activation (Figure 52 D) due to the elongated effective tension length. Deformations of  $\gamma = 40\%$  ( $\sigma_N = 1.45$  MPa) revealed CuAAC conversions up to 5%, 60% deformation ( $\sigma_N = 2.14$  MPa) caused an increase up to 12%, while 80% deformation ( $\sigma_N = 2.79$  MPa) finally increase the CuAAC conversion up to 17%. A further enhanced deformation could not be realized due to limitations in the experimental setup (full turn of the fixing drums).

Table 12. Calculated conversions for the fluorogenic “click” reaction of the non-fluorescent 8-azidonaphthalen-2-ol (26) with 3-hydroxyphenylacetylene (27) yielding fluorescent 7 fluorescent 8-(4-(3-hydroxyphenyl)-1,2,3-triazol-1-yl)naphthalen-2-ol (28) by varying experimental parameters ( $\text{DeformationPUXX}^{\text{Frequency}}$   $\text{Precondensation time}$ )

Ent.	Poly(urethane) network				
	Compound	Deformation [%]	Stress rate [ $\text{s}^{-1}$ ]	Precond. time [min]	Conversion [%]
<b>Control experiments</b>					
1	W/O	80	0.50	10	2
2	LMW				0
3	25°C				1
4	60°C			10	6
<b>Precondensation time dependence</b>					
5	Pu-60 <sub>0</sub>	80	0.50	0	11
6	PU-60 <sub>10</sub>			10	18
7	PU-60 <sub>30</sub>			30	16
<b>Frequency dependence</b>					
8	PU-60 <sup>0.25</sup>	80	0.25	10	12
9	PU-60 <sup>0.50</sup>		0.50		14
10	PU-60 <sup>0.75</sup>		0.75		14
11	PU-60 <sup>1.00</sup>		1.00		12
<b>Deformation dependence</b>					
12	<sup>40</sup> Pu-60	40	0.50	10	6
13	<sup>60</sup> PU-60	60			14
14	<sup>80</sup> PU-60	80			18
<b>Crosslinking density dependence</b>					
16	PU30	80	0.50	10	16 <sup>a)</sup>
17	PU40				25 <sup>a)</sup>
18	PU50				11 <sup>a)</sup>
19	PU60				9 <sup>a)</sup>
20	PU70				5 <sup>a)</sup>

a) Conversion after 24 h.

PU-foils with precisely adjusted densities (**PU20 – PU80**) were prepared by varying the ratio of bivalent (chain-extending) and trivalent (crosslinking) functionalities as previous discussed. The crosslinking density was determined by stress strain experiments via gradual increasing of deformation ( $0.01 \leq \gamma \leq 2.00\%$ ) revealing the E-modulus by determining the slope within the linear elastic area ( $0.01 \leq \gamma \leq 0.50\%$ ) and thus obtaining the crosslinking densities which increase exponential with increasing crosslinker feed. (Figure 53 A). Subsequently, fluorescence measurements were performed to quantify the influence of the crosslinking density in response to their mechanochemical activation (Figure 53 B, C) applying the previously discussed optimal activation conditions (80% deformation and  $0.50 \text{ s}^{-1}$  stress rate). As expected, the overall activation of mechanophore is enhanced with decreasing crosslinking density (**PU70 – 5.2%** and **PU 60 – 8.5%** and **PU 50 – 10.1%**), due to the longer chain

extension between crosslinking points and the accompanying enhancement of the mechanochemical response. However, the highest conversion of 25% could be determined for **PU 40** with  $v_x$  of 24 mol m<sup>-3</sup>. We propose that in this region the optimal OH-ratio of the chain extended polymer chains act as handles for the copper(I)-bis(NHC) complex and thus improve its mechanochemical response and trivalent crosslinker, which directs the acting force three-dimensionally (Figure 51). With further decreasing crosslinking density, a lower conversion is observed caused by excessive chain extension between crosslinking points, resulting in a suboptimal force transmission whereby the activation of mechanophores is deteriorated.

Summarized, the developed all-in-one mechanocatalytical PU system, which contains a covalently incorporated low molecular weight copper(I)-bis(NHC) complex (**3**) and incorporated fluorogenic dye precursors (**31**, **32**), proved its potential for the application as damage sensing material. Thus, the disadvantages of the coumarin based system could be overcome by the exclusion of an external matrix, the implemented material transparency as well as the easy tunability of material properties in terms of elasticity and force transmission. Thus, a completely transparent force responsive poly(urethane) material is designed, beneficial and easy to adapt.

#### 3.5.4. Self-healing ability

In order to expand the mechanophore concept a material should be generated which gives an optical response and can form an additional covalent network solely due to effect of mechanical stress.

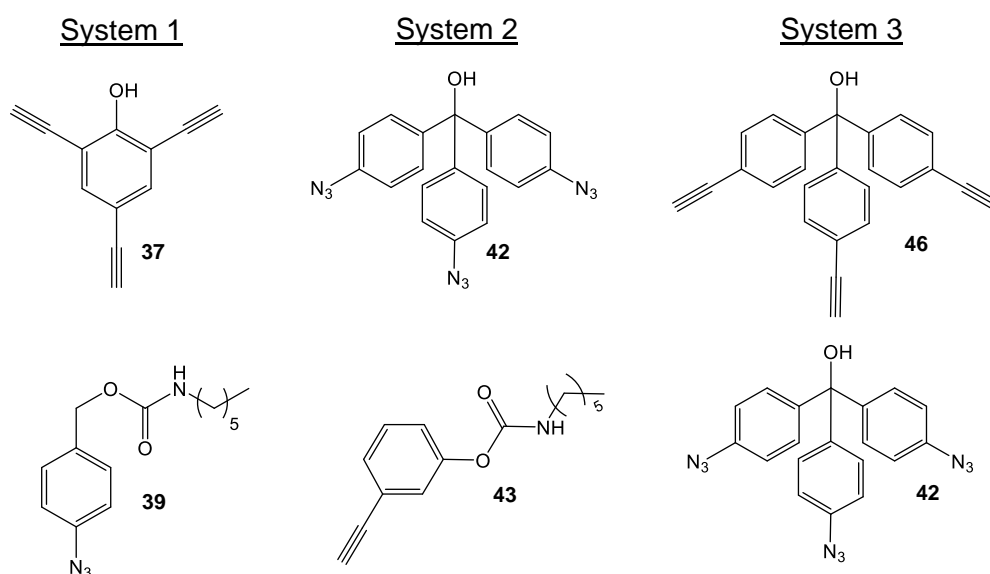


Figure 54. Several fluorogenic systems for potential use as stress-sensing approach accompanies by simultaneous self-healing.

By using multivalent fluorogenic dyes the force induced CuAAC could initiate a crosslinking reaction which could lead to an autonomous self-healing ability. For this purpose, a trivalent alkyne (**37**) was synthesized in which the stepwise expansion of the conjugated system during CuAAC should lead to a fluorescence signal with a shifting emission maximum depending on the degree of crosslinking. The determination of optical properties (see Figure A 90) in solution revealed the occurrence of an initial fluorescence caused by substrates as well as the overlapping of the emission maxima of trivalent alkyne and the “click” product. This allows the potential usage for additional crosslinking agents but hindered the detection as well as the quantification of ongoing self-healing reaction.

To circumvent the limitations further crosslinking agent (**42**) were synthesized that exhibited fluorescence behavior solely initiated by mechanical stress. This could approve by determination of their optical properties in solution (see Figure 55 A, B) in which the embedding of **42** and **43** in the previous discussed PU networks and the subsequent activation via extensional rheology offered an increase in optical response (see Figure 55 C).

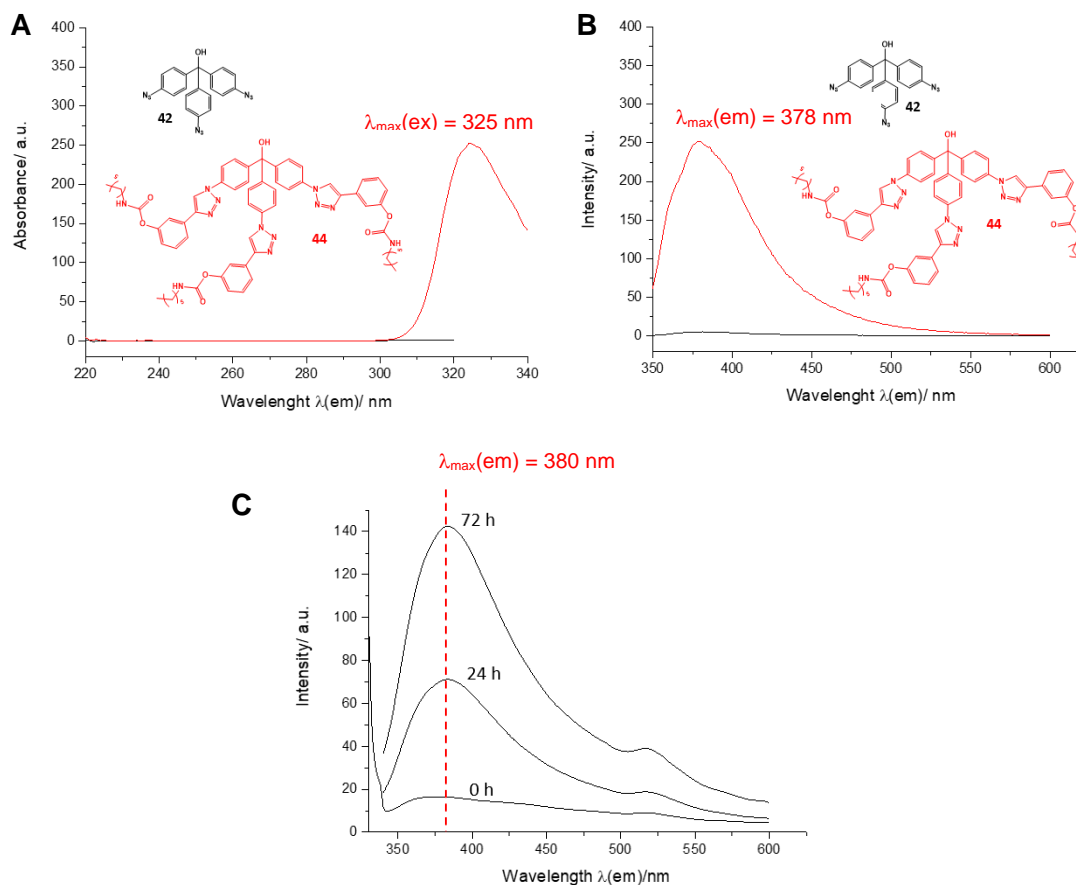


Figure 55. Optical properties of the trivalent fluorogenic system. (A) UV-spectrum of **42** (black) and **44** (red) in THF and (B) fluorescence spectrum of **42** (black) and **44** (red) in THF after excitation at  $\lambda_{\text{ex}} \approx 341 \text{ nm}$ . (C) Fluorescence intensity after excitation at  $\lambda_{\text{ex}} \approx 341 \text{ nm}$  during activation process of **42** and **32** embedded within a PU matrix via extensional rheology ( $f = 0.5 \text{ s}^{-1}$ ,  $\gamma = 80\%$ ).

This could further expand by the simultaneous usage of the trivalent azide **42** and a new synthesized trivalent alkyne **46** in which preliminary results emphasize these dyes as potential candidates for the combination of stress-sensing and self-healing approaches.

## 4. Experimental Part

### 4.1. Methods and materials

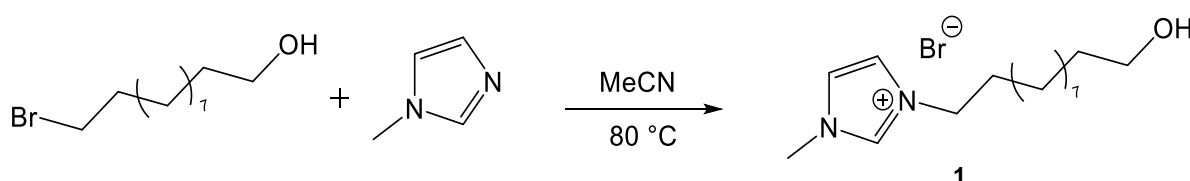
All reactions were carried out under dry inert argon atmosphere using common Schlenk techniques unless noted. All solvents were purchased in technical grade and were distilled before use, while dry solvents were prepared using standard drying techniques and degassed by freeze-pump-thaw-cycles. Chemicals were purchased from Sigma-Aldrich or VWR and used as received. *N*-methylimidazole were dried over molecular sieve and distilled after purchasing. Copper(I)-bromide was washed three times with acetic anhydride, dry ethanol and finally with dry diethyl ether and was stored in a Schlenk tube within the glove box. High molecular weight PTHF matrix ( $M_{n(\text{GPC})} = 112\,000\text{ g mol}^{-1}$ ) was synthesized via cationic ring opening polymerization using methyl trifluoromethanesulfonate as initiator and methanol for quenching. Column chromatography was performed on Merck silica gel 60 (230 – 400 mesh). PTHF was purchased from Sigma Aldrich with a molecular weight of  $M_n = 2900\text{ g mol}^{-1}$  and polydispersity of  $\bar{D} = 1.60$ . Fluorescence measurements were carried out in the bulk state on a Cary Eclipse fluorescence spectrometer from Agilent, fixing the samples with a solid sample holder between two quartz glass slides. Emission spectra were recorded after excitation at 377 nm with a maximum at 438 nm and repeated at least three times. UV measurements were carried out via Perkin Elmer UV/vis Lambda 365 using Helma analytics quartz glass cuvettes ( $d = 10\text{ mm}$ ) with a concentration of  $0.20\text{ mmol L}^{-1}$  in THF. NMR spectra were recorded on a Varian Gemini 400 or 500 spectrometer at  $27^\circ\text{C}$ . Chemical shifts ( $\delta$ ) are reported in ppm and referred to the solvent residual signal ( $\text{CDCl}_3$  7.26 ppm for  $^1\text{H}$  and 77.0 ppm for  $^{13}\text{C}$ ;  $\text{THF-}d_8$  3.58 and 1.72 ppm for  $^1\text{H}$  as well as 67.2 and 25.3 ppm for  $^{13}\text{C}$ ;  $\text{DMSO-}d_6$  2.50 ppm for  $^1\text{H}$  and 39.5 ppm for  $^{13}\text{C}$ ). GPC was performed on a Viscotek GPCmax VE 2001 with a set of a  $\text{H}_{\text{HR}}\text{-H Guard-17369}$  and a  $\text{GM}_{\text{HR}}\text{-N-18055}$  main column in DMF with  $0.75\text{ mM LiNTf}_2$  at  $60^\circ\text{C}$ . Detection was realized with a refractive index VE 3580 RI detector from Viscotek at  $35^\circ\text{C}$ . The injection volume was  $100\text{ }\mu\text{L}$  with a standard sample concentration of  $5\text{ mg mL}^{-1}$  in DMF and the flow rate was adjusted to  $1\text{ mL min}^{-1}$ . External calibration was done using poly(styrene) (PS) standards (purchased from PSS) with a molecular weight range from 1050 to  $115\,000\text{ g mol}^{-1}$ . Preparative GPC was performed on a VWR HITACHI Chromaster using a KD-2002.5 column from Shodex in DMF at  $55^\circ\text{C}$ . The detection of the refractive index was performed with a RI detector from VWR at  $50^\circ\text{C}$ . The concentration of the samples was adjusted to  $50 - 100\text{ mg mL}^{-1}$  and a flow rate of  $0.35\text{ mL min}^{-1}$  to  $0.70\text{ mL min}^{-1}$  resulting in pressures ranging from 6 to 21 bar. EZChrom Elite (version 3.3.2 SP2) was used for analyzing the data.

ESI-TOF-MS measurements were performed on a Bruker Daltonics microTOF via direct injection with a flow rate of  $180\text{ }\mu\text{L h}^{-1}$  using the positive or negative mode with an acceleration voltage of 4.5 kV. Samples were prepared by dissolving in HPLC grade solvent at a concentration of  $1\text{ mg mL}^{-1}$  without additional salt. MALDI-TOF-MS experiments were conducted on a Bruker Autoflex III system equipped with a smart beam laser (355 nm, 532 nm, 808 nm and  $1064\text{ nm} \pm 5\text{ nm}$ ; 3 ns pulse width; up to 2500 Hz repetition rate) accelerated by a voltage of 20 kV and detected as positive ions operating either in reflectron or linear mode. The ratio of matrix:analyte:salt was 100:10:1 and  $1\text{ }\mu\text{L}$  of a solution was spotted on a MALDI-target plate adjusting samples concentration of  $10\text{ mg mL}^{-1}$  in THF, matrix concentration (dithranol or DCTB) of  $20\text{ mg mL}^{-1}$  in THF and LiTFA or NaTFA salt concentration of  $10\text{ mg mL}^{-1}$  in THF. ATR-IR spectra were recorded on a Bruker Tensor Vertex 70 additionally

equipped with a Golden Gate Heated Diamond ATR Top-plate. For analyzing data Opus 6.5 and OriginPro 8G SR4 (v8.0951) was applied. Differential scanning calorimetry (DSC) experiments were performed in aluminium pans using a DSC 204 F1 Phoenix provided from NETZSCH. Samples were measured in a temperature range of  $-40^{\circ}\text{C}$  to  $180^{\circ}\text{C}$  with a heating rate of  $10\text{ K min}^{-1}$  and data interpretation was accomplished using Proteus Thermal Analysis (V 5.2.1). The crystallinity was determined with  $172\text{ J/g}$  as  $\Delta H_{m0}$  for 100% crystallinity<sup>311</sup>. Melting rheology experiments were performed on Anton Paar (Physica) MCR 101/SN 80753612 using parallel plate-plate geometry ( $d = 8\text{ mm}$ ). The temperature was controlled with a thermoelectric cooler/heater in a chamber filled with dry air. Extensional oscillatory and rotational rheology experiments of thin films were conducted on Anton Paar (Physica) MCR 101/SN 80753612 via Universal Extensional Fixture (UXF) at  $20^{\circ}\text{C}$ . Therefore, the films with rectangular shape ( $40 \times 15 \times 0.15\text{ mm}$ ) containing  $0.85\text{ }\mu\text{mol}_{(\text{Cu})}\text{ g}^{-1}_{(\text{sample})}$  were fixed in the UXF sample holder and subjected to oscillating stretch experiments. To investigate the influence of the strain rate towards the mechanochemical activation of the Cu(I)-bis(NHC) catalysts, the strain rate was varied from  $0.25\text{ s}^{-1}$ ,  $0.5\text{ s}^{-1}$ ,  $0.75\text{ s}^{-1}$  to  $1.0\text{ s}^{-1}$ , while keeping the deformation constant at  $\gamma = 60\%$ . The deformation dependency of the mechanochemical activation was investigated varying the deformation from 40%, 60% to 80% and keeping the frequency constant at  $0.5\text{ s}^{-1}$ . Crosslinking dependence investigations were done with a strain rate of  $0.5\text{ s}^{-1}$  and deformation of 80%.

## 4.2. Synthesis of low molecular weight copper(I)-bis(NHC) complexes

### 4.2.1. Synthesis of 3-(11-hydroxyundecyl)-1-methylimidazolium bromide (1)



Scheme 1. Synthesis of 3-(11-hydroxyundecyl)-1-methylimidazolium bromide (1).

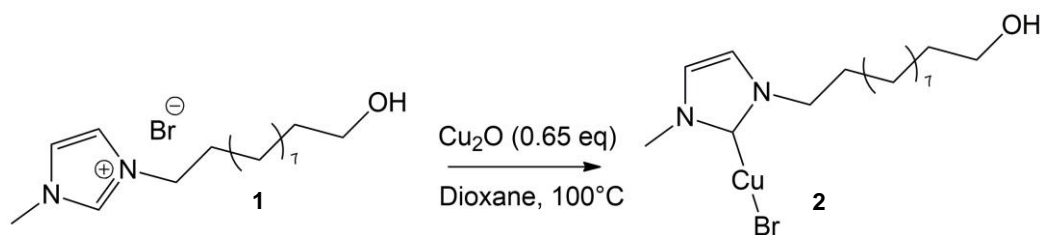
1-Methylimidazole (3.01 mL, 38 mmol) was added to a suspension of 11-bromoundecan-1-ol (10.00 g, 40 mmol) in acetonitrile (MeCN) (50 mL) at room temperature (RT) and was stirred for 24 h at  $80^{\circ}\text{C}$ . The reaction mixture was allowed to come to RT and was diluted with diethyl ether ( $\text{Et}_2\text{O}$ ) (120 mL). The resulting precipitate was filtered off, washed again with  $\text{Et}_2\text{O}$  (3 x 50 mL) and **1** was obtained as colorless solid after drying in high vacuum (12.41 g, 37.24 mmol, 98%).

**$^1\text{H-NMR}$  (DMSO- $d_6$ , 400 MHz):**  $\delta$  [ppm] 9.20 (*d*,  $^3J_{\text{H,H}} = 1.7\text{ Hz}$ , 1H, NCHN), 7.80 (*t*,  $^3J_{\text{H,H}} = 1.8\text{ Hz}$ , 1H, NCHCHN), 7.73 (*t*,  $^3J_{\text{H,H}} = 1.8\text{ Hz}$ , 1H, NCHCHN), 4.31 (*t*,  $^3J_{\text{H,H}} = 5.1\text{ Hz}$ , 1H, OH), 4.16 (*t*,  $^3J_{\text{H,H}} = 7.2\text{ Hz}$ , 2H, NCH<sub>2</sub>), 3.86 (*s*, 3H, NCH<sub>3</sub>), 3.36 (*td*,  $^3J_{\text{H,H}} = 6.5$ ,  $^4J_{\text{H,H}} = 4.9\text{ Hz}$ , 2H, OCH<sub>2</sub>), 1.83 – 1.69 (*m*, 2H, NCH<sub>2</sub>CH<sub>2</sub>), 1.39 (*p*,  $^3J_{\text{H,H}} = 6.7\text{ Hz}$ , 2H, OCH<sub>2</sub>CH<sub>2</sub>), 1.20 – 1.31 (*m*, 14H, (CH<sub>2</sub>)<sub>7</sub>).

**$^{13}\text{C NMR}$  (DMSO- $d_6$ , 100 MHz):**  $\delta$  [ppm] 136.5 (NCHN), 123.5 (CH<sub>3</sub>NCHCHN), 122.2 (CH<sub>3</sub>NCHCHN), 60.6 (OCH<sub>2</sub>), 48.7 (NCH<sub>2</sub>), 35.7 (NCH<sub>3</sub>), 32.5 (OCH<sub>2</sub>CH<sub>2</sub>), 29.3, 29.0, 28.9, 28.9, 28.8, 28.3, 25.5, 25.4.

ESI-TOF MS (positive mode, MeOH,  $m/z$ ):  $[M-Br]^+$  found 253.228, simulated 253.227 for  $C_{15}H_{29}N_2O^+$ .

#### 4.2.2. Synthesis of copper(I) mono(NHC) complex (**2**)



Scheme 2. Synthesis of Cu(I) mono(NHC) complex (**2**) using copper(I) oxide method.

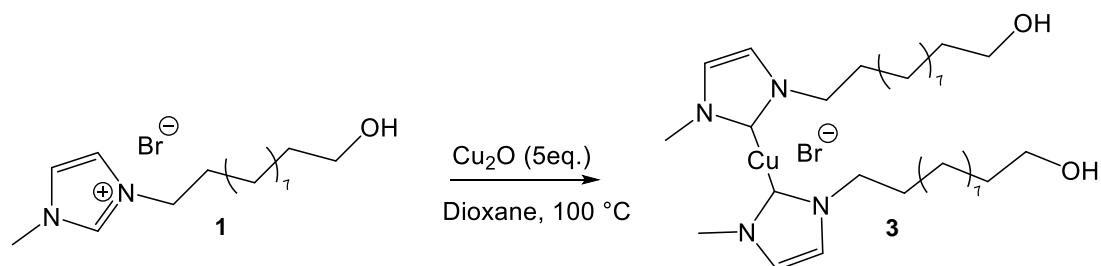
Compound **1** (780 mg, 2.34 mmol) and copper(I)-oxide (220 mg, 1.52 mmol, 0.65 eq.) were suspended in dry 1,4-dioxane (4.8 mL) and stirred at 100°C for 24 h. After cooling to RT, the reaction mixture was filtered twice, and the solvent was removed under reduced pressure. The residue was dissolved in dichloromethane (DCM) (10 mL) and was precipitated in *n*-hexane (15 mL). Cu(I) mono(NHC) complex (**2**) was obtained as a colorless solid (1.07 g, 2.70 mmol, 90%) after drying in high vacuum.

$^1H$ -NMR (THF- $d_6$ , 500 MHz):  $\delta$  [ppm] 7.15 (d,  $^3J_{H,H} = 17.2$  Hz, 2H, NCHCHN), 4.13 (t,  $^3J_{H,H} = 7.0$  Hz, 2H, NCH<sub>2</sub>), 3.81 (s, 3H, NCH<sub>3</sub>), 3.46 (q,  $^3J_{H,H} = 5.9$  Hz, 2H, OCH<sub>2</sub>), 3.26 (t,  $^3J_{H,H} = 4.7$  Hz, 1H, OH), 1.86 (p,  $^3J_{H,H} = 7.2$  Hz, 2H, NCH<sub>2</sub>CH<sub>2</sub>), 1.45 (p,  $^3J_{H,H} = 6.9$  Hz, 2H, OCH<sub>2</sub>CH<sub>2</sub>), 1.39 – 1.25 (m, 14H, (CH<sub>2</sub>)<sub>7</sub>).

$^{13}C$ -NMR (THF- $d_6$ , 125 MHz):  $\delta$  [ppm] 171.3 (NCCuN), 121.7 (CH<sub>3</sub>NCHCHN), 120.5 (CH<sub>3</sub>NCHCHN), 61.6 (NCH<sub>3</sub>), 50.7 (NCH<sub>2</sub>), 37.1 (OCH<sub>2</sub>), 33.1 (NCH<sub>2</sub>CH<sub>2</sub>), 31.4 OCH<sub>2</sub>CH<sub>2</sub>, 29.6, 29.5, 29.5, 29.4, 29.1, 26.3, 25.9.

ESI-TOF MS (negative mode, THF,  $m/z$ ):  $[M+Br]^-$  found 474.982, simulated 474.984 for  $C_{15}H_{28}Br_2CuN_2O^-$ .

#### 4.2.3. Synthesis of OH end-capped copper(I)-bis(NHC) complex (**3**)



Scheme 3. Synthesis of copper(I)-bis(NHC) complex (**3**) using copper(I) oxide method.

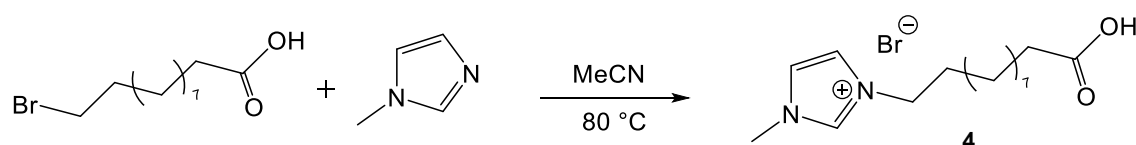
Compound **1** (2.0 g, 6.0 mmol) and copper(I)-oxide (4.3 g, 30.0 mmol, 5 eq.) were suspended in dioxane (50 mL) and stirred at 100°C for 3 days. After cooling to RT, excess of Cu<sub>2</sub>O was filtered off. The solvent was removed under reduced pressure. Compound **3** (1.55 g, 2.4 mmol, 40%) was obtained after column chromatography on silica by gradually changing the polarity of solvent from pure CHCl<sub>3</sub> to CHCl<sub>3</sub>/MeOH 20/1 ( $R_f = 0.40$  CHCl<sub>3</sub>/MeOH 20/1) as a light yellow solid.

$^1\text{H-NMR}$  (THF- $d_6$ , 400 MHz):  $\delta$  [ppm] 6.27 – 6.23 (m, 4H, NCHCHN), 3.51 (t,  $^3J_{\text{H,H}} = 7.2$  Hz, 4H, NCH<sub>2</sub>), 3.46 (q,  $^3J_{\text{H,H}} = 6.4$  Hz, 4H, OCH<sub>2</sub>), 3.35 (t,  $^3J_{\text{H,H}} = 5.2$  Hz, 2H, OH), 3.12 (s, 6H, NCH<sub>3</sub>), 1.60 (p,  $^3J_{\text{H,H}} = 7.2$  Hz, 4H, NCH<sub>2</sub>CH<sub>2</sub>), 1.47 (p,  $^3J_{\text{H,H}} = 6.9$  Hz, 4H, OCH<sub>2</sub>CH<sub>2</sub>), 1.31 (m, 28H, (CH<sub>2</sub>)<sub>14</sub>).

$^{13}\text{C-NMR}$  (CDCl<sub>3</sub>, 100 MHz):  $\delta$  [ppm] 153.2 (NCCuN), 111.1 (CH<sub>3</sub>NCHCHN), 109.9 (CH<sub>3</sub>NCHCHN), 62.9 (NCH<sub>2</sub>), 43.6 (OCH<sub>2</sub>), 32.8, 30.3, 29.5, 29.5, 29.4, 29.4, 29.3, 29.1, 26.5, 25.6.

ESI-TOF MS (positive mode, THF,  $m/z$ ): [M]<sup>+</sup> found 567.362, simulated 567.369 for C<sub>30</sub>H<sub>56</sub>CuN<sub>4</sub>O<sub>2</sub><sup>+</sup>.

#### 4.2.4. Synthesis of 3-(11-hydroxyundecyl)-1-methylimidazolium bromide (**4**)



Scheme 4. Synthesis of 3-(11-hydroxyundecyl)-1-methylimidazolium bromide (**4**).

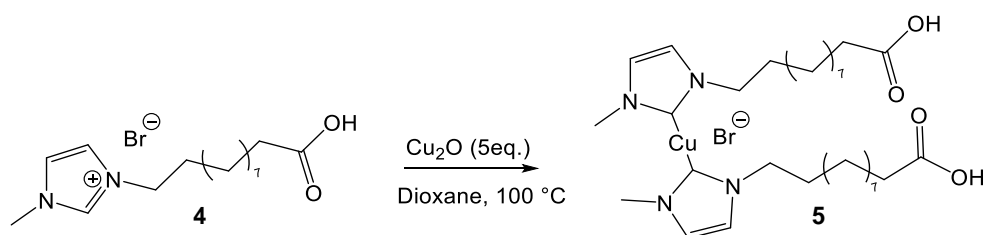
1-Methylimidazole (1.50 mL, 19 mmol) was added to a suspension of 11-bromoundecanoic acid (5.30 g, 20 mmol) in acetonitrile (MeCN) (20 mL) at room temperature (RT) and was stirred for 24 h at 80°C. The reaction mixture was allowed to come to RT and was diluted with diethyl ether (Et<sub>2</sub>O) (80 mL). The resulting precipitate was filtered off, washed again three times with Et<sub>2</sub>O (3 x 50 mL) and compound **4** was obtained as colorless solid after drying in high vacuum (6.31 g, 18.17 mmol, 95%).

$^1\text{H-NMR}$  (DMSO- $d_6$ , 400 MHz):  $\delta$  [ppm] 11.94 (s, 2H, COOH), 9.13 (s, 2H, NCHN), 7.76 (s, 2H, NCHCHN), 7.69 (s, 2H, NCHCHN), 4.14 (t,  $^3J_{\text{H,H}} = 7.2$  Hz, 4H, NCH<sub>2</sub>), 3.83 (s, 6H, NCH<sub>3</sub>), 2.16 (t,  $^3J_{\text{H,H}} = 7.3$  Hz, 4H, OCH<sub>2</sub>), 1.75 (m, 4H, NCH<sub>2</sub>CH<sub>2</sub>), 1.46 (m, 4H, OCH<sub>2</sub>CH<sub>2</sub>), 1.22 (m, 24H, (CH<sub>2</sub>)<sub>6</sub>).

$^{13}\text{C NMR}$  (DMSO- $d_6$ , 100 MHz):  $\delta$  [ppm] 174.9 (COOH), 137.0 (NCHN), 124.0 (CH<sub>3</sub>NCHCHN), 122.7 (CH<sub>3</sub>NCHCHN), 49.2 (NCH<sub>2</sub>), , 36.2 (NCH<sub>3</sub>), 34.1 (OCH<sub>2</sub>), 29.8 (OCH<sub>2</sub>CH<sub>2</sub>), 29.2, 29.2, 29.1, 29.0, 28.8, 25.9, 24.9.

ESI-TOF MS (positive mode, MeOH,  $m/z$ ): [M-Br]<sup>+</sup> found 267.206, simulated 267.207 for C<sub>15</sub>H<sub>27</sub>N<sub>2</sub>O<sub>2</sub><sup>+</sup>.

#### 4.2.5. Synthesis of OH end-capped copper(I)-bis(NHC) complex (**5**)



Scheme 5. Synthesis of OH end-capped copper(I)-bis(NHC) complex (**5**)

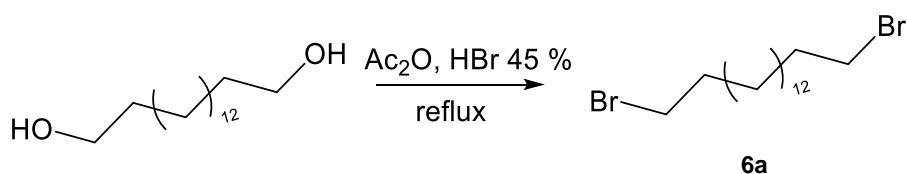
Compound **4** (2.08 g, 6.0 mmol) and copper(I)-oxide (4.30 g, 30.0 mmol, 5 eq.) were suspended in dioxane (50 mL) and were stirred at 100°C for 3 days. After cooling to RT, the excess of Cu<sub>2</sub>O was filtered off and the solvent was removed under reduced pressure.

Compound **5** (0.54 g, 0.8 mmol, 13%) was obtained after column chromatography on silica by gradually changing the polarity of solvent from pure  $\text{CHCl}_3$  to  $\text{CHCl}_3/\text{MeOH}$  10/1 ( $R_f = 0.24$   $\text{CHCl}_3/\text{MeOH}$  20/1) as a white solid.

$^1\text{H-NMR}$  ( $\text{CDCl}_3$ , 400 MHz):  $\delta$  [ppm] 6.18 (q, 4H,  $\text{NCHCHN}$ ), 3.60 (t,  $^3J_{\text{H,H}} = 7.3$  Hz, 4H,  $\text{NCH}_2$ ), 3.12 (s, 6H,  $\text{NCH}_3$ ), 2.34 (t,  $^3J_{\text{H,H}} = 7.2$  Hz, 4H,  $\text{OCCCH}_2$ ), 1.71 – 1.58 (m, 8H,  $\text{NCH}_2\text{CH}_2$ ), 1.31 (m, 24H,  $(\text{CH}_2)_{12}$ ).

$^{13}\text{C-NMR}$  ( $\text{CDCl}_3$ , 100 MHz):  $\delta$  [ppm] 174.3 ( $\text{C=O}$ ), 153.2 ( $\text{NCCuN}$ ), 111.0 ( $\text{CH}_3\text{NCHCHN}$ ), 109.9 ( $\text{CH}_3\text{NCHCHN}$ ), 51.4 ( $\text{NCH}_2$ ), 43.6 ( $\text{NCH}_3$ ), 34.1 ( $\text{OCH}_2$ ), 30.3, 29.5, 29.4, 29.3, 29.5, 29.1, 28.1, 26.6, 24.9.

#### 4.2.6. Synthesis of 1,5-dibromododecane (**6a**)



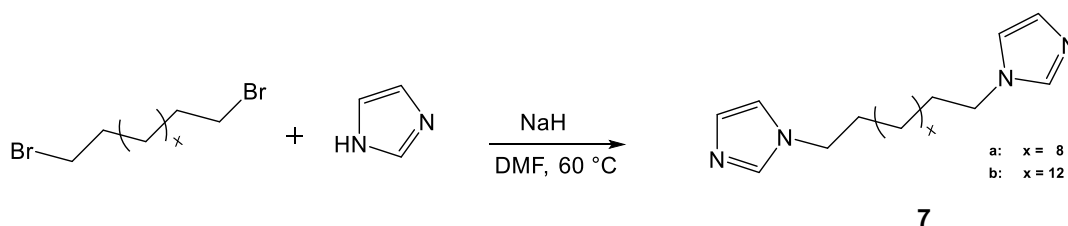
Scheme 6. Synthesis of 1,5-dibromododecane (**6a**).

HBr (48% in  $\text{H}_2\text{O}$ , 63.0 mL, 380 mmol) was added dropwise to  $\text{Ac}_2\text{O}$  (108 mL, 1.1 mol) at  $0^\circ\text{C}$  followed by the addition of compound 1,16-dihydroxyhexadecane (4.47 g, 17 mmol). The reaction mixture was stirred at reflux for 24 h. After cooling to RT, the solution was extracted with hexanes (3 x 50 mL) and washed with  $\text{H}_2\text{O}$  (3 x 100 mL). The solvent was removed under reduced pressure and compound **6** (17 mmol, 6.55 g, 99%) was obtained as a white solid.

$^1\text{H-NMR}$  ( $\text{CDCl}_3$ , 400 MHz):  $\delta$  [ppm] 3.41 (t,  $^3J_{\text{H,H}} = 6.9$  Hz, 4H,  $\text{BrCH}_2$ ), 1.85 (p,  $^3J_{\text{H,H}} = 6.9$  Hz, 4H,  $\text{BrCH}_2\text{CH}_2$ ), 1.48 – 1.36 (m, 4H,  $\text{BrCH}_2\text{CH}_2\text{CH}_2$ ), 1.27 (m, 20H,  $(\text{CH}_2)_{10}$ ).

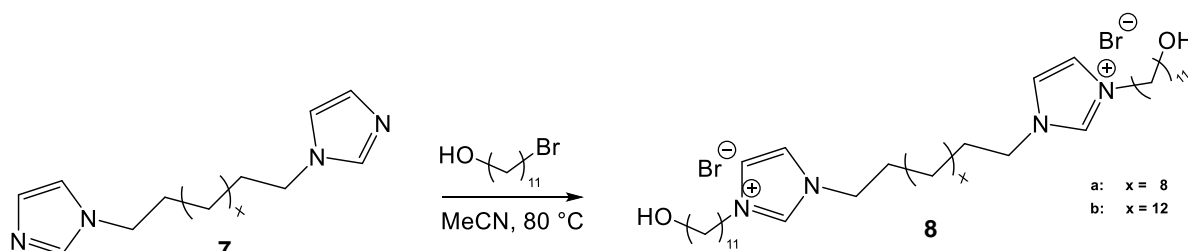
$^{13}\text{C-NMR}$  ( $\text{CDCl}_3$ , 100 MHz):  $\delta$  [ppm] 34.0 ( $\text{BrCH}_2$ ), 32.8 ( $\text{BrCH}_2\text{CH}_2$ ), 29.6 ( $\text{Br}(\text{CH}_2)_2\text{CH}_2$ ), 29.6 ( $\text{Br}(\text{CH}_2)_3\text{CH}_2$ ), 29.5 ( $\text{Br}(\text{CH}_2)_4\text{CH}_2$ ), 29.4 ( $\text{Br}(\text{CH}_2)_5\text{CH}_2$ ), 28.8 ( $\text{Br}(\text{CH}_2)_6\text{CH}_2$ ), 28.2 ( $\text{Br}(\text{CH}_2)_7\text{CH}_2$ ).

#### 4.2.7. Synthesis of 1,5-di(imidazolyl) alkane (**7**)



Scheme 7. Synthesis of 1,5-di(imidazolyl) alkane (**7**) with different chain length.

NaH (80.0 mmol, 60%) was suspended in DMF (50 mL) and was cooled to  $0^\circ\text{C}$  followed by the dropwise addition of imidazole (72.4 mmol). After stirring for 15 min at  $0^\circ\text{C}$ ,  $\alpha,\omega$ -dibromoalkane (30.0 mmol) was added. The reaction mixture was heated up to  $70^\circ\text{C}$  and was further stirred for 4 h. The reaction mixture was allowed to come to RT, diluted with ethyl acetate (120 mL) and was washed with water (3 x 50 mL). The combined organic phases were dried via  $\text{NaSO}_4$ . After solvent evaporation was under reduced pressure compound **7** was obtained as colorless solid.

Characterization of 7a (X = 8):Yield: (8.60 g, 28.5 mmol, 95%)<sup>1</sup>H-NMR (CDCl<sub>3</sub>, 400 MHz): δ [ppm] 7.46 (s, 2H, NCHN), 7.06 (s, 2H, CH<sub>2</sub>NCHCHN), 6.90 (s, 2H, CH<sub>3</sub>NCHCHN), 3.91 (t, <sup>3</sup>J<sub>H,H</sub> = 7.1 Hz, 4H, NCH<sub>2</sub>), 1.76 (p, <sup>3</sup>J<sub>H,H</sub> = 6.8 Hz, 4H, NCH<sub>2</sub>CH<sub>2</sub>), 1.36 – 1.18 (m, 16H, (CH<sub>2</sub>)<sub>8</sub>).<sup>13</sup>C-NMR (CDCl<sub>3</sub>, 100 MHz): δ [ppm] 137.0 (NCHN), 129.4 (NCHCHN), 118.7 (NCHCHN), 47.0 (NCH<sub>2</sub>), 31.0 (NCH<sub>2</sub>CH<sub>2</sub>), 29.4 (N(CH<sub>2</sub>)<sub>2</sub>CH<sub>2</sub>), 29.3 (N(CH<sub>2</sub>)<sub>3</sub>CH<sub>2</sub>), 29.0 (N(CH<sub>2</sub>)<sub>4</sub>CH<sub>2</sub>), 26.5 (N(CH<sub>2</sub>)<sub>5</sub>CH<sub>2</sub>).ESI-TOF MS (positive mode, THF, m/z): [M+Na]<sup>+</sup> found 325.235, simulated 325.236 for C<sub>18</sub>H<sub>30</sub>N<sub>4</sub>Na<sup>+</sup>.Characterization of 7b (X = 12):Yield: (9.98 g, 27.9 mmol, 93%)<sup>1</sup>H-NMR (DMSO-*d*<sub>6</sub>, 400 MHz): δ [ppm] 7.58 (s, 2H, NCHN), 7.13 (s, 2H, CH<sub>2</sub>NCHCHN), 6.85 (s, 2H, CH<sub>3</sub>NCHCHN), 3.91 (t, <sup>3</sup>J<sub>H,H</sub> = 7.1 Hz, 4H, NCH<sub>2</sub>), 1.66 (p, <sup>3</sup>J<sub>H,H</sub> = 7.2 Hz, 4H, NCH<sub>2</sub>CH<sub>2</sub>), 1.20 (m, 24H, (CH<sub>2</sub>)<sub>12</sub>).<sup>13</sup>C-NMR (DMSO-*d*<sub>6</sub>, 125 MHz): δ [ppm] 137.7 (NCHN), 128.7 (NCHCHN), 119.7 (NCHCHN), 46.4 (NCH<sub>2</sub>), 40.0 (NCH<sub>2</sub>CH<sub>2</sub>), 31.0 (N(CH<sub>2</sub>)<sub>2</sub>CH<sub>2</sub>), 29.5 (N(CH<sub>2</sub>)<sub>3</sub>CH<sub>2</sub>), 29.4 (N(CH<sub>2</sub>)<sub>4</sub>CH<sub>2</sub>), 29.6 (N(CH<sub>2</sub>)<sub>5</sub>CH<sub>2</sub>), 28.9 (N(CH<sub>2</sub>)<sub>6</sub>CH<sub>2</sub>), 26.3 (N(CH<sub>2</sub>)<sub>7</sub>CH<sub>2</sub>).ESI-TOF MS (positive mode, THF, m/z): [M+H]<sup>+</sup> found 359.316, simulated 359.317 for C<sub>22</sub>H<sub>39</sub>N<sub>4</sub>O<sub>2</sub><sup>+</sup>.4.2.8. Synthesis of 1,1'-(alkane-1,5-diyl)bis(3-(hydroxyundecyl)imidazolium) bromide (**8**)Scheme 8. Synthesis of 1,1'-(alkane-1,5-diyl)bis(3-(hydroxyundecyl)imidazolium) bromide (**8**) with different chain length.

Compound **7** (13.25 mmol) was added to a suspension of 11-bromoundecan-1-ol (7.50 g, 30.00 mmol) in acetonitrile (MeCN) (100 mL) at RT and was stirred for 24 h at 80°C. The reaction mixture was allowed to come to RT and was diluted with diethyl ether (Et<sub>2</sub>O) (120 mL). The resulting precipitate was filtered off, washed again with Et<sub>2</sub>O (3 x 50 mL) and **8** was obtained as colorless solid after drying in high vacuum.

Characterization of 8a (X = 8):Yield: (10.46 g, 13.0 mmol, 98%)

$^1\text{H-NMR}$  (DMSO- $d_6$ , 500 MHz):  $\delta$  [ppm] 9.21 (s, 2H, NCHN), 7.80 (s, 4H, NCHCHN), 4.30 (t,  $^3J_{\text{H,H}} = 5.1$  Hz, 2H, OH), 4.15 (t,  $^3J_{\text{H,H}} = 7.0$  Hz, 8H,  $\text{CH}_2\text{NCHNCH}_2$ ), 3.36 (q,  $^3J_{\text{H,H}} = 6.4$  Hz, 4H,  $\text{OCH}_2$ ), 1.77 (m, 8H,  $\text{CH}_2\text{CH}_2\text{NCHNCH}_2\text{CH}_2$ ), 1.38 (p,  $^3J_{\text{H,H}} = 6.7$  Hz, 4H,  $\text{OCH}_2\text{CH}_2$ ), 1.29 – 1.11 (m, 44H,  $(\text{CH}_2)_{22}$ ).

$^{13}\text{C-NMR}$  (DMSO- $d_6$ , 125 MHz):  $\delta$  [ppm] 136.4 (NCN), 122.9 (NCHCHN), 61.2 ( $\text{OCH}_2$ ), 49.3 ( $\text{NCH}_2$ ), 40.6, 40.4, 40.2, 40.0, 39.9, 33.0, 29.7, 29.7, 29.5, 29.5, 29.4, 29.4, 29.3, 29.3, 28.9, 28.8, 26.0, 26.0, 25.9.

ESI-TOF MS (positive mode, THF,  $m/z$ ):  $[\text{M}-2\text{Br}]^{2+}$  found 322.299, simulated 322.298 for  $\text{C}_{40}\text{H}_{76}\text{N}_4\text{O}_2^{2+}$ .

Characterization of **8b** (X = 12):

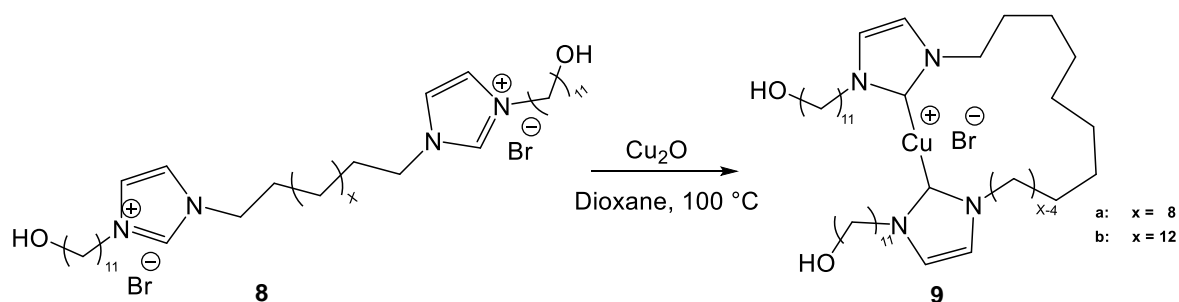
Yield: (10.85 g, 12.6 mmol, 95%)

$^1\text{H-NMR}$  (DMSO- $d_6$ , 400 MHz):  $\delta$  [ppm] 9.19 (s, 2H, NCHN), 7.78 (s, 4H, NCHCHN), 4.29 (t,  $^3J_{\text{H,H}} = 5.1$  Hz, 2H, OH), 4.14 (t,  $^3J_{\text{H,H}} = 7.0$  Hz, 8H,  $\text{CH}_2\text{NCHNCH}_2$ ), 3.36 (q,  $^3J_{\text{H,H}} = 6.4$  Hz, 4H,  $\text{OCH}_2$ ), 1.78 (p,  $^3J_{\text{H,H}} = 7.4$  Hz, 8H,  $\text{CH}_2\text{CH}_2\text{NCHNCH}_2\text{CH}_2$ ), 1.37 (p,  $^3J_{\text{H,H}} = 6.8$  Hz, 4H,  $\text{OCH}_2\text{CH}_2$ ), 1.28 – 1.13 (m, 52H,  $(\text{CH}_2)_{26}$ ).

$^{13}\text{C-NMR}$  (DMSO- $d_6$ , 125 MHz):  $\delta$  [ppm] 136.4 (NCN), 122.9 (NCHCHN), 61.1 ( $\text{OCH}_2$ ), 49.3 ( $\text{NCH}_2$ ), 40.4, 40.2, 40.0, 39.8, 39.6, 33.0, 29.7, 29.6, 29.6, 29.5, 29.5, 29.4, 29.3, 29.3, 28.8, 28.8, 26.0, 25.90.

ESI-TOF MS (positive mode, THF,  $m/z$ ):  $[\text{M}-2\text{Br}]^{2+}$  found 350.327, simulated 350.329 for  $\text{C}_{44}\text{H}_{84}\text{N}_4\text{O}_2^{2+}$ .

4.2.9. Synthesis of OH end-capped copper(I)-bis(NHC) complexes with safety line (**9**)



Scheme 9. Synthesis of OH end-capped copper(I)-bis(NHC) complexes (**9**) with different length of safety line using copper(I) oxide method.

Compound **8** (6.00 mmol) and copper(I)-oxide (4.3 g, 30.00 mmol, 5 eq.) were suspended in dioxane (300 mL) and was stirred at 100°C overnight. After cooling to RT, excess of  $\text{Cu}_2\text{O}$  was filtered off and the solvent was removed under reduced pressure. Compound **9** was obtained after column chromatography on silica by gradually changing the polarity of solvent from pure  $\text{CHCl}_3$  to  $\text{CHCl}_3/\text{MeOH}$  20/1 ( $R_f = 0.42$   $\text{CHCl}_3/\text{MeOH}$  20/1) as a light yellow solid.

Characterization of **9a** (X = 8):

Yield: (0.40 g, 0.60 mmol, 10%)

$^1\text{H-NMR}$  (THF- $d_8$ , 400 MHz):  $\delta$  [ppm] 6.26 (s, 4H, NCHCHN), 3.52 (t,  $^3J_{\text{H,H}} = 7.1$  Hz, 8H,  $\text{CH}_2\text{NCHNCH}_2$ ), 3.46 (q,  $^3J_{\text{H,H}} = 5.9$  Hz, 4H,  $\text{OCH}_2$ ), 3.42 (t,  $^3J_{\text{H,H}} = 4.8$  Hz, 2H, OH), 1.65 – 1.56 (m, 8H,  $\text{CH}_2\text{CH}_2\text{NCHNCH}_2\text{CH}_2$ ), 1.47 (p,  $^3J_{\text{H,H}} = 6.8$ , 4H,  $\text{OCH}_2\text{CH}_2$ ), 1.41 – 1.22 (m, 44H,  $(\text{CH}_2)_{22}$ ).

$^{13}\text{C-NMR}$  (THF- $d_8$ , 100 MHz):  $\delta$  [ppm] 152.9 (NCCuN), 109.9 (NCHCHN), 109.9 (NCHCHN), 63.0 ( $\text{OCH}_2$ ), 43.5 ( $\text{NCH}_2$ ), 43.4 ( $\text{NCH}_2$ ), 32.8, 29.7, 29.5, 29.5, 29.5, 29.4, 29.3, 29.2, 29.1, 26.6, 26.5, 25.7.

ESI-TOF MS (positive mode, THF,  $m/z$ ):  $[\text{M} + \text{CH}_3\text{OH}]^+$  found 737.138, simulated 737.538 for  $\text{C}_{41}\text{H}_{77}\text{CuN}_4\text{O}_3^+$

Characterization of **9b** (X = 12):

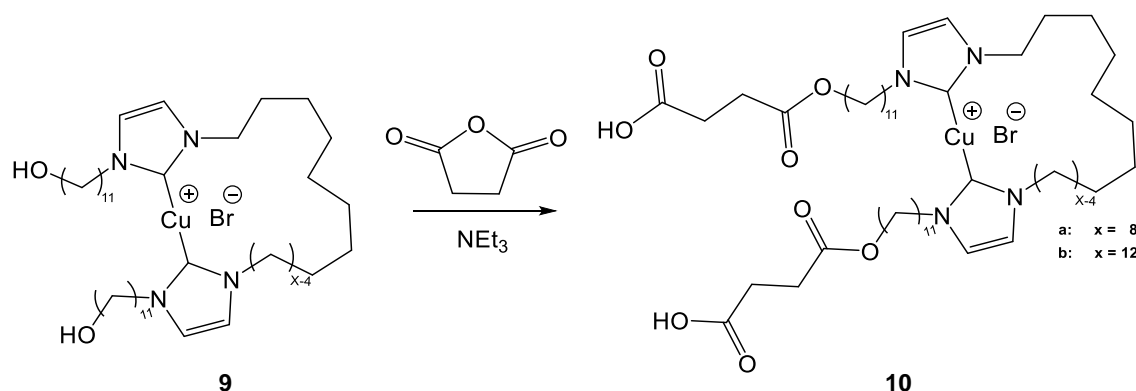
Yield: (0.73 g, 0.96 mmol, 16%)

$^1\text{H-NMR}$  (THF- $d_8$ , 400 MHz):  $\delta$  [ppm] 6.24 (s, 4H, NCHCHN), 3.51 (t,  $^3J_{\text{H,H}} = 7.1$  Hz, 8H,  $\text{CH}_2\text{NCHNCH}_2$ ), 3.46 (q,  $^3J_{\text{H,H}} = 6.4$  Hz, 4H,  $\text{OCH}_2$ ), 3.34 (t,  $^3J_{\text{H,H}} = 5.2$  Hz, 2H, OH), 1.60 (p,  $^3J_{\text{H,H}} = 7.3$  Hz, 8H,  $\text{CH}_2\text{CH}_2\text{NCHNCH}_2\text{CH}_2$ ), 1.46 (p,  $^3J_{\text{H,H}} = 6.7$  Hz, 4H,  $\text{OCH}_2\text{CH}_2$ ), 1.38 – 1.13 (m, 52H,  $(\text{CH}_2)_{26}$ ).

$^{13}\text{C-NMR}$  ( $\text{CDCl}_3$ , 100 MHz):  $\delta$  [ppm] 152.9 (NCCuN), 109.9 (NCHCHN), 109.8 (NCHCHN), 63.0 ( $\text{OCH}_2$ ), 43.5 ( $\text{NCH}_2$ ), 43.4 ( $\text{NCH}_2$ ), 32.8, 29.6, 29.6, 29.5, 29.5, 29.5, 29.5, 29.4, 29.3, 29.2, 29.1, 26.6, 26.6, 25.7.

ESI-TOF MS (positive mode, THF,  $m/z$ ):  $[\text{M}-\text{Br}+\text{Cl}+\text{H}]^+$  found 797.605, simulated 797.549 for  $\text{C}_{44}\text{H}_{83}\text{CuN}_4\text{O}_2\text{Cl}^+$

4.2.10. Synthesis of COOH end-capped copper(I)-bis(NHC) complexes with safety line (**10**)



Scheme 10. Synthesis of COOH end-capped copper(I)-bis(NHC) complexes (**7**) with different length of safety line.

Compound **9** (0.15 mmol) was dissolved in THF (5 mL) followed by addition of  $\text{NEt}_3$  (50  $\mu\text{L}$ , 0.35 mmol). The reaction mixture was stirred at RT overnight, washed with HCl (10 mL, 1M) and was extracted with  $\text{CH}_2\text{Cl}_2$  (3 x 20 mL). The combined organic phases were concentrated under reduced pressure. Compound **10** was obtained after precipitation with hexane as a colorless solid ( $R_f = 0.37$   $\text{CHCl}_3/\text{MeOH}$  20/1).

Characterization of **10a** (X = 8):

Yield: (0.18 g, 0.12 mmol, 80%)

$^1\text{H-NMR}$  ( $\text{CDCl}_3$ , 500 MHz):  $\delta$  [ppm] 6.19 (s, 4H,  $\text{NCHCHN}$ ), 4.10 (t,  $^3J_{\text{H,H}} = 6.3$  Hz, 4H,  $\text{OCH}_2$ ), 3.61 (m, 8H,  $\text{CH}_2\text{NCHNCH}_2$ ), 2.64 (m, 8H,  $\text{OCCH}_2\text{CH}_2\text{CO}$ ), 1.63 (m, 12H,  $\text{CH}_2\text{CH}_2\text{NCHNCH}_2\text{CH}_2 + \text{OCH}_2\text{CH}_2$ ), 1.40 – 1.07 (m, 36H,  $(\text{CH}_2)_{18}$ ).

$^{13}\text{C-NMR}$  ( $\text{CDCl}_3$ , 100 MHz):  $\delta$  [ppm] 172.4 ( $\text{HOC=O}$ ), 170.5 ( $\text{CH}_2\text{OC=O}$ ), 152.8 ( $\text{NCCuN}$ ), 110.3 ( $\text{CH}_3\text{NCHCHN}$ ), 110.2 ( $\text{CH}_3\text{NCHCHN}$ ), 64.8 ( $\text{OCH}_2$ ), 43.7 ( $\text{NCH}_2$ ), 43.5 ( $\text{NCH}_2$ ), 29.5 ( $\text{HOC=OCH}_2$ ), 29.5 ( $\text{CH}_2\text{OC=OCH}_2$ ), 29.4, 29.2, 29.1, 29.0, 29.0, 28.9, 28.8, 28.4, 28.3, 26.5, 26.3, 25.7.

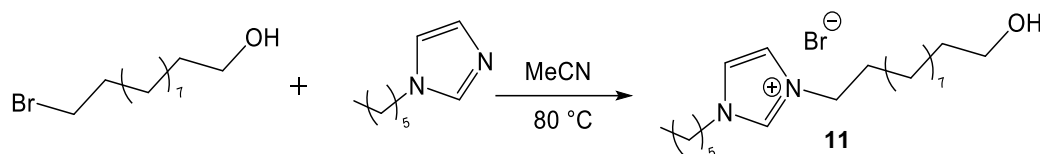
#### Characterization of **10b** (X = 12):

Yield: (0.11 g, 0.10 mmol, 72%)

$^1\text{H-NMR}$  ( $\text{CDCl}_3$ , 500 MHz):  $\delta$  [ppm] 6.19 (s, 4H,  $\text{NCHCHN}$ ), 4.10 (t,  $^3J_{\text{H,H}} = 6.3$  Hz, 4H,  $\text{OCH}_2$ ), 3.61 (td,  $J = 7.3, 2.9$  Hz, 8H,  $\text{CH}_2\text{NCHNCH}_2$ ), 2.64 (dq,  $J = 10.6, 5.8$  Hz, 8H,  $\text{OCCH}_2\text{CH}_2\text{CO}$ ), 1.63 (m, 12 H,  $\text{CH}_2\text{CH}_2\text{NCHNCH}_2\text{CH}_2 + \text{OCH}_2\text{CH}_2$ ), 1.39 – 1.20 (m, 44H,  $(\text{CH}_2)_{22}$ ).

$^{13}\text{C-NMR}$  ( $\text{CDCl}_3$ , 100 MHz):  $\delta$  [ppm] 172.4 ( $\text{HOC=O}$ ), 170.5 ( $\text{CH}_2\text{OC=O}$ ), 152.8 ( $\text{NCCuN}$ ), 110.3 ( $\text{CH}_3\text{NCHCHN}$ ), 110.2 ( $\text{CH}_3\text{NCHCHN}$ ), 64.8 ( $\text{OCH}_2$ ), 43.7 ( $\text{NCH}_2$ ), 43.5 ( $\text{NCH}_2$ ), 29.5 ( $\text{HOC=OCH}_2$ ), 29.5 ( $\text{CH}_2\text{OC=OCH}_2$ ), 29.4, 29.2, 29.1, 29.0, 29.0, 28.9, 28.9, 28.8, 28.8, 28.6, 28.5, 28.4, 28.3, 26.5, 26.3, 25.7.

#### 4.2.11. Synthesis of 3-(11-hydroxyundecyl)-1-hexylimidazolium bromide (**11**)



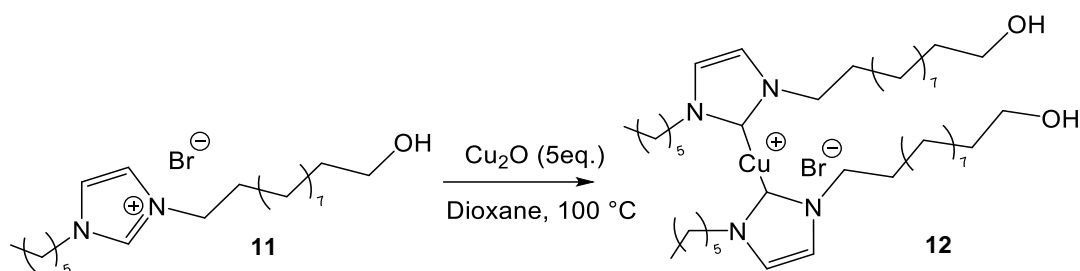
Scheme 11. Synthesis of 3-(11-hydroxyundecyl)-1-hexylimidazolium bromide (**11**).

1-Hexylimidazole (1.52 mL, 10.00 mmol) was added to a suspension of 11-bromoundecan-1-ol (2.38 g, 9.50 mmol) in acetonitrile (MeCN) (20 mL) at room temperature (RT) and was stirred for 24 h at 80°C. The reaction mixture was allowed to come to RT and was diluted with diethyl ether ( $\text{Et}_2\text{O}$ ) (120 mL). The resulting precipitate was filtered off, washed again with  $\text{Et}_2\text{O}$  (3 x 50 mL) and **11** was obtained as colorless solid after drying in high vacuum (3.75 g, 9.30 mmol, 98%).

$^1\text{H-NMR}$  ( $\text{DMSO-}d_6$ , 500 MHz):  $\delta$  [ppm] 9.21 (s, 1H,  $\text{NCHN}$ ), 7.79 (m, 2H,  $\text{NCHCHN}$ ), 4.29 (t,  $^3J_{\text{H,H}} = 5.1$  Hz, 1H,  $\text{OH}$ ), 4.14 (t,  $^3J_{\text{H,H}} = 7.0$  Hz, 4H,  $\text{NCH}_2$ ), 3.36 (q,  $^3J_{\text{H,H}} = 5.4$  Hz, 2H,  $\text{OCH}_2$ ), 1.77 (p,  $^3J_{\text{H,H}} = 7.2$  Hz, 4H,  $\text{NCH}_2\text{CH}_2$ ), 1.37 (p,  $^3J_{\text{H,H}} = 6.7$  Hz, 2H,  $\text{OCH}_2\text{CH}_2$ ), 1.28 – 1.15 (m, 20H,  $(\text{CH}_2)_{10}$ ), 0.84 (t,  $^3J_{\text{H,H}} = 6.9$  Hz, 3H,  $\text{CH}_3$ ).

$^{13}\text{C NMR}$  ( $\text{DMSO-}d_6$ , 125 MHz):  $\delta$  [ppm] 136.4 ( $\text{NCHN}$ ), 122.9 ( $\text{NCHCHN}$ ), 61.1 ( $\text{OCH}_2$ ), 49.3 ( $\text{NCH}_2$ ), 32.9 ( $\text{OCH}_2\text{CH}_2$ ), 30.9, 29.7, 29.7, 29.5, 29.4, 28.8, 26.0, 25.9, 25.6, 22.3, 14.24 ( $\text{CH}_3$ ).

ESI-TOF MS (positive mode, MeOH,  $m/z$ ):  $[\text{M-Br}]^+$  found 323.304, simulated 323.306 for  $\text{C}_{20}\text{H}_{39}\text{N}_2\text{O}^+$ .

4.2.12. Synthesis of 6,11 - OH end-capped copper(I)-bis(NHC) complex (**12**)Scheme 12. Synthesis of 6,11 copper(I)-bis(NHC) complex (**12**) using copper(I)-oxide method.

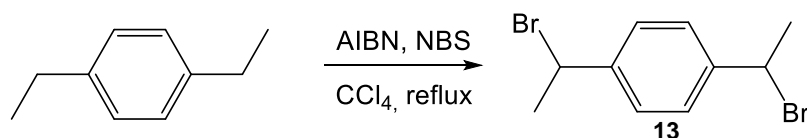
Compound **11** (1.20 g, 3.00 mmol) and copper(I)-oxide (2.15 g, 15.00 mmol, 5 eq.) were suspended in dioxane (20 mL) and were stirred at 100°C for 3 days. After cooling to RT, the excess of  $\text{Cu}_2\text{O}$  was filtered off and the solvent was removed under reduced pressure. Compound **12** (0.66 g, 0.84 mmol, 28%) was obtained after column chromatography on silica by gradually changing the polarity of solvent from pure  $\text{CHCl}_3$  to  $\text{CHCl}_3/\text{MeOH}$  20/1 ( $R_f = 0.40$   $\text{CHCl}_3/\text{MeOH}$  20/1) as a colorless solid.

**$^1\text{H-NMR}$  ( $\text{CDCl}_3$ , 400 MHz):**  $\delta$  [ppm] 6.16 (s, 4H,  $\text{NCHCHN}$ ), 3.63 (q,  $^3J_{\text{H,H}} = 6.5$  Hz, 4H,  $\text{OCH}_2$ ), 3.58 (t,  $^3J_{\text{H,H}} = 7.3$  Hz, 8H,  $\text{NCH}_2$ ), 1.70 – 1.60 (m, 8H,  $\text{NCH}_2\text{CH}_2$ ), 1.56 (p,  $^3J_{\text{H,H}} = 6.8$  Hz, 4H,  $\text{OCH}_2\text{CH}_2$ ), 1.37 – 1.20 (m, 40H,  $(\text{CH}_2)_{20}$ ), 0.87 (t,  $^3J_{\text{H,H}} = 6.5$  Hz, 6H,  $\text{CH}_3$ ).

**$^{13}\text{C-NMR}$  ( $\text{CDCl}_3$ , 100 MHz):**  $\delta$  [ppm] 152.9 ( $\text{NCCuN}$ ), 109.9 ( $\text{CH}_3\text{NCHCHN}$ ), 62.9 ( $\text{NCH}_2$ ), 62.9 ( $\text{NCH}_2$ ), 43.4 ( $\text{OCH}_2$ ), 32.8, 31.4, 29.6, 29.5, 29.5, 29.4, 29.3, 29.1, 26.6, 26.3, 25.7, 22.5, 14.0 ( $\text{CH}_3$ ).

**ESI-TOF MS (positive mode, THF,  $m/z$ ):**  $[\text{M-Br}]^+$  found 707.548, simulated 707.526 for  $\text{C}_{40}\text{H}_{76}\text{CuN}_4\text{O}_2^+$ .

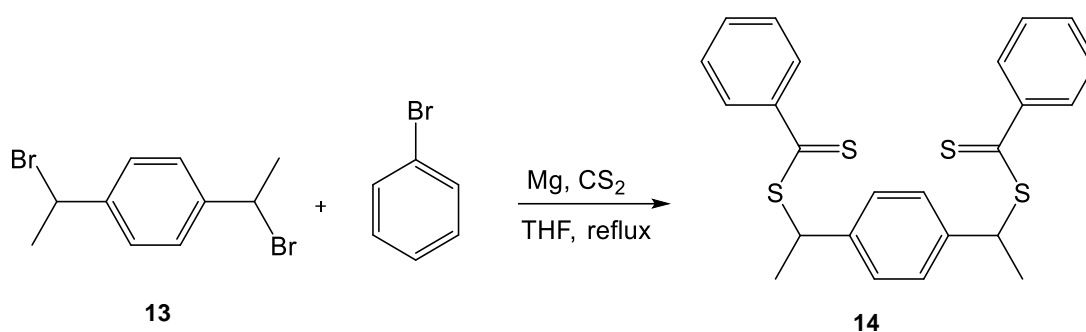
## 4.3. Synthesis of chain extended polymeric copper(I)-bis(NHC) complexes

4.3.1. Synthesis of 1,4-bis(1-bromoethyl)benzene (**13**)Scheme 13. Synthesis of 1,4-bis(1-bromoethyl)benzene (**13**) via radical bromination.

1,4-Diethylbenzene (5.00 g, 33.60 mmol) was dissolved in tetrachloromethane (50 mL) followed by the addition of *N*-bromo succinimide (NBS) (13.23 g, 74.30 mmol) and azobisisobutyronitrile (AIBN) (57 mg, 0.33 mmol). The obtained solution was heated overnight under reflux. Subsequently, the cold suspension was filtered, the solvent was removed and the resulting solid was recrystallized three times in diethyl ether to obtain **13** (9.11 g, 31.25 mmol) as a white solid in a yield of 93%.

**$^1\text{H-NMR}$  ( $\text{CDCl}_3$ , 400 MHz):**  $\delta$  [ppm] 7.41 (s, 4H,  $\text{CH}_{\text{Ar}}$ ), 5.19 (q,  $^3J_{\text{H,H}} = 6.9$  Hz, 2H,  $\text{BrCH}$ ), 2.04 (d,  $^3J_{\text{H,H}} = 6.9$  Hz, 6H,  $\text{CHCH}_3$ ).

**$^{13}\text{C-NMR}$  ( $\text{CDCl}_3$ , 100 MHz):**  $\delta$  [ppm] 143.8 ( $\text{CCH}$ ), 127.6 ( $\text{C}_{\text{Ar}}$ ), 49.2 ( $\text{BrCH}$ ), 27.2 ( $\text{CHCH}_3$ ).

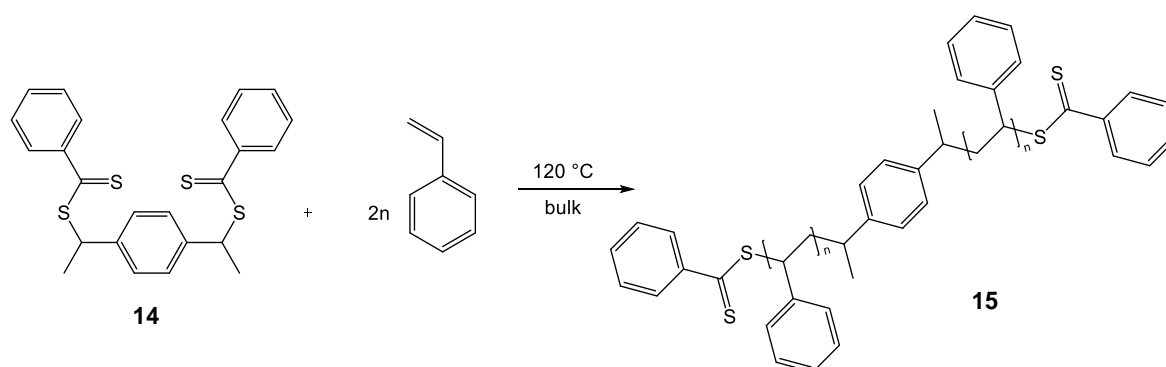
4.3.2. Synthesis of 1,4-phenylenebis(ethane-1,1-diyl) dibenzodithioate (**14**)Scheme 14. Synthesis of 1,4-phenylenebis(ethane-1,1-diyl) dibenzodithioate (**14**) via Grignard reaction.

Bromobenzene (1.43 mL, 13.71 mmol) and magnesium (0.33 g, 13.71 mmol) were suspended in dry THF (30 mL) and a small amount of iodine was added to etch the magnesium. The reaction mixture was heated under reflux for 2 hours, subsequently cooled in an ice bath and carbon disulfide (0.83 mL, 13.71 mmol) was added slowly at 0°C. After refluxing for 2 hours, **13** (1.00 g, 3.43 mmol) was added and the solution was refluxed for further 48 hours. Afterwards, the solvent was removed, the crude product was re-dissolved in DCM (50 mL) and washed with HCl (1M, 20 mL) and water (50 mL). The combined organic layers were dried over Na<sub>2</sub>SO<sub>4</sub>, the solvent was removed under vacuo and the crude product was purified via chromatography on silica with n-hexane/DCM 4/1 (*R<sub>f</sub>* = 0.25) obtaining **14** (1.00 g, 2.30 mmol) as a red viscous liquid in a yield of 67%.

**<sup>1</sup>H-NMR (CDCl<sub>3</sub>, 400 MHz):** δ [ppm] 7.95 (d, <sup>3</sup>*J*<sub>H,H</sub> = 7.3 Hz, 4H, *CH*<sub>ortho</sub>), 7.50 (t, <sup>3</sup>*J*<sub>H,H</sub> = 7.4 Hz, 2H, *CH*<sub>para</sub>), 7.42 (s, 4H, CHCCHCCH), 7.35 (t, <sup>3</sup>*J*<sub>H,H</sub> = 7.8 Hz, 4H, *CH*<sub>meta</sub>), 5.26 (q, <sup>3</sup>*J*<sub>H,H</sub> = 7.1 Hz, 2H, SCHCH<sub>3</sub>), 1.79 (d, *J* = 7.1 Hz, 6H, SCHCH<sub>3</sub>).

**<sup>13</sup>C-NMR (CDCl<sub>3</sub>, 100 MHz):** δ [ppm] 226.9 (C=S), 144.9 (CC=S), 140.7 (CCH), 132.3 (C<sub>para</sub>), 128.3 (C<sub>ortho</sub>), 128.1 (C<sub>meta</sub>), 126.9 (CHCCHCCH), 49.8 (CCH), 20.7 (CHCH<sub>3</sub>).

**ESI-TOF MS (positive mode, THF, *m/z*):** [M+Na]<sup>+</sup> found 461.096, simulated 461.050 for C<sub>24</sub>H<sub>22</sub>S<sub>4</sub>Na<sup>+</sup>.

4.3.3. General RAFT polymerization for bivalent poly(styrene)s (**15**)Scheme 15. Synthesis of bivalent dithiobenzoate end-capped poly(styrene) (**15**) via RAFT polymerization in bulk.

All RAFT polymerizations were carried out in bulk under dry and inert conditions using common Schlenk techniques. For the synthesis compound **14** was placed together with destabilized and freshly distilled styrene in a Schlenk tube and subjected to several freeze-pump-thaw

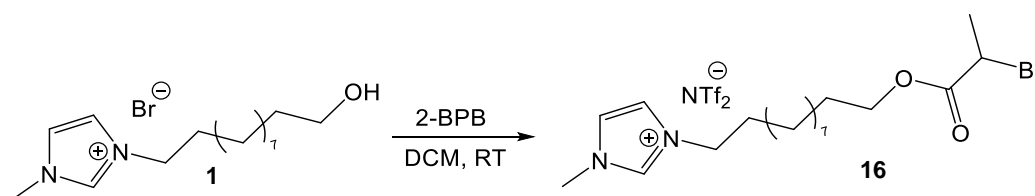
cycles. Subsequently, the reaction mixture was placed in a pre-heated oil bath and stirred for 16 hours at 120°C. Cooling fast to room temperature by means of an ice bath terminated the reaction and the crude product was purified by diluting the reaction mixture with a small amount of toluene and precipitating three times in ice-cold MeOH. The pure product (**15**) was obtained after drying the sample in high vacuum for several hours.

<sup>1</sup>H-NMR (CDCl<sub>3</sub>, 400 MHz): δ [ppm] 7.87 (s, 4H), 7.48 (s, 4H), 7.12 (s, Ar-*H* of phenyl-residue), 1.65 (s, CH<sub>2</sub>- + CH-groups of repetitive units).

Table 13. Reaction conditions and characterization data of bivalent poly(styrene) (**15**) via RAFT.

Ent.	Comp.	CTA:M	n(CTA) [mmol]	n(M) [mmol]	T [°C]	M <sub>n</sub> (GPC) [g mol <sup>-1</sup> ]	M <sub>n</sub> (NMR) [g mol <sup>-1</sup> ]	Đ	yield [%]
1	<b>15a</b>	10: 500	1.75			4400	5000	1.10	37
2	<b>15b</b>	10: 750	1.16	87.4	120	9000	8300	1.18	25
3	<b>15c</b>	10:1000	0.87			15500	14800	1.17	13

#### 4.3.4. Synthesis of 3-(11-(2-bromopropionyloxy)undecyl)-methyl-1-imidazolium bis(trifluoromethane)sulfonimide (**16**)



Scheme 16. Synthesis of 3-(11-(2-bromopropionyloxy)undecyl)-methyl-1-imidazolium bis(trifluoromethane)sulfonimide (**16**).

3-(11-Hydroxyundecyl)-1-methylimidazolium bromide (**1**) (3.5 g, 10.5 mmol) was dissolved in dry dichloromethane (DCM) (30.0 mL) followed by addition of 2-bromopropionyl bromide (3.3 mL, 6.8 g, 31.5 mmol). The obtained reaction mixture was subsequently stirred for 48 hours at room temperature. The solvent was removed in vacuo and the oily residue was transferred to a separation funnel diluted with water (50 mL) and washed with DCM (3 x 50 mL). The aqueous phase was mixed with lithium bis(trifluoromethane)sulfonimide (3.3 g, 11.6 mmol) and the reaction mixture was stirred for 24 hours at room temperature followed by extraction with DCM (3 x 50.0 mL). The combined organic layers were dried over Na<sub>2</sub>SO<sub>4</sub>, the solvent was removed in vacuo and **16** was obtained as colorless oil in a yield of 83%.

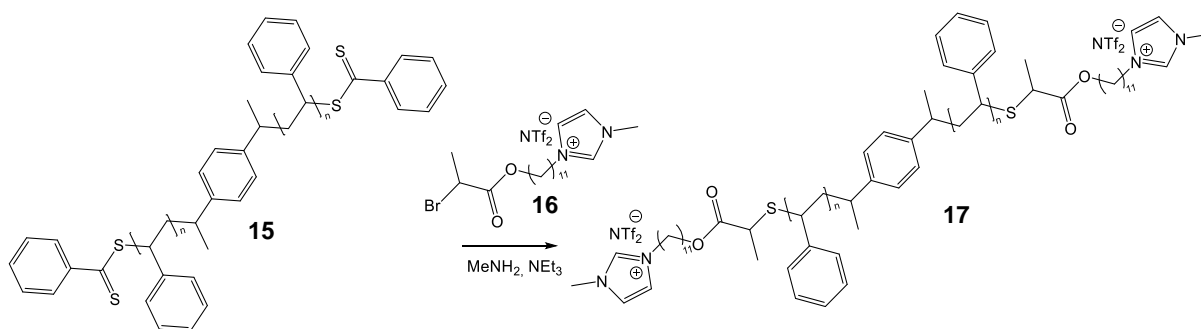
<sup>1</sup>H-NMR (CDCl<sub>3</sub>, 400 MHz): δ [ppm] 8.79 (s, 1H, NCHN), 7.30 (t, <sup>3</sup>J<sub>H,H</sub> = 1.8 Hz, 1H, CH<sub>2</sub>NCHCHN), 7.27 (t, <sup>3</sup>J<sub>H,H</sub> = 1.8 Hz, 1H, NCHCHNCH<sub>3</sub>), 4.36 (q, <sup>3</sup>J<sub>H,H</sub> = 6.8 Hz, 1H, BrCH), 4.24 – 4.05 (m, 4H, NCH<sub>2</sub> + OCH<sub>2</sub>), 3.95 (s, 3H, NCH<sub>3</sub>), 1.94 – 1.83 (m, 2H, OCH<sub>2</sub>CH<sub>2</sub>), 1.82 (d, <sup>3</sup>J<sub>H,H</sub> = 6.9 Hz, 3H, CH<sub>3</sub>CHBr), 1.72 – 1.60 (m, 2H, NCH<sub>2</sub>CH<sub>2</sub>), 1.44 – 1.19 (m, 14H, (CH<sub>2</sub>)<sub>7</sub>).

<sup>13</sup>C-NMR (CDCl<sub>3</sub>, 100 MHz): δ [ppm] 170.5 (C=O), 136.1 (NCHN), 123.6 (NCHCHNCH<sub>3</sub>), 122.3 (NCHCHNCH<sub>3</sub>), 119.9 (q, <sup>3</sup>J<sub>C,F</sub> = 321.2 Hz, CF<sub>3</sub>), 66.2 (OCH<sub>2</sub>), 50.4 (NCH<sub>2</sub>), 40.5 (BrCH), 36.6 (NCH<sub>3</sub>), 30.2, 29.3, 29.3, 29.2, 29.1, 28.8, 28.3, 26.1, 25.6, 21.7.

<sup>19</sup>F-NMR (CDCl<sub>3</sub>, 375 MHz): δ [ppm] -79.00 (CF<sub>3</sub>).

ESI-TOF MS (positive mode, THF,  $m/z$ ):  $[M-Br]^+$  found 387.154, simulated 387.162 for  $C_{18}H_{32}BrN_2O_2^+$  and ESI-TOF MS (negative mode, THF,  $m/z$ ):  $[NTf_2]^-$  found 279.951, simulated 279.918 for  $C_2F_6NO_4S_2^-$ .

#### 4.3.5. Synthesis of bivalent imidazolium-telechelic poly(styrene) (**17**)



Scheme 17. Synthesis of bivalent 1-methylimidazolium end-capped poly(styrene) (**17**) via thio bromo “click” reaction.

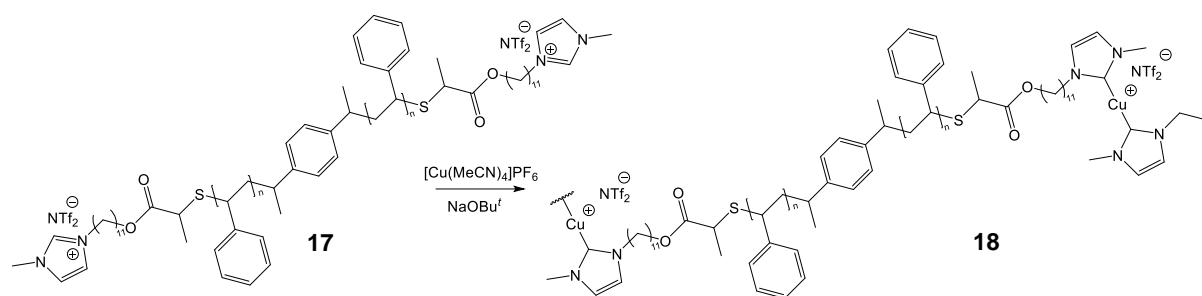
The bivalent PS precursor **15** (1.0 g, 1.0 eq.) was placed in a Schlenk flask and was dissolved in a mixture of dry THF/MeCN 1:1 (10 mL) followed by five freeze-pump-thaw cycles. Afterwards, tributyl phosphine (0.1 eq.) and methylamine (2M in THF, 2.2 eq.) were added. The reaction mixture was stirred at room temperature for one hour until the red color completely disappeared. Subsequently, triethylamine (4.4 eq.) and **16** (4.4 eq.) were added and stirred for 24 h at 40°C. After evaporating the solvent, a small amount of toluene was added, and the sample was precipitated in methanol. The pure product **17** were obtained by column chromatography on silica changing the polarity of the eluent gradually from pure DCM to DCM/MeOH 4/1 ( $R_f = 0.40$ , DCM/MeOH 4/1) in almost quantitative yields.

$^1H$ -NMR (THF- $d_8$ , 400 MHz):  $\delta$  [ppm] 8.97 (d, 2H,  $^3J_{H,H} = 1.9$  Hz,  $NC_HN$ ), 7.54 (d, 4H,  $^3J_{H,H} = 14.5$  Hz,  $NCHCHN$ ), 6.91 (bs, Ar- $H$  of phenyl-residue), 4.23 (t,  $^3J_{H,H} = 8.0$  Hz, 4H,  $OCH_2$ ), 3.93 (s, 6H,  $NCH_3$ ), 3.77 (s, 4H,  $NCH_2$ ), 1.51 (bs,  $CH_2^- + CH^-$  of repetitive unit,

ESI-TOF-MS of **17a** (positive mode, THF,  $m/z$ ):  $[M-2NTf_2]^{2+}$  found 2645.338, simulated 2645.321 for  $C_{390}H_{420}N_4O_4S_2^{2+}$ .

Table 14. Characterization data of bivalent imidazolium end-capped poly(styrene) (**17**) via thio-bromo “click” reaction.

Ent.	Comp.	Prec.	n(15) [mmol]	n(16) [mmol]	m(16) [mg]	$M_n$ (GPC) [g mol $^{-1}$ ]	$M_n$ (NMR) [g mol $^{-1}$ ]	$\bar{D}$	yield [%]
1	<b>17a</b>	<b>15a</b>	0.200	0.880	587	4500	4800	1.12	98
2	<b>17b</b>	<b>15b</b>	0.120	0.528	352	9000	8500	1.15	89
3	<b>17c</b>	<b>15c</b>	0.068	0.299	199	15100	18200	1.17	53

4.3.6. Synthesis of chain-extended copper(I)-bis(NHC) complexes (**18**)Scheme 18. Synthesis of chain extended mechanocatalysts (**18**) using strong base method.

Polymer **17** was dissolved in dry toluene adjusting a concentration of 0.15 mmol mL<sup>-1</sup> followed by five freeze-thaw cycles in order to remove oxygen. After adding NaO<sup>t</sup>Bu (2.6 eq.), the reaction mixture was stirred at room temperature for 15 minutes followed by the addition of tetrakis(acetonitrile)copper(I) hexafluorophosphate (1 eq). The solvent was removed under vacuo and the crude product was purified by preparative GPC to obtain **18** as a light yellow solid.

<sup>1</sup>H-NMR (THF-*d*<sub>6</sub>, 400 MHz): δ [ppm] 7.27 – 6.35 (m, Ar-*H* of phenyl-residue), 6.23 (d, <sup>3</sup>J<sub>H,H</sub> = 2.9 Hz, 2H, NCHCHN), 3.50 (s, 4H, NCH<sub>2</sub> + OCH<sub>2</sub>), 3.50 (s, 3H, NCH<sub>3</sub>), 2.39 – 1.08 (m, CH<sub>2</sub> + CH-groups of repetitive unit).

Table 15. Conversion in complexation reaction of **17a** using different concentration.

Ent.	c <sup>17a</sup> [mmol * mL <sup>-1</sup> ]	M <sub>n</sub> (GPC) <sup>17a</sup> [g mol <sup>-1</sup> ]	M <sub>n</sub> (GPC) <sup>18a</sup> [g mol <sup>-1</sup> ]	Đ	Conv. <sup>a)</sup> [%]
1	0.02		5000	1.3	5
2	0.04	4500	7400	1.3	8
3	0.08		9100	1.5	39
4	0.15		15000	1.5	87

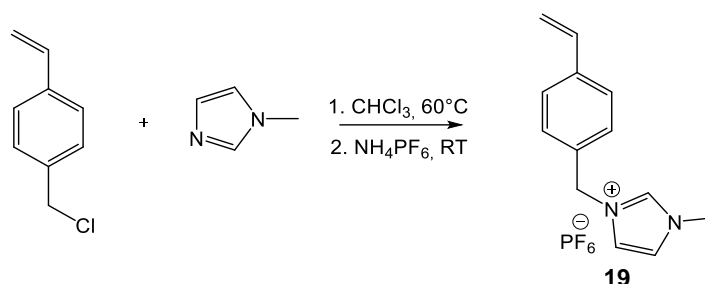
a) Determined via <sup>1</sup>H-NMR spectroscopy of the crude reaction mixture by integration of precursor signals at 7.54 ppm and the resonances at 6.25 ppm assigned to the copper(I)-bis(NHC) complex.

Table 16. Reaction conditions of Cu(I) bis(NHC)-complexes (**18**) formation.

Ent.	Comp.	Prec.	n(prec) [mmol] <sup>a)</sup>	n(NaO <sup>t</sup> Bu) [mmol]	m(NaO <sup>t</sup> Bu) [mg]	n(Cu) [mmol]	m(Cu) [mg]	M <sub>n</sub> (GPC) <sup>18</sup> [g mol <sup>-1</sup> ] <sup>b)</sup>	Đ
1	<b>18a</b>	<b>17a</b>	0.104	0.270	25.99	0.104	38.76	15000	1.6
2	<b>18b</b>	<b>17b</b>	0.059	0.153	14.74	0.059	21.99	21500	1.5
3	<b>18c</b>	<b>17c</b>	0.027	0.071	06.83	0.027	10.06	31000	1.4

a) Determined by using molecular weight via NMR, b) Determined via GPC (DMF + LiNTf<sub>2</sub>) using PS standard calibration.

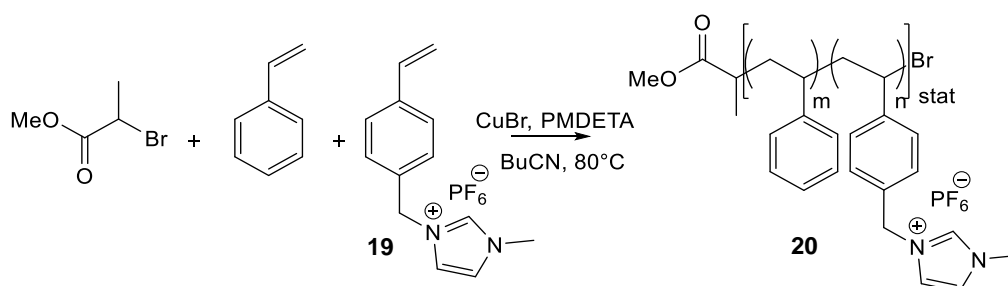
## 4.4. Synthesis of network-based copper(I)-bis(NHC) complexes

4.4.1. Synthesis of (bis(3-(vinylbenzyl)-1-methyl-imidazole-2-yl)copper(I)-hexafluorophosphate (**19**))Scheme 19. Synthesis of (bis(3-(vinylbenzyl)-1-methyl-imidazole-2-yl)copper(I)-hexafluorophosphate (**19**)).

4-Vinylbenzylchloride (5.10 mL, 37.50 mmol,) was dissolved in  $\text{CHCl}_3$  (25 mL) followed by the addition of 1-methylimidazole (37.50 mmol, 3.00 mL) and was stirred for 18 h at  $60^\circ\text{C}$ . The resulted solution was mixed with water (100 mL) and washed with diethyl ether (3 x 50 mL). The aqueous phase was concentrated under reduced pressure and methanol was added (100 mL). After addition of ammonium hexafluorophosphate (6.10 g, 37.50 mmol), the reaction mixture was stirred for 24 h at RT, the formed precipitate was filtered off and finally washed with methanol (3 x 20 mL). Compound **19** (34.50 mmol, 11.86 g, 92% was obtained after drying in high vacuum as a colorless powder.

$^1\text{H-NMR}$  ( $\text{DMSO-}d_6$ , 400 MHz):  $\delta$  [ppm] = 9.40 (s, 1H, NCHN), 7.79 (dt,  $^3J_{\text{H,H}} = 35.5$ ,  $^4J_{\text{H,H}} = 1.7$  Hz, 2H, NCHCH), 7.54 – 7.39 (m, 4H,  $\text{CH}_{\text{Ar}}$ ), 6.74 (dd,  $^3J_{\text{H,H}} = 17.6$ ,  $^4J_{\text{H,H}} = 10.9$  Hz, 1H,  $\text{CH}_2\text{CHC}$ ), 5.86 (dd,  $^3J_{\text{H,H}} = 17.7$ ,  $^4J_{\text{H,H}} = 0.9$  Hz, 1H,  $\text{CH}_2\text{CHC}$ ), 5.44 (s, 2H,  $\text{NCH}_2$ ), 5.29 (dd,  $^3J_{\text{H,H}} = 10.9$ ,  $^3J_{\text{H,H}} = 0.8$  Hz, 1H,  $\text{CH}_2\text{CHC}$ ), 3.86 (s, 3H,  $\text{NCH}_3$ ).

$^{13}\text{C-NMR}$  ( $\text{DMSO-}d_6$ , 100 MHz):  $\delta$  [ppm] = 137.9 ( $\text{CH}_2\text{CHC}$ ), 137.2 ( $\text{CH}_2\text{CHC}$ ), 136.4 (NCHN), 134.8 ( $\text{CCH}_2\text{N}$ ), 129.2 ( $\text{CH}_2\text{CHCCH}$ ), 127.1 ( $\text{CH}_2\text{CCH}$ ), 124.4 ( $\text{CH}_3\text{NCHCHN}$ ), 122.7 ( $\text{CH}_3\text{NCHCHN}$ ), 115.7 ( $\text{CH}_2\text{CHC}$ ), 51.9 ( $\text{NCH}_2$ ), 36.3 ( $\text{NCH}_3$ ).

4.4.2. Copolymerization of poly[(styrene)-*stat*-1-methyl-3-(4-vinylbenzyl)-1H-imidazol-3-ium hexafluorophosphate] (**20**)Scheme 20. Synthesis of copolymers (**20**) consisting of styrene and **19** via ATRP.

Styrene, 1-methyl-3-(4-vinylbenzyl)-1H-imidazol-3-ium hexafluorophosphate (**19**) (mol ratio 10:1 for **20a**, 3:1 for **20b** and 1:1 for **20c**), 2-bromopropionate (11.0  $\mu\text{l}$ , 0.08 mmol),

*N,N,N',N'',N'''*-pentamethyl diethylenetriamine (PMDETA) (31.7  $\mu\text{l}$ , 0.15 mmol) and butyronirile (3.0 mL) were placed in a Schlenk tube. The reaction mixture was subjected to several freeze-pump-thaw cycles. Subsequently, copper(I) bromide (10.9 mg, 0.08 mmol) was added inside a glove box. The solution was stirred 15 minutes at room temperature and was placed afterwards in a preheated oil bath at 80°C until the desired molecular weight was achieved (GPC control). After fast cooling to room temperature, the reaction mixture was diluted with MeCN and precipitated in MeOH/HCl (conc.) (10:1 v/v%) three times to obtain poly[(styrene)-*stat*-1-methyl-3-(4-vinylbenzyl)-1H-imidazol-3-ium hexafluorophosphate] (**20**) as a light yellow solid.

$^1\text{H-NMR}$  (DMSO- $d_6$ , 400 MHz):  $\delta$  [ppm] 9.15 (bs, 9H), 7.70 (bs, 19H), 6.78 (bs,  $\text{C}_6\text{H}_5$  repetitive unit), 5.30 (bs, 20H), 3.85 (bs, 30H), 1.44 (bs, CH and  $\text{CH}_2$  repetitive unit), 0.88 (bs, 3H).

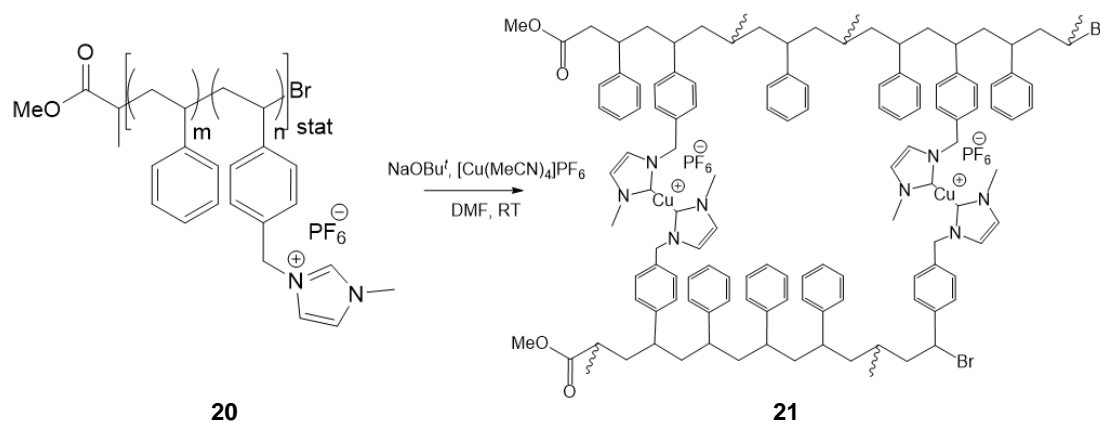
$^{13}\text{C-NMR}$  (DMSO- $d_6$ , 100 MHz):  $\delta$  [ppm] 145.6, 127.9, 125.6, 136.9, 124.4, 122.5, 52.0, 45.9 – 44.3, 36.3.

Table 17. Overview of synthesized copolymers (**20**) as well as their monomer feed and polymer composition.

Ent.	Copolymer	Feed styr./19	Polymer styr./19	$M_n(\text{NMR})$ [g mol $^{-1}$ ] <sup>a)</sup>	$M_n(\text{GPC})$ [g mol $^{-1}$ ]	$\bar{D}$	Funct. groups	$T_g^{\text{b)}$ [°C]
1	<b>20a</b>	10:1	11:1	7500	6300	1.4	5	106
2	<b>20b</b>	3:1	3:1	7200	5900	1.4	11	127
3	<b>20c</b>	1:1	1:1	6000	5700	1.4	15	138

a) Determined via  $^1\text{H-NMR}$  spectroscopy using the resonances at 0.88 ppm ( $\text{CH}_3\text{OC}(\text{O})\text{CH}(\text{CH}_3)$  of initiator) and the aromatic protons of the repetitive units 6.52 – 7.02 ppm respective of the ionic species at 5.25 ppm ( $\text{NCH}_2\text{C}_6\text{H}_4$ ).  
b) Heating rate 10 K min $^{-1}$ .

#### 4.4.3. Synthesis of poly(styrene) copper(I)-bis(NHC) networks (**21**)



Scheme 21. Synthesis of network based mechanocatalysts (**21**) using strong base method.

In a typical procedure, **20a** (1.00 g, 0.13 mmol,  $M_n$  (NMR) = 7500 g mol $^{-1}$ , 5 functional groups per polymer chain) were dissolved in DMF (1.0 mL) adjusting a concentration of 1.00 g mL $^{-1}$  followed by three freeze-pump-thaw cycles in order to remove oxygen. After adding  $\text{NaO}^t\text{Bu}$  (81 mg, 0.85 mmol, 1.3 eq. per functional group), the reaction mixture was stirred at room temperature for 15 min subsequently followed by addition of tetrakis(acetonitrile)copper(I)hexafluorophosphate (0.12 g, 0.33 mmol, 0.5 eq. per functional group) which caused immediately the formation of a precipitate. The solvent was removed, and the residue was washed with THF and MeCN to obtain network **21a** as a yellow-brown solid.

Table 18. Characterization data for copper(I)-bis(NHC) based networks (**21**).

Ent.	Comp.	Ratio styr./19 <sup>a)</sup>	$\vartheta_{exp}$ [mol m <sup>-3</sup> ] <sup>b)</sup>	Amount Cu <sub>exp</sub> [mmol <sub>Cu</sub> /100 mg <sub>sample</sub> ] <sup>c)</sup>	Amount Cu <sub>theo</sub> [mmol <sub>Cu</sub> /100 mg <sub>sample</sub> ] <sup>d)</sup>	Conv. [%]
1	21a	11:1	120	0.055	0.072	83
2	21b	3:1	710	0.142	0.152	93
3	21c	1:1	2360	0.178	0.225	79

a) Determined via <sup>1</sup>H-NMR spectroscopy.

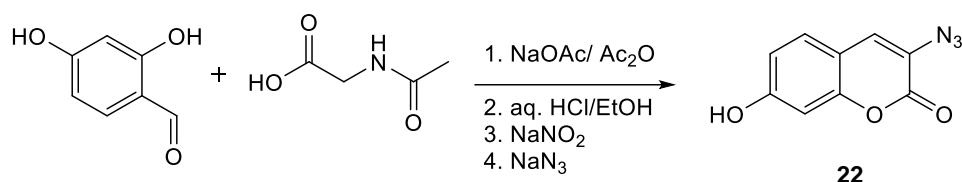
b) Crosslinking density  $\vartheta_{exp}$  in swollen state.

c) Determined by FAAS.

d) Theoretical value for full conversion of imidazole moieties (**20**).

#### 4.5. Mechanochemical activation of copper(I)-bis(NHC) complexes in bulk via compression

##### 4.5.1. Synthesis of 3-azido-7-hydroxycoumarin (**22**)



Scheme 22. Synthesis of 3-azido-7-hydroxycoumarin (**22**).

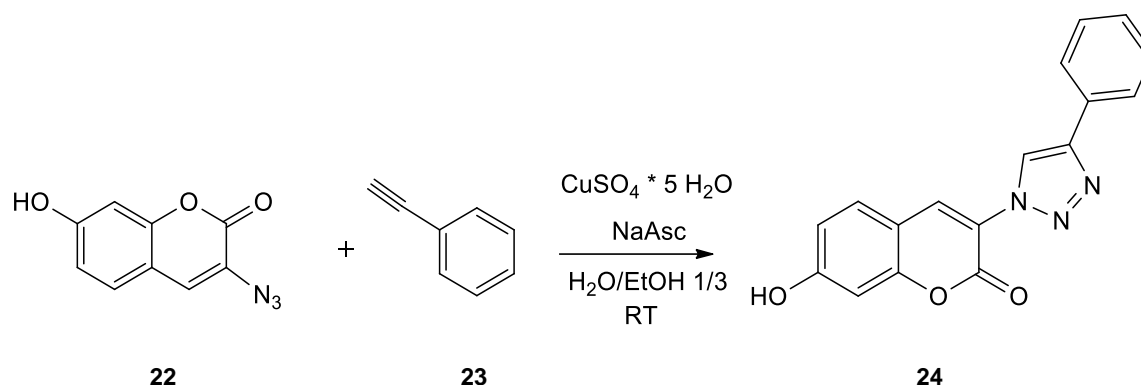
2,4-Dihydroxybenzaldehyde (8.31 g, 60 mmol), *N*-acetyl glycine (7.05 g, 60 mmol) and sodium acetate (18.3 g, 240 mmol) was suspended in Ac<sub>2</sub>O (300 mL) and was stirred for 250 min under reflux. The reaction mixture was allowed to come to room temperature and poured in an ice bath (500 mL). The precipitate was filtered off and was washed with cold water (3 x 70 mL). The crude residue was dissolved in HCl (36 wt.%) /EtOH 2:1 (90 mL) and heated up for 60 min under reflux. After addition of ice water (70 mL), the reaction mixture was cooled to – 5°C. Sodium nitrite (8.31 g, 120 mmol) was added followed by the dropwise addition of sodium azide (11.70 g, 180 mmol). In this step, the temperature of 0°C was not exceeded. The resulting suspension was stirred for 15 min at RT, the precipitate was filtered off and finally dried in high vacuum to obtain compound **22** (1.53 g, 7.80 mmol, 13%) as a brown solid.

**<sup>1</sup>H-NMR (DMSO-*d*<sub>6</sub>, 400 MHz):**  $\delta$  [ppm] 10.53 (bs, 1H, OH), 7.59 (s, 1H, CHCN<sub>3</sub>), 7.48 (d, <sup>3</sup>*J*<sub>H,H</sub> = 8.5 Hz, 1H, OCCHCHC), 6.81 (dd, <sup>3</sup>*J*<sub>H,H</sub> = 8.52, <sup>4</sup>*J*<sub>H,H</sub> = 3.00 Hz, 1H, OCCHCHC), 6.76 (d, <sup>3</sup>*J*<sub>H,H</sub> = 2.2 Hz, 1H, OCCHC).

**<sup>13</sup>C-NMR (DMSO-*d*<sub>6</sub>, 100 MHz):**  $\delta$  [ppm] 160.7 (COH), 157.7 (C=O), 153.2 (COC=O), 129.5 (CHCHCOH), 128.2 (CCHCOH), 121.5 (CN<sub>3</sub>), 114.2 (CHCHCOH), 111.7 (CCHCN<sub>3</sub>), 102.5 (CHCN<sub>3</sub>).

**ESI-TOF-MS (positive mode, THF, *m/z*):** [M+H]<sup>+</sup> found 204.053, simulated 204.040 for C<sub>9</sub>H<sub>6</sub>N<sub>3</sub>O<sub>3</sub><sup>+</sup> and [M-N<sub>2</sub>]<sup>+</sup> found 175.026, simulated 175.074 for C<sub>9</sub>H<sub>5</sub>NO<sub>3</sub><sup>+</sup>.

**FT-IR (ATR):** 1/ $\lambda$  [cm<sup>-1</sup>] = 3298 (m), 3051 (w), 2363 (w), 2114 (s), 1678 (s), 1618 (s), 1599 (s), 1511 (w), 1453 (w), 1371 (w), 1342 (w), 1317 (m), 1257 (m), 1222 (m), 1155 (m), 1122 (m), 1066 (w), 980 (w), 923 (w), 857 (w), 836 (w), 814 (w), 746 (w), 721 (w), 626 (w), 582 (w).

4.5.2. Synthesis of 7-hydroxy-3-(4-phenyl-[1,2,3]triazol-1-yl)-coumarin (**24**)Scheme 23. Synthesis of 7-hydroxy-3-(4-phenyl-[1,2,3]triazole-1-yl)-coumarin (**24**)

3-Azido-7-hydroxycoumarin **22** (0.49 mmol, 100 mg) was added to a solution of phenylacetylene (**23**) (54  $\mu$ l, 0.51 mmol), copper(II)-sulfate-pentahydrate (460  $\mu$ l, 0.03 mmol, 0.1 M in H<sub>2</sub>O) and sodiumascorbate (23.80 mg, 0.12 mmol) in 5.0 mL water/EtOH 1/3 and stirred for 18 h at RT. Ice water was added to the brownish suspension, EtOH was removed under reduced pressure, the residue was filtered off and finally washed with ice water (3 x 4 mL). After drying in high vacuum compound **24** (132 mg, 0.43 mmol, 90%) was obtained as brown solid.

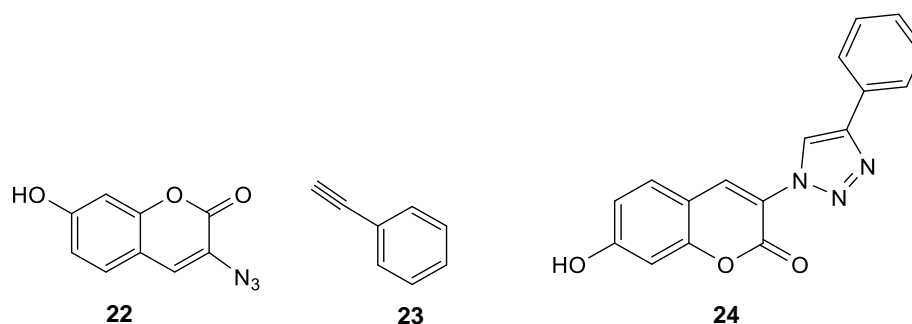
<sup>1</sup>H-NMR (DMSO-*d*<sub>6</sub>, 400 MHz):  $\delta$  [ppm] 10.92 (s, 1H, OH), 8.99 (s, 1H, triazole), 8.64 (s, 1H, CHCN), 7.95 (d, <sup>3</sup>J<sub>HH</sub> = 7.2 Hz, 2H, CH<sub>ortho</sub>), 7.77 (d, <sup>3</sup>J<sub>HH</sub> = 8.5 Hz, OCCHCHC), 7.49 (t, <sup>3</sup>J<sub>HH</sub> = 7.49 Hz, 2H, CH<sub>meta</sub>), 7.38 (t, <sup>3</sup>J<sub>HH</sub> = 7.4 Hz, 1H, CH<sub>para</sub>), 6.92 (d, <sup>3</sup>J<sub>HH</sub> = 8.6 Hz, 1H, OCCHCH), 6.87 (s, 1H, CCHCO).

<sup>13</sup>C-NMR (DMSO-*d*<sub>6</sub>, 100 MHz):  $\delta$  [ppm] 163.4 (C=O), 156.8 (COH), 155.3 (CHCO), 146.9 (NCHC), 137.3 (CHCCN), 131.5 (CHCCN), 130.5 (C<sub>ortho</sub>), 129.5 (O=CCN), 128.7 (C<sub>meta</sub>), 125.8 (HOCCHCH), 122.6 (C<sub>para</sub>), 119.5 (CCHCN), 114.9 (CCHCN), 110.6 (HOCCHC), 102.7 (HOCCHC).

ESI-TOF-MS (positive mode, THF, *m/z*): [M+Na]<sup>+</sup> found 328.050, simulated 328.069 for C<sub>17</sub>H<sub>11</sub>N<sub>3</sub>NaO<sub>3</sub><sup>+</sup> and [M-C<sub>8</sub>H<sub>6</sub>N<sub>2</sub>Na]<sup>+</sup> found 217.128, simulated 217.034 for C<sub>9</sub>H<sub>8</sub>O<sub>4</sub>NNa<sup>+</sup>.

FT-IR (ATR): 1/ $\lambda$  [cm<sup>-1</sup>] = 3169 (w), 3134 (w), 3083 (w), 1731 (m), 1711 (m), 1603 (s), 1478 (w), 1449 (w), 1411 (m), 1338 (w), 1238 (m), 1176 (w), 1130 (w), 1077 (w), 1051 (w), 995 (w), 925 (w), 860 (w), 817 (w), 764 (w), 694 (w), 634 (w).

## 4.5.3. Fluorescence calibration for fluorogenic "click" reaction



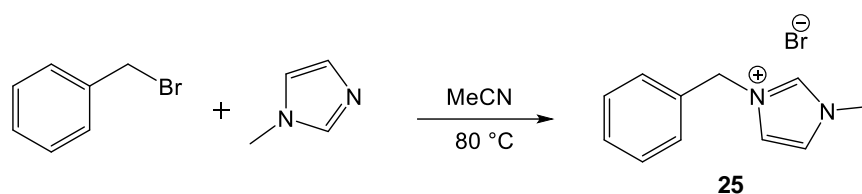
Scheme 24. Components involved in calibration for fluorogenic "click" reaction.

Calibration of fluorescence spectrometer was done by embedding the clicked fluorogenic dye **24** in different concentrations in a high molecular weight pTHF matrix. Fluorescence quenching effects based on the chromaticity of the dye were neglected adjusting an overall concentration of coumarin based dyes (**22** + **24**) constant at  $1.6 \cdot 10^{-4} \text{ mmol mg}^{-1}$ . The experimentally used concentrations ( $c_{(24)} = 0, 1.5 \cdot 10^{-6}, 2.9 \cdot 10^{-6}, 7.7 \cdot 10^{-6}, 1.6 \cdot 10^{-5}, 3.2 \cdot 10^{-5}, 6.4 \cdot 10^{-5}, 1.6 \cdot 10^{-4} \text{ mmol}_{(24)} \text{ mg}_{\text{sample}}^{-1}$ ) of **24** were adjusted dissolving the pTHF matrix (200 mg,  $M_n = 112\,000 \text{ g mol}^{-1}$ ), the corresponding amounts of **24** and **22** in dry THF. After the solution became homogenous, the solvent was removed under reduced pressure and the sample was brought roughly into a cylindrical form (diameter  $\sim 13 \text{ mm}$ ) using spatula and tweezer and was allowed to crystallize for one week into dark. After crystallization, the samples were compressed using an automatic hydraulic press together with a 13 mm pellet compression tool applying 10 tons pressure (corresponding to 0.74 GPa). The fluorescence intensity was measured at 427 nm after excitation at 360 nm. The obtained fluorescence was finally fitted versus the conversion.

Table 19. Detailed data for the calibration of the fluorescence intensity versus the concentration of the 7-hydroxy-3-(4-phenyl-1H-[1,2,3]triazole-1-yl)-coumarin (**24**) in a pTHF matrix.

Ent.	$n_{(24)}$ [mmol]	$m_{(24)}$ [mg]	$n_{(22)}$ [mmol]	$m_{(22)}$ [mg]	I <sub>Fl.</sub> (427 nm) Sample1 [a.u.]	I <sub>Fl.</sub> (427 nm) Sample 2 [a.u.]	I <sub>Fl.</sub> (427 nm) Sample 3 [a.u.]	I <sub>Fl.</sub> (427 nm) Average [a.u.]	conv. <sup>a)</sup> [%]
1	0	0	$3.4 \cdot 10^{-2}$	6.98	17	17	17	17	0
2	$3.0 \cdot 10^{-4}$	0.10	$3.4 \cdot 10^{-2}$	6.91	23	24	25	24	1
3	$6.0 \cdot 10^{-4}$	0.20	$3.4 \cdot 10^{-2}$	6.85	25	26	26	25	2
4	$1.6 \cdot 10^{-3}$	0.50	$3.2 \cdot 10^{-2}$	6.65	44	49	49	47	5
5	$3.2 \cdot 10^{-3}$	1.00	$3.1 \cdot 10^{-2}$	6.31	74	78	88	80	10
6	$6.6 \cdot 10^{-3}$	2.02	$2.8 \cdot 10^{-2}$	5.63	160	170	182	170	19
7	$1.3 \cdot 10^{-2}$	4.08	$2.1 \cdot 10^{-2}$	4.26	477	483	510	490	39
8	$3.4 \cdot 10^{-2}$	10.50	0	0	939	973	989	967	100

a) Conversion was calculated according to  $y = 6.01 \cdot 10^6 (\pm 2.94 \cdot 10^5) x + 1.12 \cdot 10^1 (\pm 1.86 \cdot 10^1)$ .

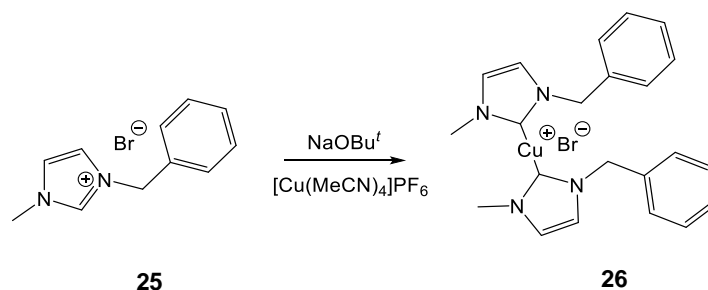
4.5.4. Synthesis of 3-benzyl-1-methylimidazolium bromide (**25**)Scheme 25. Synthesis of 3-benzyl-1-methylimidazolium bromide (**25**).

1-Methylimidazole (2.42 mL, 30 mmol) was added dropwise to a solution of benzyl bromide (6.48 mL, 30 mmol) in acetonitrile (MeCN) (15 mL) at 0°C and was stirred for 24 h at 60°C. The crude product was diluted with water (20 mL) and washed with  $\text{CHCl}_3$  (3 x 20 mL) followed by evaporation of water at reduced pressure. After drying in high vacuum **25** (7.41 g, 29.40 mmol, 98%) was obtained as colorless highly viscous oil.

$^1\text{H-NMR}$  ( $\text{CDCl}_3$ , 400 MHz):  $\delta$  [ppm] 10.24 (s, 1H,  $\text{NCHN}$ ), 7.47 (m, 3H,  $\text{CH}_{para} + \text{CH}_{ortho}$ ), 7.38 – 7.28 (m, 4H,  $\text{CH}_{para} + \text{NCHCHN}$ ), 5.55 (s, 2H,  $\text{NCH}_2$ ), 4.02 (s, 3H,  $\text{NCH}_3$ ).

$^{13}\text{C-NMR}$  ( $\text{CDCl}_3$ , 100 MHz):  $\delta$  [ppm] 137.0 ( $\text{NCHN}$ ), 133.1 ( $\text{CCH}_2\text{N}$ ), 129.4 ( $\text{C}_{para}$ ), 129.3 ( $\text{C}_{ortho}$ ), 128.9 ( $\text{C}_{meta}$ ), 123.8 ( $\text{CH}_3\text{NCHCHN}$ ), 122.0 ( $\text{CH}_3\text{NCHCHN}$ ), 53.1 ( $\text{NCH}_2$ ), 36.7 ( $\text{NCH}_3$ ).

ESI-TOF-MS (positive mode, MeOH,  $m/z$ ):  $[\text{M-Br}]^+$  found 173.108, simulated 173.107 for  $\text{C}_{11}\text{H}_{13}\text{N}_2^+$ .

4.5.5. Synthesis of low molecular weight copper(I)-bis(NHC) complex (**26**)Scheme 26. Synthesis of low molecular weight copper(I)-bis(NHC) complex (**26**) using strong base method.

To a solution of **25** (1.0 g, 3.97 mmol) in dry MeCN (15 mL) sodium *tert*-butoxide (0.42 g, 4.37 mmol, 1.3 eq.) was added and the solution was stirred for 15 minutes at room temperature followed by addition of copper(I) bromide (0.28 g, 1.98 mmol, 0.5 eq.). The reaction mixture was stirred at 60°C for further 48 hours. The resulting suspension was filtered, and the solvent was removed under reduced pressure. After column chromatography on silica by gradually changing the polarity of solvent from EA/MeOH 50/1 to EA/MeOH 10/1 ( $R_f = 0.48$  EA/MeOH 10/1) bis(3-benzyl-1-methyl-imidazol-2-yl)copper(I)-bromide (**26**) (1.19 g, 2.42 mmol, 61%) was obtained as a colorless solid.

$^1\text{H-NMR}$  ( $\text{CDCl}_3$ , 400 MHz):  $\delta$  [ppm] 7.41 – 7.21 (m, 10H,  $\text{CH}_{Ar}$ ), 6.12 (dd,  $^3J_{\text{H,H}} = 21.8$ ,  $^4J_{\text{H,H}} = 2.9$  Hz, 4H,  $\text{NCHCHN}$ ), 4.78 (s, 4H,  $\text{NCH}_2$ ), 3.27 (s, 6H,  $\text{NCH}_3$ ).

$^{13}\text{C-NMR}$  ( $\text{CDCl}_3$ , 100 MHz):  $\delta$  [ppm] 153.4 ( $\text{NCCuN}$ ), 137.0 ( $\text{CCH}_2\text{N}$ ), 128.7 ( $\text{C}_{para}$ ), 127.8 ( $\text{C}_{ortho}$ ), 127.7 ( $\text{C}_{meta}$ ), 111.6 ( $\text{CH}_3\text{NCHCHN}$ ), 109.8 ( $\text{CH}_3\text{NCHCHN}$ ), 47.2 ( $\text{NCH}_2$ ), 30.5 ( $\text{NCH}_3$ ).

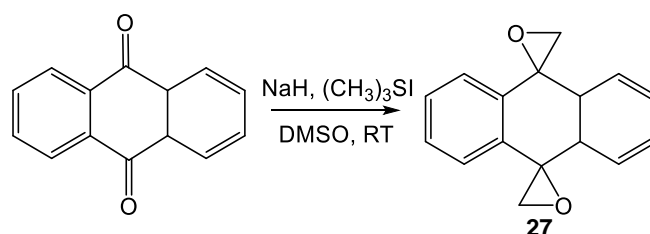
## 4.5.6. Mechanochemical activation

The catalytic activity of different latent copper(I)-bis(NHC) complexes was demonstrated by embedding 0.033 eq. of the bis(NHC) complexes and an equimolar ratio of phenylacetylene (**23**) and 3-azido-7-hydroxy-coumarin (**22**) in a high molecular weight pTHF matrix with a copper(I) concentration of  $5.4 \cdot 10^{-6}$  mmol  $\text{mg}_{\text{sample}}^{-1}$ . After crystallizing the sample for one week, the sample was transferred in a KBr pellet die compression tool. A compression force of 10 tons (corresponding to 0.74 GPa) was applied via a hydraulic press into 20 compression cycles folding the sample between each compression cycle. The fluorescence was determined before and after compression with an emission maximum at a wavelength of  $\lambda_{\text{em}} = 427$  nm after an excitation at  $\lambda_{\text{ex}} = 360$  nm. Previous calibration of the fluorescence spectrometer with respect to the dye concentration enabled a quantitative comparison of catalytic efficiency.

Table 20. Summary of catalytic activity of force activated chain-extended (**18**), network-based (**21**) and low molecular weight (**26**) mechanocatalysts, towards the fluorogenic “click” reaction from (**22**) with phenylacetylene (**24**).

Ent.	Cu(I) catalyst	$M_n(\text{GPC})$ [g mol <sup>-1</sup> ]	Conversion [%] after compression cycle					
			0	1 <sup>st</sup>	2 <sup>nd</sup>	3 <sup>rd</sup>	10 <sup>th</sup>	20 <sup>th</sup>
Control experiments								
<b>1</b>		without	0	0	0	0	0	0
<b>2</b>	<b>25</b>	Low MW	0	0	0	0	0	0
Chain extended copper(I)-bis(NHC) complexes								
<b>3</b>	<b>18a</b>	15000	1	5	6	7	14	16
<b>4</b>	<b>18b</b>	21500	3	5	16	28	40	44
Network based copper(I)-bis(NHC) complexes								
<b>5</b>	<b>21a</b>	11:1	0	20	24	33	44	44
<b>6</b>	<b>21b</b>	3:1	0	4	7	9	11	12
<b>7</b>	<b>21c</b>	1:1	0	7	8	11	12	12

## 4.6. Synthesis of poly(urethane) networks

4.6.1. Synthesis of trans-dispiro[oxirane-2,9[10'H]-anthracene-10',2''-oxirane] (**27**)

Scheme 27. Synthesis of trans-dispiro[oxirane-2,9[10'H]-anthracene-10',2''-oxirane] (**27**) via COREY-CHAYKOVSKY epoxidation.

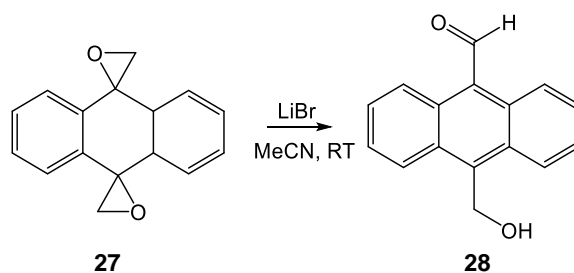
To a suspension of NaH (0.50 g, 13.00 mmol, 60% in oil) in dry DMSO (30 mL) trimethyl sulfonium iodide (2.85 g, 12.64 mmol) was added dropwise in the dark. After stirring for 8 hours, anthraquinone (1.17 g, 5.62 mmol) in DMSO (20 mL) was added and subsequently stirred at RT for additional 16 h. The reaction mixture was poured into an ice bath, the resulting

precipitate was collected and after recrystallization in ethanol compound **27** (1.11 g, 4.66 mmol, 78%) was obtained a colorless solid.

$^1\text{H-NMR}$  ( $\text{CDCl}_3$ , 400 MHz):  $\delta$  [ppm] 7.56 – 7.25 (m, 8H,  $\text{CH}_{Ar}$ ), 3.25 (s, 4H,  $\text{CH}_2$ ).

$^{13}\text{C-NMR}$  ( $\text{CDCl}_3$ , 100 MHz):  $\delta$  [ppm] 135.4 ( $\text{CHCCO}$ ), 128.4 ( $\text{CHCHC}$ ), 122.3 ( $\text{CHCHC}$ ), 63.8 ( $\text{CH}_2\text{O}$ ), 54.4 ( $\text{CCH}_2\text{O}$ ).

#### 4.6.2. Synthesis of 10-(hydroxymethyl) anthracene-9-carbaldehyde (**28**)



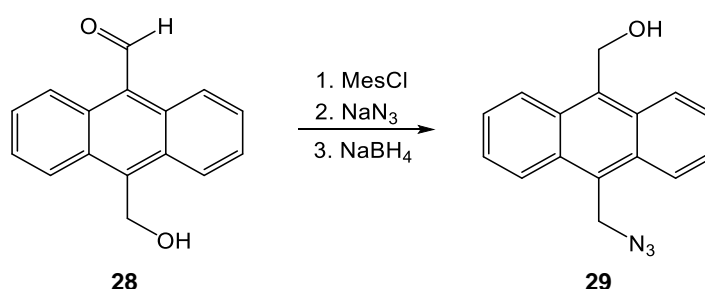
Scheme 28. Synthesis of 10-(hydroxymethyl) anthracene-9-carbaldehyde (**28**).

LiBr (1.00 g, 11.50 mmol) was added to a solution of compound **27** (0.59 g, 2.50 mmol) in MeCN (80 mL) and was stirred in the dark overnight. The reaction mixture was concentrated by removing MeCN under reduced pressure. After crystallization at 20°C, compound **28** (0.53 g, 2.25 mmol, 90%) was obtained as light-yellow crystals.

$^1\text{H-NMR}$  ( $\text{CDCl}_3$ , 400 MHz):  $\delta$  [ppm] 11.53 (s, 1H,  $\text{HC}=\text{O}$ ), 8.94 – 8.91 (m, 2H,  $\text{CHCCC}=\text{O}$ ), 8.56 – 8.53 (m, 8H,  $\text{CHCCCH}_2\text{OH}$ ), 7.74 – 7.62 (m, 4H,  $\text{CH}_{Ar}$ ), 5.74 (d,  $^3J_{\text{H,H}} = 5.8$  Hz, 4H,  $\text{CH}_2$ ).

$^{13}\text{C-NMR}$  ( $\text{CDCl}_3$ , 100 MHz):  $\delta$  [ppm] 193.8 ( $\text{HC}=\text{O}$ ), 138.6 ( $\text{CCH}_2\text{OH}$ ), 131.4 ( $\text{CCCH}_2\text{OH}$ ), 129.8 ( $\text{CHCHCCC}=\text{O}$ ), 128.4 ( $\text{CCC}=\text{O}$ ), 126.6 ( $\text{CHCHCCCH}_2\text{OH}$ ), 124.7 ( $\text{CHCCCH}_2\text{OH}$ ), 124.2 ( $\text{CC}=\text{O}$ ), 57.6 ( $\text{CH}_2\text{OH}$ ).

#### 4.6.3. Synthesis of (10-Azidomethylantracene-9-yl)methanol (**29**)



Scheme 29. Synthesis of (10-Azidomethylantracene-9-yl)methanol (**29**).

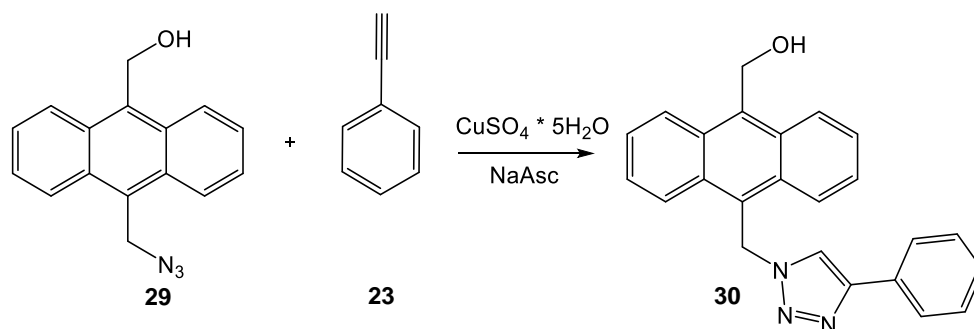
Triethylamine (0.46 mL, 3.30 mmol) was added to a suspension of compound **28** (0.52 g, 2.20 mmol) in DCM/MeCN 1/1 (40 mL) followed by the addition of methane sulfonyl chloride 0.32 g, 2.75 mmol). The reaction mixture was stirred at RT for 4 h, HCl (30 mL, 1 M) was added and the organic layer was washed with water (2 x 50 mL) and brine (50 mL) and was dried over anhydrous  $\text{Na}_2\text{SO}_4$ . After removing the solvent under reduced pressure, the residue was dissolved in DMF (50 mL),  $\text{NaN}_3$  (0.21 g, 3.30 mmol) was added, the reaction mixture was stirred overnight. After the addition of water (100 mL), the solution was extracted with EA (3 x

50 mL). The combined organic layers were dried over anhydrous  $\text{Na}_2\text{SO}_4$  and the solvent was removed under reduced pressure. Finally, the obtained residue was suspended in ethanol (50 mL),  $\text{NaBH}_4$  (0.12 g, 3.30 mmol) was added in small portions at  $0^\circ\text{C}$  and the reaction mixture was stirred at RT overnight. Afterwards, concentrated HCl (5.00 mL, 37%) was added. Then, the reaction mixture was diluted with  $\text{H}_2\text{O}$  (150 mL) and was extracted with DCM (3 x 70 mL). The combined organic layers were dried over anhydrous  $\text{Na}_2\text{SO}_4$ . After flash chromatography on silica (EA/Hex 1/4), compound **29** (0.30 g, 1.14 mmol, 52%) was obtained as a yellow solid.

**$^1\text{H-NMR}$  (DMSO- $d_6$ , 400 MHz):**  $\delta$  [ppm] 8.57 – 8.50 (m, 2H,  $\text{CHCCCH}_2\text{OH}$ ), 8.49 – 8.42 (m, 2H,  $\text{CHCCCH}_2\text{N}_3$ ), 7.66 – 7.58 (m, 4H,  $\text{CH}_{Ar}$ ), 5.50 (s, 2H,  $\text{CH}_2\text{N}_3$ ), 5.46 (d,  $^3J_{\text{H,H}} = 5.3$  Hz, 3H,  $\text{CH}_2\text{OH}$ ), 5.38 (t,  $^3J_{\text{H,H}} = 5.3$  Hz, 1H, OH).

**$^{13}\text{C-NMR}$  (DMSO- $d_6$ , 100 MHz):**  $\delta$  [ppm] 135.4 ( $\text{CCH}_2\text{OH}$ ), 130.6 ( $\text{CCCH}_2\text{OH}$ ), 130.0 ( $\text{CCCH}_2\text{N}_3$ ), 127.3 ( $\text{CHCHCCCH}_2\text{N}_3$ ), 126.8 ( $\text{CHCHCCCH}_2\text{OH}$ ), 126.1 ( $\text{CHCCCH}_2\text{OH}$ ), 126.1 ( $\text{CHCCCH}_2\text{N}_3$ ), 124.9 ( $\text{CCH}_2\text{N}_3$ ), 55.9 ( $\text{CH}_2\text{OH}$ ), 46.1 ( $\text{CH}_2\text{N}_3$ ).

#### 4.6.4. Synthesis of [10-(4-Phenyl-[1,2,3]triazol-1-ylmethyl)-anthracen-9-yl] methanol (**30**)

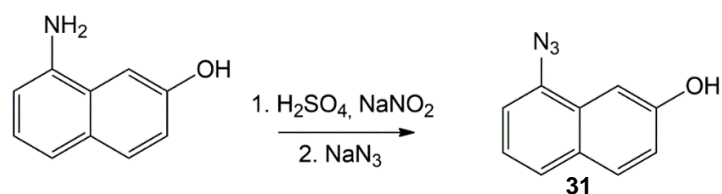


Scheme 30. “Click” reaction of (10-Azidomethylanthracen-9-yl)methanol (**29**) and phenylacetylene (**23**).

Compound **29** (78.99 mg, 0.30 mmol) and phenylacetylene **23** were suspended in DMF/water 3/1 (28 mL) followed by the addition of  $\text{CuSO}_4 \cdot 5\text{H}_2\text{O}$  (7.00 mg, 0.05 mmol), NaAsc (14.00 mg, 0.09 mmol) and TBTA (8.00 mg, 0.02 mmol). The reaction mixture was stirred at RT for 24 h, water was added, and the solution was extracted by EA (3 x 25 mL). The combined organic layers were dried over anhydrous  $\text{Na}_2\text{SO}_4$ . After column chromatography on silica changing the polarity of solvent from EA/Hex 9/1 to EA/Hex 4/1, compound **30** (98.66 mg, 0.27 mmol, 93%) was obtained as a yellow solid.

**$^1\text{H-NMR}$  (DMSO- $d_6$ , 400 MHz):**  $\delta$  [ppm]  $\delta$  8.66 – 8.59 (m, 2H,  $\text{CHCCCH}_2\text{N}$ ), 8.59 – 8.52 (m, 2H,  $\text{CHCCCH}_2\text{OH}$ ), 8.37 (s, 1H, triazole), 7.80 – 7.71 (m, 2H,  $\text{CH}_{ortho}$ ), 7.69 – 7.57 (m, 4H,  $\text{CH}_{Ar}$ ), 7.36 – 7.31 (m, 2H,  $\text{CH}_{meta}$ ), 7.27 – 7.18 (m, 1H,  $\text{CH}_{para}$ ), 6.68 (s, 2H,  $\text{CH}_2\text{N}$ ), 5.48 (d,  $^3J_{\text{H,H}} = 5.1$  Hz, 2H,  $\text{CH}_2\text{OH}$ ), 5.39 (t,  $^3J_{\text{H,H}} = 5.4$  Hz, 1H, OH).

**$^{13}\text{C-NMR}$  (DMSO- $d_6$ , 100 MHz):**  $\delta$  [ppm] 146.7 (NCC), 135.9 ( $\text{CCCH}_2\text{OH}$ ), 131.0 ( $\text{CCCH}_2\text{N}$ ), 130.7 (NCC), 130.1 ( $\text{CCCH}_2\text{OH}$ ), 129.2 ( $\text{CCCH}_2\text{N}$ ), 128.2 ( $\text{CH}_{para}$ ), 127.1 ( $\text{CHCHCCCH}_2\text{N}$ ), 126.4 ( $\text{CH}_{ortho}$ ), 126.1 ( $\text{CH}_{meta}$ ), 126.0 ( $\text{CHCHCCCH}_2\text{OH}$ ), 125.6 ( $\text{CHCCCH}_2\text{OH}$ ), 124.9 ( $\text{CHCCCH}_2\text{N}$ ), 121.43 (NCHC), 55.9 ( $\text{CH}_2\text{OH}$ ), 46.4 ( $\text{CH}_2\text{N}$ ).

4.6.5. Synthesis of 8-azidonaphthalen-2-ol (**31**)Scheme 31. Synthesis of 8-azidonaphthalen-2-ol (**31**).

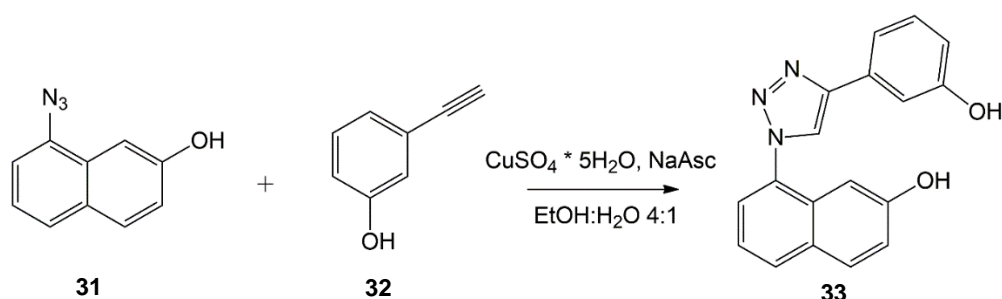
HCl (8 mL, 36 wt.%) was added dropwise to a suspension of 8-amino-2-naphthol (2.00 g, 12.5 mmol) in water (70 mL) and was cooled to  $-5^{\circ}\text{C}$ . A solution of  $\text{NaNO}_2$  (1.30 g, 18.75 mmol) in water (10 mL) was added slowly and the mixture was stirred for 30 min at  $-5^{\circ}\text{C}$ . Over a time of 40 min, a solution of  $\text{NaN}_3$  (1.21 g, 18.75 mmol) in ice cold water (15 mL) was added and the reaction mixture was stirred at RT for 1 h. Afterwards, the solution was extracted with  $\text{Et}_2\text{O}$  and washed with water. The combined organic layers were dried via  $\text{Na}_2\text{SO}_4$  and the solvent was evaporated under reduced pressure. After purification via flash chromatography on silica with *n*-hexane/EA 5/1 ( $R_f = 0.51$ ), compound **31** (1.46 g, 7.88 mmol, 63%) was obtained as a pale brown solid.

$^1\text{H-NMR}$  ( $\text{CDCl}_3$ , 400 MHz):  $\delta$  [ppm] 7.73 (d,  $^3J_{\text{H,H}} = 8.8$  Hz, 1H, CCHCHCO), 7.57 (d,  $^3J_{\text{H,H}} = 8.2$  Hz, 1H, CHCHCN<sub>3</sub>), 7.39 (d,  $^3J_{\text{H,H}} = 2.5$  Hz, 1H, N<sub>3</sub>CCHCHCH), 7.32 (t,  $^3J_{\text{H,H}} = 8.1$  Hz, 1H, OCCHC), 7.22 (d,  $^3J_{\text{H,H}} = 7.1$  Hz, 1H, CHCN<sub>3</sub>), 7.14 (dd,  $^3J_{\text{H,H}} = 8.8$ ,  $^4J_{\text{H,H}} = 2.6$  Hz, 1H, OCCH), 5.10 (s, 1H, OH).

$^{13}\text{C-NMR}$  ( $\text{CDCl}_3$ , 100 MHz):  $\delta$  [ppm] 153.7 (COH), 134.9 (CN<sub>3</sub>), 129.8 (N<sub>3</sub>CC), 129.8 (HOCCHCH), 127.5 (N<sub>3</sub>CHCH), 124.6 (N<sub>3</sub>CHCHCH), 123.3 (N<sub>3</sub>CCH), 118.7 (CHCCH), 114.5 (HOCCH), 104.7 (HOCCHC).

ESI-TOF MS (negative mode, THF:MeOH 99:1,  $m/z$ ):  $[\text{M-H}]^-$  found 184.066, simulated 184.052 for  $\text{C}_{10}\text{H}_7\text{N}_3\text{O}^-$ .

FT-IR (ATR):  $1/\lambda$  [ $\text{cm}^{-1}$ ] = 3316 (br), 2121 (s), 1631 (w), 1594 (m), 1524 (w), 1465 (m), 1394 (w), 1354 (w), 1294 (s), 1233 (m), 1199 (w), 1175 (s), 1137 (m), 1071 (w), 1012 (w), 916 (w), 884 (w), 858 (w), 827 (s), 780 (w), 759 (w), 738 (m), 721 (w), 666 (w), 634 (w).

4.6.6. Synthesis of 8-(4-(3-hydroxyphenyl)-1,2,3-triazol-1-yl)naphthalen-2-ol (**33**)Scheme 32. Synthesis of 8-(4-(3-hydroxyphenyl)-1,2,3-triazol-1-yl)naphthalen-2-ol (**33**).

A stock solution of  $\text{CuSO}_4 \cdot 5\text{H}_2\text{O}$  (54.0  $\mu\text{mol}$ , 13.4 mg in 0.5 mL water) and a stock solution of sodium ascorbate (NaAsc) (80.0  $\mu\text{mol}$ , 16.1 mg in 0.5 mL water) were added to a mixture of **31** (100.0 mg, 0.54 mmol) and 3-hydroxyphenylacetylene (**32**) (67.1 mg, 0.54 mmol) in EtOH (4 mL). The resultant solution was stirred overnight at RT. The reaction mixture was diluted

with water 15 mL, extracted with  $\text{CHCl}_3$  (3 x 10 mL) and dried over  $\text{Na}_2\text{SO}_4$ . The solvent was evaporated under reduced pressure. After purification via column chromatography with  $\text{CHCl}_3/\text{MeOH}$  20/1 ( $R_f = 0.30$ ), compound **33** (154.0 mg, 0.51 mmol, 94%) was obtained as a yellow solid.

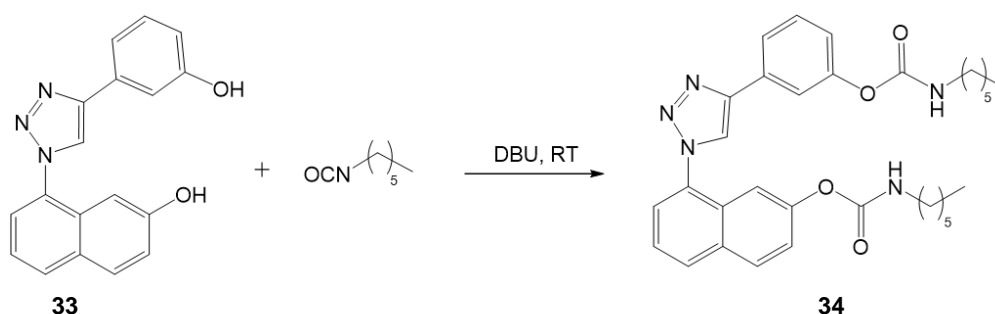
**$^1\text{H-NMR}$  (DMSO- $d_6$ , 400 MHz):**  $\delta$  [ppm] 10.01 (s, 1H,  $\text{OH}_{\text{naph}}$ ), 9.59 (s, 1H,  $\text{OH}_{\text{phe}}$ ), 8.99 (s, 1H, triazole), 8.04 (d,  $^3J_{\text{H,H}} = 8.2$  Hz, 1H,  $\text{OCCHCH}_{\text{naph}}$ ), 7.96 (d,  $^3J_{\text{H,H}} = 8.9$  Hz, 1H,  $\text{CHCHCHCN}_{\text{naph}}$ ), 7.66 (d,  $^3J_{\text{H,H}} = 7.2$  Hz, 1H,  $\text{NCCH}$ ), 7.47 – 7.40 (m, 2H,  $\text{OCCHC} + \text{NCCCHCH}$ ), 7.37 (d,  $^3J_{\text{H,H}} = 7.7$  Hz, 1H,  $\text{CCHCH}_{\text{phe}}$ ), 7.27 (t,  $^3J_{\text{H,H}} = 7.8$  Hz, 1H,  $\text{CCHCH}_{\text{phe}}$ ), 7.18 (dd,  $^3J_{\text{H,H}} = 8.9$ ,  $^4J_{\text{H,H}} = 2.3$  Hz, 1H,  $\text{CCHCO}_{\text{phe}}$ ), 6.78 (dd,  $^3J_{\text{H,H}} = 2.5$  Hz,  $^4J_{\text{H,H}} = 1.0$  Hz, 1H,  $\text{OCCHCH}_{\text{phe}}$ ), 6.76 (d,  $^3J_{\text{H,H}} = 2.4$  Hz, 1H,  $\text{OCCHCH}_{\text{naph}}$ ).

**$^{13}\text{C-NMR}$  (DMSO- $d_6$ , 100 MHz):**  $\delta$  [ppm] 158.3 ( $\text{HOC}_{\text{phe}}$ ), 157.5 ( $\text{HOC}_{\text{naph}}$ ), 147.0 ( $\text{NCCHN}$ ), 132.3 ( $\text{NCCH}$ ), 132.1 ( $\text{HOCCHCH}$ ), 130.7 ( $\text{CHCHCCHCH}$ ), 130.5 ( $\text{NCCCH}$ ), 130.5 ( $\text{HOCCHC}_{\text{phe}}$ ), 130.4 ( $\text{HOCCHCH}_{\text{naph}}$ ), 128.9 ( $\text{NCCHCHCH}$ ), 124.7 ( $\text{NCCHCHCH}$ ), 124.5 ( $\text{NCHCN}$ ), 122.3 ( $\text{NCCH}$ ), 120.3 ( $\text{HOCCH}_{\text{phe}}$ ), 116.7 ( $\text{NCCCH}$ ), 115.6 ( $\text{HOCCH}_{\text{naph}}$ ), 112.6 ( $\text{HOCCHC}_{\text{phe}}$ ), 103.5 ( $\text{HOCCHC}$ ).

**ESI-TOF MS (negative mode, THF:MeOH 99:1,  $m/z$ ):**  $[\text{M-H}]^-$  found 302.041, simulated 302.094 for  $\text{C}_{18}\text{H}_{13}\text{N}_3\text{O}_2^-$ .

**FT-IR (ATR):**  $1/\lambda$  [ $\text{cm}^{-1}$ ] = 3136 (br), 1602 (m), 1516, 1453 (m), 1428 (w), 1383 (w), 1356 (w), 1239 (s), 1200 (s), 1163 (w), 1080 (w), 1046 (w), 1000 (w), 968 (w), 910 (w), 871 (m), 829 (s), 782 (s), 743 (m), 717 (w), 687 (m), 663 (w), 573 (w).

#### 4.6.7. Synthesis of 3-(1-(7-((hexylcarbamoyl)oxy)naphthalen-1-yl)-1H-1,2,3-triazol-4-yl)phenyl hexylcarbamate (**34**)



Scheme 33. Synthesis of model dye (**34**) for determination of optical properties in solution.

Hexamethylene isocyanate (187  $\mu\text{l}$ , 1.28 mmol) was added to a mixture of **33** (150.0 mg, 0.49 mmol) followed by the addition of DBU (0.05 eq) and the resultant solution was stirred 4 h at RT. The reaction mixture was diluted with water 15 mL, was extracted with  $\text{CHCl}_3$  (3 x 10 mL), dried over  $\text{Na}_2\text{SO}_4$  and the solvent was evaporated under reduced pressure. After purification via flash chromatography with  $\text{CHCl}_3/\text{MeOH}$  20/1 compound **34** (234.0 mg, 0.42 mmol, 86%) was obtained as a pale brownish solid.

**$^1\text{H-NMR}$  (DMSO- $d_6$ , 500 MHz):**  $\delta$  [ppm] 9.17 (s, 1H, triazole), 8.23 (d,  $^3J_{\text{H,H}} = 8.3$  Hz, 1H,  $\text{OCCHCH}_{\text{naph}}$ ), 8.17 (d,  $^3J_{\text{H,H}} = 9.0$  Hz, 1H,  $\text{NCCHCHCH}$ ), 7.85 – 7.82 (m, 2H,  $\text{NCCH} + \text{CCHCHCH}_{\text{phe}}$ ), 7.80 (t,  $^3J_{\text{H,H}} = 5.7$  Hz, 2H,  $\text{NH}$ ), 7.75 – 7.66 (m, 2H,  $\text{OCCHC}_{\text{naph}} + \text{CCCH}_{\text{phe}}$ ), 7.54 – 7.46 (m, 2H,  $\text{NCCHCH} + \text{CCHCO}_{\text{phe}}$ ), 7.25 (d,  $^3J_{\text{H,H}} = 2.0$  Hz, 1H,  $\text{OCCH}_{\text{naph}}$ ), 7.12 (dd,  $^3J_{\text{H,H}} = 7.9$ ,  $^4J_{\text{H,H}} = 1.9$  Hz, 1H,  $\text{OCCHCH}_{\text{phe}}$ ), 3.08 (q,  $^3J_{\text{H,H}} = 6.8$  Hz, 2H,  $\text{CH}_2\text{NH}_{\text{naph}}$ ), 3.03 (q,

$^3J_{H,H} = 6.8$  Hz, 2H,  $CH_2NH_{phe}$ ), 1.52 – 1.39 (m, 4H,  $CH_2CH_2NH$ ), 1.36 – 1.18 (m, 12H,  $(CH_2)_6$ ), 0.87 (t,  $^3J_{H,H} = 6.8$  Hz, 3H,  $CH_3_{naph}$ ), 0.83 (t,  $^3J_{H,H} = 6.7$  Hz, 3H,  $CH_3_{phe}$ ).

$^{13}C$ -NMR (DMSO- $d_6$ , 125 MHz):  $\delta$  [ppm] 154.7 ( $C=O_{naph}$ ), 154.4 ( $C=O_{phe}$ ), 152.2 ( $O=COC_{naph}$ ), 151.1 ( $O=COC_{phe}$ ), 146.5 (C<sub>3</sub>N<sub>3</sub>NCH), 133.2 (N<sub>2</sub>CCCH), 132.0 (CCHCOH), 131.7 (NCCHCHCH), 130.7 (NNNCHC), 130.4 (OCCHCH<sub>naph</sub>), 130.3 (OCCHCH<sub>phe</sub>), 128.9 (CHCHCCHCH), 125.3 (CHCHCCHCH), 124.9 (CHCCH<sub>phe</sub>), 124.9 (CHCCH<sub>phe</sub>), 123.7 (NCCHCH<sub>naph</sub>), 122.3 (NCCHCH), 122.1 (OCCH<sub>phe</sub>), 119.2 (OCCH<sub>naph</sub>), 113.1 (OCCH<sub>naph</sub>), 41.0 ( $CH_2NH_{naph}$ ), 40.9 ( $CH_2NH_{phe}$ ), 31.4 ( $CH_2CH_2NH_{naph}$ ), 31.4 ( $CH_2CH_2NH_{phe}$ ), 29.7 ( $(CH_2)_2CH_2NH_{naph}$ ), 29.5 ( $(CH_2)_2CH_2NH_{phe}$ ), 26.4 ( $(CH_2)_3CH_2NH_{naph}$ ), 26.3 ( $(CH_2)_3CH_2NH_{phe}$ ), 22.5 ( $(CH_2)_4CH_2NH_{naph}$ ), 22.5 ( $(CH_2)_4CH_2NH_{phe}$ ), 14.4 ( $CH_3$ ), 14.3 ( $CH_3$ ).

#### 4.6.8. Fluorescence calibration for fluorogenic “click” reaction

The calibration of the fluorescence spectroscope was done embedding the clicked fluorogenic dye **33** in defined amounts into the poly(urethane) networks at the end of the crosslinking process in which followed leaching experiments guarantee the complete covalently incorporation. To compensate potential internal quenching effects of the dye, the overall concentration of naphthalene-based dyes (sum of mmol **31** and mmol **33**) were kept constant at  $8.50 \mu\text{mol g}^{-1}_{\text{sample}}$ . Afterwards, the fluorescence intensity was determined at 437 nm (excitation wavelength: 377nm) at least three times on three different positions to neglect potential inhomogeneities within the material. This results in a direct proportionality of dye concentration and fluorescence intensity and which allowed to determine the conversion of **33** during activation process (Figure 55 B) and thus offered information about the mechanochemical response of the incorporated mechanocatalyst (**3**).

Table 21 Detailed data for the calibration of the fluorescence intensity versus the concentration of (**3**) and (**5**) in PU matrix.

Ent.	$n_{(33)}$ [mmol]	$m_{(33)}$ [mg]	$n_{(31)}$ [mmol]	$m_{(31)}$ [mg]	I <sub>Fl.</sub>	I <sub>Fl.</sub>	I <sub>Fl.</sub>	I <sub>Fl.</sub>	conv. a) [%]
					(438 nm) Sample1 [a.u.]	(438 nm) Sample 2 [a.u.]	(438 nm) Sample 3 [a.u.]	(438 nm) Average [a.u.]	
1	0.000	0.00	0.03	5.55	15	15	15	15	0
2	0.005	1.52	0.025	4.63	108	110	112	110	17
3	0.015	4.55	0.015	2.77	352	355	364	357	50
4	0.020	6.06	0.010	1.85	492	492	492	492	67
5	0.025	7.58	0.005	0.92	652	657	662	657	83
6	0.030	9.09	0.000	0.00	821	822	826	823	100

a) Conversion was calculated according to  $y = 8.0519x - 15.96$ .

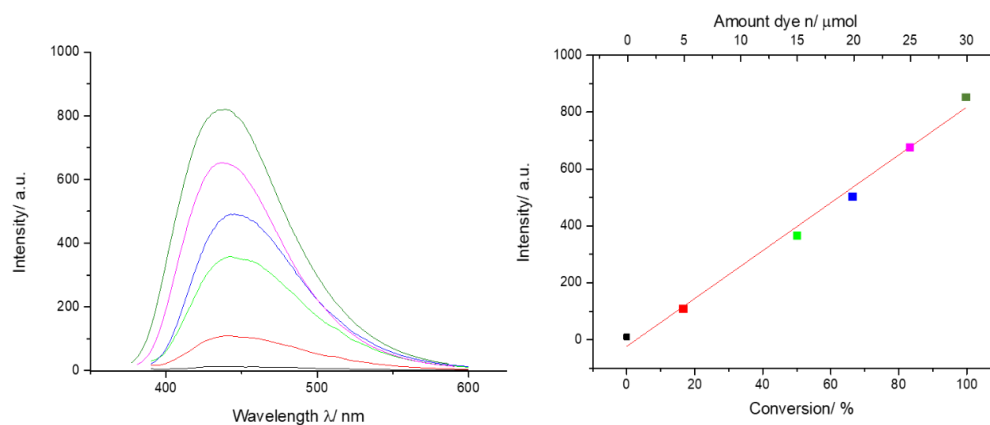
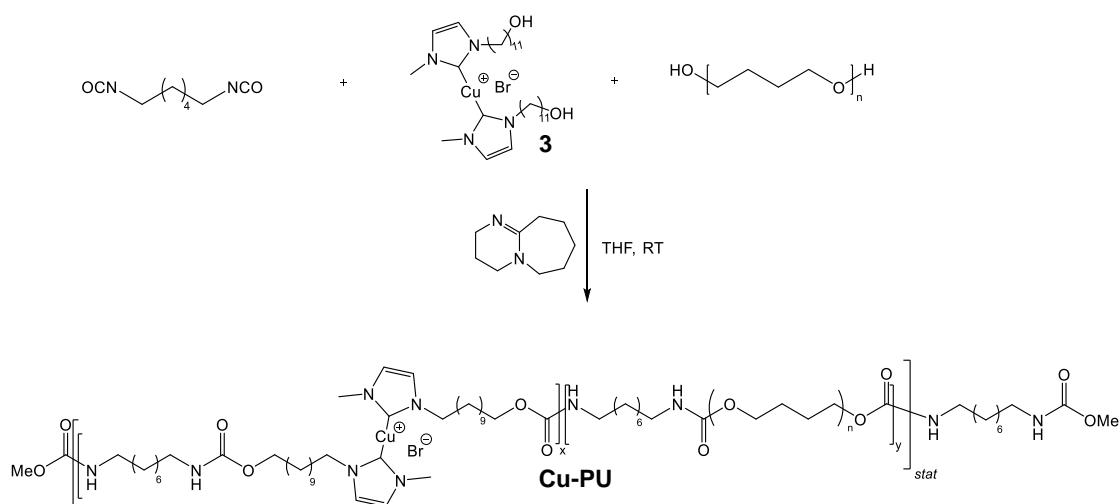


Figure 56. Emission spectra of **29**, which was directly incorporated into poly(urethane) matrix in different concentration leads to an increase in fluorescence intensity with increasing amount of **29** showing up a linear dependency, which can be used to quantify the mechanochemical activation of **PUXX**.

#### 4.6.9. Synthesis of thermoplastic poly(urethane)s as prepolymers (**Cu-PU**)



Scheme 34. Synthesis of thermoplastic poly(urethane)s (**Cu-PU**) by polyaddition reaction.

Table 22. Representative examples for molecular weight and polydispersity of PU during pre-condensation (**Cu-PU**) process.

Ent.	Time [min]	$M_n^{a)}$ [g mol <sup>-1</sup> ]	$\bar{D}$
1	0	2900	1.6
2	10	3800	1.6
3	20	4400	1.7
4	30	5100	1.7
5	40	5400	1.7
6	50	5900	1.7
7	60	6000	1.7

a) Determined via comparison of <sup>1</sup>H-NMR and GPC measurements applying a correction factor of 0.68.

pTHF (3.00 g, 1.03 mmol) and **3** (2.70 mg, 4.00  $\mu\text{mol}$ ) were dissolved in THF (5 mL) followed by addition of hexamethylene diisocyanate (HDI) (411.2  $\mu\text{L}$ , 2.56 mmol) and catalytic amounts of 1,8-diazabicycloundec-7-ene (DBU). The reaction mixture was stirred at RT and after defined times, samples ( $\sim 250 \mu\text{L}$ ) were precipitated in MeOH (5 mL) and investigated via GPC.

#### 4.6.10. Synthesis of PU networks (**PUXX**)

The synthesis was accomplished under inert conditions to exclude humidity, which in turn could lead to foam formation. In a representative procedure, e.g., for **PU60**, the precondensate was formed by dissolving pTHF (3.0 g, 1.03 mmol) and **3** (2.0 mg, 3.00  $\mu\text{mol}$ ) in THF (5 mL) followed by addition of hexamethylene diisocyanate (HDI) (411.2  $\mu\text{L}$ , 2.56 mmol) and catalytic amounts of DBU. The reaction mixture was stirred at RT and after a 10 min, trimethylolpropane (TMP) (83.3 mg, 0.62 mmol) dissolved in THF (1.00 mL) was added as crosslinker. The reaction mixture was stirred at RT until the desired viscosity was reached (absence of capillary attraction). After **31** (5.5 mg, 0.03 mmol) and 3-hydroxyphenylacetylene (**32**) (3.73 mg, 0.03 mmol) were added and was stirred again at RT for 5 min. The highly viscous liquid was poured in a Petri dish and was kept condensing further at RT for 1 h. The resulting foil ( $\sim 0.1$  mm thickness) was cut into shape (40 x 10 mm), were dried in high vacuum for 8 h in the dark and finally stored under  $\text{N}_2$  atmosphere for 1 day.

Table 23. Reaction conditions of polyurethane network synthesis (**PU20 – PU60**).

Ent.	Comp.	m (pTHF) [g]	n (pTHF) [mmol]	n (TMP) [mmol]	m (TMP) [mg]	n (HDI) [mmol]	V (HDI) [ $\mu\text{L}$ ]	n ( <b>3</b> ) [ $\mu\text{mol}$ ]	m ( <b>3</b> ) [mg]	n ( <b>31/32</b> ) [ $\mu\text{mol}$ ]	m ( <b>31</b> ) [mg]
1	<b>PU20</b>			0.21	27.8	1.75	280	2.17	1.4	21.70	4.0
2	<b>PU30</b>			0.31	41.6	1.95	314	2.39	1.6	23.90	4.4
3	<b>PU40</b>			0.41	55.5	2.15	347	2.61	1.7	26.10	4.8
4	<b>PU50</b>	3.00	1.03	0.52	69.4	2.35	379	2.84	1.8	28.40	5.3
5	<b>PU60</b>			0.62	83.3	2.56	411	3.00	2.0	30.00	5.6
6	<b>PU70</b>			0.72	97.2	2.76	446	3.29	2.1	32.90	6.1
7	<b>PU80</b>			0.83	111.1	2.96	474	3.50	2.3	35.00	6.5

## 4.7. Mechanical properties of PU networks

### 4.7.1. Determination of E-modulus

Table 24. Young's moduli of **PU20 – PU80** networks and calculated  $G'$  and  $\nu_x$ .

Ent.	Comp.	OH ratio <sup>a)</sup>	E modulus <sup>b)</sup> [MPa]	$G'$ <sup>c)</sup> [MPa]	$\nu_x$ <sup>d)</sup> [mol/m <sup>3</sup> ]
1	<b>PU20</b>	0.2	0.04	0.01	4
2	<b>PU30</b>	0.3	0.10	0.03	12
3	<b>PU40</b>	0.4	0.19	0.06	24
4	<b>PU50</b>	0.5	0.32	0.11	45
5	<b>PU60</b>	0.6	0.68	0.22	90
6	<b>PU70</b>	0.7	1.00	0.34	139
7	<b>PU80</b>	0.8	1.20	0.41	168

a) OH ratio of bivalent (pTHF, (**3**)) and trivalent (TMP).

b) Determined according to  $E = \Delta\sigma/\Delta\varepsilon$ .

c) Determined according to  $G' = E / (2(1+\mu))$ .

d) Determined according to  $\nu' = G'/(RT)$ .

The E-moduli determination of PU foils (**PU20 – PU80**) with different crosslinker densities was done via tensile rheological experiments. The applied strain (ranging from 0.01% to 2.00%) correlated with the determined stress values. The E-moduli were calculated by using the slope of the linear regression in the low strain range from 0.01% to 0.50%. Crosslinking densities  $\nu_x$  were calculated from tensile rheological experiments (see chapter 1.3.3.2) by means of  $G'$  assuming a Poisson Ratio  $\mu = 0.49$ <sup>312</sup>.

#### 4.7.2. Determination of crystallinity (DSC analysis)

Table 25. Melting enthalpy  $\Delta H_m$  values and calculated crystallinity of PU networks (**PU20 – PU80**)

Ent.	Comp.	OH ratio	$\Delta H_m$ [J g <sup>-1</sup> ]	$\alpha$ <sup>a)</sup> [%]
1	<b>PU20</b>	0.2	46.2	26.8
2	<b>PU30</b>	0.3	45.3	26.2
3	<b>PU40</b>	0.4	44.4	25.8
4	<b>PU50</b>	0.5	43.5	25.2
5	<b>PU60</b>	0.6	41.1	23.8
6	<b>PU70</b>	0.7	40.2	23.3
7	<b>PU80</b>	0.8	38.3	22.3

a) Crystallinity  $X_c$  was calculated according to  $\alpha = (\Delta H_m / \Delta H_{m0}) * 100\%$  with a melting enthalpy of  $\Delta H_{m0} = 172 \text{ J g}^{-1}$  for pTHF ( $X_c = 100\%$ ).

#### 4.7.3. Swelling experiments

Swelling experiments were performed by placing the PU-foil (~50 mg) in THF (25 mL) and storing overnight at RT inside a closed system. Afterwards, the excess of THF was removed and the foil was dried by means of a filter paper. After weighing the sample in swollen state, the solvent was removed by using high vacuum for at least 24 h until a constant weight was reached.

Table 26. THF uptake of PU networks.

Ent.	Comp.	OH ratio	THF uptake [%]
1	<b>PU20</b>	0.2	1160
2	<b>PU40</b>	0.4	819
3	<b>PU60</b>	0.6	517
4	<b>PU80</b>	0.8	422

a) THF uptake was calculated according to  $\text{THF uptake\%} = (m(\text{swollen}) / m(\text{dry})) * 100\%$ .

### 4.8. Mechanochemical activation of copper(I)-bis(NHC) complex containing PU networks via uniaxial tensile rheology

#### 4.8.1. Fluorescence calibration

The calibration of the fluorescence spectrometer was done by embedding the clicked fluorogenic dye **33** in different concentration in the polyurethane matrix consisting out of pTHF, HDI, **3** and TMP in accordance with the synthetic procedure of **PU60**. To compensate potential internal quenching effects of the dye, the overall concentration of naphthalene-based dyes

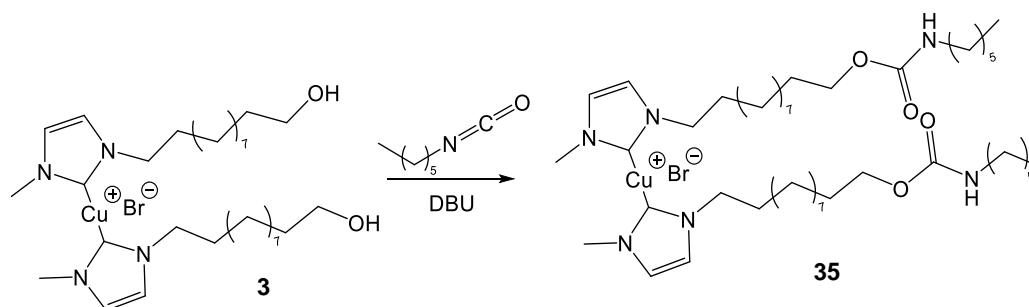
(sum of mmol **31** and mmol **33**) were kept constant at  $8.50 \mu\text{mol g}^{-1}_{\text{sample}}$ . **33** and corresponding amounts of **31** (details see Table 27) were dissolved in dry THF (100  $\mu\text{L}$ ), added to the reaction mixture as mentioned above and were stirred for 5 min at RT before pouring into a petri dish. After drying the PU foil, the sample was cut into the desired shape (40 x 20 x 0.15 mm) and dried in high vacuo. The foil was stored under  $\text{N}_2$  atmosphere at RT for one day. Afterwards, the fluorescence intensity was measured at 447 nm after excitation at 377 nm and plotted versus the conversion (calculated according to concentrations of dye **33** to dye **31**). Linear fitting yield in a calibration equation used for calculating the conversion of the mechanochemically triggered “click” reaction based on the measured fluorescence. For the calibration of PU with different crosslinking densities (**PU20** – **PU60**) fluorescence intensity was adapted to respective maximum amount of dye.

Table 27. Detailed data for the calibration of PU matrix (**PU60**).

Ent.	n( <b>31</b> ) [mmol]	m( <b>31</b> ) [mg]	n( <b>33</b> ) [mmol]	m( <b>33</b> ) [mg]	I <sub>Fl. S1</sub> [a.u.]	I <sub>Fl. S2</sub> [a.u.]	I <sub>Fl. S3</sub> [a.u.]	I <sub>Fl.</sub> [a.u.]	Conv. [%]
1	0.000	0.00	0.030	5.55	15	15	15	15	0
2	0.005	1.52	0.025	4.63	108	110	112	110	17
3	0.015	4.55	0.015	2.77	352	355	364	357	50
4	0.020	6.06	0.010	1.85	492	492	492	492	67
5	0.025	7.58	0.005	0.92	652	657	662	657	83
6	0.030	9.09	0.000	0.00	821	822	826	823	100

a) Conversion was calculated according to the equation of linear regression  $y = 8.0519x - 15.96$ .

#### 4.8.2. Synthesis of OH end-capped copper(I)-bis(NHC) complex (**35**)



Scheme 35. Synthesis of urethane terminated copper(I)-bis(NHC) complex (**35**).

**<sup>1</sup>H-NMR (THF-*d*<sub>8</sub>, 400 MHz):**  $\delta$  [ppm] 6.28 – 6.21 (m, 4H, NCHCHN), 3.94 (t,  $^3J_{\text{H,H}} = 6.6$  Hz, 4H, OCH<sub>2</sub>), 3.58 (s, 6H, NCH<sub>3</sub>), 3.50 (t,  $^3J_{\text{H,H}} = 7.1$  Hz, 4H, NCH<sub>2</sub>), 3.06 (p,  $^3J_{\text{H,H}} = 6.9$  Hz, 4H, NHCH<sub>2</sub>), 1.68 – 1.38 (m, 12H, NCH<sub>2</sub>CH<sub>2</sub>), 1.31 (m, 40H, (CH<sub>2</sub>)<sub>20</sub>).

**<sup>13</sup>C-NMR (CDCl<sub>3</sub>, 100 MHz):**  $\delta$  [ppm] 156.2 (C=O), 152.9 (NCCuN), 110.5 (CH<sub>3</sub>NCHCHN), 109.4 (CH<sub>3</sub>NCHCHN), 63.6 (OCH<sub>2</sub>), 42.8 (NCH<sub>2</sub>), 40.6 (NHCH<sub>2</sub>), 39.8 (NCH<sub>3</sub>), 31.55, 30.55, 30.03, 29.46, 29.43, 29.39, 29.25, 29.12, 28.99, 26.45, 26.41, 25.88, 22.51, 13.37.

#### 4.8.3. Activation of PU networks

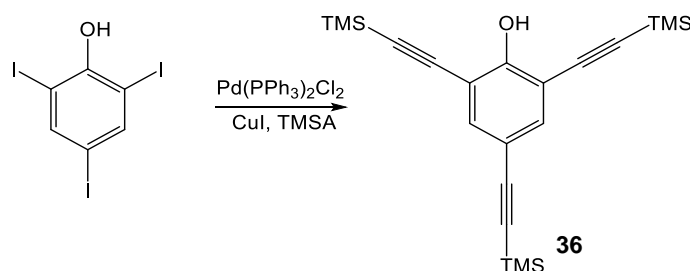
Extensional oscillatory and rotational rheology experiments of thin films were conducted on Anton Paar (Physica) MCR 101/SN 80753612 via Universal Extensional Fixture (UXF) at 20°C. Therefore, the films with rectangular shape (40 x 10 x 0.10 mm) (containing  $0.85 \mu\text{mol}_{(\text{Cu})} \text{g}^{-1}_{(\text{sample})}$ ) were fixed in the UXF sample holder and subjected to oscillating stretch experiments. To investigate the influence of the strain rate towards the mechanochemical

activation of the Cu(I)-bis(NHC) catalysts (**3**), the strain rate was varied from 0.25 s<sup>-1</sup>, 0.5 s<sup>-1</sup>, 0.75 s<sup>-1</sup> to 1.00 s<sup>-1</sup> while keeping the deformation constant at  $\gamma = 60\%$ . The deformation dependency of the mechanochemical activation was investigated varying the deformation from 40%, 60% to 80% and keeping the strain rate constant at 0.5 s<sup>-1</sup>. Crosslinking dependence investigations were done with a strain rate of 0.5 s<sup>-1</sup> and deformation of 80%.

Table 28. Summary of catalytic activity of force activated poly(urethane) networks towards the fluorogenic “click” reaction from **27** with 3-hydroxyphenylacetylene (**28**).

Ent.	Poly(urethane) network				Time [h]	“click” conversion [%] <sup>a)</sup>					
	Comp.	Def. [%]	Frequ. [Hz]	Precond. [min]							
<b>Control experiments</b>											
1	W/O	60	0.50	10	Time [h]	0	24	48	96		
					Conversion [%]	1	2	2	2		
2	LMW				Time [h]	0	24	48	96		
					conversion [%]	1	2	1	2		
3	Therm (25°C)	-	-	10	Time [h]	0	24	48	96		
					Conversion [%]	1	1	0	1		
4	Therm (60°C)				Time [h]	0	24	48	96		
					Conversion [%]	1	4	6	6		
<b>Precondensation time dependency</b>											
5	Pu-60 <sub>00</sub>			00	Time [h]	0	24	48	72	96	
					Conversion [%]	1	7	9	10	11	
6	PU-60 <sub>10</sub>	80	0.50	10	Time [h]	0	24	48	72	96	
					Conversion [%]	0	9	15	18	18	
7	PU-60 <sub>30</sub>			30	Time [h]	0	24	48	72	96	
					Conversion [%]	1	10	13	15	16	
<b>Frequency dependency</b>											
8	PU-60 <sup>0.25</sup>		0.25		Time [h]	0	48	96	144	288	
					Conversion [%]	1	5	8	10	12	
9	PU-60 <sup>0.50</sup>	80	0.50	10	Time [h]	0	24	48	96	-	
					Conversion [%]	0	4	9	14	-	
10	PU-60 <sup>0.75</sup>		0.75		Time [h]	0	12	24	48	72	
					Conversion [%]	0	8	13	13	14	
11	PU-60 <sup>1.00</sup>		1.00		Time [h]	0	8	16	24	-	
					Conversion [%]	0	12	13	12	-	
<b>Deformation dependency</b>											
12	<sup>40</sup> Pu-60	40			Time [h]	0	24	48	72	96	
					Conversion [%]	0	4	5	5	6	
13	<sup>60</sup> Pu-60	60	0.50	10	Time [h]	0	24	48	72	96	
					Conversion [%]	0	4	9	13	14	
14	<sup>80</sup> Pu-60	80			Time [h]	0	24	48	72	96	
					Conversion [%]	0	9	15	17	18	
<b>Crosslinking density dependency</b>											
15	PU-30				Time [h]	0		24			
					Conversion [%]	1		16			
16	PU-40	80	0.50	10	Conversion [%]	1		25			
17	PU-50				Conversion [%]	1		11			
18	PU-60	Conversion [%]	0		9						
19	PU-70	Conversion [%]	0		5						

## 4.9. Synthesis of multivalent fluorogenic dyes

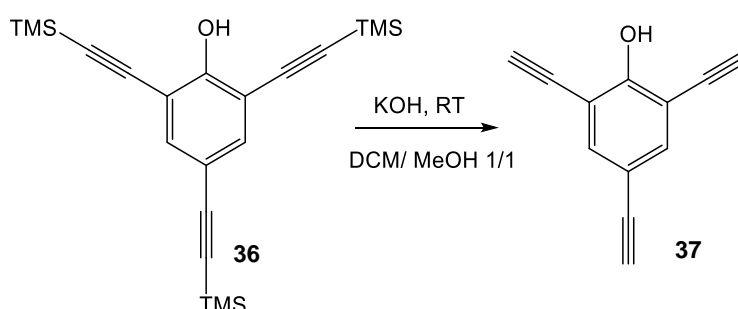
4.9.1. Synthesis of 2,4,6-tris((trimethylsilyl)ethynyl)phenol (**36**)Scheme 36. Synthesis of 2,4,6-tris((trimethylsilyl)ethynyl)phenol (**36**) via SONOGASHIRA coupling.

$\text{Pd}(\text{PPh}_3)_2\text{Cl}_2$  (0.15 g, 0.21 mmol) and copper(I) iodide (40.00 mg, 0.21 mmol) were added to a solution of 2,4,6 triiodo phenol (1.00 g, 2.12 mmol) in DMF (20 mL) followed by the addition of  $\text{NEt}_3$  (10 mL) and trimethylsilyl acetylene (TMSA) (1.05 mL, 7.37 mmol). The reaction mixture was stirred at RT for 6 h, HCl (50 mL, 1M) was added and the solution was extracted with diethyl ether (3 x 50 mL) three times. The combined organic layers were dried over anhydrous  $\text{Na}_2\text{SO}_4$ . After column chromatography on silica (EA/Hex 1/40) compound **36** (0.75 g, 1.95 mmol, 92%) was obtained as a pale-yellow solid.

$^1\text{H-NMR}$  ( $\text{CDCl}_3$ , 400 MHz):  $\delta$  [ppm] 7.45 (s, 2H,  $\text{CH}_{\text{Ar}}$ ), 6.33 (s, 1H, OH), 0.26 (s, 18H,  $\text{SiCH}_{3\text{ortho}}$ ), 0.21 (s, 9H,  $\text{SiCH}_{3\text{para}}$ ).

$^{13}\text{C-NMR}$  ( $\text{CDCl}_3$ , 100 MHz):  $\delta$  [ppm] 157.7 (COH), 136.3 ( $\text{CH}_{\text{Ar}}$ ), 115.4 ( $\text{C}_{\text{para}}\text{C}\equiv\text{C}$ ), 110.3 ( $\text{C}_{\text{ortho}}\text{C}\equiv\text{C}$ ), 103.1 ( $\text{C}\equiv\text{CSi}_{\text{ortho}}$ ), 101.9 ( $\text{C}\equiv\text{CSi}_{\text{ortho}}$ ), 97.9 ( $\text{C}\equiv\text{CSi}_{\text{para}}$ ), 93.4 ( $\text{C}\equiv\text{CSi}_{\text{para}}$ ), -0.2 ( $\text{SiCH}_3$ ).

$^{29}\text{Si-NMR}$  ( $\text{CDCl}_3$ , 80 MHz):  $\delta$  [ppm] -16.8 ( $\text{Si}_{\text{ortho}}$ ), -17.7 ( $\text{Si}_{\text{para}}$ )

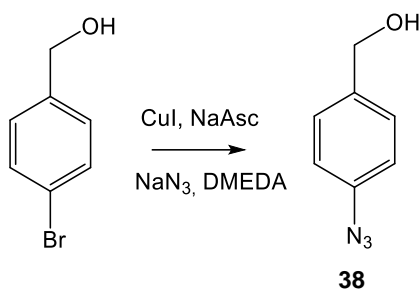
4.9.2. Synthesis of 2,4,6-triethynylphenol (**37**)Scheme 37. Synthesis of 2,4,5-triethynylphenol (**37**) via basic deprotection.

Compound **36** (0.46 g, 1.20 mmol) was dissolved in DCM (10 mL) followed by the addition of KOH (0.28 g, 5.00 mmol) in MeOH (10 mL). The reaction mixture was stirred at RT for 4 h, HCl (30 mL, 1 M) was added and the solution was extracted with DCM (3 x 20 mL). The combined organic layers were dried over anhydrous  $\text{Na}_2\text{SO}_4$ , the solvent was removed under reduced pressure and compound **37** (0.14 g, 0.82 mmol) was obtained after recrystallization in hexane as a pale brown solid.

$^1\text{H-NMR}$  ( $\text{CDCl}_3$ , 400 MHz):  $\delta$  [ppm] 7.53 (s, 2H,  $\text{CH}_{\text{Ar}}$ ), 6.30 (s, 1H, OH), 3.43 (s, 2H,  $\text{C}\equiv\text{CH}_{\text{ortho}}$ ), 2.99 (s, 1H,  $\text{C}\equiv\text{CH}_{\text{para}}$ ).

$^{13}\text{C-NMR}$  ( $\text{CDCl}_3$ , 100 MHz):  $\delta$  [ppm] 157.7 (COH), 136.3 ( $\text{CH}_{\text{Ar}}$ ), 115.4 ( $\text{C}_{\text{para}}\text{C}\equiv\text{C}$ ), 110.3 ( $\text{C}_{\text{ortho}}\text{C}\equiv\text{C}$ ), 103.1 ( $\text{C}\equiv\text{C}_{\text{para}}$ ), 101.9 ( $\text{C}\equiv\text{C}_{\text{ortho}}$ ), 97.9 ( $\text{C}\equiv\text{CH}_{\text{ortho}}$ ), 93.4 ( $\text{C}\equiv\text{CH}_{\text{para}}$ ).

#### 4.9.3. Synthesis of (4-azidophenyl)methanol (**38**)



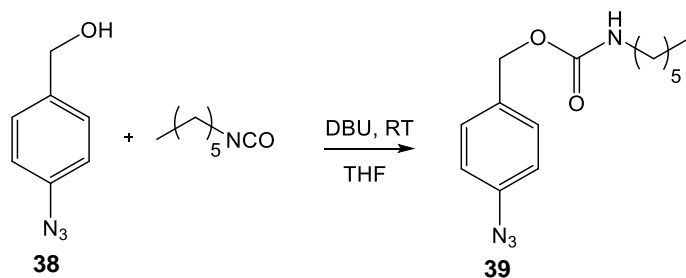
Scheme 38. Synthesis of (4-azidophenyl)methanol (**38**) via modified ULLMANN reaction.

4-(bromophenyl)methanol (0.50 g, 2.67 mmol) was dissolved in EtOH/H<sub>2</sub>O 7/3 (5 mL) and copper(I) iodide (49.51 mg, 0.26 mmol), NaAsc (25.75 mg, 0.13 mmol) and NaN<sub>3</sub> (0.35 g, 5.34 mmol) were added followed by the addition of DMEDA (88  $\mu\text{L}$ , 0.40 mmol). The reaction mixture was stirred at 80°C for 1 h, HCl (10 mL, 1 M) was added and the solution was extracted with EA (3 x 20 mL). The combined organic layers were dried over anhydrous Na<sub>2</sub>SO<sub>4</sub>, the solvent was removed under reduced pressure and after flash chromatography on silica (EA/Hex 1/4) compound **38** (0.38 g, 2.53 mmol, 95%) was obtained as a brown solid.

$^1\text{H-NMR}$  ( $\text{DMSO-}d_6$ , 400 MHz):  $\delta$  [ppm] 7.36 – 7.31 (m, 2H,  $\text{CHCN}_3$ ), 7.08 – 7.02 (m, 2H,  $\text{CHCCH}_2\text{OH}$ ), 5.17 (bs, 1H, OH), 4.45 (s, 2H,  $\text{CH}_2$ ).

$^{13}\text{C-NMR}$  ( $\text{DMSO-}d_6$ , 100 MHz):  $\delta$  [ppm] 140.1 ( $\text{CCH}_2\text{OH}$ ), 138.1 ( $\text{CN}_3$ ), 128.5 ( $\text{CHCN}_3$ ), 119.2 ( $\text{CHCCH}_2\text{OH}$ ), 62.8 ( $\text{CH}_2\text{OH}$ ).

#### 4.9.4. Synthesis of 4-azidobenzyl hexylcarbamate (**39**)



Scheme 39. Synthesis of 4-azidobenzyl hexylcarbamate (**39**).

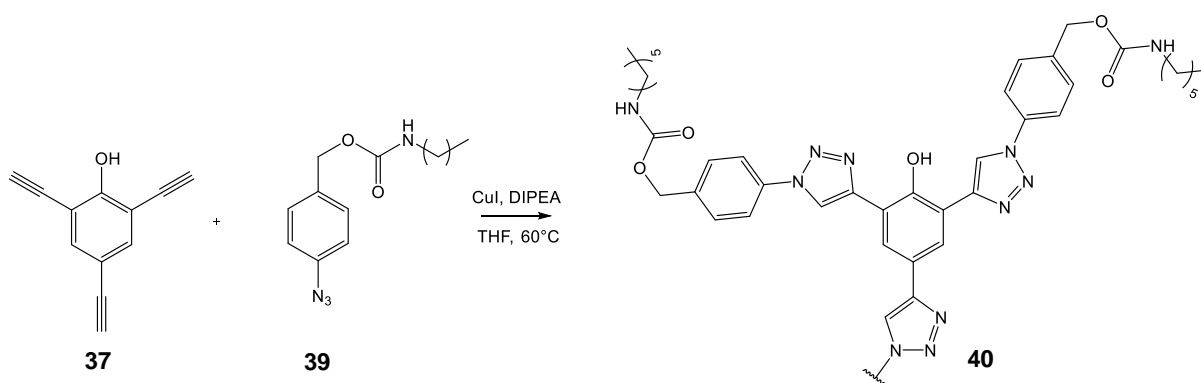
Hexamethylene isocyanate (192  $\mu\text{L}$ , 1.34 mmol) was added to a mixture of **38** (0.20 g, 1.34 mmol) followed by the addition of DBU (0.05 eq) and the resultant solution was stirred 4 h at RT. The reaction mixture was diluted with water (15 mL), was extracted with EA (3 x 10 mL), dried over Na<sub>2</sub>SO<sub>4</sub> and the solvent was evaporated under reduced pressure to obtain compound **39** (0.36 g, 1.31 mmol, 98%) as a yellow solid.

$^1\text{H-NMR}$  (DMSO- $d_6$ , 400 MHz):  $\delta$  [ppm] 7.39 – 7.34 (m, 2H,  $\text{CHCN}_3$ ), 7.19 (t,  $^3J_{\text{H,H}} = 5.8$  Hz, 1H, NH), 7.13 – 7.06 (m, 2H,  $\text{CHCCH}_2\text{OH}$ ), 4.96 (s, 2H,  $\text{CH}_2$ ), 2.95 (q, 2H,  $^3J_{\text{H,H}} = 6.8$  Hz,  $\text{CH}_2\text{NH}$ ), 1.36 (p,  $^3J_{\text{H,H}} = 7.1$  Hz, 2H,  $\text{CH}_2\text{CH}_2\text{NH}$ ), 1.27 – 1.16 (m, 6H,  $(\text{CH}_2)_3$ ), 0.83 (t,  $^3J_{\text{H,H}} = 6.9$  Hz, 3H,  $\text{CH}_3$ ).

$^{13}\text{C-NMR}$  (DMSO- $d_6$ , 100 MHz):  $\delta$  [ppm] 156.5 (C=O), 139.3 ( $\text{CCH}_2\text{O}$ ), 134.7 ( $\text{CN}_3$ ), 130.0 ( $\text{CHCN}_3$ ), 119.5 ( $\text{CHCCH}_2\text{OH}$ ), 64.9 ( $\text{CH}_2\text{OH}$ ), 40.7 ( $\text{NHCH}_2$ ), 31.4 ( $\text{NHCH}_2\text{CH}_2$ ), 29.8 ( $\text{NH}(\text{CH}_2)_2\text{CH}_2$ ), 26.3 ( $\text{NH}(\text{CH}_2)_3\text{CH}_2$ ), 22.5 ( $\text{NH}(\text{CH}_2)_4\text{CH}_2$ ), 14.3 ( $\text{NH}(\text{CH}_2)_5\text{CH}_3$ ).

ESI-TOF MS (positive mode, THF:MeOH 99:1, NaI,  $m/z$ ):  $[\text{M}+\text{Na}]^+$  found 299.172, simulated 299.148 for  $\text{C}_{14}\text{H}_{20}\text{N}_4\text{O}_2\text{Na}^+$ .

#### 4.9.5. Synthesis of trivalent conjugated dye (**40**)



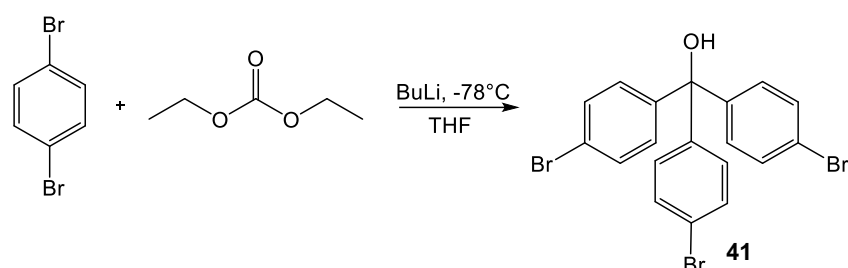
Scheme 40. Synthesis of trivalent conjugated dye (**40**) via CuAAC.

Compounds **37** (0.25 g, 1.50 mmol) and **39** (1.20 g, 4.50 mmol) were dissolved in THF (25 mL) followed by the addition of copper(I)-iodide (57.00 mg, 0.30 mmol) and DIPEA (107  $\mu\text{L}$ , 0.60 mmol). The reaction mixture was stirred at 60 °C overnight, HCL (20 mL, 1 M) was added, the solution was extracted with DCM (3 x 20 mL) and finally washed with water (20 mL). The combined organic layers were dried over anhydrous  $\text{Na}_2\text{SO}_4$ . The solvent was removed under reduced pressure and compound **40** (1.19 g, 1.20 mmol, 80%) was obtained after column chromatography on silica ( $\text{CHCl}_3/\text{MeOH}$  30/1) as a colorless solid.

$^1\text{H-NMR}$  (THF- $d_8$ , 400 MHz):  $\delta$  [ppm] 9.01 (t,  $^3J_{\text{H,H}} = 0.9$  Hz, 3H, triazole), 8.77 (d,  $^3J_{\text{H,H}} = 1.8$  Hz, 1.5H), 8.38 (dd,  $^3J_{\text{H,H}} = 1.8, 0.6$  Hz, 1.5H), 8.00 (dd,  $^3J_{\text{H,H}} = 8.5, 2.1$  Hz, 6H,  $\text{CHCN}$ ), 7.98 (d,  $^3J_{\text{H,H}} = 2.2$  Hz, 1.5H), 7.59 (t,  $^3J_{\text{H,H}} = 7.6$  Hz, 6H,  $\text{CHCCH}_2\text{OH}$ ), 7.04 (d,  $^3J_{\text{H,H}} = 2.2$  Hz, 1.5H), 6.46 (q,  $^3J_{\text{H,H}} = 5.6$  Hz, 3H, NH), 5.13 (d,  $^3J_{\text{H,H}} = 4.5$  Hz, 6H,  $\text{CH}_2$ ), 3.17 – 3.09 (m, 6H,  $\text{CH}_2\text{NH}$ ), 1.50 (p,  $^3J_{\text{H,H}} = 7.1$  Hz, 6H,  $\text{CH}_2\text{CH}_2\text{NH}$ ), 1.39 – 1.28 (m, 18H,  $(\text{CH}_2)_3$ ), 0.90 (t,  $^3J_{\text{H,H}} = 6.8$  Hz, 9H).

$^{13}\text{C-NMR}$  (THF- $d_8$ , 100 MHz):  $\delta$  [ppm] 156.0, 150.9, 148.0, 146.0, 142.3, 138.5, 138.1, 136.9, 136.7, 128.88, 128.7, 126.8, 120.3, 119.9, 119.5, 119.1, 117.8, 117.7, 115.4, 107.5, 64.6, 64.6, 40.7, 31.5, 23.0, 26.4, 22.5, 13.4.

ESI-TOF MS (negative mode, THF:MeOH 99:1,  $m/z$ ):  $[\text{M}-\text{H}]^-$  found 993.509, simulated 993.509 for  $\text{C}_{54}\text{H}_{65}\text{N}_{12}\text{O}_7^-$ .

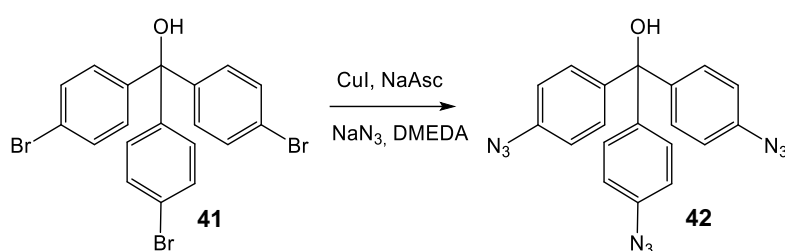
4.9.6. Synthesis of tris(4-bromophenyl)methanol (**41**)Scheme 41. Synthesis of (4-bromophenyl)methanol (**41**).

To a solution of 1,4-dibromobenzene (8.70 g, 37.20 mmol) in THF (135 mL) which was cooled to -78°C, BuLi (13.5 mL, 33.80 mmol, 2.5 M in hexane) was added dropwise and was stirred for 3 h at 78°C. Afterwards the solution was transferred to a separate prepared solution of diethyl carbonate (1.02 mL, 8.50 mmol) in THF (3 mL), which was also cooled to 78°C and subsequently was allowed to come to room temperature. After stirring for 6 h, the reaction mixture was quenched with saturated aqueous NH<sub>4</sub>Cl (50 mL), was extracted with EA (3 x 20 mL) and the combined organic layers was finally dried over anhydrous Na<sub>2</sub>SO<sub>4</sub>. After purification via column chromatography on silica changing the polarity of solvent from hexane to EA/Hex 3/1 compound **41** (3.28 g, 6.63 mmol, 78%) was obtained as a colorless solid.

<sup>1</sup>H-NMR (DMSO-*d*<sub>6</sub>, 400 MHz): δ [ppm] 7.54 – 7.48 (m, 6H, CHCBr), 7.15 – 7.07 (m, 6H, CHCCOH), 6.74 (s, 1H, OH).

<sup>13</sup>C-NMR (DMSO-*d*<sub>6</sub>, 100 MHz): δ [ppm] 144.9 (CCOH), 131.3 (CHCBr), 129.5 (CHCCOH), 122.0 (CBr), 81.1 (COH).

ESI-TOF MS (negative mode, THF:MeOH 99:1, *m/z*): [M-H]<sup>-</sup> found 494.855, simulated 494.841 for C<sub>19</sub>H<sub>12</sub>Br<sub>3</sub>O<sup>-</sup>.

4.9.7. Synthesis of tris(4-azidophenyl)methanol (**42**)Scheme 42. Synthesis of (4-azidophenyl)methanol (**42**) via modified ULLMANN reaction.

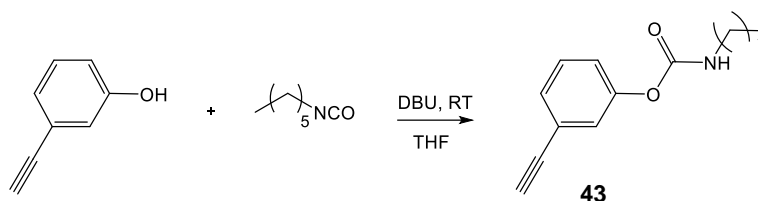
Compound **41** (1.32 g, 2.67 mmol) was dissolved in EtOH/H<sub>2</sub>O 7/3 (10 mL) and copper(I) iodide (49.51 mg, 0.26 mmol), NaAsc (25.75 mg, 0.13 mmol) and NaN<sub>3</sub> (0.35 g, 5.34 mmol) were added followed by the addition of DMEDA (88 μL, 0.40 mmol). The reaction mixture was stirred at 80°C for 8 h, HCl (10 mL, 1 M) was added and the solution was extracted with EA (3 x 20 mL). The combined organic layers were dried over anhydrous Na<sub>2</sub>SO<sub>4</sub>, the solvent was removed under reduced pressure and after flash chromatography on silica (EA/Hex 1/7) compound **42** (0.82 g, 2.13 mmol, 80%) was obtained as a brown viscous liquid which crystallize slowly at 4 °C.

$^1\text{H-NMR}$  ( $\text{DMSO-}d_6$ , 400 MHz):  $\delta$  [ppm] 7.24 – 7.18 (m, 6H,  $\text{CHCN}_3$ ), 7.09 – 7.01 (m, 6H,  $\text{CHCCOH}$ ), 6.58 (s, 1H,  $\text{OH}$ ).

$^{13}\text{C-NMR}$  ( $\text{DMSO-}d_6$ , 100 MHz):  $\delta$  [ppm] 144.8 ( $\text{CCOH}$ ), 138.4 ( $\text{CN}_3$ ), 129.7 ( $\text{CN}_3$ ), 118.8 ( $\text{CHCCOH}$ ), 80.1 ( $\text{COH}$ ).

ESI-TOF MS (negative mode,  $\text{THF}:\text{MeOH}$  99:1,  $m/z$ ):  $[\text{M-H}]^-$  found 382.128, simulated 382.116 for  $\text{C}_{19}\text{H}_{12}\text{N}_9\text{O}^-$ .

#### 4.9.8. Synthesis of 3-ethynylphenyl hexylcarbamate (**43**)



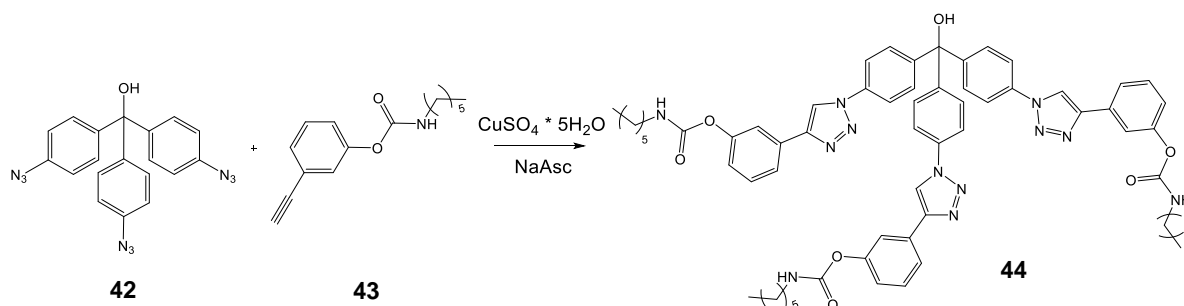
Scheme 43. Synthesis of 3-ethynylphenyl hexylcarbamate (**43**).

Hexamethylene isocyanate (192  $\mu\text{l}$ , 1.34 mmol) was added to a solution of 3-hydroxyphenylacetylene (**32**) (0.17 g, 1.34 mmol, 95%) followed by the addition of DBU (0.05 eq) and the resultant solution was stirred overnight at RT. The reaction mixture was diluted with HCl (10 mL), was extracted with EA (3 x 10 mL), was dried over  $\text{Na}_2\text{SO}_4$  and the solvent was evaporated under reduced pressure to obtain compound **43** (0.31 g, 1.26 mmol, 94%) as a yellow solid.

$^1\text{H-NMR}$  ( $\text{CDCl}_3$ , 400 MHz):  $\delta$  [ppm] 7.36 – 7.25 (m, 3H,  $\text{CHCHCH}$ ), 7.15 (dt,  $^3J_{\text{H,H}} = 7.4$ , 2.1 Hz, 1H,  $\text{CCHC}$ ), 5.04 (s, 1H,  $\text{NH}$ ), 3.27 (q,  $^3J_{\text{H,H}} = 6.7$  Hz, 2H,  $\text{CH}_2\text{NH}$ ), 3.08 (s, 1H,  $\text{OH}$ ), 1.58 (p,  $^3J_{\text{H,H}} = 7.3$  Hz, 1H,  $\text{CH}_2\text{CH}_2\text{NH}$ ), 1.42 – 1.27 (m, 6H,  $(\text{CH}_2)_3$ ), 0.91 (t,  $^3J_{\text{H,H}} = 6.9$  Hz, 3H,  $\text{CH}_3$ ).

$^{13}\text{C-NMR}$  ( $\text{CDCl}_3$ , 100 MHz):  $\delta$  [ppm] 154.2 ( $\text{C=O}$ ), 150.9 ( $\text{COC=O}$ ), 129.2 ( $\text{CCHCH}$ ), 129.0 ( $\text{CCHCH}$ ), 125.2 ( $\text{CCHC}$ ), 123.2 ( $\text{CC}\equiv\text{CH}$ ), 122.5 ( $\text{CHCHCO}$ ), 82.8 ( $\text{CC}\equiv\text{CH}$ ), 77.7 ( $\text{CC}\equiv\text{CH}$ ), 41.3 ( $\text{NHCH}_2$ ), 31.4 ( $\text{NHCH}_2\text{CH}_2$ ), 29.8 ( $\text{NH}(\text{CH}_2)_2\text{CH}_2$ ), 26.4 ( $\text{NH}(\text{CH}_2)_3\text{CH}_2$ ), 22.5 ( $\text{NH}(\text{CH}_2)_4\text{CH}_2$ ), 14.0 ( $\text{CH}_3$ ).

#### 4.9.9. Synthesis of trivalent “click” dye (**44**)



Scheme 44. Synthesis of trivalent “click” dye (**44**) via CuAAC.

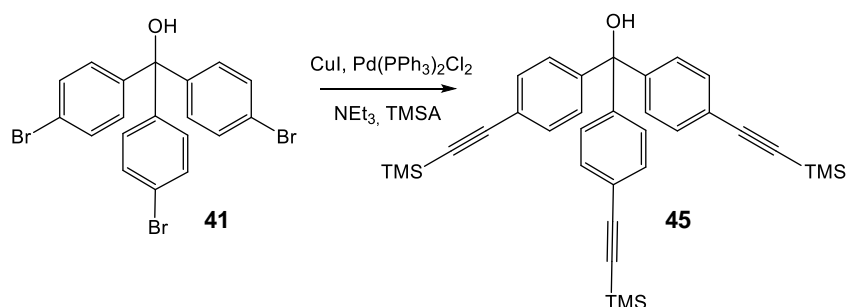
A stock solution of  $\text{CuSO}_4 \cdot 5\text{H}_2\text{O}$  (54.0  $\mu\text{mol}$ , 13.4 mg in 0.5 mL water) and a stock solution of sodium ascorbate (NaAsc) (80.0  $\mu\text{mol}$ , 16.1 mg in 0.5 mL water) were added to a mixture of **42** (0.21 g, 0.54 mmol) and **43** (0.39 g, 1.62 mmol) in EtOH (4 mL) and the resultant solution was stirred overnight at RT. The solution was diluted with water (20 mL), was extracted with

DCM (3 x 20 mL) and finally washed with brine (20 mL). The combined organic layers were dried over anhydrous Na<sub>2</sub>SO<sub>4</sub>, the solvent was removed under reduced pressure and compound **44** (0.56 g, 0.50 mmol, 92%) was obtained after flash chromatography on silica (CHCl<sub>3</sub>/MeOH 30/1) as a colorless solid.

**<sup>1</sup>H-NMR (DMSO-*d*<sub>6</sub>, 400 MHz):** δ [ppm] 9.35 (s, 1H, triazole), 7.97 (d, *J* = 8.6 Hz, 6H, CHCCOH), 7.79 (m, , 6H, CHCHCH), 7.66 (m, 3H, CHCHCH), 7.58 (d, <sup>3</sup>*J*<sub>H,H</sub> = 8.7 Hz, 6H, CHCN), 7.48 (t, <sup>3</sup>*J*<sub>H,H</sub> = 7.9 Hz, 3H, NH), 7.10 (ddt, <sup>3</sup>*J*<sub>H,H</sub> = 8.0, 2.4, 1.2 Hz, 3H, CCHC), 7.06 (s, 1H, OH), 3.07 (q, <sup>3</sup>*J*<sub>H,H</sub> = 6.6 Hz, 6H, CH<sub>2</sub>NH), 1.47 (p, <sup>3</sup>*J*<sub>H,H</sub> = 7.1 Hz, 2H, CH<sub>2</sub>CH<sub>2</sub>NH), 1.38 – 1.20 (m, 18H, (CH<sub>2</sub>)<sub>3</sub>), 0.86 (t, <sup>3</sup>*J*<sub>H,H</sub> = 6.6 Hz, 9H, CH<sub>3</sub>).

**<sup>13</sup>C-NMR (DMSO-*d*<sub>6</sub>, 125 MHz):** δ [ppm] 154.7 (C=O), 152.2 (COC=O), 147.9 (CCHN), 147.1 (CN), 135.9 (CCOH), 131.9 (CCN), 130.4 (CHCCOH), 129.7 (CHCHCH), 122.2 (CHCHCN), 122.1 (CHCO), 120.5 (CHCCN), 120.1 (OCCHC), 119.2 (CCHN), 80.4 (COH), 40.9 (NHCH<sub>2</sub>), 31.4 (NHCH<sub>2</sub>CH<sub>2</sub>), 29.6 (NH(CH<sub>2</sub>)<sub>2</sub>CH<sub>2</sub>), 26.4 (NH(CH<sub>2</sub>)<sub>3</sub>CH<sub>2</sub>), 22.5 (NH(CH<sub>2</sub>)<sub>4</sub>CH<sub>2</sub>), 14.4 (CH<sub>3</sub>).

#### 4.9.10. Synthesis of tris(4-((trimethylsilyl)ethynyl)phenyl)methanol (**45**)



Scheme 45. Synthesis of tris(4-((trimethylsilyl)ethynyl)phenyl)methanol (**45**) via SONOGASHIRA coupling.

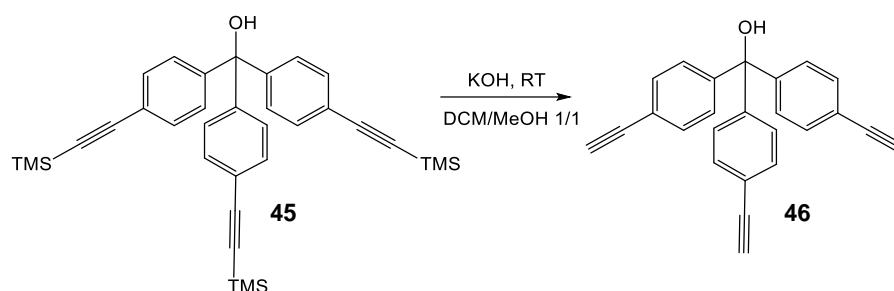
Pd(PPh<sub>3</sub>)<sub>2</sub>Cl<sub>2</sub> (0.15 g, 0.21 mmol) and copper(I) iodide (40.00 mg, 0.21 mmol) were added to a solution of compound **41** (1.05 g, 2.12 mmol) in DMF (20 mL) followed by the addition of NEt<sub>3</sub> (10 mL) and TMSA (1.05 mL, 7.37 mmol). The reaction mixture was stirred at RT for 6 h, HCl (50 mL, 1M) was added and the solution was extracted with EA (3 x 50 mL) three times. The combined organic layers were dried over anhydrous Na<sub>2</sub>SO<sub>4</sub> and after column chromatography on silica (EA/Hex 1/40) compound **45** (1.12 g, 2.04 mmol, 96%) was obtained as a pale yellow solid.

**<sup>1</sup>H-NMR (CDCl<sub>3</sub>, 400 MHz):** δ [ppm] 7.42 – 7.37 (m, 6H, CHCC≡C), 7.18 – 7.12 (m, 6H, CHCCOH), 0.24 (s, 5H, SiCH<sub>3</sub>).

**<sup>13</sup>C-NMR (CDCl<sub>3</sub>, 125 MHz):** δ [ppm] 146.2 (CCOH), 131.7 (CHCC≡C), 127.7 (CHCCOH), 122.4 (CC≡CSi), 104.6 (CC≡CSi), 94.9 (CC≡CSi), 81.5 (CHOH), -0.1 (SiCH<sub>3</sub>).

**<sup>29</sup>Si-NMR (CDCl<sub>3</sub>, 80 MHz):** δ [ppm] -17.7 (Si<sub>para</sub>).

**ESI-TOF MS (positive mode, THF:MeOH 99:1, NaI, *m/z*):** [M+Na]<sup>+</sup> found 571.197, simulated 571.228 for C<sub>34</sub>H<sub>40</sub>OSi<sub>3</sub>Na<sup>+</sup>.

4.9.11. Synthesis of tris(4-(ethynyl)phenyl)methanol (**46**)Scheme 46. Synthesis of tris(4-(ethynyl)phenyl)methane (**46**) via basic deprotection.

Compound **45** (0.55 g, 1.00 mmol) was dissolved in DCM (10 mL) followed by addition of KOH (0.22 g, 4.00 mmol) in MeOH (10 mL). The reaction mixture was stirred at RT for 4 h, HCl (30 mL, 1 M) was added and the solution was extracted with DCM (3 x 20 mL). The combined organic layers were dried over anhydrous Na<sub>2</sub>SO<sub>4</sub>, the solvent was removed under reduced pressure and compound **46** (0.23 g, 0.68 mmol, 68%) was obtained after flash chromatography on silica (EA/Hex 1/10) as a pale-yellow oil.

<sup>1</sup>H-NMR (CDCl<sub>3</sub>, 400 MHz): δ [ppm] 7.48 – 7.44 (m, 6H, CHCC≡C), 7.25 – 7.21 (m, 6H, CHCCOH), 3.09 (s, 3H, C≡CH).

<sup>13</sup>C-NMR (CDCl<sub>3</sub>, 125 MHz): δ [ppm] 146.6 (CCOH), 131.9 (CHCC≡C), 127.8 (CHCCOH), 121.5 (CC≡CH), 83.2 (CC≡CH), 81.5 (COH), 77.7 (CC≡CH).

ESI-TOF MS (positive mode, THF:MeOH 99:1, NaI, m/z): [M+Na]<sup>+</sup> found 355.113, simulated 355.111 for C<sub>25</sub>H<sub>16</sub>O.

## 5. Summary

In summary a series of cyclic as well as acyclic low molecular weight copper(I)-bis(NHC) complexes (**3**, **10**) were synthesized via the copper(I)-oxide method at high temperatures and modified with carboxylic end groups either directly or by post functionalization. In order to determine the rupture forces of the mechanochemically active copper-carbon bond, these complexes were subjected to SMFS via AFM. The occurrence of force on the immobilized complexes led to single as well as double rupture events and resulted in forces up to 1600 to 2600 pN, which was in good agreement with the calculated values of 1500 pN, enabled future estimations to connect macro- and microscopic forces.

Furthermore, the mechanochemical activation in bulk state was improved by varying the mechanophoric architecture.

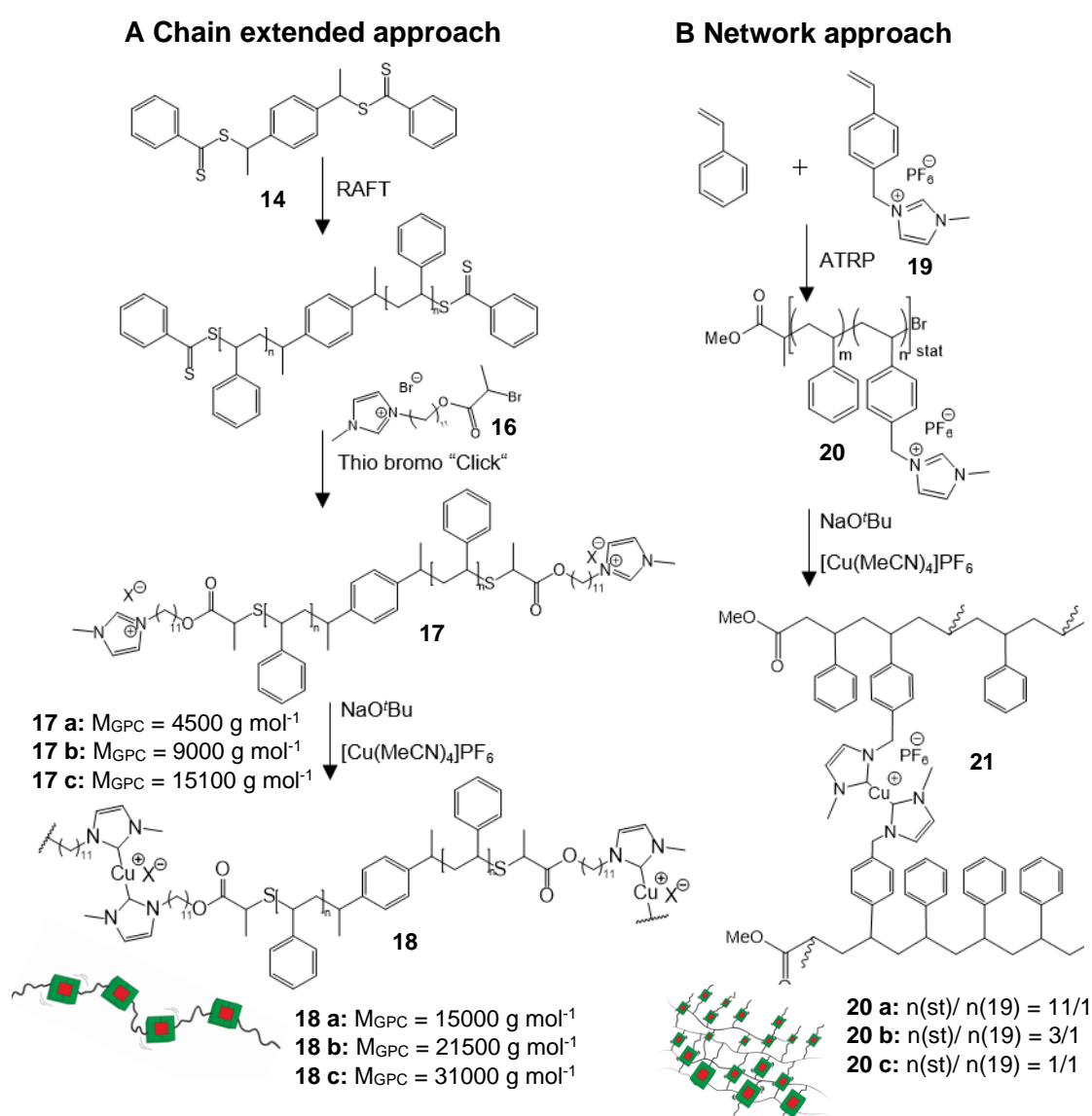


Figure 57. (A) Synthetic pathway for the chain extended mechanocatalysts (**18**) as well as (B) Synthetic pathway of the network based mechanocatalyst (**21**).

In case of the 3-azido-7-hydroxycoumarin system (**22**, **23**), the mechanochemically activation efficiency was enhanced by the increase in the effective polymer chain length via multi copper(I)-centers, which in turn led to a facilitated force transmission. In order to improve the

latency of catalysts, covalent crosslinking points were implemented, which allowed to redirect the applied force through the network structure and thus enabled the additional activation of the perpendicular to the force orientated mechanophores.

The synthesis of the chain extended mechanophores (**18**) (Figure 57 A) started with the thermal induced polymerization of styrene via controlled radical technique (RAFT), yielded in three different molecular weights, ranging from 4 400 g mol<sup>-1</sup> to 15 500 g mol<sup>-1</sup> offering narrow molecular weight distributions with PDIs of 1.1. This guaranteed the well-defined positioning of the labile copper(I) bond which was necessary for an optimal activation process. The subsequent integration of imidazolium moiety was performed via highly efficient thio bromo “click” reaction in mostly quantitative yield. After deprotonation and subsequent complexation of the bivalent end capped NHC precursor (**17**), a chain extended mechanophore (**18**) could be obtained in which the initial molecular weight of the macro ligand as well as concentration effects influenced the number of obtained copper(I) centers as well as the overall chain length. In order to obtain the mechanochemically active networks (Figure 57 B), an imidazolium containing monomer (**19**) was developed and subsequent copolymerized via atomic transfer radical polymerization with styrene adjusting the ratio of both monomers from 1/1 to 11/1. This allowed to control the amount of potential crosslinking points within the mechanophore (**21**) which were generated by deprotonation and subsequent complexation of imidazolium moieties, revealed crosslinking densities in the equilibrium swelling state of 120 mol m<sup>-3</sup> for **21a** (11/1), 710 mol m<sup>-3</sup> for **21b** (3/1) and 2160 mol m<sup>-3</sup> for **21c** (1/1).

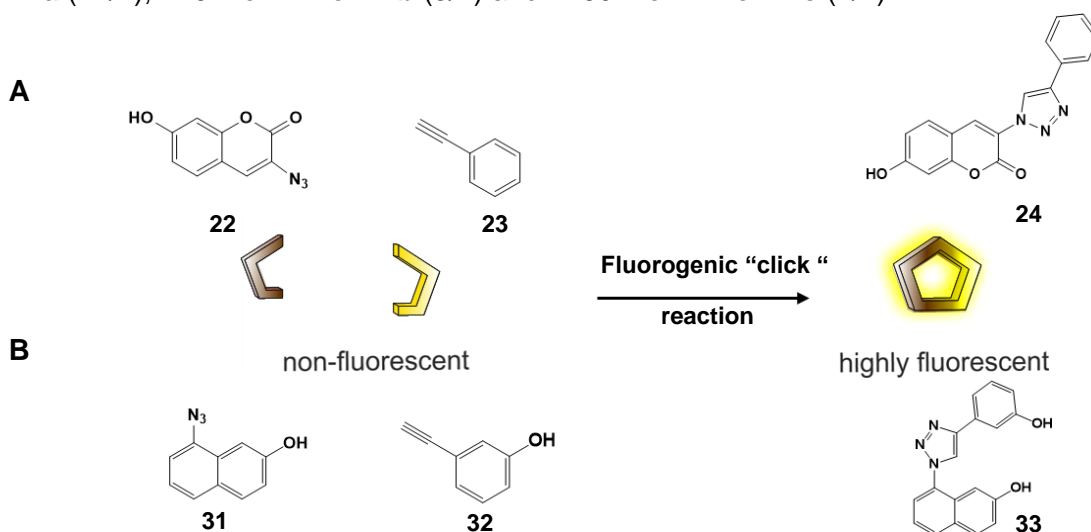


Figure 58. Fluorogenic “click” reaction of non-fluorescent substrate to highly fluorescent dyes.

The catalytic activity of chain extended (**18**) and network based (**21**) mechanophores were tested in a high molecular weight pTHF matrix generated a rise of fluorescence intensity due to copper(I)-triggered fluorogenic “click” reaction of **22** and **23**. This revealed a high fluorescent dye **24** (Figure 58 A). Therefore, the catalytic active site was generated by the compression induced cleavage of one shielding ligand. The increase in chain length, and thus, the accompanying duplication of copper(I) centers within the chain extended concept led to conversion up to 16% for the catalyst **18a**. Further extension of chain length (**18b**) revealed a high increase in fluorescence intensity reached conversion up to 44% but could not maintained the required latency (initial conversions of 3 – 4%). By testing the network-based mechanophore resulted in values up to 44% for **21a** (11/1), 12% for **21b** (3/1) and 12% for **21c** (1/1) while the fully latency could be retained in contrast to the chain extended concept. This emphasized the network structured mechanophore as the most promising candidate in terms of architectural influences on mechanochemical activation.

Furthermore, an all-in-one approach was developed, in which all required components for the fluorogenic “click” reaction as well as the mechanocatalyst itself were anchored covalently into a poly(urethane) based matrix. This approach enabled a circumvention of matrix blending effects, time-consuming adaptations of the catalyst-polymer linkage and prevents leaching of dye components. Moreover, a simple tunability of material properties in terms of strength and stiffness by varying the number of crosslinking points could be established. Within the poly(urethane) networks (**PUXX**), the linear components (pTHF, HDI) controlled the elasticity and stiffness whereas TMP acted as trivalent crosslinker. The simultaneous integration of mechanophore (**3**) during DBU catalyzed poly(addition) reaction and the final implementation of fluorogenic substrates (**31**, **32**) allowed forming a suitable material (Figure 58 B). It displayed a sufficient stiffness as well as a necessary mobility for the subsequent mechanochemical activation. While the concentration of **3**, **31** and **32** were kept constant, the adjustment of the OH ratio (bivalent and trivalent OH functionalities) enabled to tune the Young’s modulus ranging from 0.04 MPa (**PU20**) to 1.20 MPa (**PU80**). This offered the possibility to calculate the crosslinking density of the formed materials ranging from 4.0 mol m<sup>-3</sup> for PU20 to 168 mol<sup>-3</sup> for **PU80**.

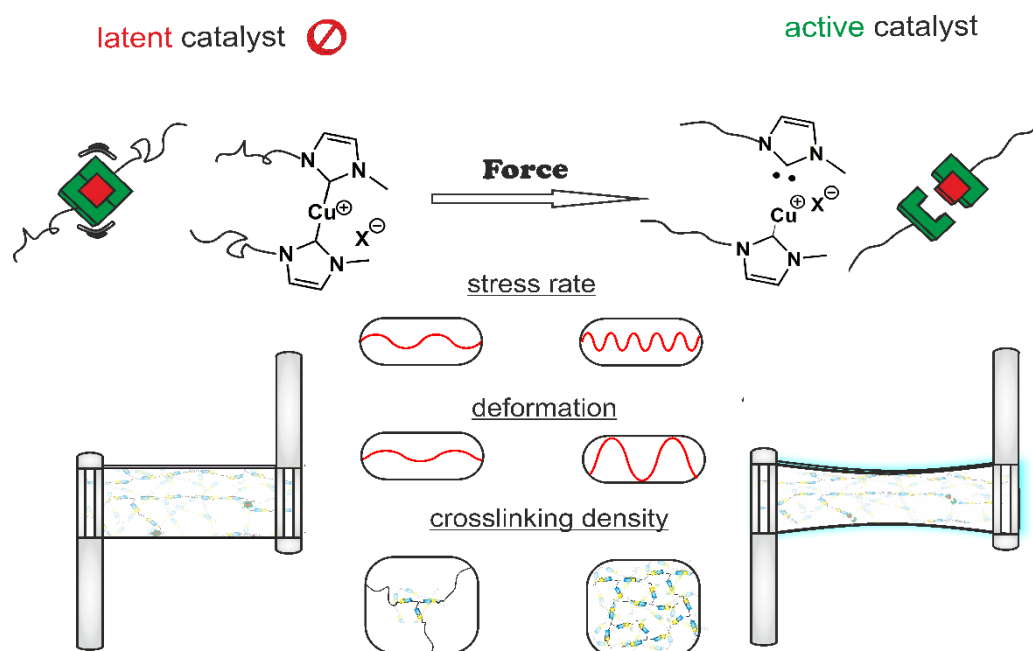


Figure 59. Mechanochemical activation of a covalently anchored low molecular weight copper(I)-bis(NHC) complex within a poly(urethane) matrix by extensional oscillating rheology triggered a fluorogenic “click” resulting in an increase in fluorescence intensity.

Finally, the catalytic activity of poly(urethane) mechanocatalysts (**PUXX**) were tested applying mechanical force on PU foils by extensional oscillating rheology (Figure 59).

The correct placement of the mechanophores turned out to be crucial for adequate results. Pre-experiments revealed that the simultaneous addition of linear components and crosslinker resulted in an inefficient activation of formed mechanophoric network. Therefore, *in situ* generated  $\alpha$ ,  $\omega$ -isocyanate-telechelic pTHF chain extended copper(I)-bis(NHC) complexes were accomplished by pre-polymerization of linear components which enabled a more efficient force transmission. As a result, the activation of the obtained mechanophore network increased while a longer pre-polymerization time of 30 min led an over extension of polymer chains ( $M_n = 6000 \text{ g mol}^{-1}$ ) and resulted in a lower mechanochemical response presumably

due to increased loops during the network formation. These loops impaired the force transmission in all directions and prevented an optimal force yield.

Stress rate dependency was investigated by varying the stress rate from  $0.25 \text{ s}^{-1}$  to  $1.00 \text{ s}^{-1}$  observing an accelerated mechanophore activation with increasing stress represented by a larger slope. Herein, the overall activation is stress rate independent (constant conversion of 12%). Within deformation dependence experiments, an enhancement of overall mechanochemical activation with increasing deformation could be observed, which could be correlated to the elongated effective tension length. Deformations of  $\gamma = 40\%$  revealed conversions up to 5%,  $\gamma = 60\%$  deformation up to 12% and  $\gamma = 80\%$  up to 17%.

Finally, the influence of the crosslinking density ( $\nu_x$ ) on the mechanochemical response were studied, in which the experimental parameters kept constant ( $\gamma =$  deformation and  $f = 0.50 \text{ s}^{-1}$ ). An enhanced overall activation of mechanophores was determined with decreasing crosslinking density for **PU70** to 5.2%, for **PU 60** to 8.5% and for **PU 50** to 10.1%. The extension of polymer strands between crosslinking points caused an enhancement in force transmission accompanied by a higher mechanochemical response. However, the highest conversion of 25% could be determined for **PU 40** with crosslinking density of  $24 \text{ mol m}^{-3}$ . In this region, the optimal OH-ratio was reached. Herein, the extended polymer strands acted as handles for efficient force transmission, whereas the trivalent crosslinker enabled to redirect the acting force three dimensionally.

Therefore, the transparent material was predestined due to its easy tunability in material properties to become a highly sensitive stress-sensor, storing the stress history of the material via the generated fluorescence as a simple optical readout.

## 6. References

- (1) Li, J.; Nagamani, C.; Moore, J. S. Polymer Mechanochemistry: From Destructive to Productive. *Accounts of Chemical Research* **2015**, *48*, 2181-2190.
- (2) Chen, Y.; Spiering, A. J. H.; Karthikeyan, S.; Peters, G. W. M.; Meijer, E. W.; Sijbesma, R. P. Mechanically induced chemiluminescence from polymers incorporating a 1,2-dioxetane unit in the main chain. *Nat Chem* **2012**, *4*, 559-562.
- (3) Beiermann, B. A.; Davis, D. A.; Kramer, S. L. B.; Moore, J. S.; Sottos, N. R.; White, S. R. Environmental effects on mechanochemical activation of spiropyran in linear PMMA. *Journal of Materials Chemistry* **2011**, *21*, 8443-8447.
- (4) Staudinger, H.; Bondy, H. F. Über Isopren und Kautschuk, 19. Mitteil.: Über die Molekülgröße des Kautschuks und der Balata. *Berichte der deutschen chemischen Gesellschaft (A and B Series)* **1930**, *63*, 734-736.
- (5) Staudinger, H.; Heuer, W. Über hochpolymere Verbindungen, 93. Mitteil.: Über das Zerreißen der Faden-Moleküle des Poly-styrols. *Berichte der deutschen chemischen Gesellschaft (A and B Series)* **1934**, *67*, 1159-1164.
- (6) Staudinger, H. Über Isopren und Kautschuk. 36. Mitteilung. Über die Konstitution des Kautschuks. *Angewandte Chemie* **1932**, *45*, 292-295.
- (7) Sohma, J. Mechano-radical formation in polypropylene by an extruder action and its after-effects. *Colloid and Polymer Science* **1992**, *270*, 1060-1065.
- (8) Ramirez, A. L. B.; Kean, Z. S.; Orlicki, J. A.; Champhekar, M.; Elsakar, S. M.; Krause, W. E.; Craig, S. L. Mechanochemical strengthening of a synthetic polymer in response to typically destructive shear forces. *Nat Chem* **2013**, *5*, 757-761.
- (9) Klukovich, H. M.; Kean, Z. S.; Ramirez, A. L. B.; Lenhardt, J. M.; Lin, J.; Hu, X.; Craig, S. L. Tension Trapping of Carbonyl Ylides Facilitated by a Change in Polymer Backbone. *Journal of the American Chemical Society* **2012**, *134*, 9577-9580.
- (10) Hickenboth, C. R.; Moore, J. S.; White, S. R.; Sottos, N. R.; Baudry, J.; Wilson, S. R. Biasing reaction pathways with mechanical force. *Nature* **2007**, *446*, 423-427.
- (11) Potisek, S. L.; Davis, D. A.; Sottos, N. R.; White, S. R.; Moore, J. S. Mechanophore-Linked Addition Polymers. *J. Am. Chem. Soc.* **2007**, *129*, 13808-13809.
- (12) Kean, Z. S.; Black Ramirez, A. L.; Yan, Y.; Craig, S. L. Bicyclo[3.2.0]heptane Mechanophores for the Non-scissile and Photochemically Reversible Generation of Reactive Bis-enones. *Journal of the American Chemical Society* **2012**, *134*, 12939-12942.
- (13) Kean, Z. S.; Niu, Z.; Hewage, G. B.; Rheingold, A. L.; Craig, S. L. Stress-Responsive Polymers Containing Cyclobutane Core Mechanophores: Reactivity and Mechanistic Insights. *Journal of the American Chemical Society* **2013**, *135*, 13598-13604.
- (14) Kryger, M. J.; Munaretto, A. M.; Moore, J. S. Structure-Mechanochemical Activity Relationships for Cyclobutane Mechanophores. *Journal of the American Chemical Society* **2011**, *133*, 18992-18998.
- (15) Kryger, M. J.; Ong, M. T.; Odom, S. A.; Sottos, N. R.; White, S. R.; Martinez, T. J.; Moore, J. S. Masked Cyanoacrylates Unveiled by Mechanical Force. *J. Am. Chem. Soc.* **2010**, *132*, 4558-4559.
- (16) Robb, M. J.; Moore, J. S. A Retro-Staudinger Cycloaddition: Mechanochemical Cycloelimination of a  $\beta$ -Lactam Mechanophore. *Journal of the American Chemical Society* **2015**, *137*, 10946-10949.
- (17) Hickenboth, C. R.; Rule, J. D.; Moore, J. S. Preparation of enediyne-crosslinked networks and their reactivity under thermal and mechanical conditions. *Tetrahedron* **2008**, *64*, 8435-8448.
- (18) Imato, K.; Natterodt, J. C.; Sapkota, J.; Goseki, R.; Weder, C.; Takahara, A.; Otsuka, H. Dynamic covalent diarylbibenzofuranone-modified nanocellulose: mechanochromic behaviour and application in self-healing polymer composites. *Polymer Chemistry* **2017**, *8*, 2115-2122.
- (19) Imato, K.; Otsuka, H. Reorganizable and stimuli-responsive polymers based on dynamic carbon-carbon linkages in diarylbibenzofuranones. *Polymer* **2018**, *137*, 395-413.

- (20) Beiermann, B. A.; Kramer, S. L. B.; May, P. A.; Moore, J. S.; White, S. R.; Sottos, N. R. The Effect of Polymer Chain Alignment and Relaxation on Force-Induced Chemical Reactions in an Elastomer. *Advanced Functional Materials* **2014**, *24*, 1529–1537.
- (21) Beiermann, B. A.; Kramer, S. L. B.; Moore, J. S.; White, S. R.; Sottos, N. R. Role of Mechanophore Orientation in Mechanochemical Reactions. *ACS Macro Letters* **2012**, *1*, 163-166.
- (22) Davis, D. A.; Hamilton, A.; Yang, J.; Cremar, L. D.; Van Gough, D.; Potisek, S. L.; Ong, M. T.; Braun, P. V.; Martinez, T. J.; White, S. R.; Moore, J. S.; Sottos, N. R. Force-induced activation of covalent bonds in mechanoresponsive polymeric materials. *Nature* **2009**, *459*, 68-72.
- (23) Lee, C. K.; Davis, D. A.; White, S. R.; Moore, J. S.; Sottos, N. R.; Braun, P. V. Force-Induced Redistribution of a Chemical Equilibrium. *Journal of the American Chemical Society* **2010**, *132*, 16107-16111.
- (24) Gossweiler, G. R.; Kouznetsova, T. B.; Craig, S. L. Force-Rate Characterization of Two Spiropyran-Based Molecular Force Probes. *Journal of the American Chemical Society* **2015**, *137*, 6148–6151.
- (25) Gossweiler, G. R.; Hewage, G. B.; Soriano, G.; Wang, Q.; Welshofer, G. W.; Zhao, X.; Craig, S. L. Mechanochemical Activation of Covalent Bonds in Polymers with Full and Repeatable Macroscopic Shape Recovery. *ACS Macro Letters* **2014**, *3*, 216-219.
- (26) Zhang, H.; Chen, Y.; Lin, Y.; Fang, X.; Xu, Y.; Ruan, Y.; Weng, W. Spiropyran as a Mechanochromic Probe in Dual Crosslinked Elastomers. *Macromolecules* **2014**, *47*, 6783–6790.
- (27) Chen, Y.; Zhang, H.; Fang, X.; Lin, Y.; Xu, Y.; Weng, W. Mechanical Activation of Mechanophore Enhanced by Strong Hydrogen Bonding Interactions. *ACS Macro Letters* **2014**, *3*, 141-145.
- (28) Fang, X.; Zhang, H.; Chen, Y.; Lin, Y.; Xu, Y.; Weng, W. Biomimetic Modular Polymer with Tough and Stress Sensing Properties. *Macromolecules* **2013**, *46*, 6566-6574.
- (29) Hong, G.; Zhang, H.; Lin, Y.; Chen, Y.; Xu, Y.; Weng, W.; Xia, H. Mechanoresponsive Healable Metallosupramolecular Polymers. *Macromolecules* **2013**, *46*, 8649-8656.
- (30) Lee, C. K.; Diesendruck, C. E.; Lu, E.; Pickett, A. N.; May, P. A.; Moore, J. S.; Braun, P. V. Solvent Swelling Activation of a Mechanophore in a Polymer Network. *Macromolecules* **2014**, *47*, 2690-2694.
- (31) Kingsbury, C. M.; May, P. A.; Davis, D. A.; White, S. R.; Moore, J. S.; Sottos, N. R. Shear activation of mechanophore-crosslinked polymers. *J. Compos. Mater.* **2011**, *21*, 8381-8388.
- (32) Degen, C. M.; May, P. A.; Moore, J. S.; White, S. R.; Sottos, N. R. Time-Dependent Mechanochemical Response of SP-Crosslinked PMMA. *Macromolecules* **2013**, *46*, 8917-8921.
- (33) Celestine, A.-D. N.; Beiermann, B. A.; May, P. A.; Moore, J. S.; Sottos, N. R.; White, S. R. Fracture-induced activation in mechanophore-linked, rubber toughened PMMA. *Polymer* **2014**, *55*, 4164-4171.
- (34) Celestine, A.-D. N.; Sottos, N. R.; White, S. R. Strain and stress mapping by mechanochemical activation of spiropyran in poly(methyl methacrylate). *Strain* **2019**, *55*, e12310.
- (35) Grady, M. E.; Beiermann, B. A.; Moore, J. S.; Sottos, N. R. Shockwave Loading of Mechanochemically Active Polymer Coatings. *ACS Applied Materials & Interfaces* **2014**, *6*, 5350-5355.
- (36) Rohde, R. C.; Basu, A.; Okello, L. B.; Barbee, M. H.; Zhang, Y.; Velev, O. D.; Nelson, A.; Craig, S. L. Mechanochromic composite elastomers for additive manufacturing and low strain mechanophore activation. *Polymer Chemistry* **2019**, *10*, 5985-5991.
- (37) Kister, G.; Moniruzzaman, M.; Khan, M.; Debnath, S. Mechanochemical activation of hydroxyl-terminated polybutadiene for the remote detection and quantification of mechanical stress. *Dyes and Pigments* **2019**, *162*, 309-314.
- (38) Xing, C.; Wang, L.; Xian, L.; Wang, Y.; Zhang, L.; Xi, K.; Zhang, Q.; Jia, X. Enhanced Thermal Ageing Stability of Mechanophore in Polyurethane Network by

Introducing Polyhedral Oligomeric Silsesquioxanes (POSS). *Macromolecular Chemistry and Physics* **2018**, *219*, 1800042.

(39) Lin, Y.; Barbee, M. H.; Chang, C.-C.; Craig, S. L. Regiochemical Effects on Mechanophore Activation in Bulk Materials. *Journal of the American Chemical Society* **2018**, *140*, 15969-15975.

(40) Kim, T. A.; Robb, M. J.; Moore, J. S.; White, S. R.; Sottos, N. R. Mechanical Reactivity of Two Different Spiropyran Mechanophores in Polydimethylsiloxane. *Macromolecules* **2018**, *51*, 9177-9183.

(41) Barbee, M. H.; Kouznetsova, T.; Barrett, S. L.; Gossweiler, G. R.; Lin, Y.; Rastogi, S. K.; Brittain, W. J.; Craig, S. L. Substituent Effects and Mechanism in a Mechanochemical Reaction. *Journal of the American Chemical Society* **2018**, *140*, 12746-12750.

(42) Brown, C. L.; Barbee, M. H.; Ko, J. H.; Maynard, H. D.; Craig, S. L. Writing Without Ink: A Mechanically and Photochemically Responsive PDMS Polymer for Science Outreach. *Journal of Chemical Education* **2017**, *94*, 1752-1755.

(43) Wang, L.-J.; Zhou, X.-J.; Zhang, X.-H.; Du, B.-Y. Enhanced Mechanophore Activation within Micelles. *Macromolecules* **2016**, *49*, 98-104.

(44) Kempe, F.; Brügner, O.; Buchheit, H.; Momm, S. N.; Riehle, F.; Hameury, S.; Walter, M.; Sommer, M. A Simply Synthesized, Tough Polyarylene with Transient Mechanochromic Response. *Angewandte Chemie International Edition* **2018**, *57*, 997-1000.

(45) Raisch, M.; Genovese, D.; Zaccheroni, N.; Schmidt, S. B.; Focarete, M. L.; Sommer, M.; Gualandi, C. Highly Sensitive, Anisotropic, and Reversible Stress/Strain-Sensors from Mechanochromic Nanofiber Composites. *Advanced Materials* **2018**, *30*, 1802813.

(46) Metzler, L.; Reichenbach, T.; Brügner, O.; Komber, H.; Lombeck, F.; Müllers, S.; Hanselmann, R.; Hillebrecht, H.; Walter, M.; Sommer, M. High molecular weight mechanochromic spiropyran main chain copolymers via reproducible microwave-assisted Suzuki polycondensation. *Polymer Chemistry* **2015**, *6*, 3694-3707.

(47) Zhang, H.; Gao, F.; Cao, X.; Li, Y.; Xu, Y.; Weng, W.; Boulatov, R. Mechanochromism and Mechanical-Force-Triggered Crosslinking from a Single Reactive Moiety Incorporated into Polymer Chains. *Angewandte Chemie* **2016**, *128*, 3092-3096.

(48) McFadden, M. E.; Robb, M. J. Force-Dependent Multicolor Mechanochromism from a Single Mechanophore. *Journal of the American Chemical Society* **2019**, *141*, 11388-11392.

(49) Robb, M. J.; Kim, T. A.; Halmes, A. J.; White, S. R.; Sottos, N. R.; Moore, J. S. Regioisomer-Specific Mechanochromism of Naphthopyran in Polymeric Materials. *Journal of the American Chemical Society* **2016**, *138*, 12328-12331.

(50) Song, Y.-K.; Lee, K.-H.; Hong, W.-S.; Cho, S.-Y.; Yu, H.-C.; Chung, C.-M. Fluorescence sensing of microcracks based on cycloreversion of a dimeric anthracene moiety. *Journal of Materials Chemistry* **2012**, *22*, 1380-1386.

(51) Göstl, R.; Sijbesma, R. P.  $\pi$ -extended anthracenes as sensitive probes for mechanical stress. *Chemical Science* **2016**, *7*, 370-375.

(52) Church, D. C.; Peterson, G. I.; Boydston, A. J. Comparison of Mechanochemical Chain Scission Rates for Linear versus Three-Arm Star Polymers in Strong Acoustic Fields. *ACS Macro Letters* **2014**, *3*, 648-651.

(53) Konda, S. S. M.; Brantley, J. N.; Varghese, B. T.; Wiggins, K. M.; Bielawski, C. W.; Makarov, D. E. Molecular Catch Bonds and the Anti-Hammond Effect in Polymer Mechanochemistry. *Journal of the American Chemical Society* **2013**, *135*, 12722-12729.

(54) Wiggins, K. M.; Syrett, J. A.; Haddleton, D. M.; Bielawski, C. W. Mechanically Facilitated Retro [4 + 2] Cycloadditions. *Journal of the American Chemical Society* **2011**, *133*, 7180-7189.

(55) Shiraki, T.; Diesendruck, C. E.; Moore, J. S. The mechanochemical production of phenyl cations through heterolytic bond scission. *Faraday Discussions* **2014**, *170*, 385-394.

(56) Kean, Z. S.; Gossweiler, G. R.; Kouznetsova, T. B.; Hewage, G. B.; Craig, S. L. A Coumarin Dimer Probe of Mechanochemical Scission Efficiency in the Sonochemical

Activation of Chain-Centered Mechanophore Polymers. *Chemical Communications* **2015**, *51*, 9157-9160.

(57) Wang, L.-J.; Yang, K.-X.; Zhou, Q.; Yang, H.-Y.; He, J.-Q.; Zhang, X.-Y. Rhodamine Mechanophore Functionalized Mechanochromic Double Network Hydrogels with High Sensitivity to Stress. *Chinese Journal of Polymer Science* **2019**.

(58) Wang, L.; Zhou, W.; Tang, Q.; Yang, H.; Zhou, Q.; Zhang, X. Rhodamine-Functionalized Mechanochromic and Mechanofluorescent Hydrogels with Enhanced Mechanoresponsive Sensitivity. *Polymers* **2018**, *10*, 994.

(59) Ma, Z.; Ji, Y.; Lan, Y.; Kuang, G.-C.; Jia, X. Two novel rhodamine-based molecules with different mechanochromic and photochromic properties in solid state. *Journal of Materials Chemistry C* **2018**, *6*, 2270-2274.

(60) Wang, T.; Zhang, N.; Dai, J.; Li, Z.; Bai, W.; Bai, R. Novel Reversible Mechanochromic Elastomer with High Sensitivity: Bond Scission and Bending-Induced Multicolor Switching. *ACS Applied Materials & Interfaces* **2017**.

(61) Chen, Y.; Sijbesma, R. P. Dioxetanes as Mechanoluminescent Probes in Thermoplastic Elastomers. *Macromolecules* **2014**, *47*, 3797-3805.

(62) Ducrot, E.; Chen, Y.; Bulters, M.; Sijbesma, R. P.; Creton, C. Toughening Elastomers with Sacrificial Bonds and Watching Them Break. *Science* **2014**, *344*, 186-189.

(63) Kean, Z. S.; Hawk, J. L.; Lin, S.; Zhao, X.; Sijbesma, R. P.; Craig, S. L. Increasing the Maximum Achievable Strain of a Covalent Polymer Gel Through the Addition of Mechanically Invisible Crosslinks. *Advanced Materials* **2014**, *26*, 6013-6018.

(64) Clough, J. M.; van der Gucht, J.; Sijbesma, R. P. Mechanoluminescent Imaging of Osmotic Stress-Induced Damage in a Glassy Polymer Network. *Macromolecules* **2017**, *50*, 2043-2053.

(65) Yang, F.; Yuan, Y.; Sijbesma, R. P.; Chen, Y. Sensitized Mechanoluminescence Design toward Mechanically Induced Intense Red Emission from Transparent Polymer Films. *Macromolecules* **2020**, *53*, 905-912.

(66) Filonenko, G. A.; Khusnutdinova, J. R. Dynamic Phosphorescent Probe for Facile and Reversible Stress Sensing. *Advanced Materials* **2017**, *29*, 1700563.

(67) Filonenko, G. A.; Sun, D.; Weber, M.; Müller, C.; Pidko, E. A. Multicolor Organometallic Mechanophores for Polymer Imaging Driven by Exciplex Level Interactions. *Journal of the American Chemical Society* **2019**, *141*, 9687-9692.

(68) Karimata, A.; Patil, P. H.; Khaskin, E.; Lapointe, S.; Fayzullin, R. R.; Stampoulis, P.; Khusnutdinova, J. R. Highly sensitive mechano-controlled luminescence in polymer films modified by dynamic CuI-based crosslinkers. *Chemical Communications* **2019**.

(69) Muramatsu, T.; Sagara, Y.; Traeger, H.; Tamaoki, N.; Weder, C. Mechanoresponsive Behavior of a Polymer-Embedded Red-Light Emitting Rotaxane Mechanophore. *ACS Applied Materials & Interfaces* **2019**, *11*, 24571-24576.

(70) Li, Z. a.; Toivola, R.; Ding, F.; Yang, J.; Lai, P.-N.; Howie, T.; Georgeson, G.; Jang, S.-H.; Li, X.; Flinn, B. D.; Jen, A. K. Y. Highly Sensitive Built-In Strain Sensors for Polymer Composites: Fluorescence Turn-On Response through Mechanochemical Activation. *Advanced Materials* **2016**, *28*, 6592-6597.

(71) Li, H.; Zhang, Y.; Liu, Y.; Sijbesma, R. P.; Heuts, J. P. A.; Zhang, Q. Preparation of mechanoresponsive hairy particles using polymeric surfactants in emulsion polymerization. *Polymer Chemistry* **2017**, *8*, 3971-3976.

(72) Karman, M.; Verde-Sesto, E.; Weder, C. Mechanochemical Activation of Polymer-Embedded Photoluminescent Benzoxazole Moieties. *ACS Macro Letters* **2018**, *7*, 1028-1033.

(73) Sulkanen, A. R.; Sung, J.; Robb, M. J.; Moore, J. S.; Sottos, N. R.; Liu, G.-y. Spatially Selective and Density-Controlled Activation of Interfacial Mechanophores. *Journal of the American Chemical Society* **2019**, *141*, 4080-4085.

(74) Yuan, Y.; Li, M.; Yuan, W.; Yang, F.; Chen, Y. Polyurethane/Siloxane Hybrid Polymers with Chemiluminescent Mechanophores as Stress Probes. *Macromolecular Materials and Engineering* **2019**, *0*, 1900056.

- (75) Paulusse, J. M. J.; Sijbesma, R. P. Selectivity of mechanochemical chain scission in mixed palladium(ii) and platinum(ii) coordination polymers. *Chemical Communications* **2008**, 4416-4418.
- (76) Paulusse, J. M. J.; Huijbers, J. P. J.; Sijbesma, R. P. Quantification of Ultrasound-Induced Chain Scission in Pd<sup>II</sup>-Phosphine Coordination Polymers. *Chemistry – A European Journal* **2006**, *12*, 4928-4934.
- (77) Paulusse, J. M. J.; Huijbers, J. P. J.; Sijbesma, R. P. Reversible, High Molecular Weight Palladium and Platinum Coordination Polymers Based on Phosphorus Ligands. *Macromolecules* **2005**, *38*, 6290-6298.
- (78) Paulusse, J. M. J.; Sijbesma, R. P. Reversible Mechanochemistry of a Pd<sup>II</sup> Coordination Polymer. *Angewandte Chemie International Edition* **2004**, *43*, 4460-4462.
- (79) Karthikeyan, S.; Potisek, S. L.; Piermattei, A.; Sijbesma, R. P. Highly Efficient Mechanochemical Scission of Silver-Carbene Coordination Polymers. *Journal of the American Chemical Society* **2008**, *130*, 14968-14969.
- (80) Groote, R.; Szyja, B. M.; Pidko, E. A.; Hensen, E. J. M.; Sijbesma, R. P. Unfolding and Mechanochemical Scission of Supramolecular Polymers Containing a Metal-Ligand Coordination Bond. *Macromolecules* **2011**, *44*, 9187-9195.
- (81) Rooze, J.; Groote, R.; Jakobs, R. T. M.; Sijbesma, R. P.; van Iersel, M. M.; Rebrov, E. V.; Schouten, J. C.; Keurentjes, J. T. F. Mechanism of Ultrasound Scission of a Silver-Carbene Coordination Polymer. *The Journal of Physical Chemistry B* **2011**, *115*, 11038-11043.
- (82) Groote, R.; van Haandel, L.; Sijbesma, R. P. The effect of molecular weight and catalyst concentration on catalytic activity in mechanochemically activated transesterification using silver(I)-N-heterocyclic carbene latent catalysts. *Journal of Polymer Science Part A: Polymer Chemistry* **2012**, *50*, 4929-4935.
- (83) Groote, R.; Jakobs, R. T. M.; Sijbesma, R. P. Performance of Mechanochemically Activated Catalysts Is Enhanced by Suppression of the Thermal Effects of Ultrasound. *ACS Macro Letters* **2012**, *1*, 1012-1015.
- (84) Piermattei, A.; Karthikeyan, S.; Sijbesma, R. P. Activating catalysts with mechanical force. *Nat Chem* **2009**, *1*, 133-137.
- (85) Jakobs, R. T. M.; Ma, S.; Sijbesma, R. P. Mechanocatalytic Polymerization and Crosslinking in a Polymeric Matrix. *ACS Macro Lett.* **2013**, *2*, 613-616.
- (86) Jakobs, R. T. M.; Sijbesma, R. P. Mechanical Activation of a Latent Olefin Metathesis Catalyst and Persistence of its Active Species in ROMP. *Organometallics* **2012**, *31*, 2476-2481.
- (87) Wiggins, K. M.; Hudnall, T. W.; Tennyson, A. G.; Bielawski, C. W. Selective scission of pyridine-boronium complexes: mechanical generation of Bronsted bases and polymerization catalysts. *Journal of Materials Chemistry* **2011**, *21*, 8355-8359.
- (88) Tennyson, A. G.; Wiggins, K. M.; Bielawski, C. W. Mechanical Activation of Catalysts for C-C Bond Forming and Anionic Polymerization Reactions from a Single Macromolecular Reagent. *Journal of the American Chemical Society* **2010**, *132*, 16631-16636.
- (89) Kersey, F. R.; Yount, W. C.; Craig, S. L. Single-Molecule Force Spectroscopy of Bimolecular Reactions: System Homology in the Mechanical Activation of Ligand Substitution Reactions. *Journal of the American Chemical Society* **2006**, *128*, 3886-3887.
- (90) Nagamani, C.; Liu, H.; Moore, J. S. Mechano-generation of Acid from Oxime Sulfonates. *Journal of the American Chemical Society* **2016**, *138*, 2540-2543.
- (91) Calvino, C.; Neumann, L.; Weder, C.; Schrettl, S. Approaches to polymeric mechanochromic materials. *Journal of Polymer Science Part A: Polymer Chemistry* **2017**, *55*, 640-652.
- (92) Ong, M. T.; Leiding, J.; Tao, H.; Virshup, A. M.; Martínez, T. J. First Principles Dynamics and Minimum Energy Pathways for Mechanochemical Ring Opening of Cyclobutene. *Journal of the American Chemical Society* **2009**, *131*, 6377-6379.
- (93) Ribas-Arino, J.; Marx, D. Covalent Mechanochemistry: Theoretical Concepts and Computational Tools with Applications to Molecular Nanomechanics. *Chemical Reviews* **2012**, *112*, 5412-5487.

- (94) Beyer, M. K. The mechanical strength of a covalent bond calculated by density functional theory. *The Journal of Chemical Physics* **2000**, *112*, 7307-7312.
- (95) Caruso, M. M.; Davis, D. A.; Shen, Q.; Odom, S. A.; Sottos, N. R.; White, S. R.; Moore, J. S. Mechanically-Induced Chemical Changes in Polymeric Materials. *Chemical Reviews* **2009**, *109*, 5755-5798.
- (96) Groote, R.; Jakobs, R. T. M.; Sijbesma, R. P. Mechanocatalysis: forcing latent catalysts into action. *Polymer Chemistry* **2013**, *4*, 4846-4859.
- (97) Beyer, M. K.; Clausen-Schaumann, H. Mechanochemistry: The Mechanical Activation of Covalent Bonds. *Chem. Rev.* **2005**, *105*, 2921-2948.
- (98) Brantley, J. N.; Wiggins, K. M.; Bielawski, C. W. Polymer mechanochemistry: the design and study of mechanophores. *Polymer International* **2013**, *62*, 2–12.
- (99) Klukovich, H. M.; Kouznetsova, T. B.; Kean, Z. S.; Lenhardt, J. M.; Craig, S. L. A backbone lever-arm effect enhances polymer mechanochemistry. *Nat Chem* **2013**, *5*, 110-114.
- (100) Wang, J.; Kouznetsova, T. B.; Kean, Z. S.; Fan, L.; Mar, B. D.; Martínez, T. J.; Craig, S. L. A Remote Stereochemical Lever Arm Effect in Polymer Mechanochemistry. *Journal of the American Chemical Society* **2014**, *136*, 15162-15165.
- (101) Wang, J.; Kouznetsova, T. B.; Niu, Z.; Rheingold, A. L.; Craig, S. L. Accelerating a Mechanically Driven anti-Woodward–Hoffmann Ring Opening with a Polymer Lever Arm Effect. *The Journal of Organic Chemistry* **2015**, *80*, 11895-11898.
- (102) Zhang, H.; Li, X.; Lin, Y.; Gao, F.; Tang, Z.; Su, P.; Zhang, W.; Xu, Y.; Weng, W.; Boulatov, R. Multi-modal mechanophores based on cinnamate dimers. *Nature Communications* **2017**, *8*, 1147.
- (103) Davila, J.; Chassepot, A.; Longo, J.; Boulmedais, F.; Reisch, A.; Frisch, B.; Meyer, F.; Voegel, J.-C.; Mésini, P. J.; Senger, B.; Metz-Boutigue, M.-H.; Hemmerlé, J.; Lavalley, P.; Schaaf, P.; Jierry, L. Cyto-mechanoresponsive Polyelectrolyte Multilayer Films. *Journal of the American Chemical Society* **2012**, *134*, 83-86.
- (104) Rios, C.; Longo, J.; Zahouani, S.; Garnier, T.; Vogt, C.; Reisch, A.; Senger, B.; Boulmedais, F.; Hemmerlé, J.; Benmlih, K.; Frisch, B.; Schaaf, P.; Jierry, L.; Lavalley, P. A new biomimetic route to engineer enzymatically active mechano-responsive materials. *Chemical Communications* **2015**, *51*, 5622-5625.
- (105) Torabi, K.; Schatz, G. C. Tensile Mechanics of  $\alpha$ -Helical Polypeptides. *Macromolecules* **2013**, *46*, 7947-7956.
- (106) Courty, S.; Gornall, J. L.; Terentjev, E. M. Induced helicity in biopolymer networks under stress. *Proceedings of the National Academy of Sciences of the United States of America* **2005**, *102*, 13457-13460.
- (107) Wang, J.; Kouznetsova, T. B.; Niu, Z.; Ong, M. T.; Klukovich, H. M.; Rheingold, A. L.; Martinez, T. J.; Craig, S. L. Inducing and quantifying forbidden reactivity with single-molecule polymer mechanochemistry. *Nat Chem* **2015**, *7*, 323-327.
- (108) Wang, J.; Kouznetsova, T. B.; Craig, S. L. Reactivity and Mechanism of a Mechanically Activated anti-Woodward–Hoffmann–DePuy Reaction. *Journal of the American Chemical Society* **2015**, *137*, 11554-11557.
- (109) Woodward, R. B.; Hoffmann, R. Stereochemistry of Electrocyclic Reactions. *Journal of the American Chemical Society* **1965**, *87*, 395-397.
- (110) Schütze, D.; Holz, K.; Müller, J.; Beyer, M. K.; Lüning, U.; Hartke, B. Pinpointing Mechanochemical Bond Rupture by Embedding the Mechanophore into a Macrocyclic. *Angewandte Chemie International Edition* **2015**, *54*, 2556-2559.
- (111) Wiita, A. P.; Ainarapu, S. R. K.; Huang, H. H.; Fernandez, J. M. Force-dependent chemical kinetics of disulfide bond reduction observed with single-molecule techniques. *Proceedings of the National Academy of Sciences* **2006**, *103*, 7222-7227.
- (112) Liang, J.; Fernández, J. M. Kinetic Measurements on Single-Molecule Disulfide Bond Cleavage. *Journal of the American Chemical Society* **2011**, *133*, 3528-3534.
- (113) Guzmán, D. L.; Randall, A.; Baldi, P.; Guan, Z. Computational and single-molecule force studies of a macro domain protein reveal a key molecular determinant for mechanical stability. *Proceedings of the National Academy of Sciences* **2010**, *107*, 1989-1994.

- (114) Garcia-Manyes, S.; Liang, J.; Szoszkiewicz, R.; Kuo, T.-L.; Fernández, J. M. Force-activated reactivity switch in a bimolecular chemical reaction. *Nature Chemistry* **2009**, *1*, 236-242.
- (115) Chung, J.; Kushner, A. M.; Weisman, A. C.; Guan, Z. Direct correlation of single-molecule properties with bulk mechanical performance for the biomimetic design of polymers. *Nature Materials* **2014**, *13*, 1055-1062.
- (116) Guan, Z.; Roland, J. T.; Bai, J. Z.; Ma, S. X.; McIntire, T. M.; Nguyen, M. Modular Domain Structure: A Biomimetic Strategy for Advanced Polymeric Materials. *Journal of the American Chemical Society* **2004**, *126*, 2058-2065.
- (117) Rief, M.; Oesterhelt, F.; Heymann, B.; Gaub, H. E. Single Molecule Force Spectroscopy on Polysaccharides by Atomic Force Microscopy. *Science* **1997**, *275*, 1295-1297.
- (118) Pill, M. F.; Holz, K.; Preußke, N.; Berger, F.; Clausen-Schaumann, H.; Lüning, U.; Beyer, M. K. Mechanochemical Cycloreversion of Cyclobutane Observed at the Single Molecule Level. *Chemistry – A European Journal* **2016**, *22*, 12034-12039.
- (119) Wang, J.; Kouznetsova, T. B.; Boulatov, R.; Craig, S. L. Mechanical gating of a mechanochemical reaction cascade. *Nature Communications* **2016**, *7*, 13433.
- (120) Kersey, F. R.; Yount, W. C.; Craig, S. L. Single-Molecule Force Spectroscopy of Bimolecular Reactions: System Homology in the Mechanical Activation of Ligand Substitution Reactions. *Journal of the American Chemical Society* **2006**, *128*, 3886-3887.
- (121) Liu, N.; Zhang, W. Feeling Inter- or Intramolecular Interactions with the Polymer Chain as Probe: Recent Progress in SMFS Studies on Macromolecular Interactions. *ChemPhysChem* **2012**, *13*, 2238-2256.
- (122) Zou, S.; Schönherr, H.; Vancso, G. J. Stretching and Rupturing Individual Supramolecular Polymer Chains by AFM. *Angewandte Chemie International Edition* **2005**, *44*, 956-959.
- (123) Pill, M. F.; East, A. L. L.; Marx, D.; Beyer, M. K.; Clausen-Schaumann, H. Mechanical activation drastically accelerates amide bond hydrolysis, matching enzyme activity. *Angewandte Chemie International Edition* **2019**, *0*.
- (124) Liu, Y.; Vancso, G. J. Polymer single chain imaging, molecular forces, and nanoscale processes by Atomic Force Microscopy: The ultimate proof of the macromolecular hypothesis. *Progress in Polymer Science* **2020**, *104*, 101232.
- (125) Basedow, A. M.; Ebert, K. H. Zum Mechanismus des Abbaus von Polymeren in Lösung durch Ultraschall. *Die Makromolekulare Chemie* **1975**, *176*, 745-757.
- (126) Price, G. J. The use of ultrasound for the controlled degradation of polymer solutions. *Advances in Sonochemistry* **1990**, *1*, 231-287.
- (127) Suslick, K. S.; Price, G. J. Application of ultrasound to materials chemistry. *Annual Review of Materials Science* **1999**, *29*, 295-326.
- (128) Suslick, K. S. Mechanochemistry and sonochemistry: concluding remarks. *Faraday Discussions* **2014**, *170*, 411-422.
- (129) Paulusse, J. M. J.; Sijbesma, R. P. Ultrasound in polymer chemistry: Revival of an established technique. *Journal of Polymer Science Part A: Polymer Chemistry* **2006**, *44*, 5445-5453.
- (130) Wiggins, K. M.; Brantley, J. N.; Bielawski, C. W. Methods for activating and characterizing mechanically responsive polymers. *Chemical Society Reviews* **2013**, *42*, 7130-7147.
- (131) Kida, J.; Imato, K.; Goseki, R.; Aoki, D.; Morimoto, M.; Otsuka, H. The photoregulation of a mechanochemical polymer scission. *Nature Communications* **2018**, *9*, 3504.
- (132) Zysman, V.; Nguyen, T. Q.; Kausch, H.-H. Degradation on freezing dilute polystyrene solutions in p-xylene. *Journal of Polymer Science Part B: Polymer Physics* **1994**, *32*, 1257-1269.
- (133) Wang, S.; Yan, X.; Ding, J.; Liu, M.; Cheng, R.; Wu, C.; Qian, R. On the cryogenic “degradation” of polystyrene in dilute solution. *Journal of Macromolecular Science, Part B* **1997**, *36*, 187-194.

- (134) Imato, K.; Irie, A.; Kosuge, T.; Ohishi, T.; Nishihara, M.; Takahara, A.; Otsuka, H. Mechanophores with a Reversible Radical System and Freezing-Induced Mechanochemistry in Polymer Solutions and Gels. *Angewandte Chemie International Edition* **2015**, *54*, 6168–6172.
- (135) Lenhardt, J. M.; Black, A. L.; Craig, S. L. gem-Dichlorocyclopropanes as Abundant and Efficient Mechanophores in Polybutadiene Copolymers under Mechanical Stress. *J. Am. Chem. Soc.* **2009**, *131*, 10818-10819.
- (136) Lenhardt, J. M.; Black, A. L.; Beiermann, B. A.; Steinberg, B. D.; Rahman, F.; Samborski, T.; Elsagr, J.; Moore, J. S.; Sottos, N. R.; Craig, S. L. Characterizing the mechanochemically active domains in gem-dihalocyclopropanated polybutadiene under compression and tension. *Journal of Materials Chemistry* **2011**, *21*, 8454-8459.
- (137) Diesendruck, C. E.; Steinberg, B. D.; Sugai, N.; Silberstein, M. N.; Sottos, N. R.; White, S. R.; Braun, P. V.; Moore, J. S. Proton-Coupled Mechanochemical Transduction: A Mechanogenerated Acid. *Journal of the American Chemical Society* **2012**, *134*, 12446-12449.
- (138) Michael, P.; Binder, W. H. A Mechanochemically Triggered “Click” Catalyst. *Angew. Chem. Int. Ed.* **2015**, *54*, 13918-13922.
- (139) Michael, P.; Biewend, M.; Binder, W. H. Mechanochemical Activation of Fluorogenic CuAAC “Click” Reactions for Stress-Sensing Applications. *Macromolecular Rapid Communications* **2018**, *39*, 1800376.
- (140) Oka, H.; Imato, K.; Sato, T.; Ohishi, T.; Goseki, R.; Otsuka, H. Enhancing Mechanochemical Activation in the Bulk State by Designing Polymer Architectures. *ACS Macro Letters* **2016**, *5*, 1124-1127.
- (141) Sohma, J. Mechanochemistry of polymers. *Progress in Polymer Science* **1989**, *14*, 451-596.
- (142) Liu, W.; Cao, Y.; Wang, W.; Gong, D.; Cao, T.; Qian, J.; Iqbal, K.; Qin, W.; Guo, H. Mechanochromic luminescent covalent organic frameworks for highly selective hydroxyl radical detection. *Chemical Communications* **2019**, *55*, 167-170.
- (143) Kosuge, T.; Zhu, X.; Lau, V. M.; Aoki, D.; Martinez, T. J.; Moore, J. S.; Otsuka, H. Multicolor Mechanochromism of a Polymer/Silica Composite with Dual Distinct Mechanophores. *Journal of the American Chemical Society* **2019**, *141*, 1898-1902.
- (144) Sung, J.; Robb, M. J.; White, S. R.; Moore, J. S.; Sottos, N. R. Interfacial Mechanophore Activation Using Laser-Induced Stress Waves. *Journal of the American Chemical Society* **2018**, *140*, 5000-5003.
- (145) Kosuge, T.; Imato, K.; Goseki, R.; Otsuka, H. Polymer-Inorganic Composites with Dynamic Covalent Mechanochromophore. *Macromolecules* **2016**, *49*, 5903–5911.
- (146) Lee, B.; Niu, Z.; Wang, J.; Slebodnick, C.; Craig, S. L. Relative Mechanical Strengths of Weak Bonds in Sonochemical Polymer Mechanochemistry. *Journal of the American Chemical Society* **2015**, *137*, 10826-10832.
- (147) May, P. A.; Moore, J. S. Polymer mechanochemistry: techniques to generate molecular force via elongational flows. *Chemical Society Reviews* **2013**, *42*, 7497-7506.
- (148) Florea, M. New use of size exclusion chromatography in kinetics of mechanical degradation of polymers in solution. *Journal of Applied Polymer Science* **1993**, *50*, 2039-2045.
- (149) Li, M.; Zhang, Q.; Zhou, Y.-N.; Zhu, S. Let spiropyran help polymers feel force! *Progress in Polymer Science* **2018**, *79*, 26-39.
- (150) Schrettl, S.; Balkenende, D. W. R.; Calvino, C.; Karman, M.; Lavrenova, A.; Neumann, L. N.; Sagara, Y.; Verde-Sesto, E.; di Giannantonio, M.; Simon, Y. C.; Fromm, K. M.; Lattuada, M.; Weder, C. Functional Polymers Through Mechanochemistry. *CHIMIA International Journal for Chemistry* **2019**, *73*, 7-11.
- (151) Yamakado, T.; Otsubo, K.; Osuka, A.; Saito, S. Compression of a Flapping Mechanophore Accompanied by Thermal Void Collapse in a Crystalline Phase. *Journal of the American Chemical Society* **2018**, *140*, 6245-6248.
- (152) Kim, S.-J.; Reneker, D. H. A mechanochromic smart material. *Polymer Bulletin* **1993**, *31*, 367-374.

- (153) Naumova, A.; Agudelo, D. C.; Villar, M. A.; Vega, D. A.; Valentin, J. L.; Saalwächter, K. Microscopic State of Polymer Network Chains upon Swelling and Deformation. *Macromolecules* **2019**, *52*, 5042-5053.
- (154) Carothers, W. H. Polymerization. *Chemical Reviews* **1931**, *8*, 353-426.
- (155) Flory, P. J. Molecular Size Distribution in Three Dimensional Polymers. I. Gelation. *Journal of the American Chemical Society* **1941**, *63*, 3083-3090.
- (156) Gu, Y.; Zhao, J.; Johnson, J. A. Polymer Networks: From Plastics and Gels to Porous Frameworks. *Angewandte Chemie International Edition* **2020**, *59*, 5022-5049.
- (157) Zou, W.; Dong, J.; Luo, Y.; Zhao, Q.; Xie, T. Dynamic Covalent Polymer Networks: from Old Chemistry to Modern Day Innovations. *Advanced Materials* **2017**, *29*, 1606100.
- (158) Voorhaar, L.; Hoogenboom, R. Supramolecular polymer networks: hydrogels and bulk materials. *Chemical Society Reviews* **2016**, *45*, 4013-4031.
- (159) Kim, H. J.; Chen, B.; Suo, Z.; Hayward, R. C. Ionomer junctions between polymer networks of fixed anions and cations. *Science* **2020**, *367*, 773-776.
- (160) Zare, P.; Stojanovic, A.; Herbst, F.; Akbarzadeh, J.; Peterlik, H.; Binder, W. H. Hierarchically Nanostructured Polyisobutylene-Based Ionic Liquids. *Macromolecules* **2012**, *45*, 2074-2084.
- (161) Herbst, F.; Döhler, D.; Michael, P.; Binder, W. H. Self-Healing Polymers via Supramolecular Forces. *Macromolecular Rapid Communications* **2013**, *34*, 203-220.
- (162) Li, J.; Mooney, D. J. Designing hydrogels for controlled drug delivery. *Nat Rev Mater* **2016**, *1*, 16071.
- (163) McKeown, N. B.; Budd, P. M. Polymers of intrinsic microporosity (PIMs): organic materials for membrane separations, heterogeneous catalysis and hydrogen storage. *Chemical Society Reviews* **2006**, *35*, 675-683.
- (164) Díaz Díaz, D.; Kühbeck, D.; Koopmans, R. J. Stimuli-responsive gels as reaction vessels and reusable catalysts. *Chemical Society Reviews* **2011**, *40*, 427-448.
- (165) Zhang, Y.; Riduan, S. N. Functional porous organic polymers for heterogeneous catalysis. *Chemical Society Reviews* **2012**, *41*, 2083-2094.
- (166) Armstrong, G.: Supramolecular Polymers (Hydrogen Bonds). In *Encyclopedia of Polymeric Nanomaterials*; Kobayashi, S., Müllen, K., Eds.; Springer Berlin Heidelberg: Berlin, Heidelberg, 2014; pp 1-10.
- (167) Wang, Y.; Astruc, D.; Abd-El-Aziz, A. S. Metallopolymers for advanced sustainable applications. *Chemical Society Reviews* **2019**, *48*, 558-636.
- (168) Fazli, A.; Rodrigue, D. Waste Rubber Recycling: A Review on the Evolution and Properties of Thermoplastic Elastomers. *Materials* **2020**, *13*, 782.
- (169) Shit, S. C.; Shah, P. A Review on Silicone Rubber. *National Academy Science Letters* **2013**, *36*, 355-365.
- (170) Sakdapipanich, J. T.; Rojruthai, P.: CHAPTER 2 Natural Rubber: Biosynthesis, Structure, Properties and Application. In *Natural Rubber Materials: Volume 1: Blends and IPNs*; The Royal Society of Chemistry, 2014; Vol. 1; pp 28-52.
- (171) Prisacariu, C.: Chemistry of polyurethane elastomers. In *Polyurethane Elastomers: From Morphology to Mechanical Aspects*; Springer Vienna: Vienna, 2011; pp 1-22.
- (172) Sadhu, S.; Bhowmick, A. K. Preparation and properties of nanocomposites based on acrylonitrile-butadiene rubber, styrene-butadiene rubber, and polybutadiene rubber. *Journal of Polymer Science Part B: Polymer Physics* **2004**, *42*, 1573-1585.
- (173) Pascault, J. P.; Williams, R. J. J.: Chapter 1 - Overview of thermosets: Present and future. In *Thermosets (Second Edition)*; Guo, Q., Ed.; Elsevier, 2018; pp 3-34.
- (174) Mullins, M. J.; Liu, D.; Sue, H. J.: Chapter 2 - Mechanical properties of thermosets. In *Thermosets (Second Edition)*; Guo, Q., Ed.; Elsevier, 2018; pp 35-68.
- (175) Krishnakumar, B.; Sanka, R. V. S. P.; Binder, W. H.; Parthasarthy, V.; Rana, S.; Karak, N. Vitrimers: Associative dynamic covalent adaptive networks in thermoset polymers. *Chemical Engineering Journal* **2020**, *385*, 123820.

- (176) Nuryawan, A.; Risnasari, I.; Sucipto, T.; Heri Iswanto, A.; Rosmala Dewi, R. Urea-formaldehyde resins: production, application, and testing. *IOP Conference Series: Materials Science and Engineering* **2017**, *223*, 012053.
- (177) Jin, F.-L.; Li, X.; Park, S.-J. Synthesis and application of epoxy resins: A review. *Journal of Industrial and Engineering Chemistry* **2015**, *29*, 1-11.
- (178) Polymer Gels, Hydrogels, and Scaffolds – An Overview. In *Disordered Pharmaceutical Materials*; pp 241-282.
- (179) Ahmed, E. M. Hydrogel: Preparation, characterization, and applications: A review. *Journal of Advanced Research* **2015**, *6*, 105-121.
- (180) Vintiloiu, A.; Leroux, J.-C. Organogels and their use in drug delivery — A review. *Journal of Controlled Release* **2008**, *125*, 179-192.
- (181) Sheiko, S. S.; Dobrynin, A. V. Architectural Code for Rubber Elasticity: From Supersoft to Superfirm Materials. *Macromolecules* **2019**, *52*, 7531-7546.
- (182) Lu, W.; Wei, Z.; Yuan, D.; Tian, J.; Fordham, S.; Zhou, H.-C. Rational Design and Synthesis of Porous Polymer Networks: Toward High Surface Area. *Chemistry of Materials* **2014**, *26*, 4589-4597.
- (183) Milisavljevic-Syed, J.; Petrovic, E.; Ćirić, I.; Mančić, M.; Marković, D.; Djordjević, M.: *TENSILE TESTING FOR DIFFERENT TYPES OF POLYMERS*, 2012.
- (184) Nielsen, L. E. Mechanical properties of polymers and composites. **1974**.
- (185) The Mechanical Properties of Polymers: General Considerations. In *Mechanical Properties of Solid Polymers*; pp 19-29.
- (186) Flory, P. J.: *Principles of polymer chemistry*; Cornell University Press: Ithaca, N.Y., 1953.
- (187) James, H. M.; Guth, E. Statistical Thermodynamics of Rubber Elasticity. *The Journal of Chemical Physics* **1953**, *21*, 1039-1049.
- (188) Rubinstein, M.: *Polymer physics*; Vol. 23.
- (189) Heinrich, G.; Straube, E.; Helmig, G. In *Tilte*, Berlin, Heidelberg1988; Springer Berlin Heidelberg.
- (190) Kloczkowski, A.; Kolinski, A.: Theoretical Models and Simulations of Polymer Chains. In *Physical Properties of Polymers Handbook*; Mark, J. E., Ed.; Springer New York: New York, NY, 2007; pp 67-81.
- (191) Staverman, A. J. In *Tilte*, Berlin, Heidelberg1982; Springer Berlin Heidelberg.
- (192) Flory, P. J. Theory of elasticity of polymer networks. The effect of local constraints on junctions. *The Journal of Chemical Physics* **1977**, *66*, 5720-5729.
- (193) Shaw, M. T.: Introduction to Polymer Rheology. In *Introduction to Polymer Rheology*; John Wiley & Sons, 2011.
- (194) Winter, H. H. Can the gel point of a crosslinking polymer be detected by the  $G'$  –  $G''$  crossover? *Polymer Engineering & Science* **1987**, *27*, 1698-1702.
- (195) Mezger, T. G.: *The Rheology Handbook*; Vincentz Network, 2012.
- (196) Basterra-Beroiz, B.; Rommel, R.; Kayser, F.; Westermann, S.; Valentin, J. L.; Heinrich, G. Swelling of polymer networks with topological constraints: Application of the Helmig-Heinrich-Straube model. *Express Polymer Letters* **2018**, *12*, 731-739.
- (197) General properties of polymer networks. In *Physical Gels from Biological and Synthetic Polymers*; Nishinari, K., Djabourov, M., Ross-Murphy, S. B., Eds.; Cambridge University Press: Cambridge, 2013; pp 97-123.
- (198) Orwoll, R. A.; Arnold, P. A.: Polymer–Solvent Interaction Parameter  $\chi$ . In *Physical Properties of Polymers Handbook*; Mark, J. E., Ed.; Springer New York: New York, NY, 2007; pp 233-257.
- (199) Hild, G. Interpretation of equilibrium swelling data on model networks using affine and ‘phantom’ network models. *Polymer* **1997**, *38*, 3279-3293.
- (200) Ding, Z. Y.; Aklonis, J. J.; Salovey, R. Model filled polymers. VI. Determination of the crosslink density of polymeric beads by swelling. *Journal of Polymer Science Part B: Polymer Physics* **1991**, *29*, 1035-1038.
- (201) Flory, P. J.; Jr., J. R. Statistical Mechanics of Cross-Linked Polymer Networks II. Swelling. *The Journal of Chemical Physics* **1943**, *11*, 521-526.

- (202) James, H. M.; Guth, E. Theory of the Elastic Properties of Rubber. *The Journal of Chemical Physics* **1943**, *11*, 455-481.
- (203) James, H. M.; Guth, E. Theory of the Increase in Rigidity of Rubber during Cure. *The Journal of Chemical Physics* **1947**, *15*, 669-683.
- (204) Flory, P. J.; Erman, B. Theory of elasticity of polymer networks. 3. *Macromolecules* **1982**, *15*, 800-806.
- (205) Rubinstein, M.; Colby, R. H.; Dobrynin, A. V.; Joanny, J.-F. Elastic Modulus and Equilibrium Swelling of Polyelectrolyte Gels. *Macromolecules* **1996**, *29*, 398-406.
- (206) Kim, J. W.; Jung, Y.; Coates, G. W.; Silberstein, M. N. Mechanoactivation of Spiropyran Covalently Linked PMMA: Effect of Temperature, Strain Rate, and Deformation Mode. *Macromolecules* **2015**, *48*, 1335-1342.
- (207) Qiu, W.; Gurr, P. A.; da Silva, G.; Qiao, G. G. Insights into the mechanochromism of spiropyran elastomers. *Polymer Chemistry* **2019**, *10*, 1650-1659.
- (208) Yenpech, N.; Intasanta, V.; Tashiro, K.; Chirachanchai, S. Color and shape reversible, recoverable and repeatable mechanochromic shape memory polycaprolactone: a single material with dual functions. *Polymer Chemistry* **2020**, *11*, 91-101.
- (209) Chen, H.; Yang, F.; Chen, Q.; Zheng, J. A Novel Design of Multi-Mechanoresponsive and Mechanically Strong Hydrogels. *Advanced Materials* **2017**, *29*, 1606900.
- (210) Li, M.; Liu, W.; Zhang, Q.; Zhu, S. Mechanical Force Sensitive Acrylic Latex Coating. *ACS Applied Materials & Interfaces* **2017**, *9*, 15156-15163.
- (211) Li, J.; Shiraki, T.; Hu, B.; Wright, R. A. E.; Zhao, B.; Moore, J. S. Mechanophore Activation at Heterointerfaces. *Journal of the American Chemical Society* **2014**, *136*, 15925-15928.
- (212) Woodcock, J. W.; Beams, R.; Davis, C. S.; Chen, N.; Stranick, S. J.; Shah, D. U.; Vollrath, F.; Gilman, J. W. Observation of Interfacial Damage in a Silk-Epoxy Composite, Using a Simple Mechanoresponsive Fluorescent Probe. *Advanced Materials Interfaces* **2017**, *4*, 1601018.
- (213) Livne, A.; Cohen, G.; Fineberg, J. Universality and Hysteretic Dynamics in Rapid Fracture. *Physical Review Letters* **2005**, *94*, 224301.
- (214) Yuan, W.; Yuan, Y.; Yang, F.; Wu, M.; Chen, Y. Improving Mechanoluminescent Sensitivity of 1,2-Dioxetane-Containing Thermoplastic Polyurethanes by Controlling Energy Transfer across Polymer Chains. *Macromolecules* **2018**, *51*, 9019-9025.
- (215) Abbas, K. B.; Porter, R. S. Polystyrene degradation induced by stresses resulting from the freezing of its solutions. *Journal of Polymer Science: Polymer Chemistry Edition* **1976**, *14*, 553-564.
- (216) Abbas, K.; Kirschner, T.; Porter, R. Cryogenic degradation of polystyrene in solution. *European Polymer Journal* **1978**, *14*, 361-367.
- (217) Imato, K.; Kanehara, T.; Nojima, S.; Ohishi, T.; Higaki, Y.; Takahara, A.; Otsuka, H. Repeatable mechanochemical activation of dynamic covalent bonds in thermoplastic elastomers. *Chemical Communications* **2016**, *52*, 10482-10485.
- (218) Balkenende, D. W. R.; Coulibaly, S.; Balog, S.; Simon, Y. C.; Fiore, G. L.; Weder, C. Mechanochemistry with Metallosupramolecular Polymers. *Journal of the American Chemical Society* **2014**, *136*, 10493-10498.
- (219) Chen, P.; Li, Q.; Grindy, S.; Holten-Andersen, N. White-Light-Emitting Lanthanide Metallogels with Tunable Luminescence and Reversible Stimuli-Responsive Properties. *Journal of the American Chemical Society* **2015**, *137*, 11590-11593.
- (220) Clough, J. M.; Balan, A.; van Daal, T. L. J.; Sijbesma, R. P. Probing Force with Mechanobase-Induced Chemiluminescence. *Angewandte Chemie International Edition* **2016**, *55*, 1445-1449.
- (221) Gao, G.; Jiao, Y.; Ma, F.; Jiao, Y.; Waclawik, E.; Du, A. Metal-free graphitic carbon nitride as mechano-catalyst for hydrogen evolution reaction. *Journal of Catalysis* **2015**, *332*, 149-155.

- (222) Di Giannantonio, M.; Ayer, M. A.; Verde-Sesto, E.; Lattuada, M.; Weder, C.; Fromm, K. M. Triggered Metal Ion Release and Oxidation: Ferrocene as a Mechanophore in Polymers. *Angewandte Chemie International Edition* **2018**, *57*, 11445-11450.
- (223) Sha, Y.; Zhang, Y.; Xu, E.; Wang, Z.; Zhu, T.; Craig, S. L.; Tang, C. Quantitative and Mechanistic Mechanochemistry in Ferrocene Dissociation. *ACS Macro Letters* **2018**, *7*, 1174-1179.
- (224) Sha, Y.; Zhang, Y.; Xu, E.; McAlister, C. W.; Zhu, T.; Craig, Stephen L.; Tang, C. Generalizing metallocene mechanochemistry to ruthenocene mechanophores. *Chemical Science* **2019**, *10*, 4959-4965.
- (225) Öfele, K. 1,3-Dimethyl-4-imidazolinylliden-(2)-pentacarbonylchrom ein neuer übergangsmetall-carben-komplex. *Journal of Organometallic Chemistry* **1968**, *12*, P42-P43.
- (226) Wanzlick, H.-W.; Schönherr, H.-J. Direct Synthesis of a Mercury Salt-Carbene Complex. *Angewandte Chemie International Edition in English* **1968**, *7*, 141-142.
- (227) Díez-González, S.; Marion, N.; Nolan, S. P. N-Heterocyclic Carbenes in Late Transition Metal Catalysis. *Chemical Reviews* **2009**, *109*, 3612-3676.
- (228) Sun, Z.; Chen, J.; Tu, T. NHC-based coordination polymers as solid molecular catalysts for reductive amination of biomass levulinic acid. *Green Chemistry* **2017**, *19*, 789-794.
- (229) Diaz, H.; Verpoort, F. ChemInform Abstract: N-Heterocyclic Carbene Transition Metal Complexes for Catalysis in Aqueous Media. *Chemical Society reviews* **2012**, *41*, 7032-7060.
- (230) Ezugwu, C. I.; Kabir, N. A.; Yusubov, M.; Verpoort, F. Metal-organic frameworks containing N-heterocyclic carbenes and their precursors. *Coordination Chemistry Reviews* **2016**, *307*, 188-210.
- (231) Fischer, E. O.; Maasböl, A. On the Existence of a Tungsten Carbonyl Carbene Complex. *Angewandte Chemie International Edition in English* **1964**, *3*, 580-581.
- (232) Mills, O. S.; Redhouse, A. D. On the Existence of Metal Carbonyl Carbene Complexes. *Angewandte Chemie International Edition in English* **1965**, *4*, 1082-1082.
- (233) Schrock, R. R. Alkylcarbene complex of tantalum by intramolecular .alpha.-hydrogen abstraction. *Journal of the American Chemical Society* **1974**, *96*, 6796-6797.
- (234) Grubbs, R. H. Olefin-Metathesis Catalysts for the Preparation of Molecules and Materials (Nobel Lecture). *Angewandte Chemie International Edition* **2006**, *45*, 3760-3765.
- (235) Chauvin, Y. Olefin Metathesis: The Early Days (Nobel Lecture). *Angewandte Chemie International Edition* **2006**, *45*, 3740-3747.
- (236) Dötz, K. H.; Stendel, J. Fischer Carbene Complexes in Organic Synthesis: Metal-Assisted and Metal-Templated Reactions. *Chemical Reviews* **2009**, *109*, 3227-3274.
- (237) Strassner, T.: Electronic Structure and Reactivity of Metal Carbenes. In *Metal Carbenes in Organic Synthesis: -/-*; Springer Berlin Heidelberg: Berlin, Heidelberg, 2004; pp 1-20.
- (238) Fischer, E. O.; Heinz Dötz, K. Übergangsmetall-Carben-Komplexe, XIX. Zur Synthese von Cyclopropanderivaten mit Übergangsmetall-Carbonyl-Carben-Komplexen. *Chemische Berichte* **1970**, *103*, 1273-1278.
- (239) Hegedus, L. S.: 1 - Introduction and Fundamentals. In *Comprehensive Organometallic Chemistry II*; Abel, E. W., Stone, F. G. A., Wilkinson, G., Eds.; Elsevier: Oxford, 1995.
- (240) Hegedus, L. S.; De Weck, G.; D'Andrea, S. Evidence for the intermediacy of chromium-ketene complexes in the synthesis of .beta.-lactams by the photolytic reaction of chromium-carbene complexes with imines. Use in amino acid synthesis. *Journal of the American Chemical Society* **1988**, *110*, 2122-2126.
- (241) Schreiber, S. L.; Klimas, M. T.; Sammakia, T. Dynamic behavior of dicobalt hexacarbonyl propargyl cations and their reactions with chiral nucleophiles. *Journal of the American Chemical Society* **1987**, *109*, 5749-5759.
- (242) Barluenga, J.; Fernández-Rodríguez, M. A.; Aguilar, E. Group 6 Fischer carbene complexes: "chemical multit talents" for multi-component reactions. *Journal of Organometallic Chemistry* **2005**, *690*, 539-587.

- (243) Dötz, K. H. Synthesis of the Naphthol Skeleton from Pentacarbonyl-[methoxy(phenyl)carbene]chromium (O) and Tolan. *Angewandte Chemie International Edition in English* **1975**, *14*, 644-645.
- (244) Dötz, K. H.; Pruskil, I.; Mühlemeier, J. Vitamin-Synthesen mit Carben-Komplexen, II. Carbonyl(carben)-Komplex-induzierte Synthese von Vitaminen der K1- und K2-Reihe. *Chemische Berichte* **1982**, *115*, 1278-1285.
- (245) Tebbe, F. N.; Parshall, G. W.; Reddy, G. S. Olefin homologation with titanium methylene compounds. *Journal of the American Chemical Society* **1978**, *100*, 3611-3613.
- (246) Astruc, D. The metathesis reactions: from a historical perspective to recent developments. *New Journal of Chemistry* **2005**, *29*, 42-56.
- (247) de Frémont, P.; Marion, N.; Nolan, S. P. Carbenes: Synthesis, properties, and organometallic chemistry. *Coordination Chemistry Reviews* **2009**, *253*, 862-892.
- (248) Tonner, R.; Heydenrych, G.; Frenking, G. Bonding Analysis of N-Heterocyclic Carbene Tautomers and Phosphine Ligands in Transition-Metal Complexes: A Theoretical Study. *Chemistry – An Asian Journal* **2007**, *2*, 1555-1567.
- (249) Herrmann, W. A.; Köcher, C. N-Heterocyclic Carbenes. *Angewandte Chemie International Edition in English* **1997**, *36*, 2162-2187.
- (250) Schaper, L.-A.; Hock, S. J.; Herrmann, W. A.; Kühn, F. E. Synthesis and Application of Water-Soluble NHC Transition-Metal Complexes. *Angewandte Chemie International Edition* **2013**, *52*, 270-289.
- (251) *N-Heterocyclic Carbenes in Transition Metal Catalysis and Organocatalysis*; Cazin, C. S. J., Ed.; Springer: Dordrecht Heidelberg London New York, 2011; Vol. 32.
- (252) Díez-González, S.; Nolan, S. P. [(NHC)<sub>2</sub>Cu]X Complexes as Efficient Catalysts for Azide–Alkyne Click Chemistry at Low Catalyst Loadings. *Angewandte Chemie International Edition* **2008**, *47*, 8881-8884.
- (253) Díez-González, S.; Stevens, E. D.; Scott, N. M.; Petersen, J. L.; Nolan, S. P. Synthesis and Characterization of [Cu(NHC)<sub>2</sub>]X Complexes: Catalytic and Mechanistic Studies of Hydrosilylation Reactions. *Chemistry – A European Journal* **2008**, *14*, 158-168.
- (254) Lazreg, F.; Slawin, A. M. Z.; Cazin, C. S. J. Heteroleptic Bis(N-heterocyclic carbene)Copper(I) Complexes: Highly Efficient Systems for the [3+2] Cycloaddition of Azides and Alkynes. *Organometallics* **2012**, *31*, 7969-7975.
- (255) Lazreg, F.; Nagra, F.; Cazin, C. S. J. Copper–NHC complexes in catalysis. *Coordination Chemistry Reviews* **2015**, *293–294*, 48-79.
- (256) Marion, N.; Díez-González, S.; Nolan, S. P. N-Heterocyclic Carbenes as Organocatalysts. *Angewandte Chemie International Edition* **2007**, *46*, 2988-3000.
- (257) Danopoulos, A. A.; Simler, T.; Braunstein, P. N-Heterocyclic Carbene Complexes of Copper, Nickel, and Cobalt. *Chemical Reviews* **2019**, *119*, 3730-3961.
- (258) Díez-González, S.; Nolan, S. P. Copper, Silver, and Gold Complexes in Hydrosilylation Reactions. *Accounts of Chemical Research* **2008**, *41*, 349-358.
- (259) Zhang, G.; Huang, X.; Li, G.; Zhang, L. Au-Containing All-Carbon 1,4-Dipoles: Generation and [4 + 2] Annulation in the Formation of Carbo-/Heterocycles. *Journal of the American Chemical Society* **2008**, *130*, 1814-1815.
- (260) Arduengo, A. J.; Dias, H. V. R.; Calabrese, J. C.; Davidson, F. Homoleptic carbene-silver(I) and carbene-copper(I) complexes. *Organometallics* **1993**, *12*, 3405-3409.
- (261) Synthetic Aspects. In *The Organometallic Chemistry of N-heterocyclic Carbenes*; pp 52-98.
- (262) Baker, M. V.; Brayshaw, S. K.; Skelton, B. W.; White, A. H.; Williams, C. C. Synthesis and structure of N-heterocyclic carbene complexes of rhodium and iridium derived from an imidazolium-linked cyclophane. *Journal of Organometallic Chemistry* **2005**, *690*, 2312-2322.
- (263) Herrmann, W. A.; Goossen, L. J.; Spiegler, M. Chiral Oxazoline/Imidazoline-2-ylidene Complexes. *Organometallics* **1998**, *17*, 2162-2168.
- (264) Danopoulos, A. A.; Winston, S.; Motherwell, W. B. Stable N-functionalised 'pincer' bis carbene ligands and their ruthenium complexes; synthesis and catalytic studies. *Chemical Communications* **2002**, 1376-1377.

- (265) Coleman, K. S.; Turberville, S.; Pascu, S. I.; Green, M. L. H. Synthesis of a new bidentate ferrocenyl N-heterocyclic carbene ligand precursor and the palladium (II) complex  $\text{trans-[PdCl}_2(\text{C}\lambda\text{f}\text{c}\lambda\text{C})]$ , where  $(\text{C}\lambda\text{f}\text{c}\lambda\text{C})=1,1'$ -di-tert-butyl-3,3'-(1,1'-dimethyleneferrocenyl)-diimidazol-2-ylidene. *Journal of Organometallic Chemistry* **2005**, *690*, 653-658.
- (266) Chun, J.; Lee, H. S.; Jung, I. G.; Lee, S. W.; Kim, H. J.; Son, S. U.  $\text{Cu}_2\text{O}$ : A Versatile Reagent for Base-Free Direct Synthesis of NHC-Copper Complexes and Decoration of 3D-MOF with Coordinatively Unsaturated NHC-Copper Species. *Organometallics* **2010**, *29*, 1518-1521.
- (267) Citadelle, C. A.; Nouy, E. L.; Bisaro, F.; Slawin, A. M. Z.; Cazin, C. S. J. Simple and versatile synthesis of copper and silver N-heterocyclic carbene complexes in water or organic solvents. *Dalton Transactions* **2010**, *39*, 4489-4491.
- (268) Tulloch, A. A. D.; Danopoulos, A. A.; Kleinhenz, S.; Light, M. E.; Hursthouse, M. B.; Eastham, G. Structural Diversity in Pyridine-N-Functionalized Carbene Copper(I) Complexes. *Organometallics* **2001**, *20*, 2027-2031.
- (269) Wang, H. M. J.; Lin, I. J. B. Facile Synthesis of Silver(I)-Carbene Complexes. Useful Carbene Transfer Agents. *Organometallics* **1998**, *17*, 972-975.
- (270) Garrison, J. C.; Youngs, W. J. Ag(I) N-Heterocyclic Carbene Complexes: Synthesis, Structure, and Application. *Chemical Reviews* **2005**, *105*, 3978-4008.
- (271) Liu, B.; Zhang, Y.; Daichao, X.; Chen, W. Synthesis of Metal N-Heterocyclic Carbene Complexes. *Chemical communications (Cambridge, England)* **2011**, *47*, 2883-2885.
- (272) Liu, B.; Zhang, Y.; Xu, D.; Chen, W. Facile synthesis of metal N-heterocyclic carbene complexes. *Chemical Communications* **2011**, *47*, 2883-2885.
- (273) Zhai, J.; Filatov, A. S.; Hillhouse, G. L.; Hopkins, M. D. Synthesis, structure, and reactions of a copper-sulfido cluster comprised of the parent  $\text{Cu}_2\text{S}$  unit:  $\{(\text{NHC})\text{Cu}\}_2(\mu\text{-S})$ . *Chemical Science* **2016**, *7*, 589-595.
- (274) Raubenheimer, H. G.; Cronje, S.; Olivier, P. J. Synthesis and characterization of mono(carbene) complexes of copper and crystal structure of a linear thiazolinylidene compound. *Journal of the Chemical Society, Dalton Transactions* **1995**, 313-316.
- (275) Fraser, P. K.; Woodward, S. Strong ligand accelerated catalysis by an Arduengo-type carbene in copper-catalysed conjugate addition. *Tetrahedron Letters* **2001**, *42*, 2747-2749.
- (276) Jurkauskas, V.; Sadighi, J. P.; Buchwald, S. L. Conjugate Reduction of  $\alpha,\beta$ -Unsaturated Carbonyl Compounds Catalyzed by a Copper Carbene Complex. *Organic Letters* **2003**, *5*, 2417-2420.
- (277) Egbert, J. D.; Cazin, C. S. J.; Nolan, S. P. Copper N-heterocyclic carbene complexes in catalysis. *Catalysis Science & Technology* **2013**, *3*, 912-926.
- (278) Kaur, H.; Zinn, F. K.; Stevens, E. D.; Nolan, S. P. (NHC)CuI (NHC = N-Heterocyclic Carbene) Complexes as Efficient Catalysts for the Reduction of Carbonyl Compounds. *Organometallics* **2004**, *23*, 1157-1160.
- (279) Díez-González, S.; Kaur, H.; Zinn, F. K.; Stevens, E. D.; Nolan, S. P. A Simple and Efficient Copper-Catalyzed Procedure for the Hydrosilylation of Hindered and Functionalized Ketones. *The Journal of Organic Chemistry* **2005**, *70*, 4784-4796.
- (280) Arnold, P. L.; Rodden, M.; Davis, K. M.; Scarisbrick, A. C.; Blake, A. J.; Wilson, C. Asymmetric lithium(i) and copper(ii) alkoxy-N-heterocyclic carbene complexes; crystallographic characterisation and Lewis acid catalysis. *Chemical Communications* **2004**, 1612-1613.
- (281) Clavier, H.; Coutable, L.; Guillemin, J.-C.; Mauduit, M. New bidentate alkoxy-NHC ligands for enantioselective copper-catalysed conjugate addition. *Tetrahedron: Asymmetry* **2005**, *16*, 921-924.
- (282) Fructos, M. R.; Belderrain, T. R.; Nicasio, M. C.; Nolan, S. P.; Kaur, H.; Díaz-Requejo, M. M.; Pérez, P. J. Complete Control of the Chemoselectivity in Catalytic Carbene Transfer Reactions from Ethyl Diazoacetate: An N-Heterocyclic Carbene-Cu System That Suppresses Diazo Coupling. *Journal of the American Chemical Society* **2004**, *126*, 10846-10847.

- (283) Fructos, M. R.; de Frémont, P.; Nolan, S. P.; Díaz-Requejo, M. M.; Pérez, P. J. Alkane Carbon–Hydrogen Bond Functionalization with (NHC)MCl Precatalysts (M = Cu, Au; NHC = N-Heterocyclic Carbene). *Organometallics* **2006**, *25*, 2237-2241.
- (284) Meldal, M.; Tornøe, C. W. In *Tilte* 2001.
- (285) Meldal, M.; Tornøe, C. W. Cu-Catalyzed Azide–Alkyne Cycloaddition. *Chemical Reviews* **2008**, *108*, 2952-3015.
- (286) Tornøe, C. W.; Christensen, C.; Meldal, M. Peptidotriazoles on Solid Phase: [1,2,3]-Triazoles by Regiospecific Copper(I)-Catalyzed 1,3-Dipolar Cycloadditions of Terminal Alkynes to Azides. *J. Org. Chem.* **2002**, *67*, 3057-3064.
- (287) Kolb, H. C.; Finn, M. G.; Sharpless, K. B. Click Chemistry: Diverse Chemical Function from a Few Good Reactions. *Angew. Chem. Int. Ed.* **2001**, *40*, 2004-2021.
- (288) Rostovtsev, V. V.; Green, L. G.; Fokin, V. V.; Sharpless, K. B. A Stepwise Huisgen Cycloaddition Process: Copper(I)-Catalyzed Regioselective “Ligation” of Azides and Terminal Alkynes. *Angew. Chem. Int. Ed.* **2002**, *41*, 2596-2599.
- (289) Wu, P.; Feldman, A. K.; Nugent, A. K.; Hawker, C. J.; Scheel, A.; Voit, B.; Pyun, J.; Fréchet, J. M. J.; Sharpless, K. B.; Fokin, V. V. Efficiency and Fidelity in a Click-Chemistry Route to Triazole Dendrimers by the Copper(I)-Catalyzed Ligation of Azides and Alkynes. *Angew. Chem., Int. Ed.* **2004**, *43*, 3928-3932.
- (290) Neumann, S.; Biewend, M.; Rana, S.; Binder, W. H. The CuAAC: Principles, Homogeneous and Heterogeneous Catalysts, and Novel Developments and Applications. *Macromolecular Rapid Communications* **2020**, *41*, 1900359.
- (291) Huisgen, R.; Szeimies, G.; Möbius, L. 1.3-Dipolare Cycloadditionen, XXXII. Kinetik der Additionen organischer Azide an CC-Mehrfachbindungen. *Chemische Berichte* **1967**, *100*, 2494-2507.
- (292) Lazreg, F.; Cordes, D. B.; Slawin, A. M. Z.; Cazin, C. S. J. Synthesis of Homoleptic and Heteroleptic Bis-N-heterocyclic Carbene Group 11 Complexes. *Organometallics* **2015**, *34*, 419-425.
- (293) Díez-González, S.; Correa, A.; Cavallo, L.; Nolan, S. P. (NHC)Copper(I)-Catalyzed [3+2] Cycloaddition of Azides and Mono- or Disubstituted Alkynes. *Chemistry – A European Journal* **2006**, *12*, 7558-7564.
- (294) Díez-González, S.; Stevens, E. D.; Nolan, S. P. A [(NHC)CuCl] complex as a latent Click catalyst. *Chemical Communications* **2008**, *0*, 4747-4749.
- (295) Díez-González, S.; Escudero-Adán, E. C.; Benet-Buchholz, J.; Stevens, E. D.; Slawin, A. M. Z.; Nolan, S. P. [(NHC)CuX] complexes: Synthesis, characterization and catalytic activities in reduction reactions and Click Chemistry. On the advantage of using well-defined catalytic systems. *Dalton Transactions* **2010**, *39*, 7595-7606.
- (296) Li, P.; Wang, L.; Zhang, Y. SiO<sub>2</sub>–NHC–Cu(I): an efficient and reusable catalyst for [3+2] cycloaddition of organic azides and terminal alkynes under solvent-free reaction conditions at room temperature. *Tetrahedron* **2008**, *64*, 10825-10830.
- (297) Teyssot, M.-L.; Nauton, L.; Canet, J.-L.; Cisnetti, F.; Chevry, A.; Gautier, A. Aromatic Nitrogen Donors for Efficient Copper(I)–NHC CuAAC under Reductant-Free Conditions. *European Journal of Organic Chemistry* **2010**, *2010*, 3507-03515.
- (298) Binder, W. H.; Sachsenhofer, R. ‘Click’ Chemistry in Polymer and Material Science: An Update. *Macromolecular Rapid Communications* **2008**, *29*, 952-981.
- (299) Döhler, D.; Michael, P.; Binder, W. H. CuAAC-Based Click Chemistry in Self-Healing Polymers. *Accounts of Chemical Research* **2017**, *50*, 2610–2620.
- (300) Meldal, M. Polymer “Clicking” by CuAAC Reactions. *Macromol. Rapid Commun.* **2008**, *29*, 1016-1051.
- (301) Catalytic Click Reactions. In *Applied Homogeneous Catalysis with Organometallic Compounds*; pp 1541-1556.
- (302) Alkyne-Azide Reactions. In *Modern Alkyne Chemistry*; pp 113-142.
- (303) Himo, F.; Lovell, T.; Hilgraf, R.; Rostovtsev, V. V.; Noodleman, L.; Sharpless, K. B.; Fokin, V. V. Copper(I)-Catalyzed Synthesis of Azoles. DFT Study Predicts Unprecedented Reactivity and Intermediates. *Journal of the American Chemical Society* **2005**, *127*, 210-216.

- (304) Worrell, B. T.; Malik, J. A.; Fokin, V. V. Direct Evidence of a Dinuclear Copper Intermediate in Cu(I)-Catalyzed Azide-Alkyne Cycloadditions. *Science* **2013**, *340*, 457-460.
- (305) Bock, V. D.; Perciaccante, R.; Jansen, T. P.; Hiemstra, H.; van Maarseveen, J. H. Click Chemistry as a Route to Cyclic Tetrapeptide Analogues: Synthesis of cyclo-[Pro-Val- $\psi$ (triazole)-Pro-Tyr]. *Organic Letters* **2006**, *8*, 919-922.
- (306) Michael, P.; Binder, W. H. A Mechanochemically Triggered "Click" Catalyst. *Angewandte Chemie* **2015**, *127*, 14124-14128.
- (307) Michael, P.; Sheidaee Mehr, S. K.; Binder, W. H. Synthesis and characterization of polymer linked copper(I) bis(N-heterocyclic carbene) mechanocatalysts. *Journal of Polymer Science Part A: Polymer Chemistry* **2017**, *55*, 3893-3907.
- (308) Döhler, D.; Kaiser, J.; Binder, W. H. Supramolecular H-bonded three-arm star polymers by efficient combination of RAFT polymerization and thio-bromo "click" reaction. *Polymer* **2017**, *122*, 148-158.
- (309) Le Droumaguet, C.; Wang, C.; Wang, Q. Fluorogenic click reaction. *Chemical Society Reviews* **2010**, *39*, 1233-1239.
- (310) Xie, F.; Sivakumar, K.; Zeng, Q.; Bruckman, M. A.; Hodges, B.; Wang, Q. A fluorogenic 'click' reaction of azidoanthracene derivatives. *Tetrahedron* **2008**, *64*, 2906-2914.
- (311) Yoshida, S.; Suga, H.; Seki, S. Thermodynamic Studies of Solid Polyethers. III. Poly(tetrahydrofuran),  $-\text{[(CH}_2\text{)}_4\text{O]}-n$ . *Polymer Journal* **1973**, *5*, 25-32.
- (312) Brandrup, J.; Immergut, E. H.; Grulke, E. A.: *Polymer Handbook*; Wiley, 2004.

## 7. Appendix

## 7.1. Synthesis of cyclic and acyclic complexes

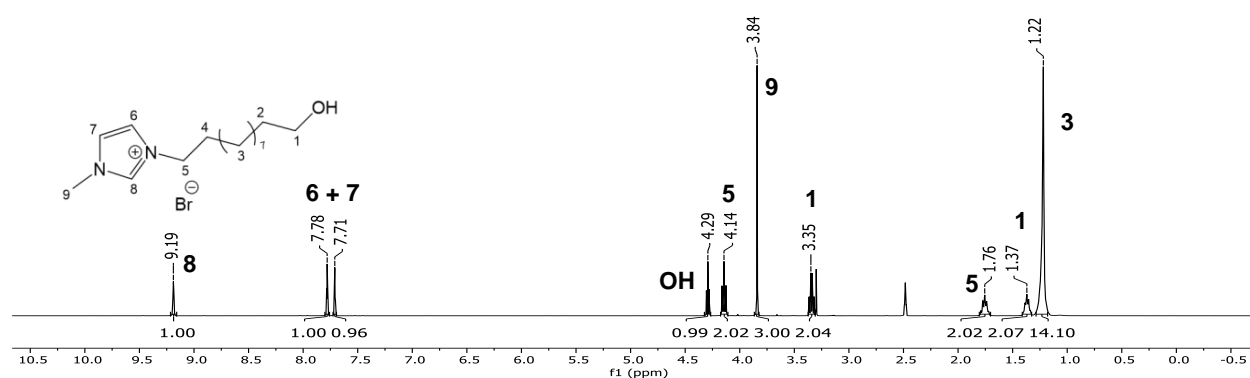
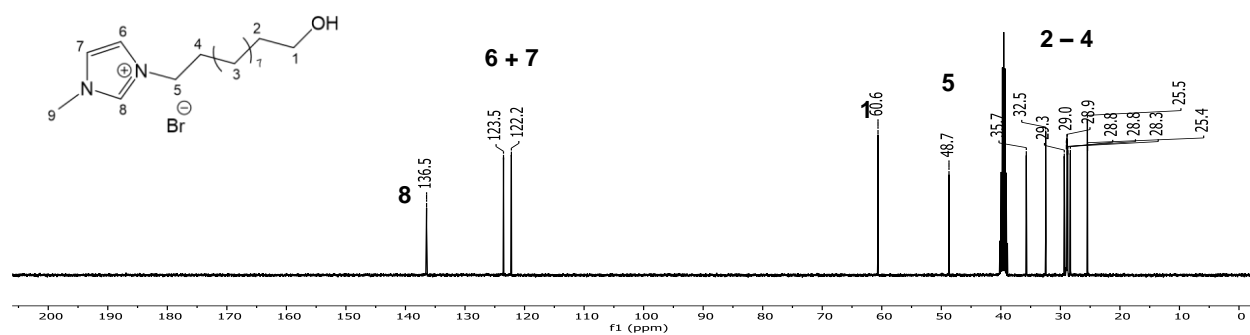
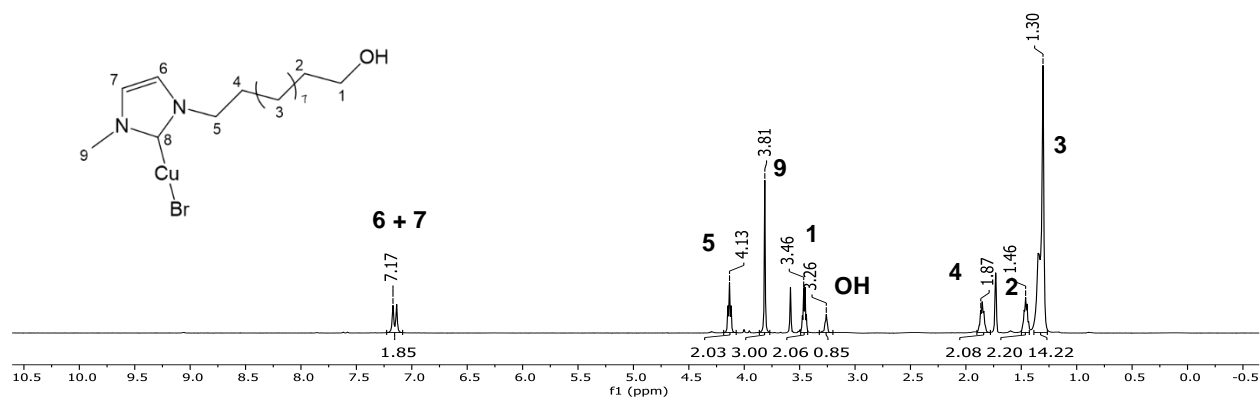
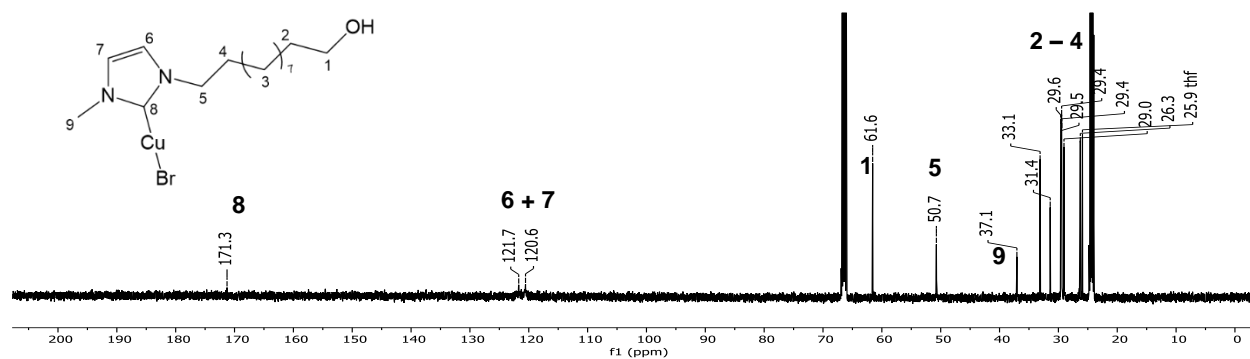
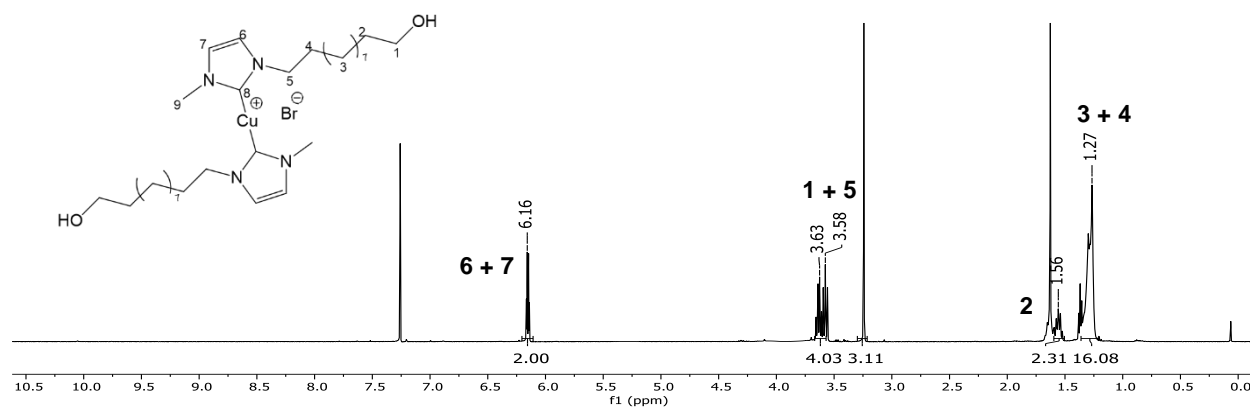
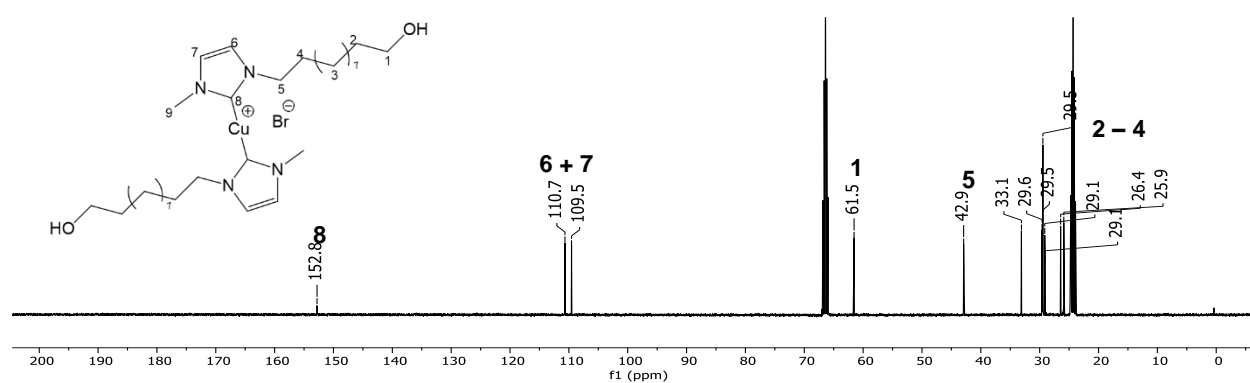
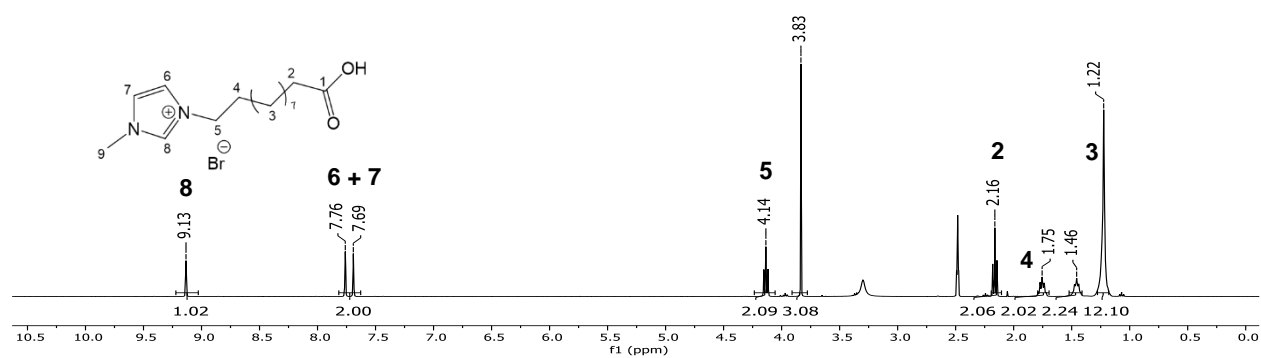
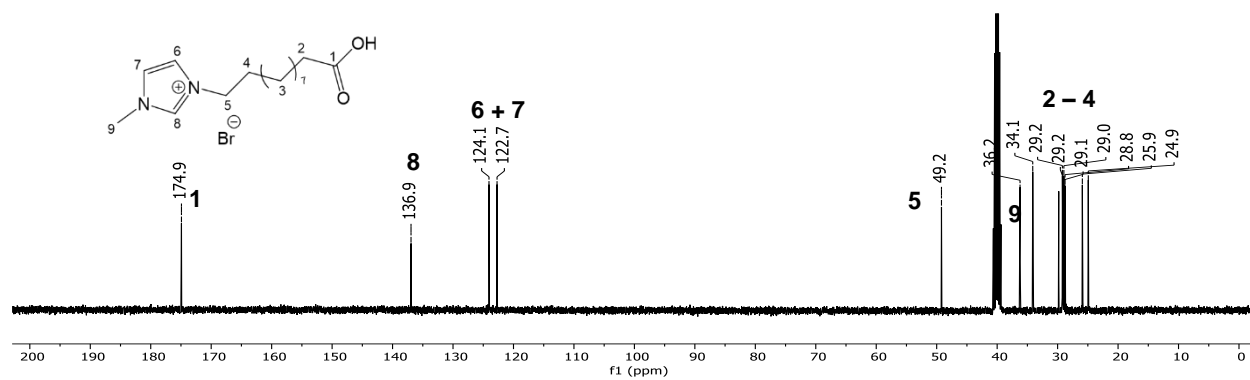
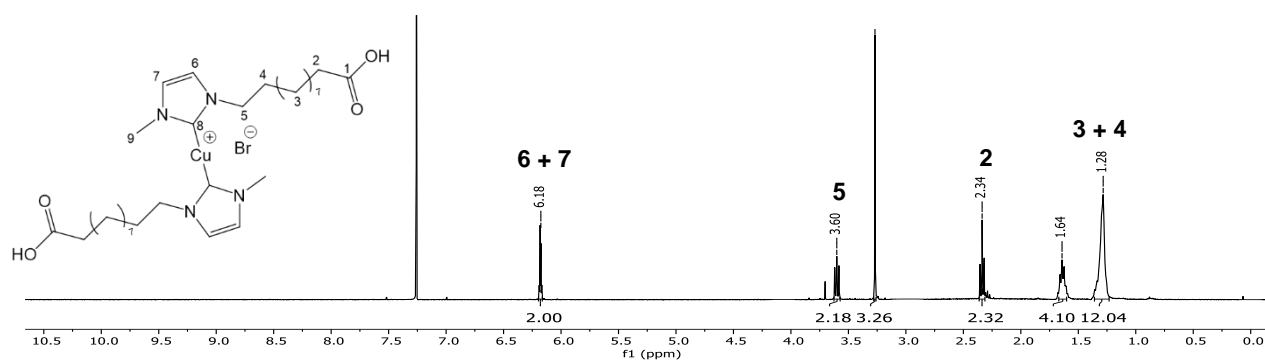
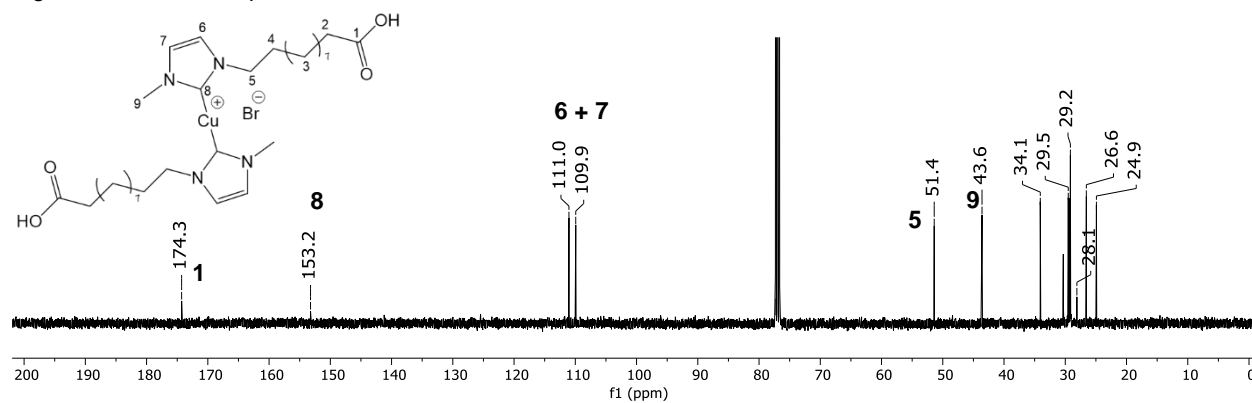
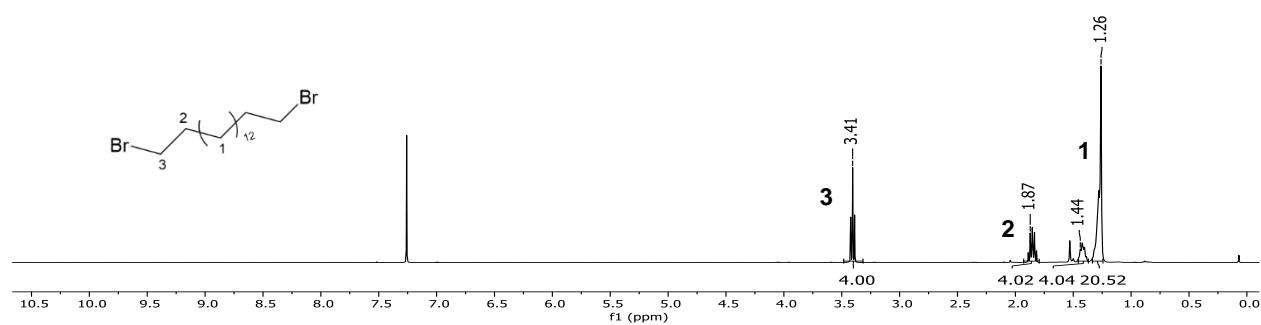
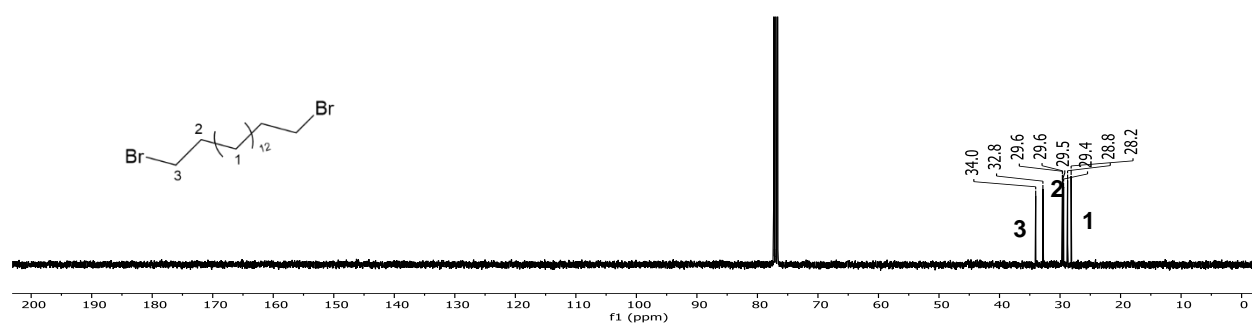
Figure A 1.  $^1\text{H-NMR}$  spectrum of **1** in  $\text{DMSO-d}_6$ .Figure A 2.  $^{13}\text{C-NMR}$  spectrum of **1** in  $\text{DMSO-d}_6$ .Figure A 3.  $^1\text{H-NMR}$  spectrum of **2** in  $\text{THF-d}_8$ .

Figure A 4.  $^{13}\text{C}$ -NMR spectrum of **2** in  $\text{THF-d}_8$ .Figure A 5.  $^1\text{H}$ -NMR spectrum of **3** in  $\text{CDCl}_3$ .Figure A 6.  $^{13}\text{C}$ -NMR spectrum of **3** in  $\text{THF-d}_8$ .Figure A 7.  $^1\text{H}$ -NMR spectrum of **4** in  $\text{DMSO-d}_6$ .Figure A 8.  $^{13}\text{C}$ -NMR spectrum of **4** in  $\text{DMSO-d}_6$ .

Figure A 9.  $^1\text{H-NMR}$  spectrum of **5** in  $\text{CDCl}_3$ .Figure A 10.  $^{13}\text{C-NMR}$  spectrum of **5** in  $\text{CDCl}_3$ .Figure A 11.  $^1\text{H-NMR}$  spectrum of **6a** in  $\text{CDCl}_3$ .Figure A 12.  $^{13}\text{C-NMR}$  spectrum of **6a** in  $\text{CDCl}_3$ .

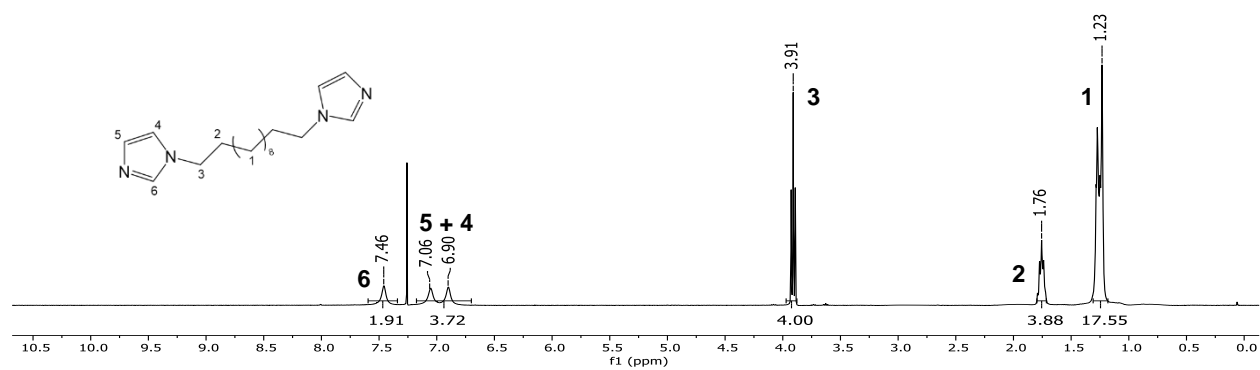


Figure A 13.  $^1\text{H-NMR}$  spectrum of **7a** in  $\text{CDCl}_3$ .

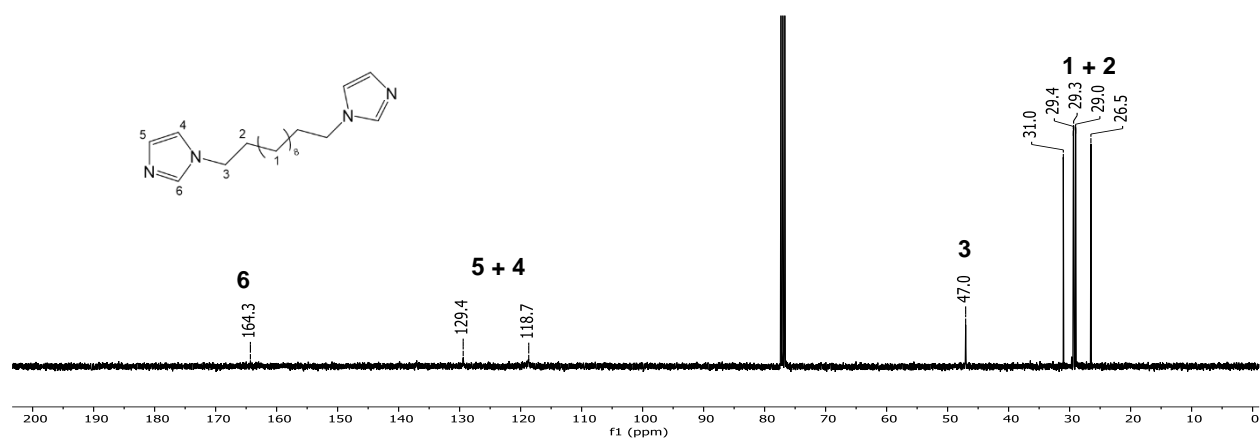


Figure A 14.  $^{13}\text{C-NMR}$  spectrum of **7a** in  $\text{CDCl}_3$ .

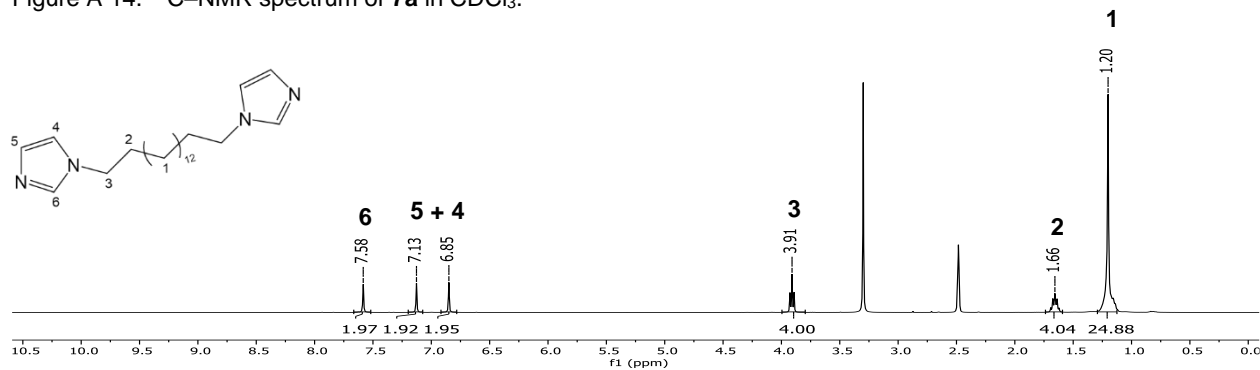


Figure A 15.  $^1\text{H-NMR}$  spectrum of **7b** in  $\text{DMSO-}d_6$ .

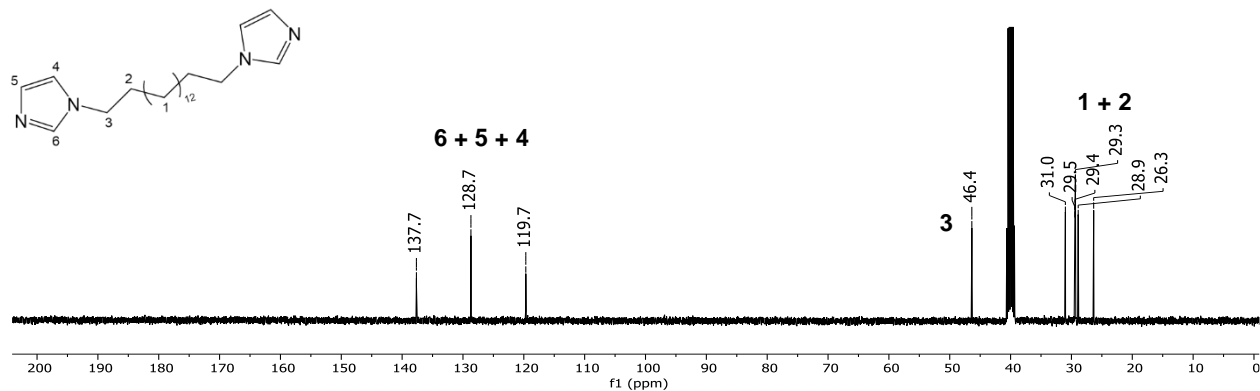
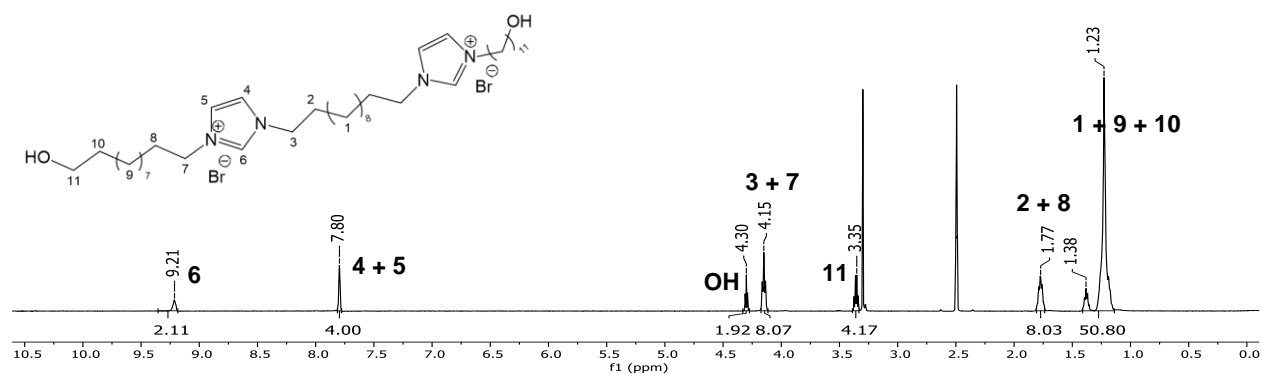
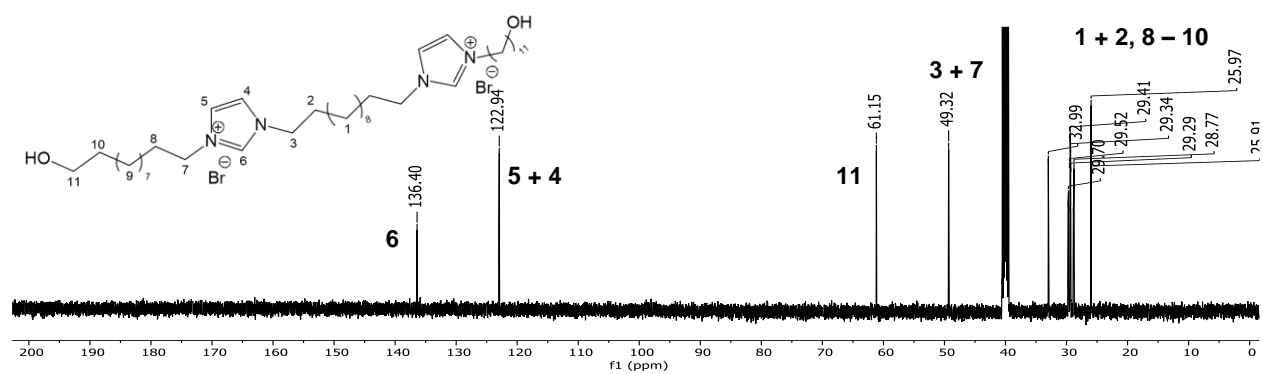
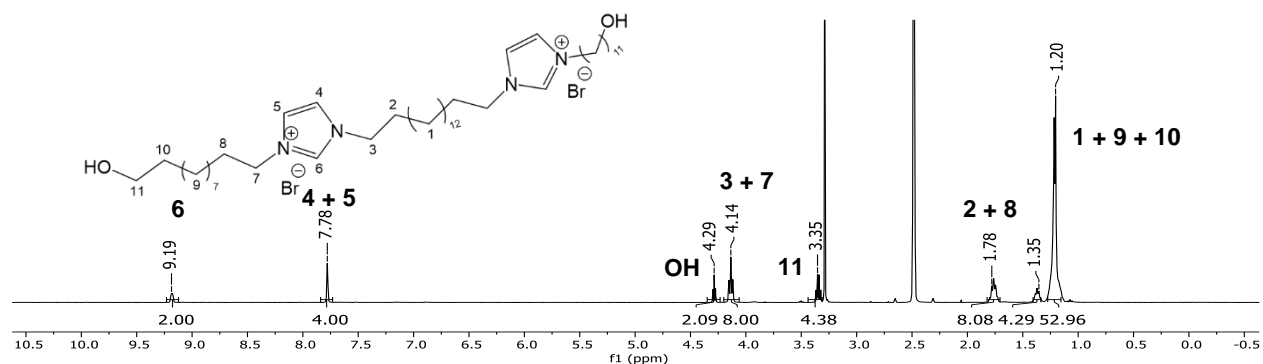
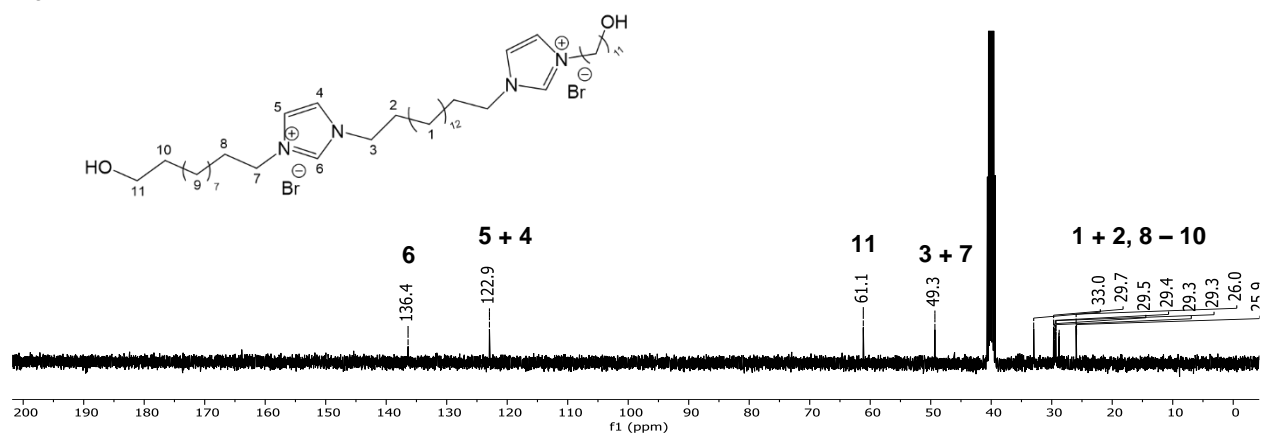
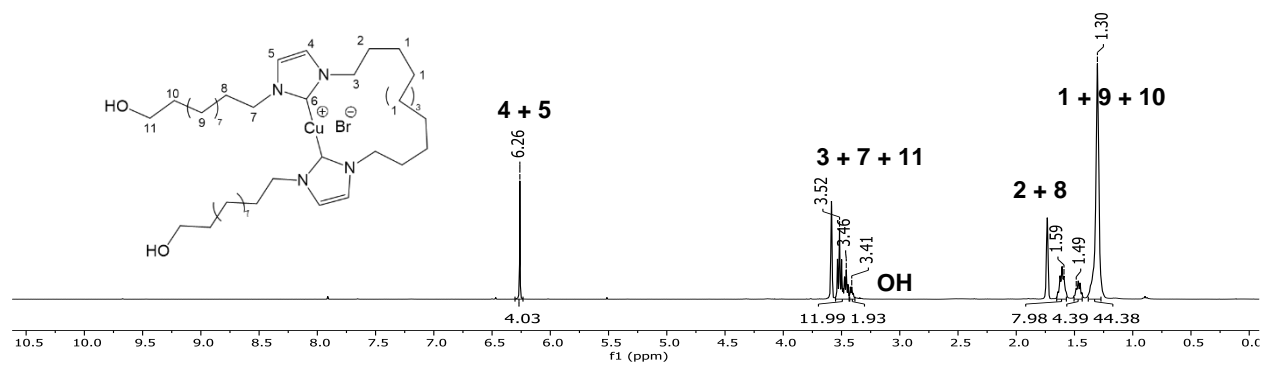
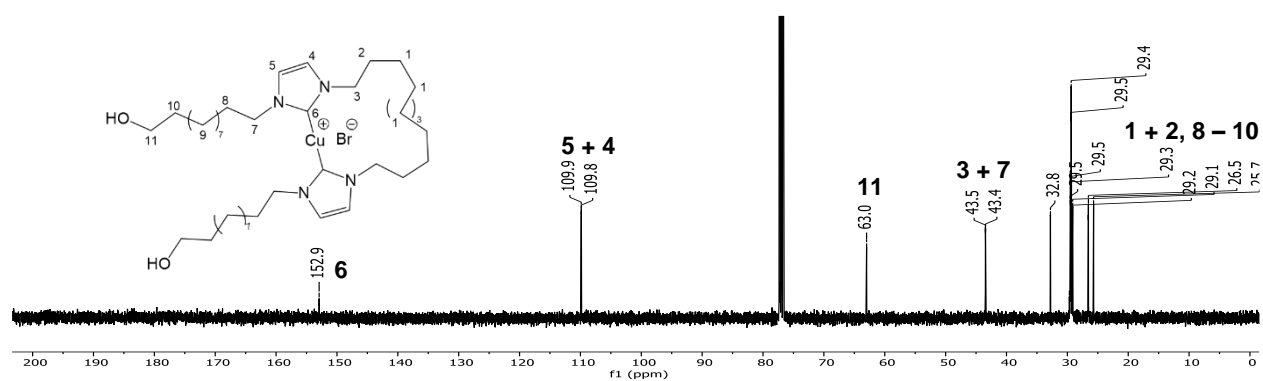
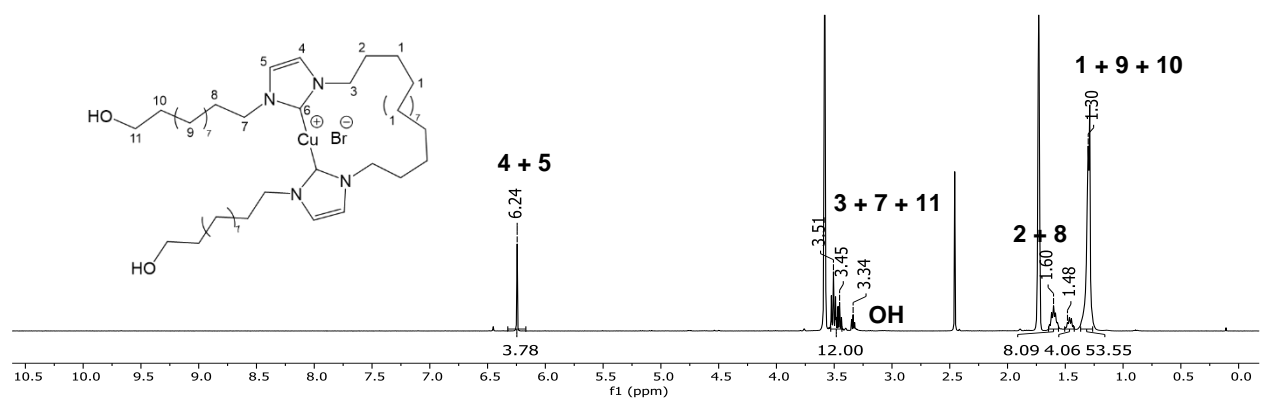
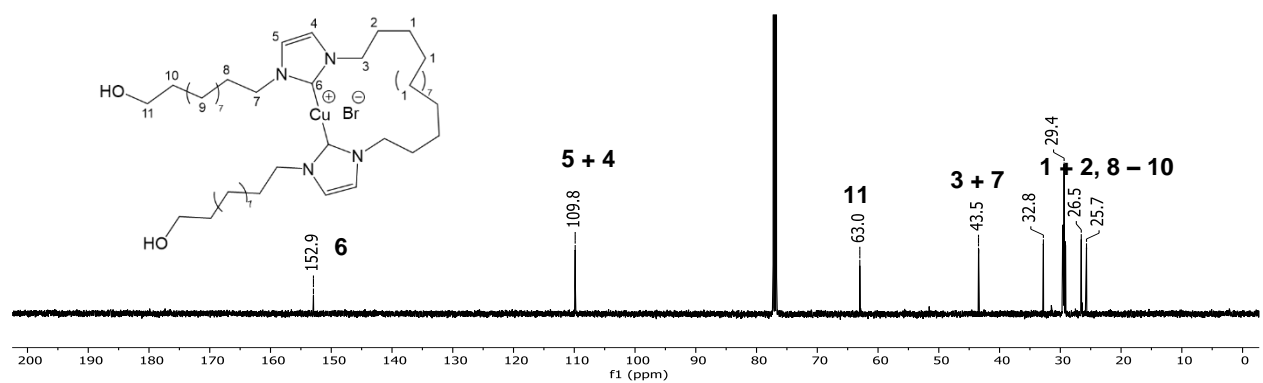
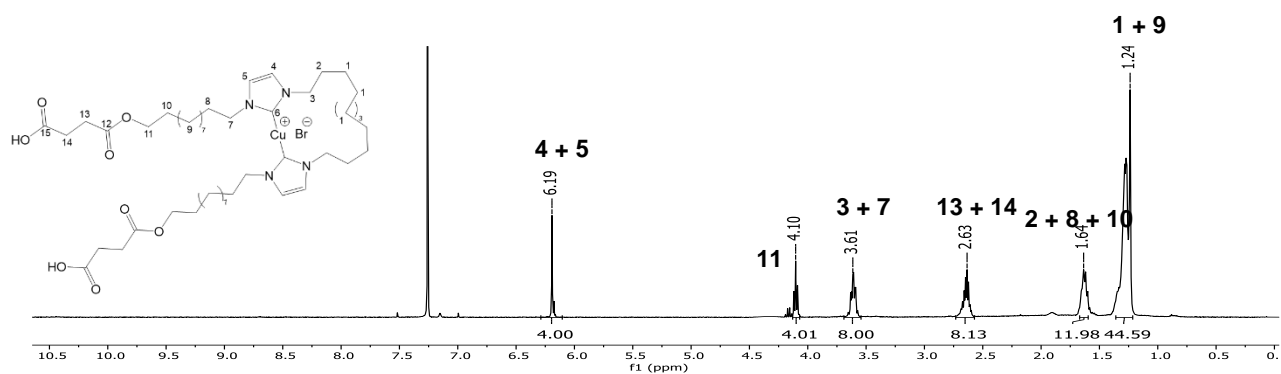
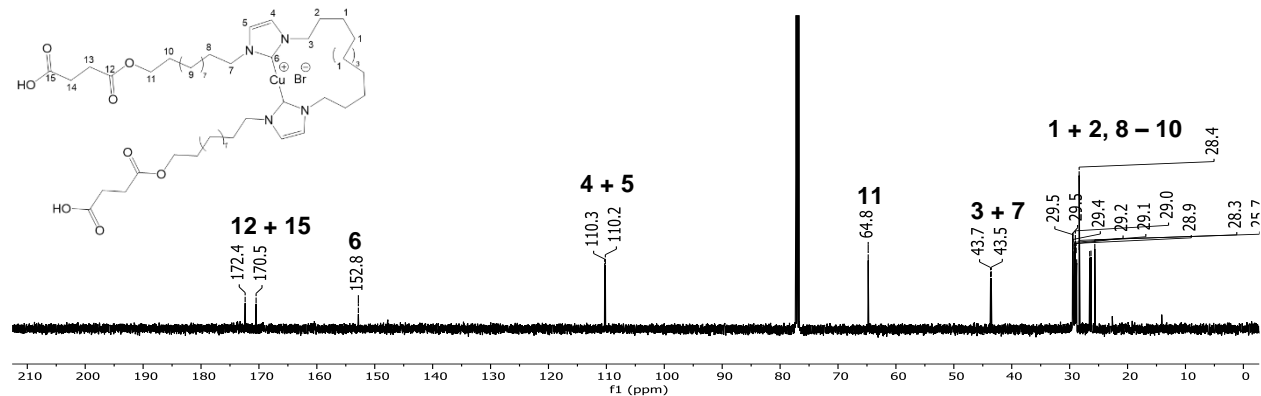
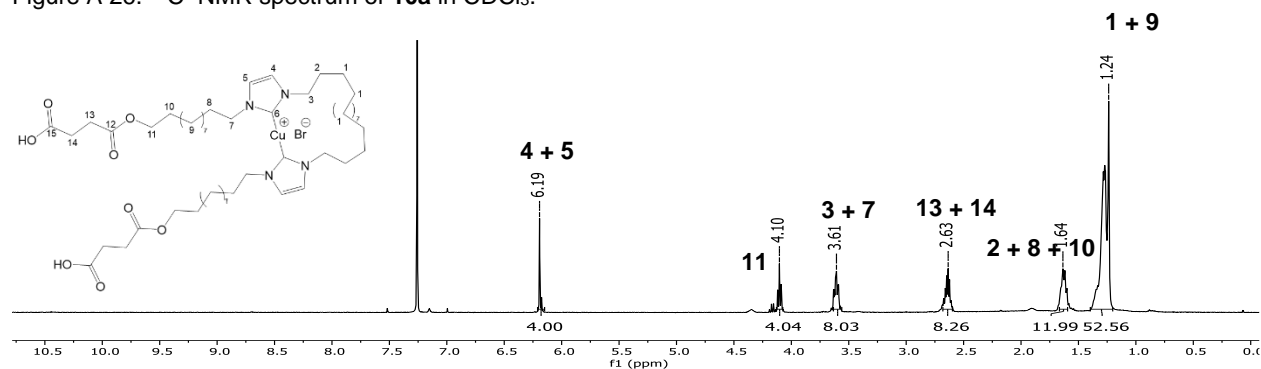
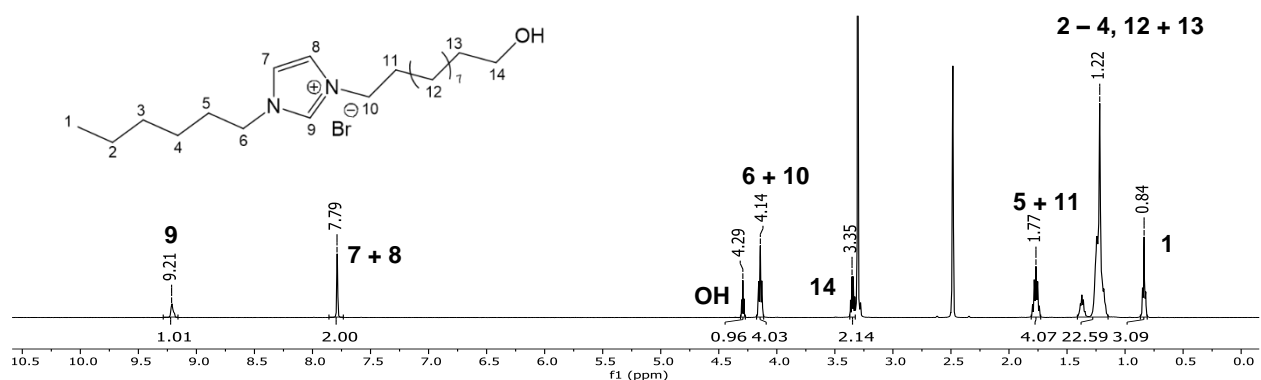
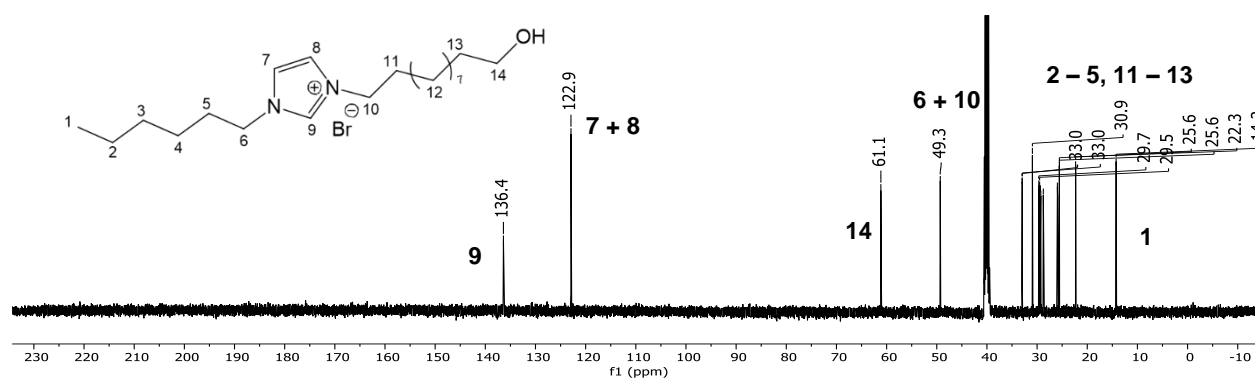
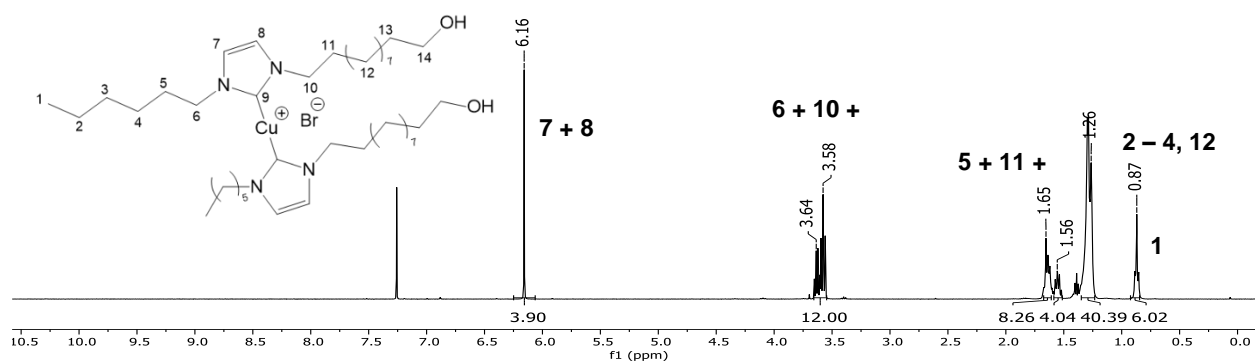
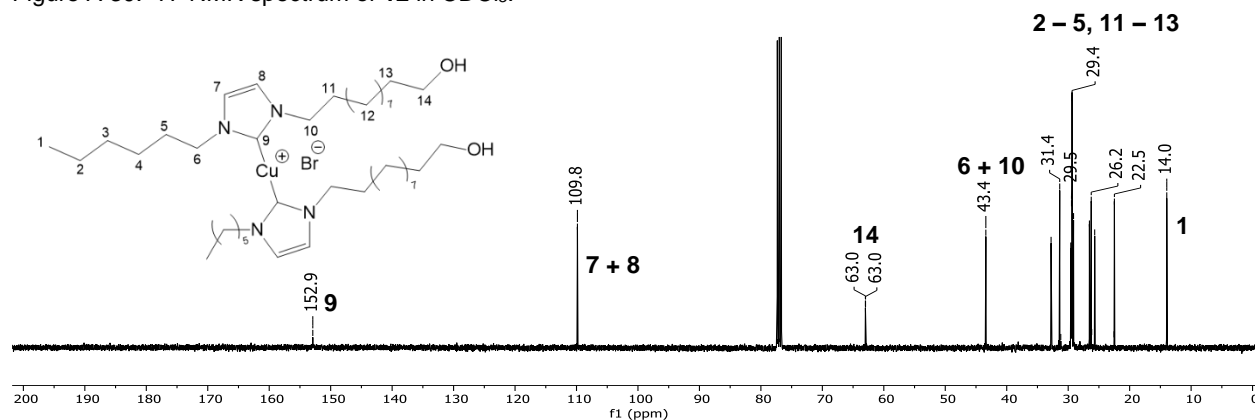
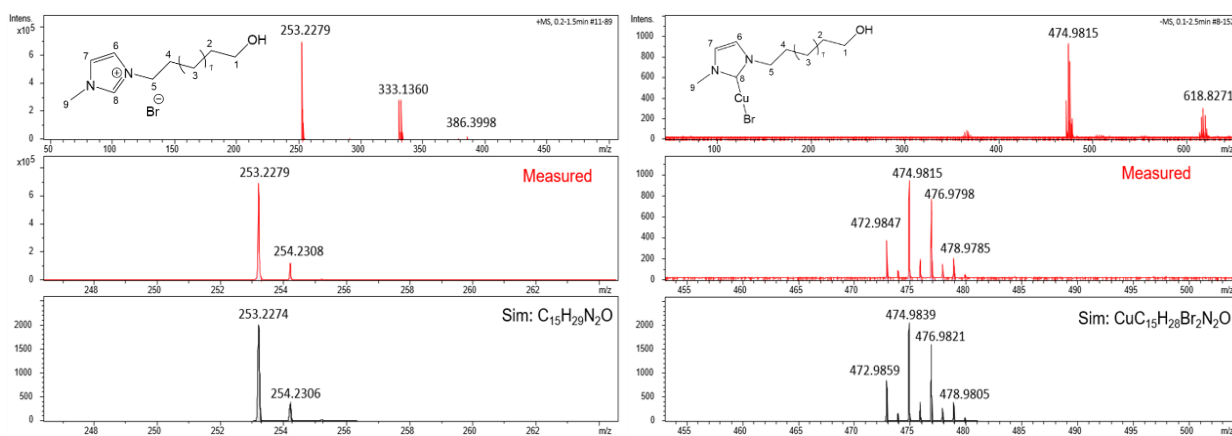


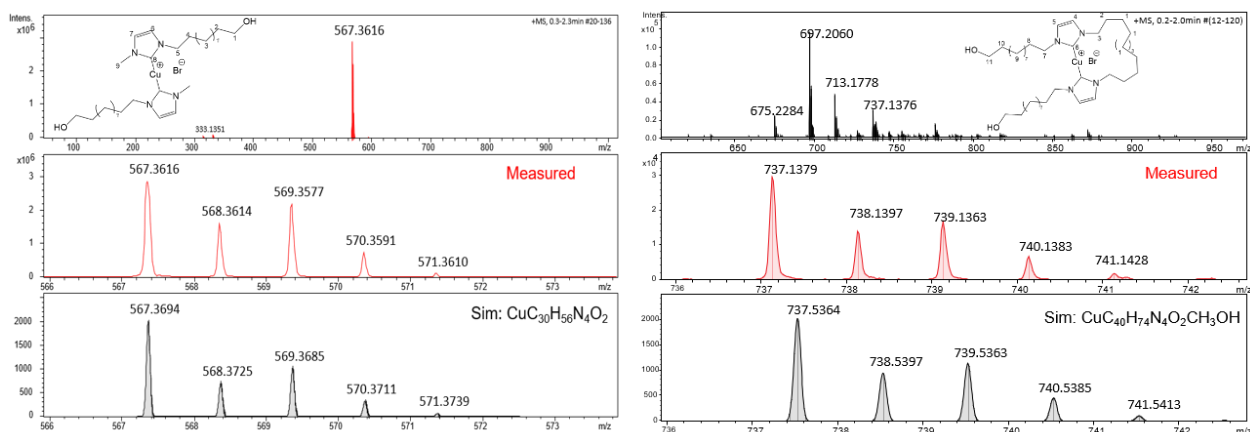
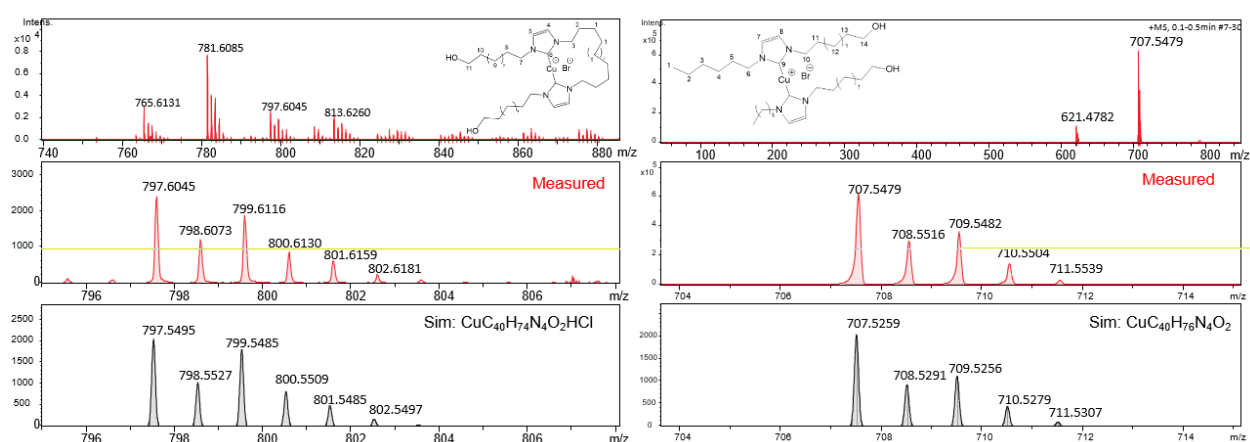
Figure A 16.  $^{13}\text{C-NMR}$  spectrum of **7b** in  $\text{DMSO-}d_6$ .

Figure A 17.  $^1\text{H}$ -NMR spectrum of **8a** in  $\text{DMSO}-d_6$ .Figure A 18.  $^{13}\text{C}$ -NMR spectrum of **8a** in  $\text{DMSO}-d_6$ .Figure A 19.  $^1\text{H}$ -NMR spectrum of **8b** in  $\text{DMSO}-d_6$ .Figure A 20.  $^{13}\text{C}$ -NMR spectrum of **8b** in  $\text{DMSO}-d_6$ .

Figure A 21.  $^1\text{H}$ -NMR spectrum of **9a** in  $\text{THF-}d_8$ .Figure A 22.  $^{13}\text{C}$ -NMR spectrum of **9a** in  $\text{THF-}d_8$ .Figure A 23.  $^1\text{H}$ -NMR spectrum of **9b** in  $\text{THF-}d_8$ .Figure A 24.  $^{13}\text{C}$ -NMR spectrum of **9b** in  $\text{THF-}d_8$ .

Figure A 25.  $^1\text{H-NMR}$  spectrum of **10a** in  $\text{CDCl}_3$ .Figure A 26.  $^{13}\text{C-NMR}$  spectrum of **10a** in  $\text{CDCl}_3$ .Figure A 27.  $^1\text{H-NMR}$  spectrum of **10b** in  $\text{CDCl}_3$ .Figure A 28.  $^1\text{H-NMR}$  spectrum of **11** in  $\text{DMSO-}d_6$ .

Figure A 29. <sup>13</sup>C-NMR spectrum of **11** in DMSO-*d*<sub>6</sub>.Figure A 30. <sup>1</sup>H-NMR spectrum of **12** in CDCl<sub>3</sub>.Figure A 31. <sup>13</sup>C-NMR spectrum of **12** in CDCl<sub>3</sub>.Figure A 32. ESI-TOF-MS spectrum of **1** (left) and **2** (right).

Figure A 33. ESI-TOF-MS spectrum of **3** (left) and **9a** (right).Figure A 34. ESI-TOF-MS spectrum of **9b** (left) and **11** (right).

## 7.2. Atomic force microscopy

Table A 1. Summary of single molecule spectroscopy measurements (AFM).

Ent.	Comp.	Length Safety line	d nm	F pN	Slope S <sup>1a)</sup>	Slope S <sup>2b)</sup>	Amount (S <sup>2</sup> /S <sup>1</sup> )
<b>Without safety line</b>							
<b>1</b>		no	2.14	2658	117.9	116.3	
<b>Safety line</b>							
<b>2</b>		12	1.41	1579	119.6	122.7	102.6
<b>3</b>			1.57	1611	127.0	126.3	99.4
<b>4</b>			1.22	1723	122.6	124.2	101.3
<b>5</b>			1.28	2141	154.4	158.4	102.6
<b>6</b>			1.41	2293	141.8	142.8	100.7
<b>7</b>			2.09	1584	137.4	140.6	102.3
<b>8</b>			2.39	1691	161.8	166.2	102.7

## 7.3. Synthesis of chain extended mechanophores

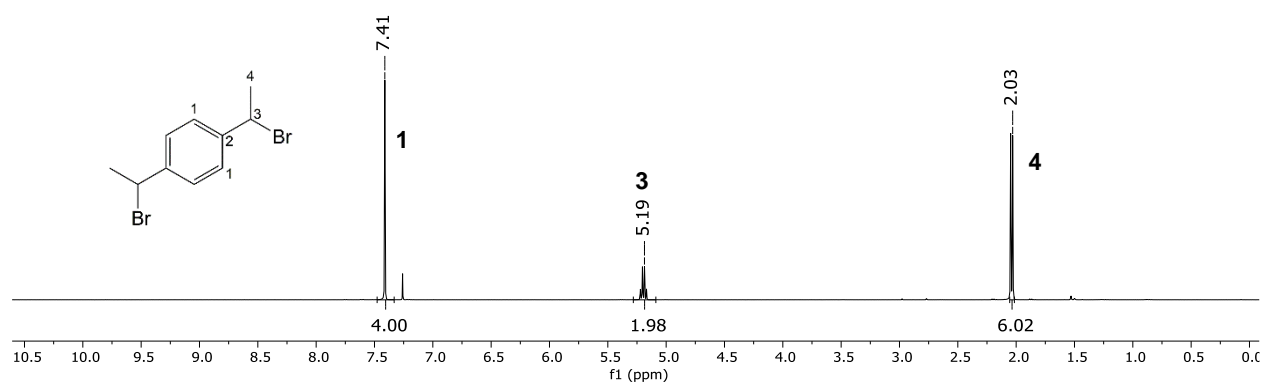


Figure A 35.  $^1\text{H-NMR}$  spectrum of **13** in  $\text{CDCl}_3$ .

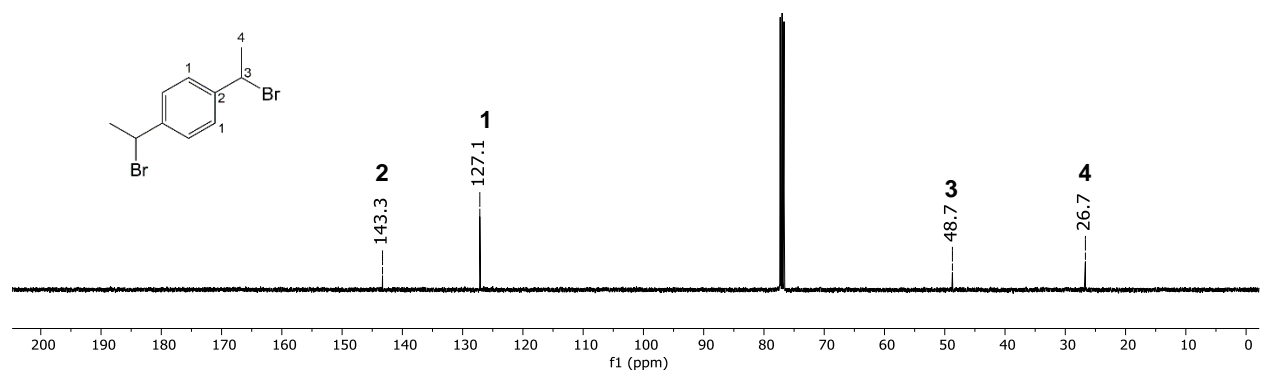


Figure A 36.  $^{13}\text{C-NMR}$  spectrum of **13** in  $\text{CDCl}_3$ .

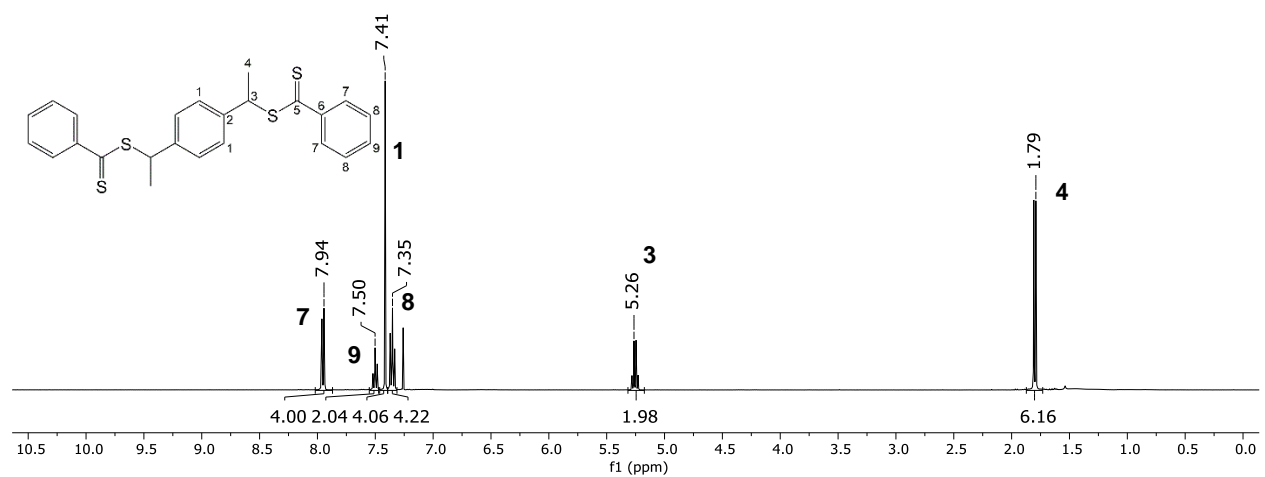
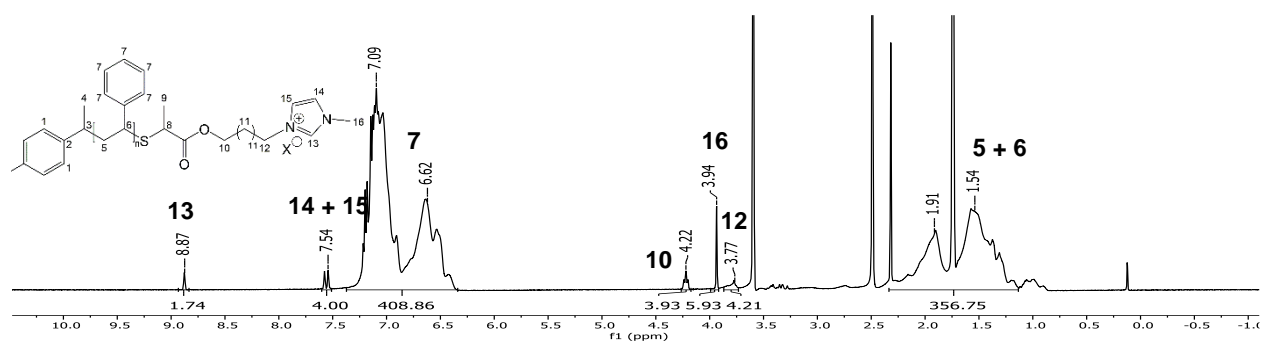
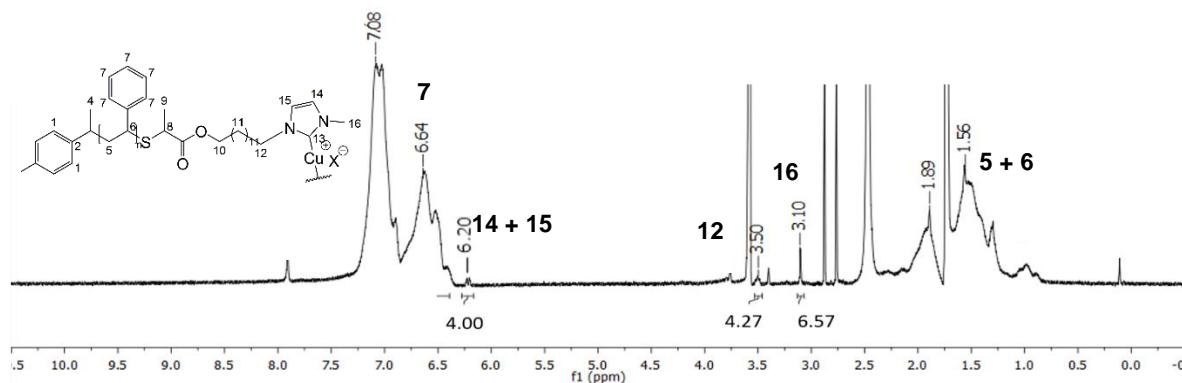
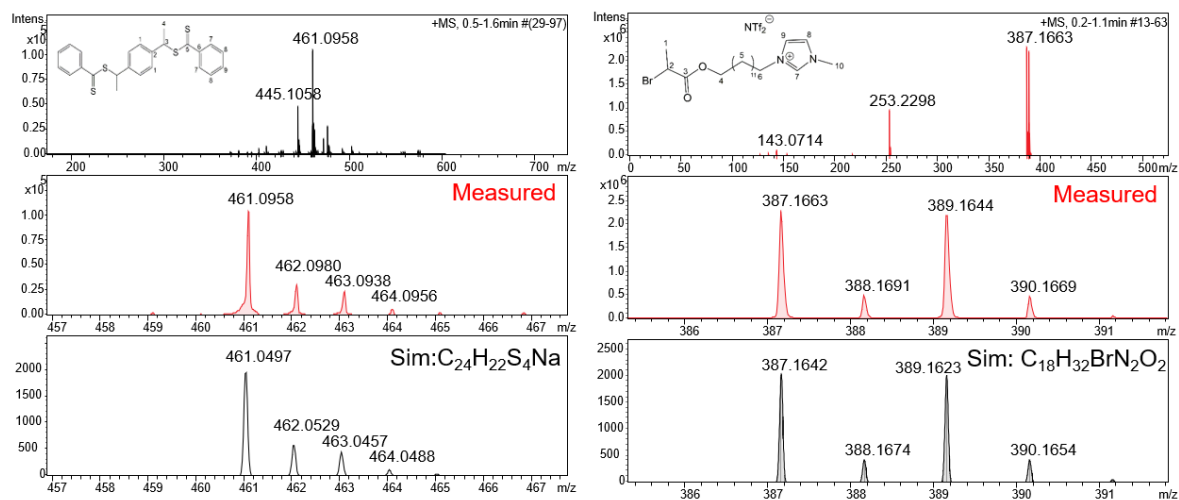
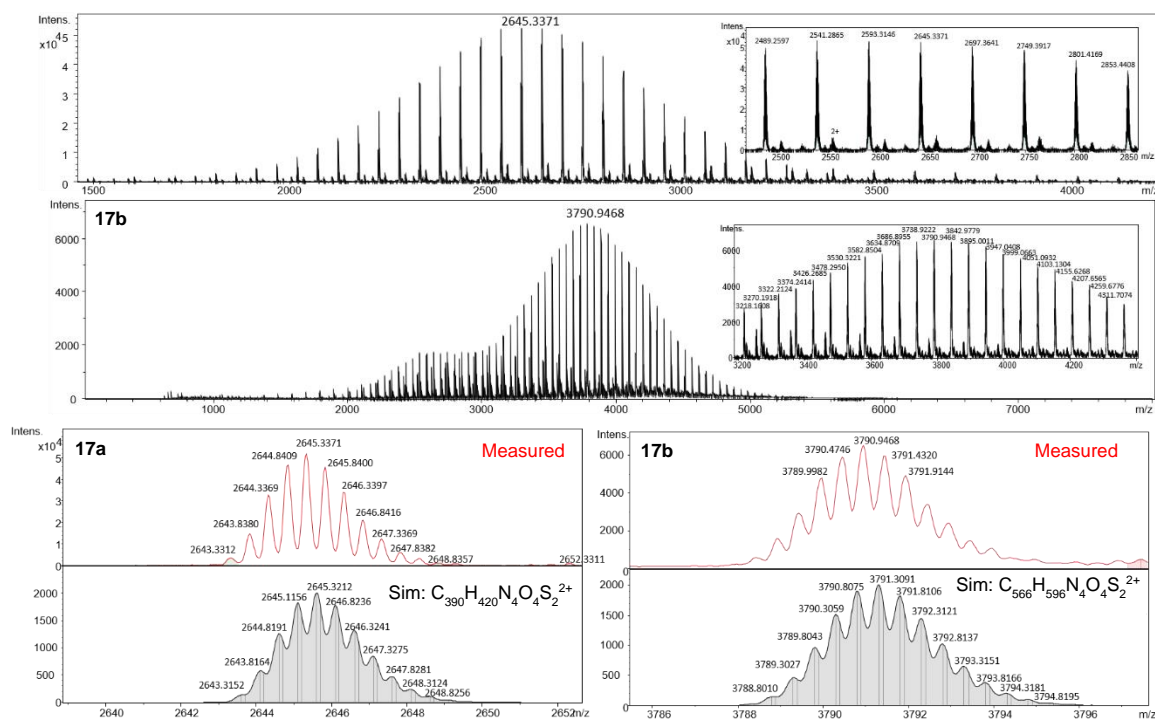


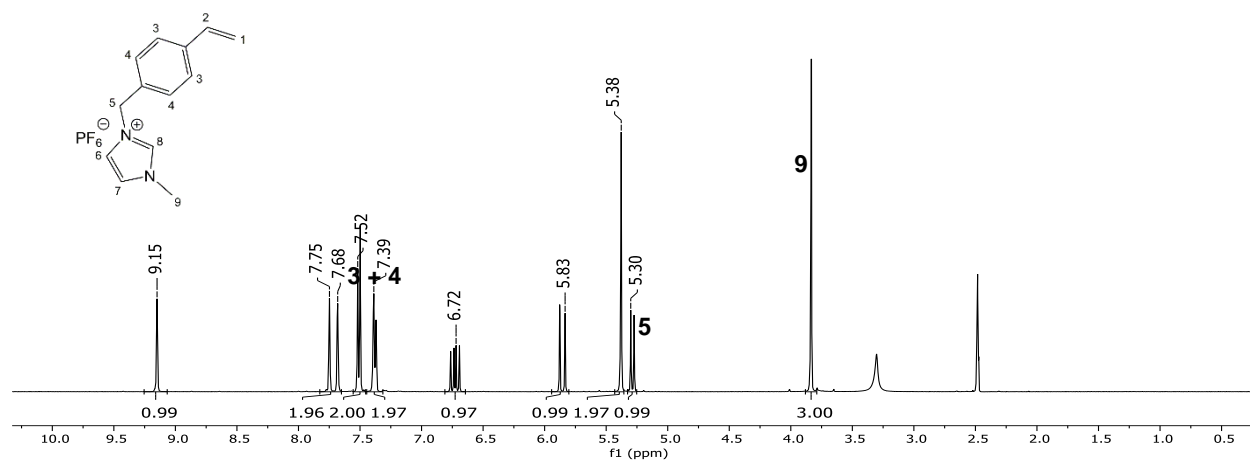
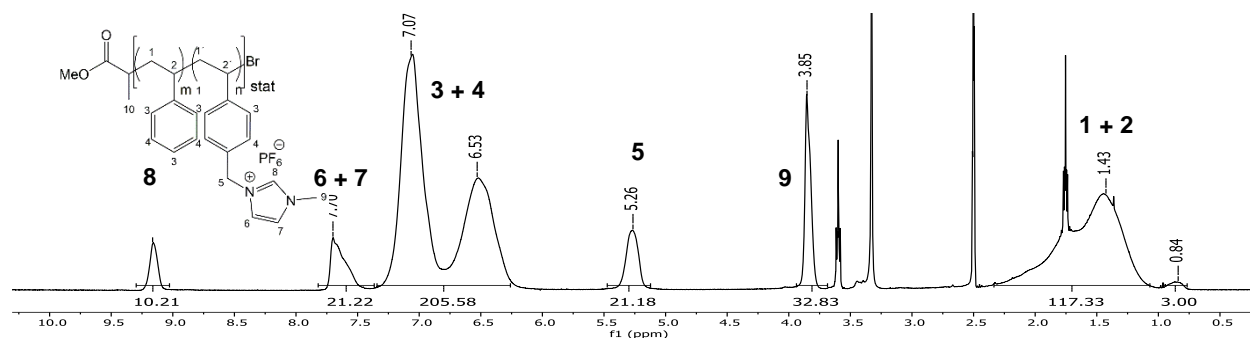
Figure A 37.  $^1\text{H-NMR}$  spectrum of **14** in  $\text{CDCl}_3$ .



Figure A 42.  $^1\text{H-NMR}$  spectrum of **17b** in  $\text{THF-d}_8$ .Figure A 43.  $^1\text{H-NMR}$  spectrum of **18b** in  $\text{THF-d}_8$ .Figure A 44. ESI-TOF-MS spectrum of **14** and **16**.

Figure A 45. ESI-TOF-MS spectrum of **17a** and **17b**.

#### 7.4. Synthesis of network based mechanophores

Figure A 46.  $^1\text{H-NMR}$  spectrum of **19** in  $\text{DMSO-}d_6$ .Figure A 47.  $^1\text{H-NMR}$  spectrum of **20a** in  $\text{THF-}d_8$ .

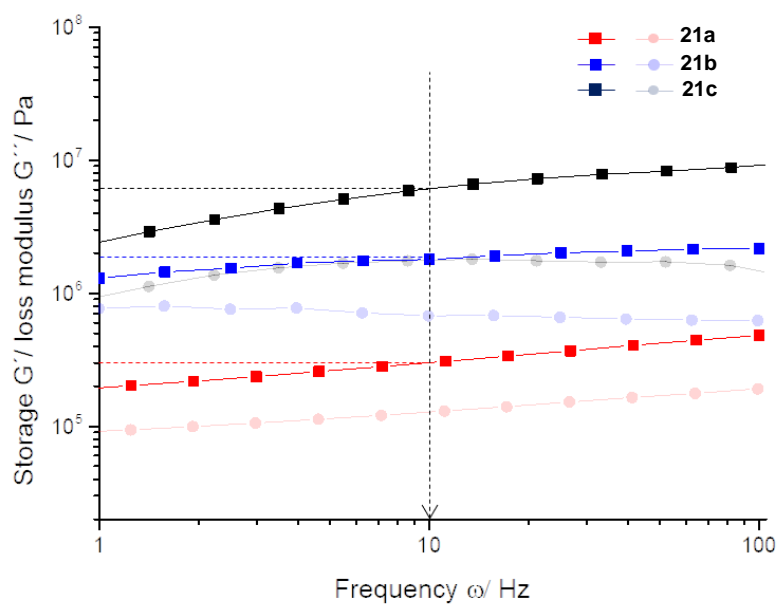


Figure A 48. Rheological investigation of **21** in the swollen state showing an increase of storage modulus  $G'$  with an increasing amount of imidazolium side chain functionalization in the copolymer precursor.

### 7.5. Synthesis of coumarin based fluorogenic system

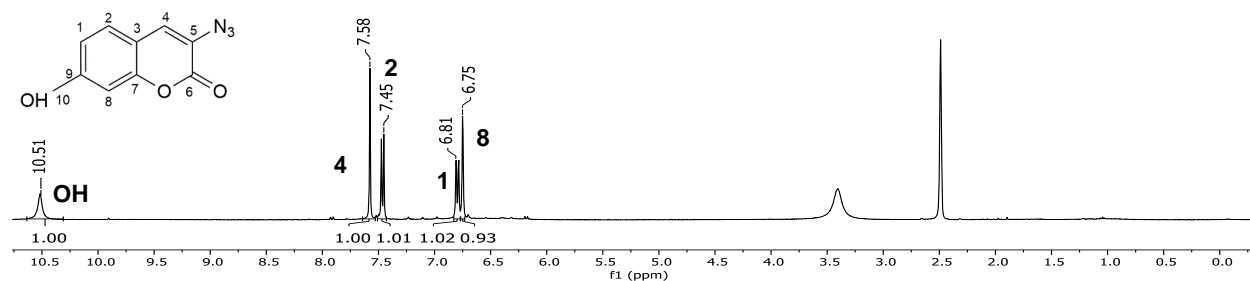


Figure A 49.  $^1\text{H}$ -NMR spectrum of **22** in  $\text{DMSO}-d_6$ .

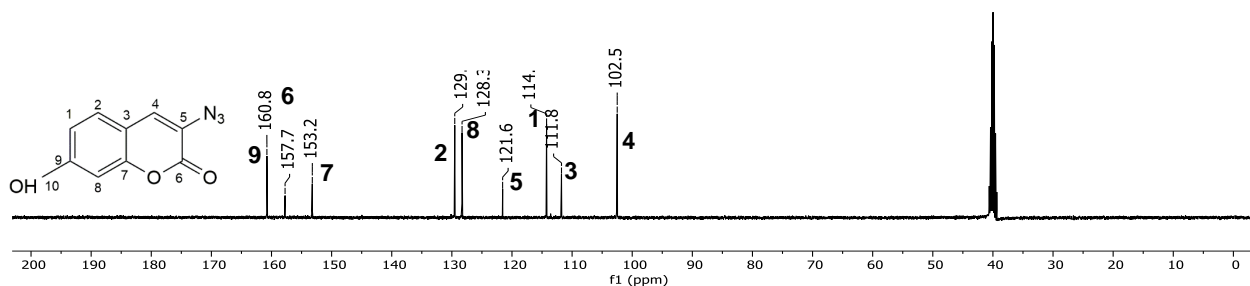
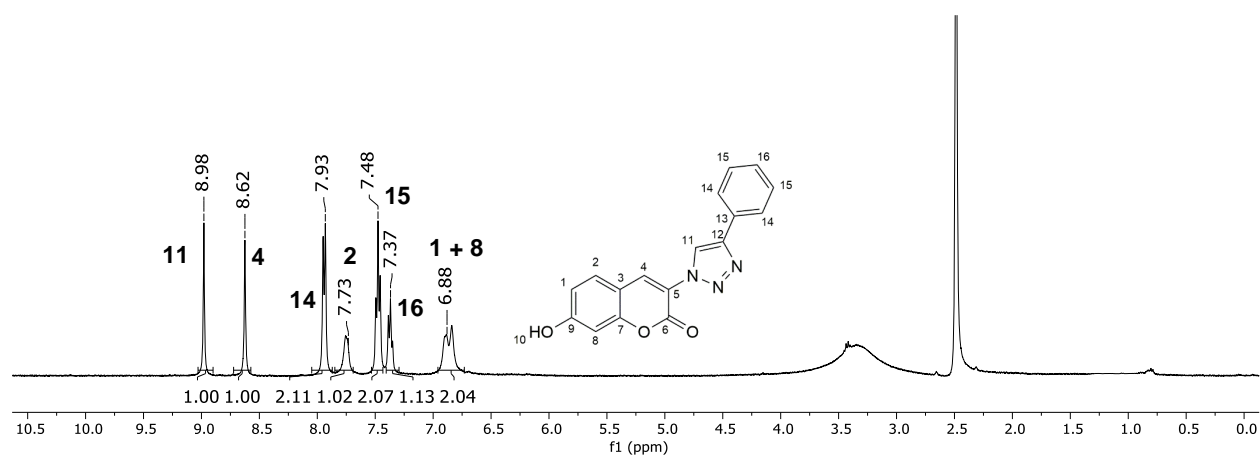
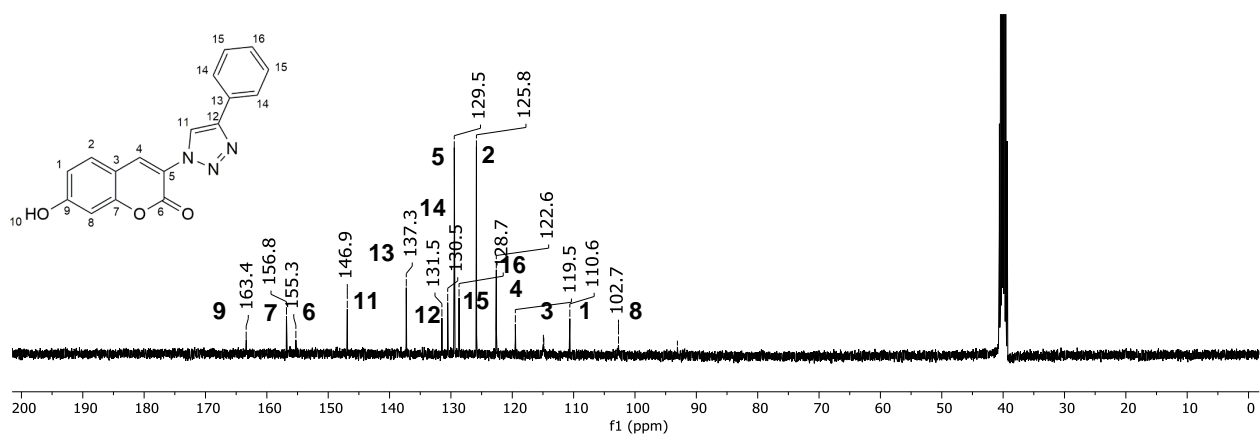
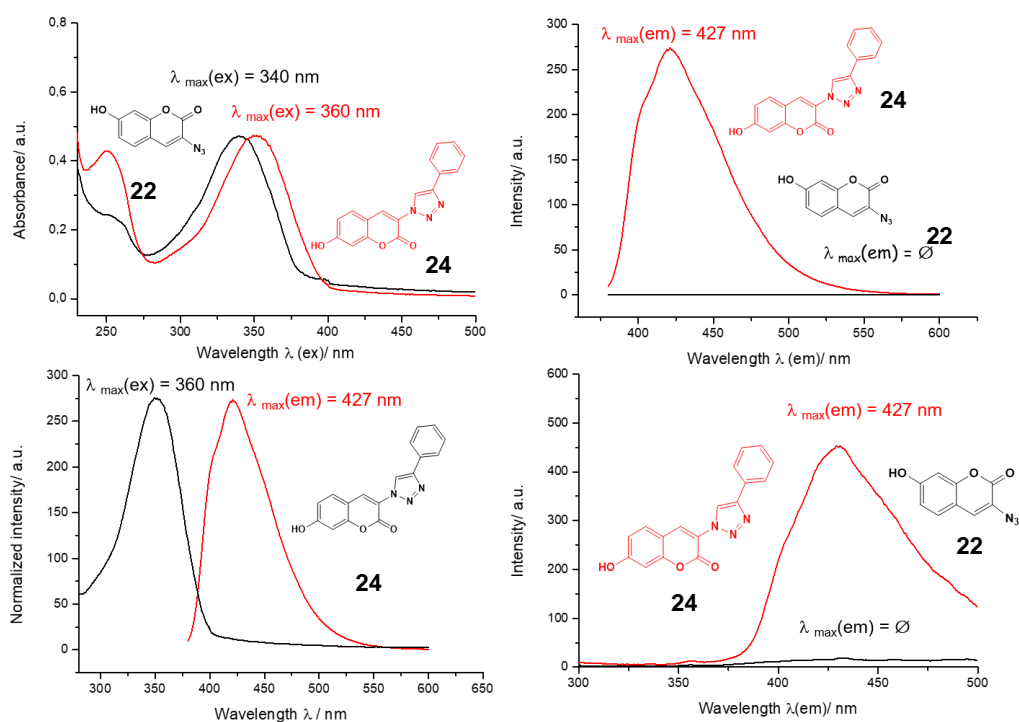
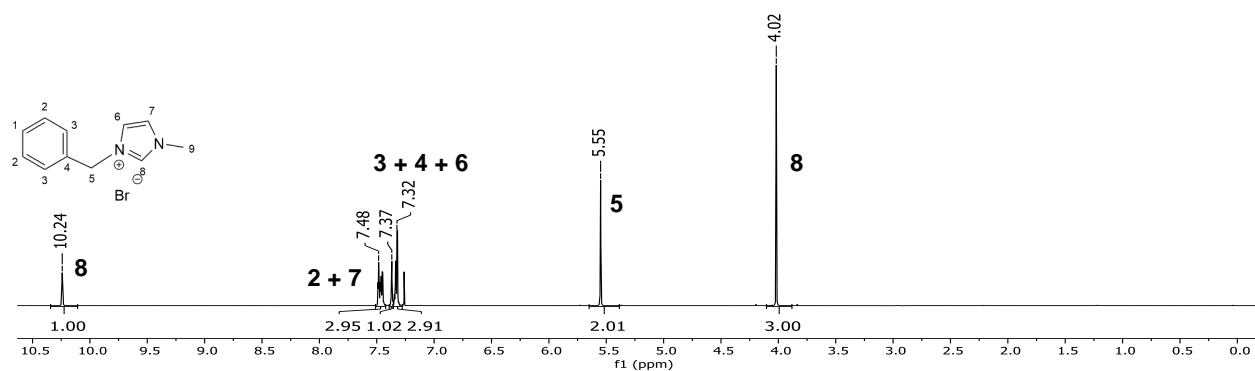
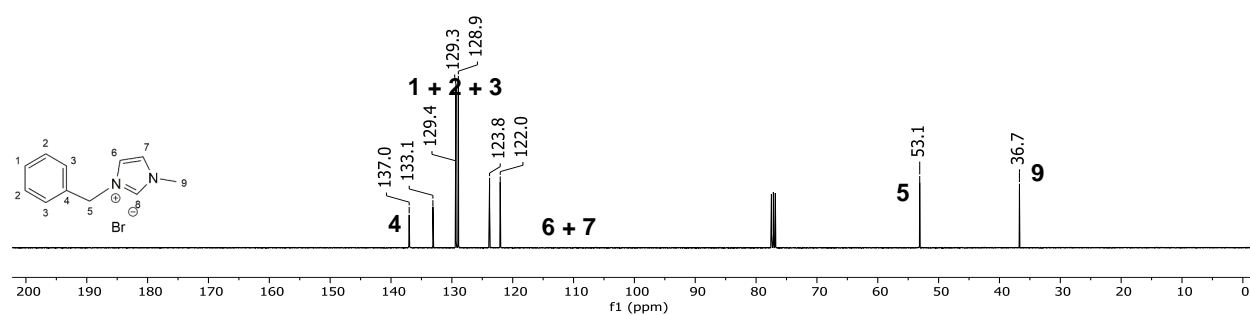
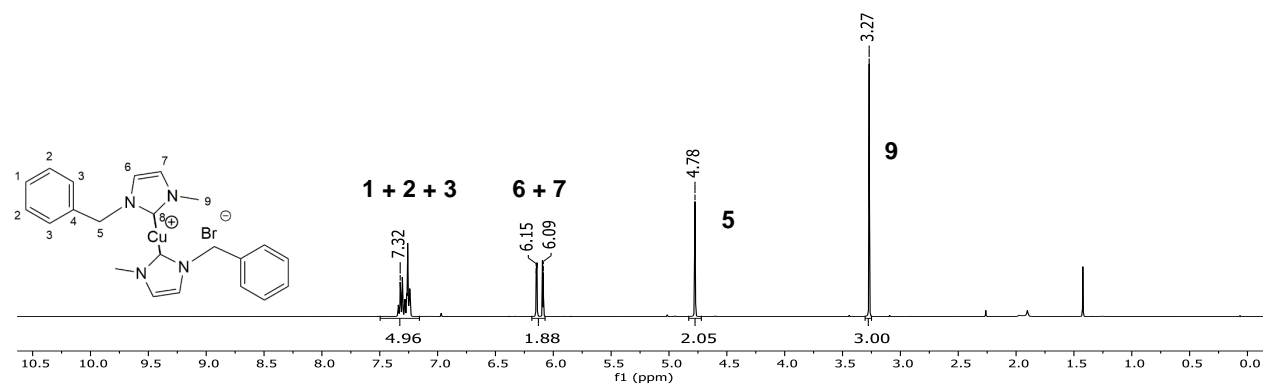
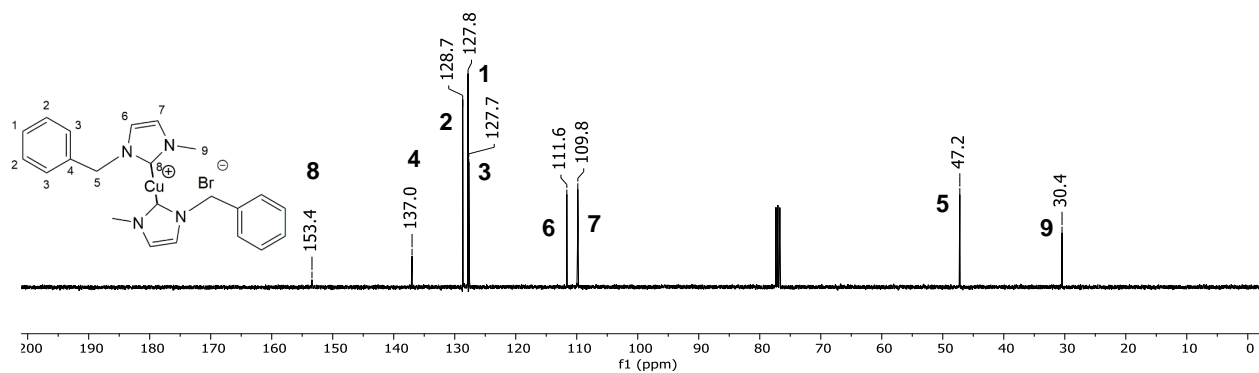


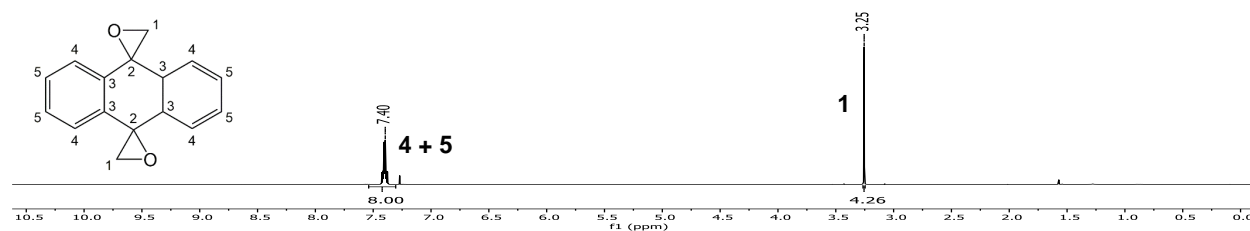
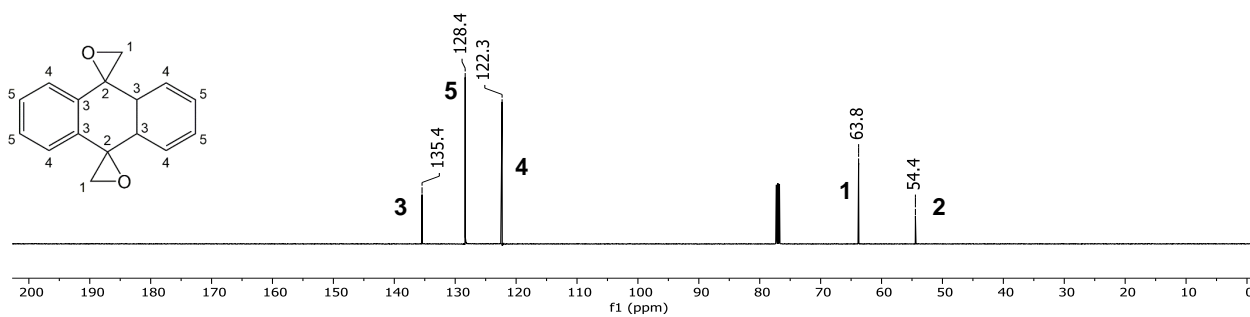
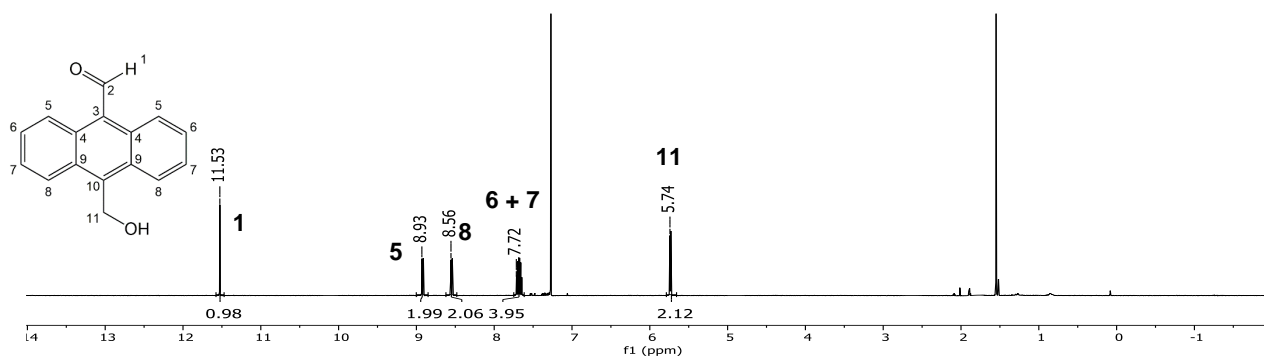
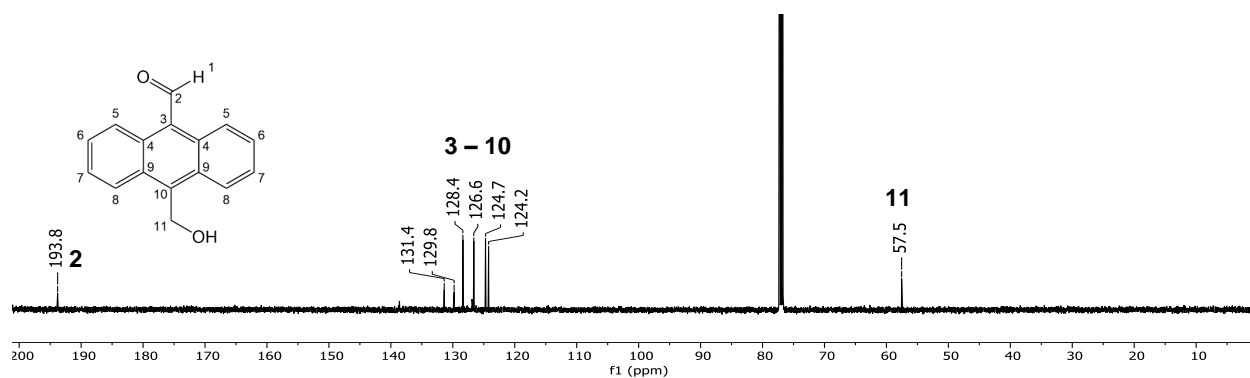
Figure A 50.  $^{13}\text{C}$ -NMR spectrum of **22** in  $\text{DMSO}-d_6$ .

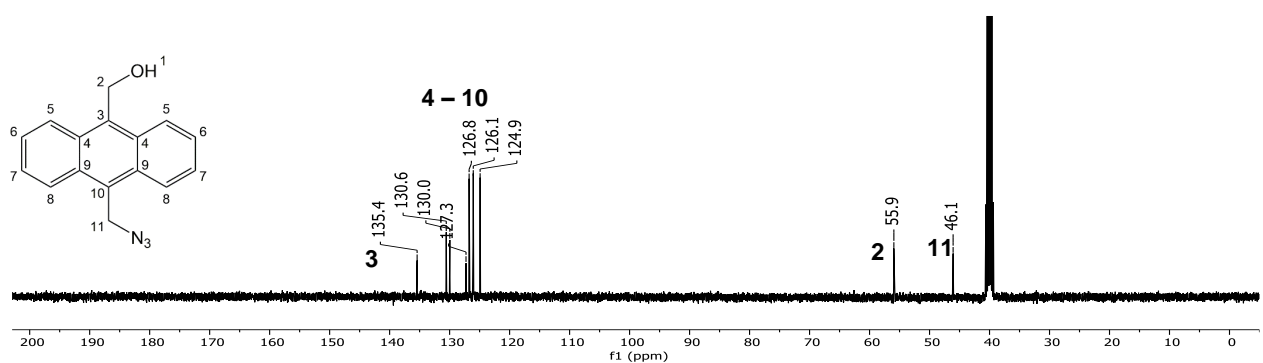
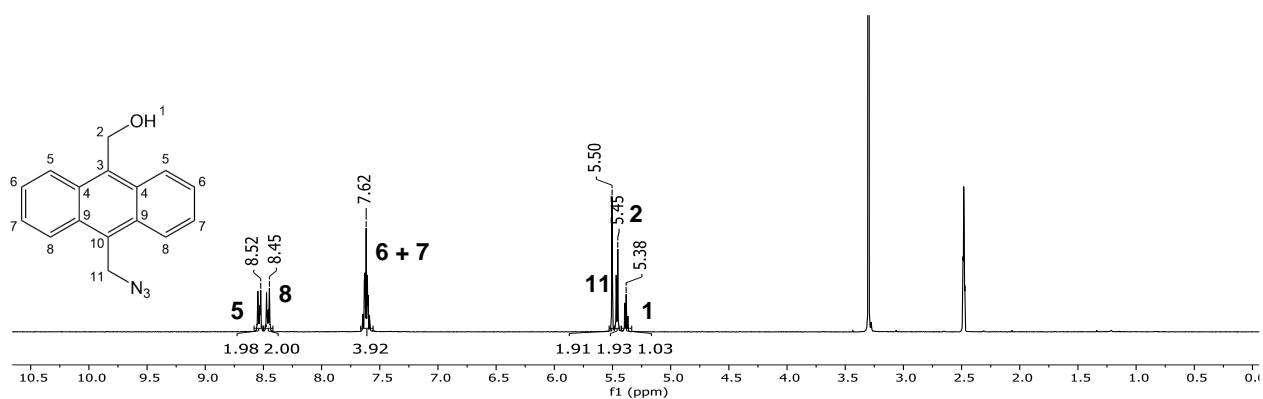
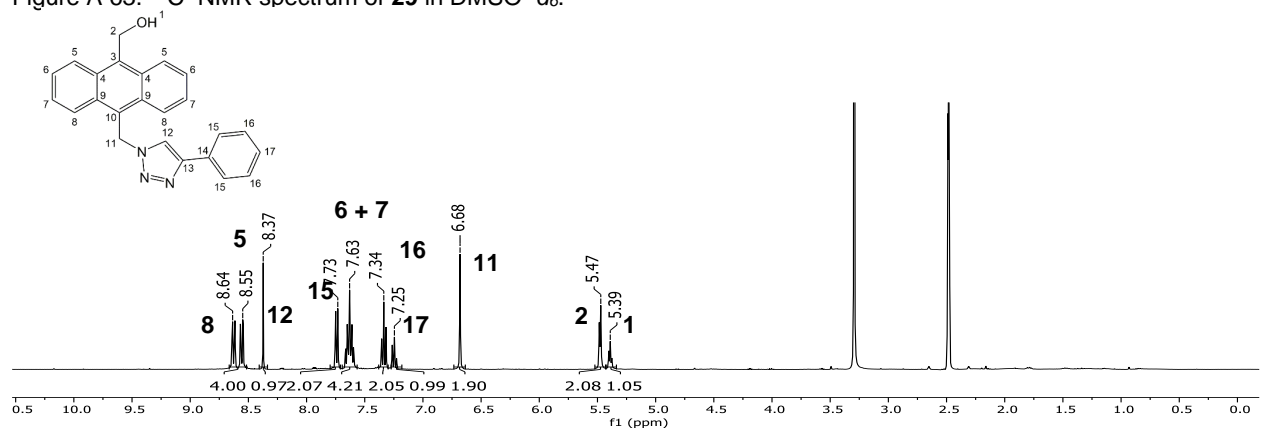
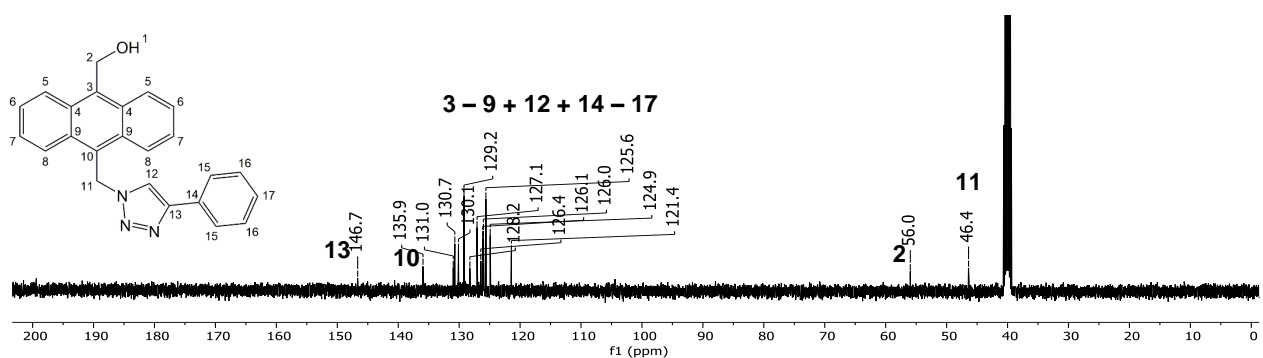
Figure A 51.  $^1\text{H}$ -NMR spectrum of **24** in  $\text{DMSO}-d_6$ .Figure A 52.  $^{13}\text{C}$ -NMR spectrum of **24** in  $\text{DMSO}-d_6$ .Figure A 53. (A) Absorption spectra of **22** (black) and **24** (red) in THF. (B) Emission spectra of **22** (black) and **24** (red) in THF. (C) Overlapping absorption (black) and emission (red) spectrum of **24** in THF and (D) Emission spectra of **22** (black) and **24** (red) in solid state.

## 7.6. Synthesis of low molecular weight model complex

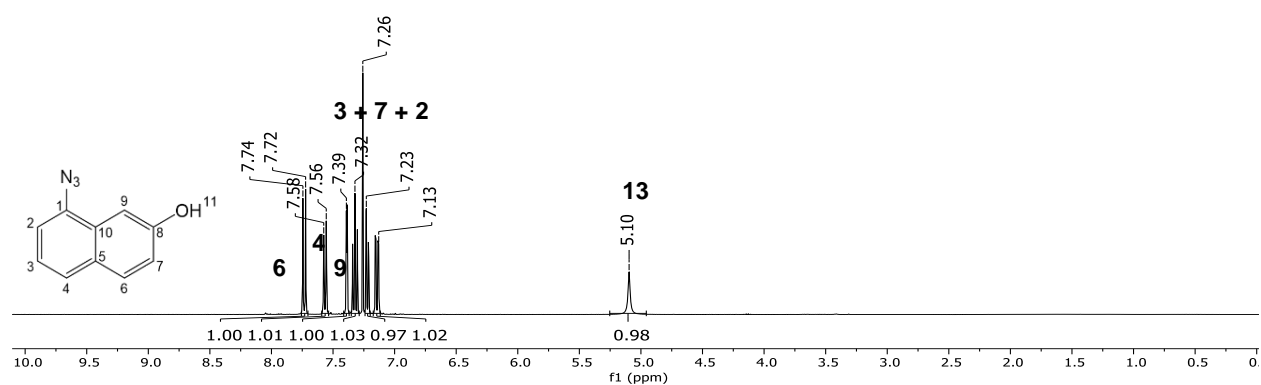
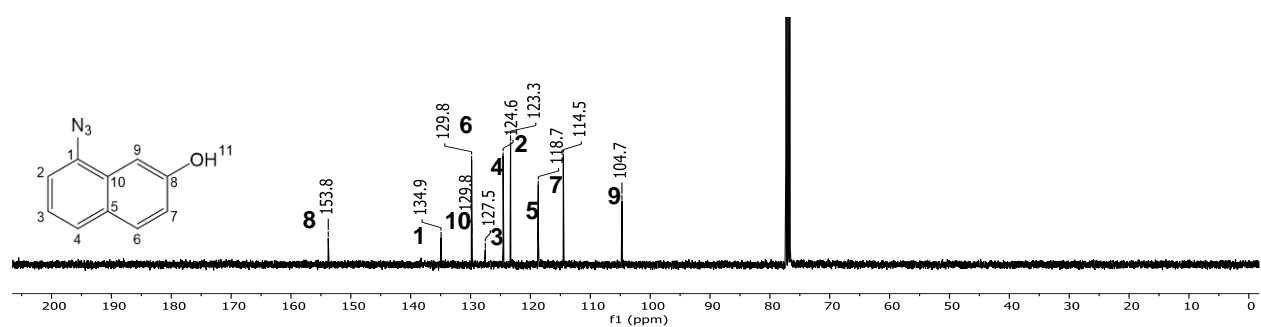
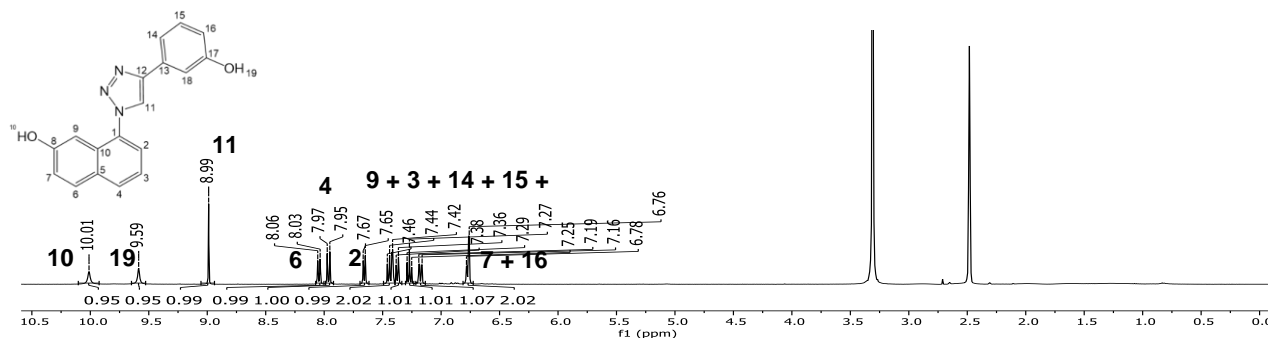
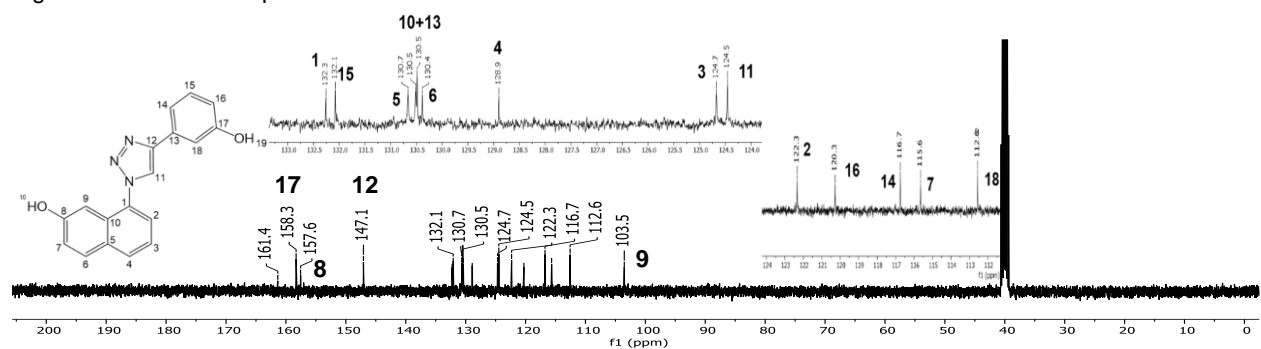
Figure A 54.  $^1\text{H}$ -NMR spectrum of **25** in  $\text{CDCl}_3$ .Figure A 55.  $^{13}\text{C}$ -NMR spectrum of **25** in  $\text{CDCl}_3$ .Figure A 56.  $^1\text{H}$ -NMR spectrum of **26** in  $\text{CDCl}_3$ .Figure A 57.  $^{13}\text{C}$ -NMR spectrum of **26** in  $\text{CDCl}_3$ .

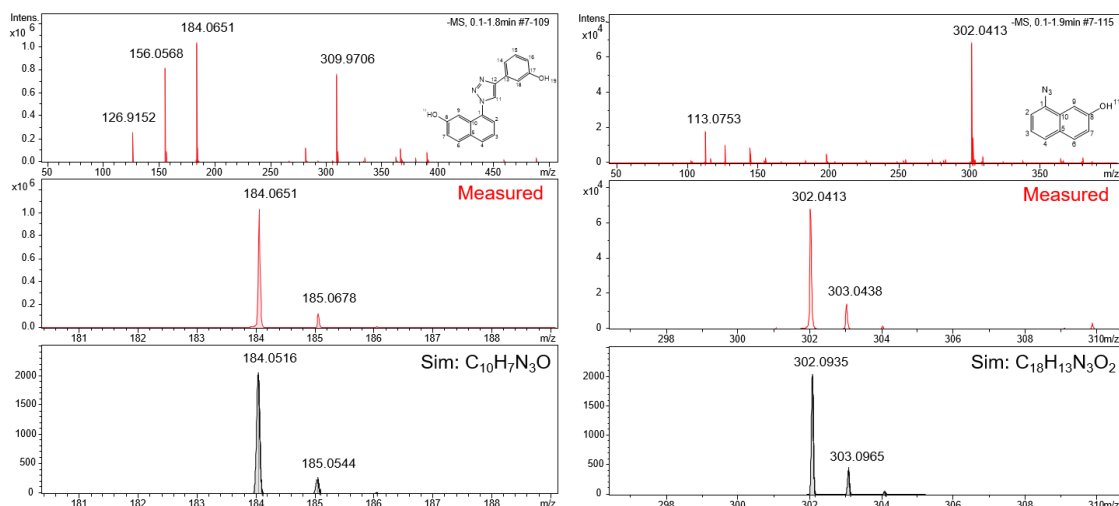
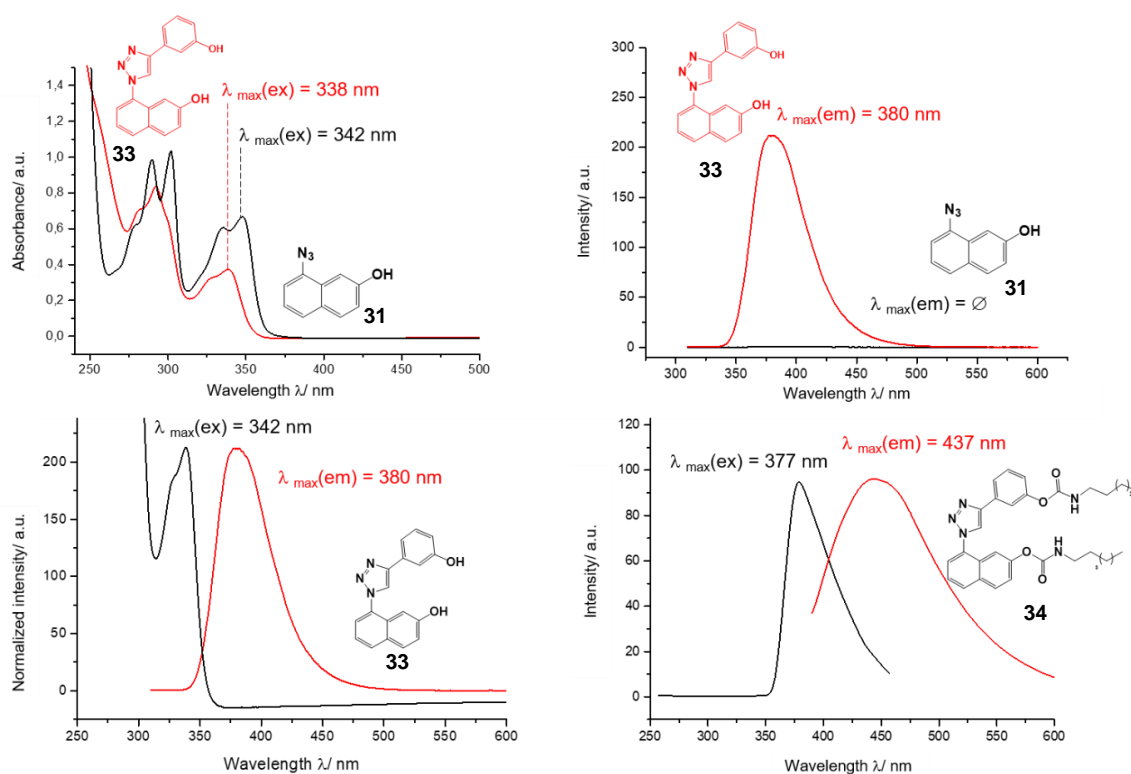
## 7.7. Synthesis of anthracene based fluorogenic “click” system

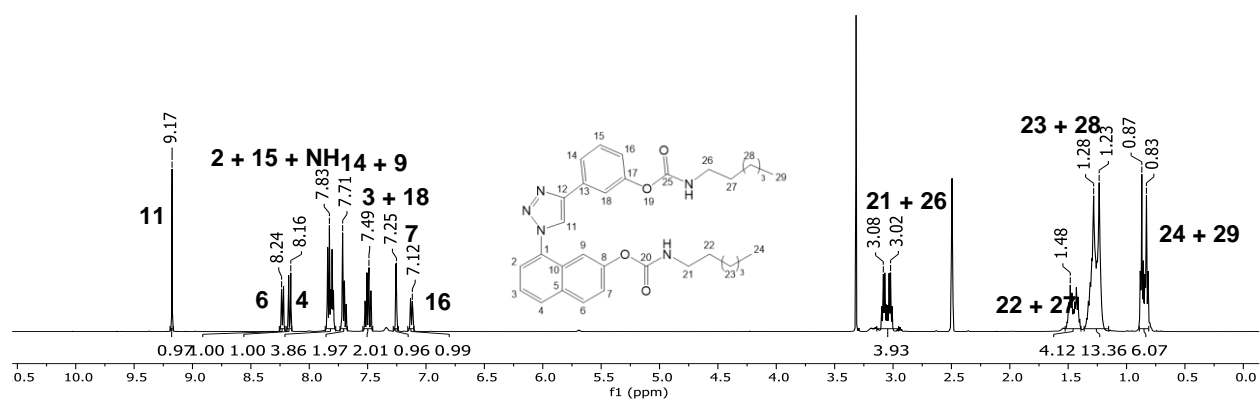
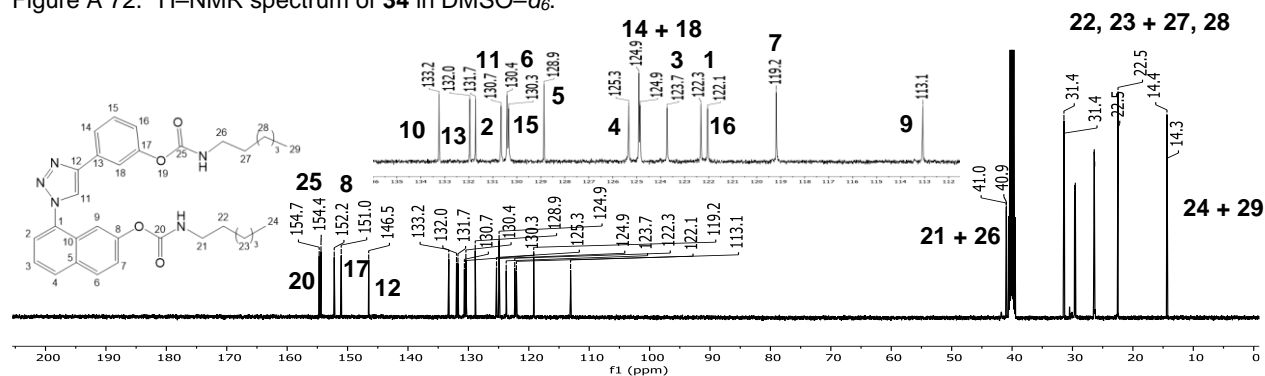
Figure A 58.  $^1\text{H}$ -NMR spectrum of **27** in  $\text{CDCl}_3$ .Figure A 59.  $^{13}\text{C}$ -NMR spectrum of **27** in  $\text{CDCl}_3$ .Figure A 60.  $^1\text{H}$ -NMR spectrum of **28** in  $\text{CDCl}_3$ .Figure A 61.  $^{13}\text{C}$ -NMR spectrum of **28** in  $\text{CDCl}_3$ .

Figure A 63.  $^{13}\text{C}$ -NMR spectrum of **29** in  $\text{DMSO}-d_6$ .Figure A 64.  $^1\text{H}$ -NMR spectrum of **30** in  $\text{DMSO}-d_6$ .Figure A 65.  $^{13}\text{C}$ -NMR spectrum of **30** in  $\text{DMSO}-d_6$ .

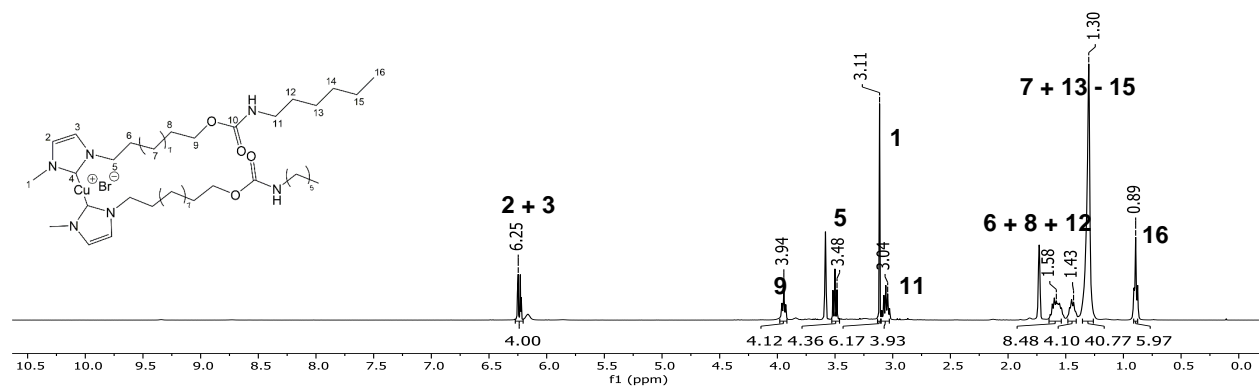
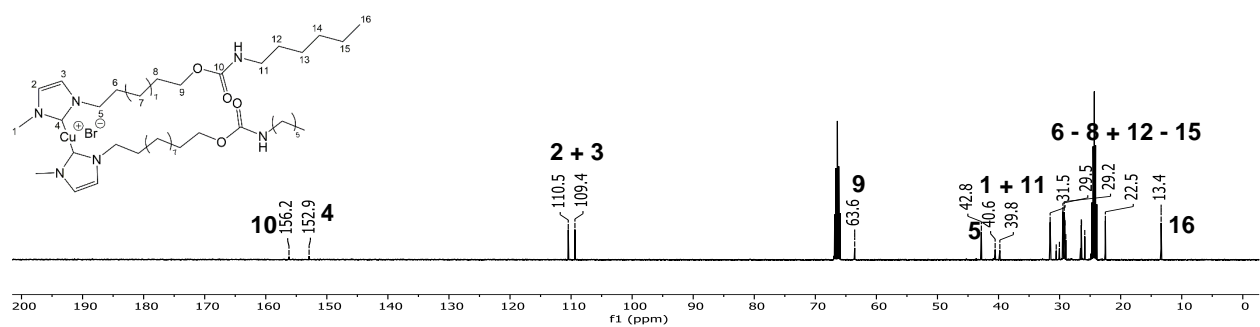
## 7.8. Synthesis of naphthalene based fluorogenic system

Figure A 66.  $^1\text{H}$ -NMR spectrum of **31** in  $\text{CDCl}_3$ .Figure A 67.  $^{13}\text{C}$ -NMR spectrum of **31** in  $\text{CDCl}_3$ .Figure A 68.  $^1\text{H}$ -NMR spectrum of **33** in  $\text{DMSO}-d_6$ .Figure A 69.  $^{13}\text{C}$ -NMR spectrum of **33** in  $\text{DMSO}-d_6$ .

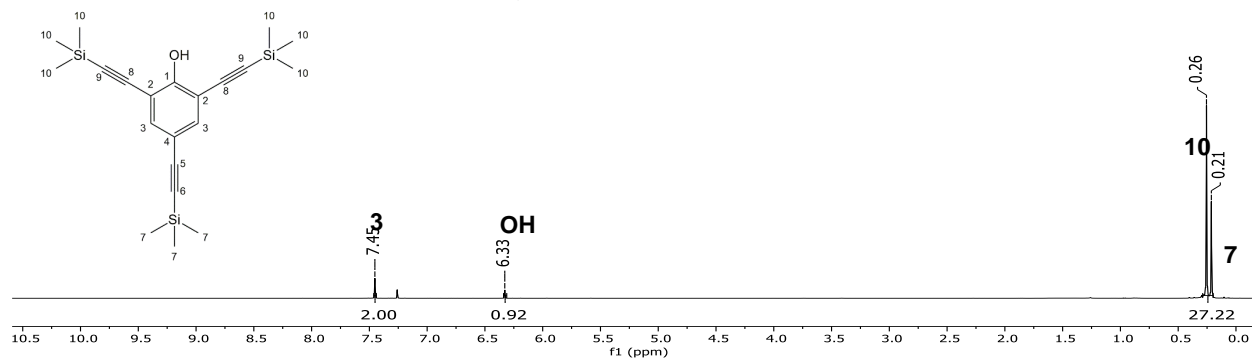
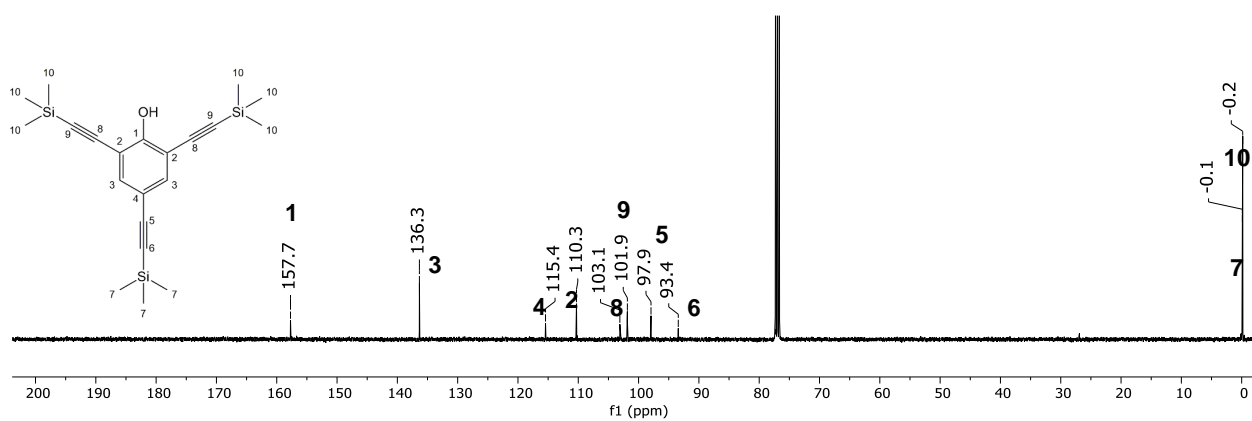
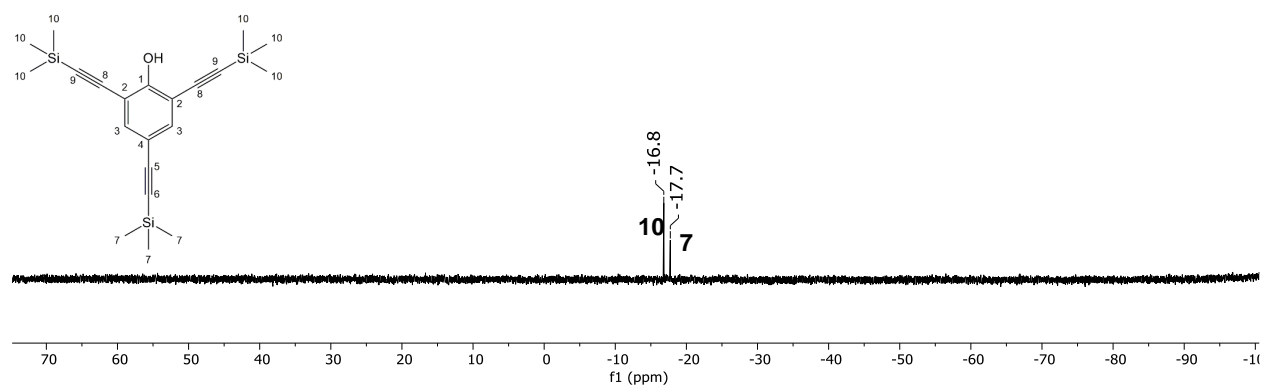
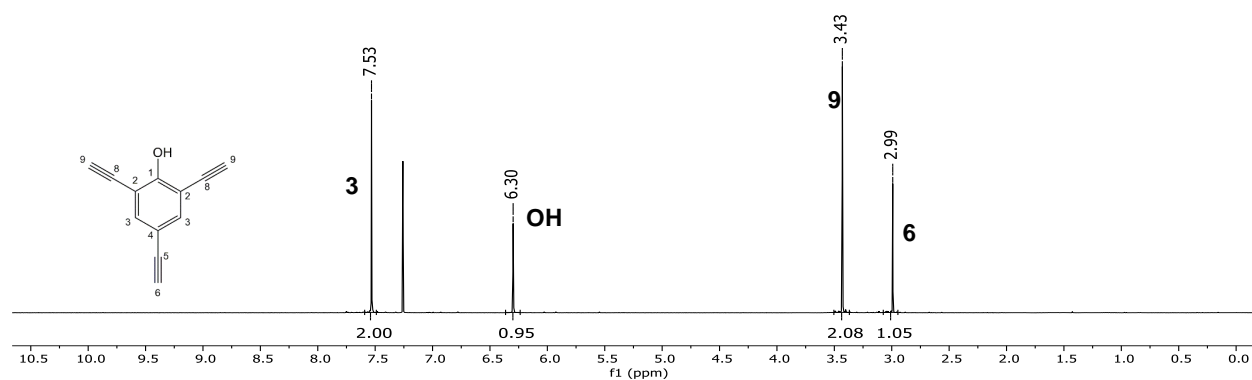
Figure A 70. ESI-TOF-MS spectrum of **31** and **33**.Figure A 71. Optical properties of the non-colored fluorogenic system. (A) UV-spectrum of **31** (black) and **33** (red) in THF. (B) Fluorescence spectrum of **31** (black) and **33** (red) in THF after excitation at  $\lambda_{\text{ex}} \approx 342$  nm. (C) Comparison of absorption (black) and emission (red) maxima of **33** and (D) Comparison of absorption (black) and emission (red) maxima of **34**.

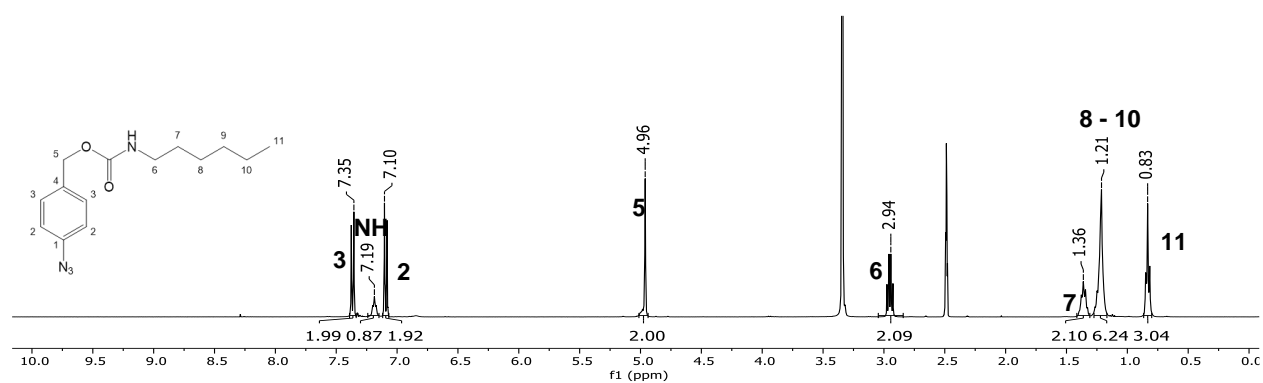
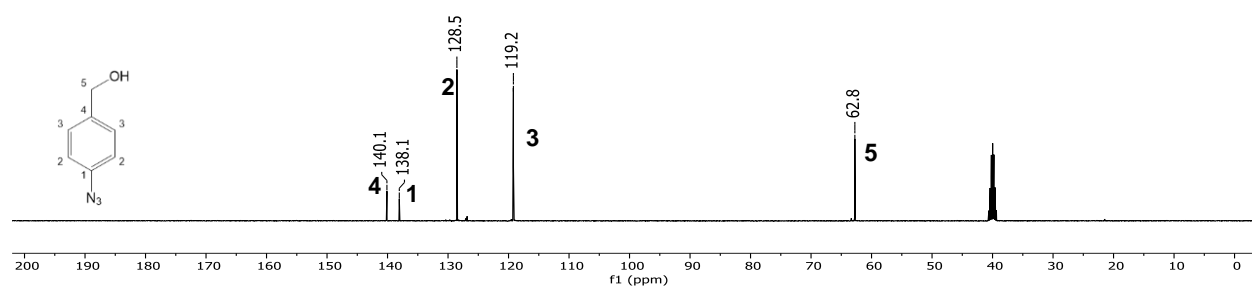
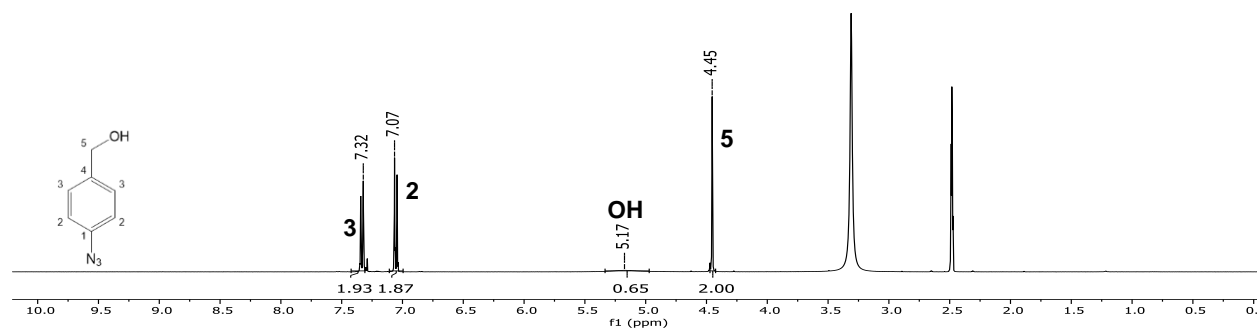
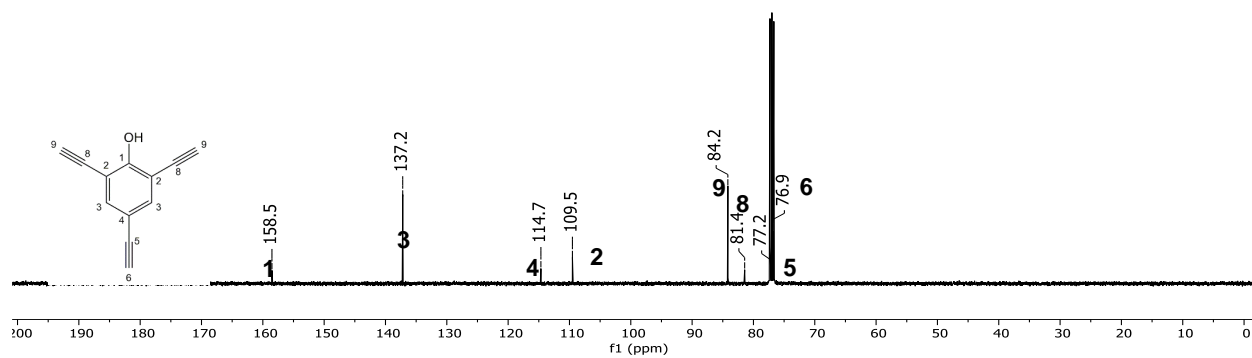
Figure A 72.  $^1\text{H}$ -NMR spectrum of **34** in  $\text{DMSO}-d_6$ .Figure A 73.  $^{13}\text{C}$ -NMR spectrum of **34** in  $\text{DMSO}-d_6$ .

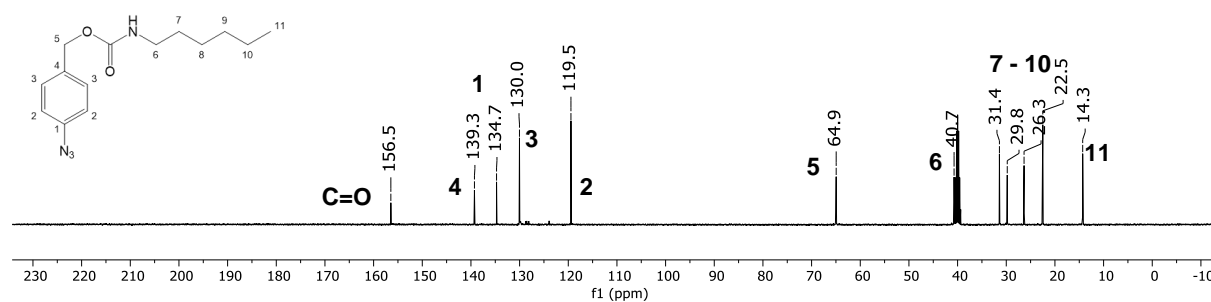
### 7.9. Synthesis of urethane quenched copper(I)-bis(NHC) complex

Figure A 74.  $^1\text{H}$ -NMR spectrum of **35** in  $\text{THF}-d_8$ .Figure A 75.  $^{13}\text{C}$ -NMR spectrum of **35** in  $\text{THF}-d_8$ .

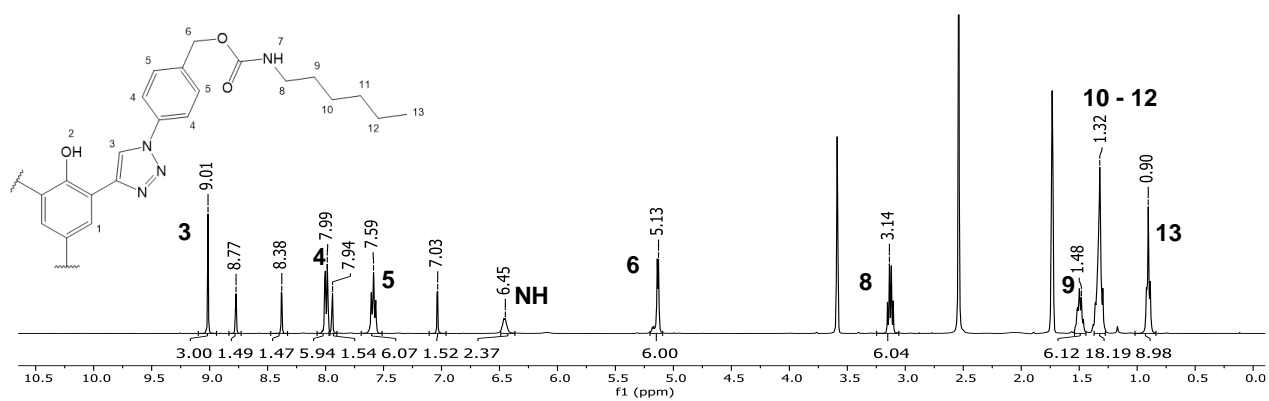
## 7.10. Synthesis of trivalent fluorogenic “click” systems

Figure A 76.  $^1\text{H}$ -NMR spectrum of **36** in  $\text{CDCl}_3$ .Figure A 77.  $^{13}\text{C}$ -NMR spectrum of **36** in  $\text{CDCl}_3$ .Figure A 78.  $^{29}\text{Si}$ -NMR spectrum of **36** in  $\text{CDCl}_3$ .Figure A 79.  $^1\text{H}$ -NMR spectrum of **37** in  $\text{CDCl}_3$ .

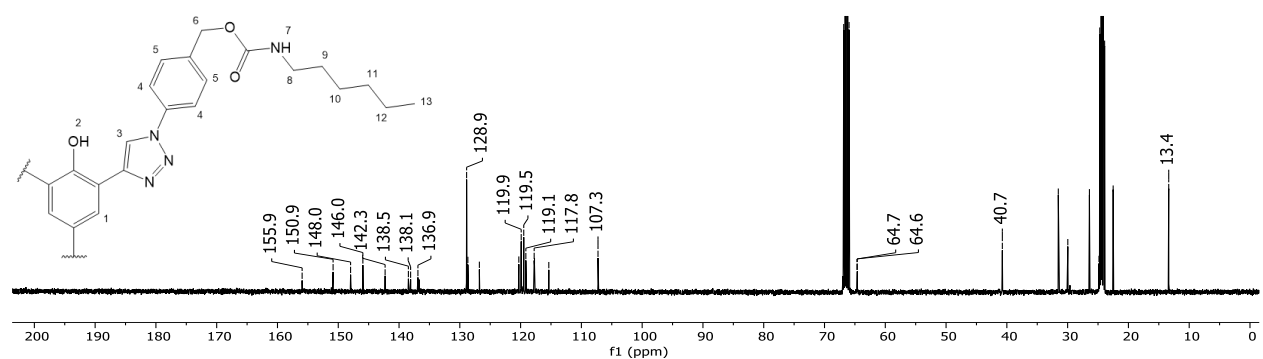




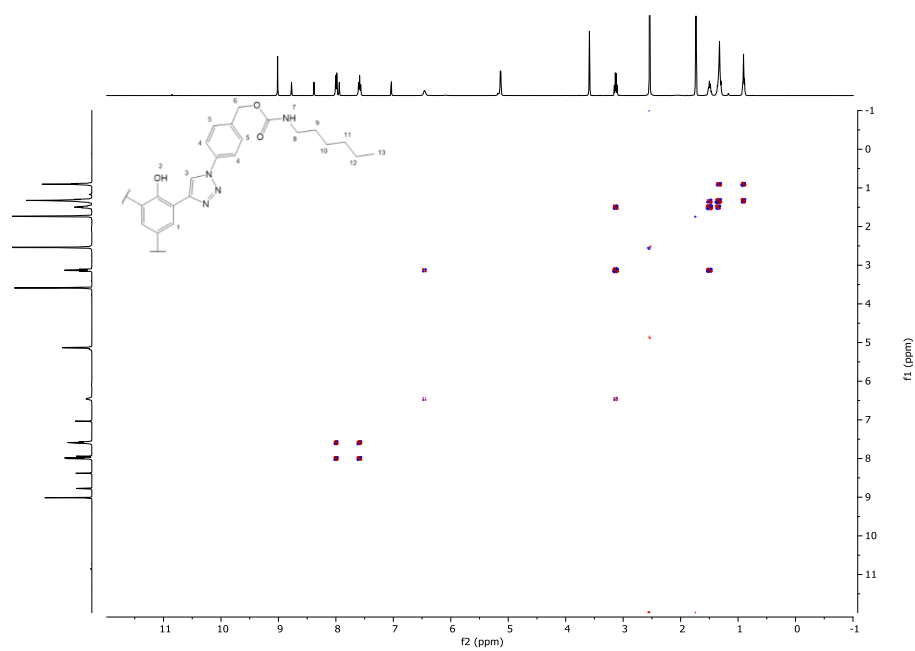
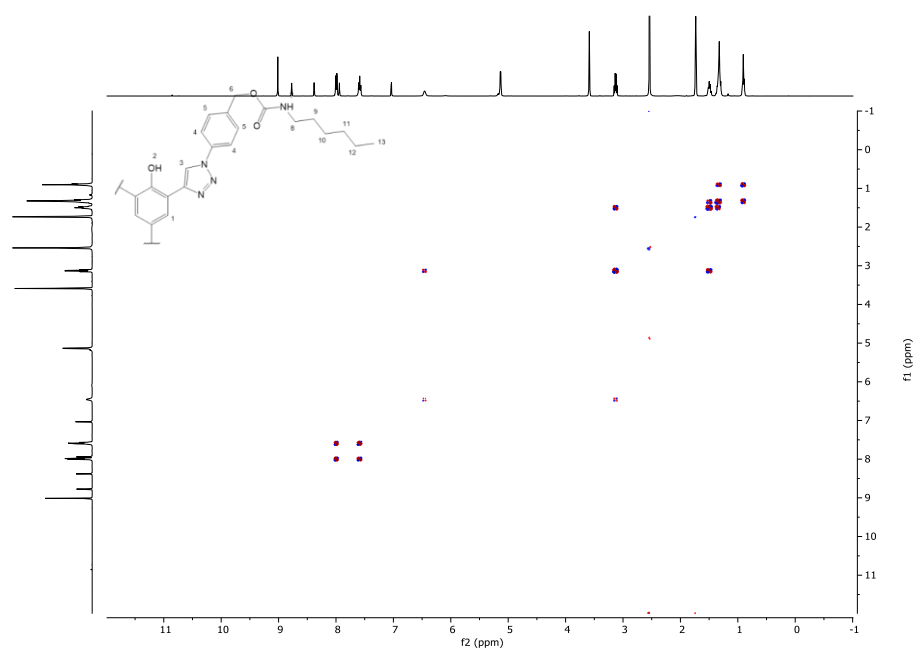
**Figure A 84.**  $^{13}\text{C}$ -NMR spectrum of **39** in  $\text{DMSO}-d_6$ .

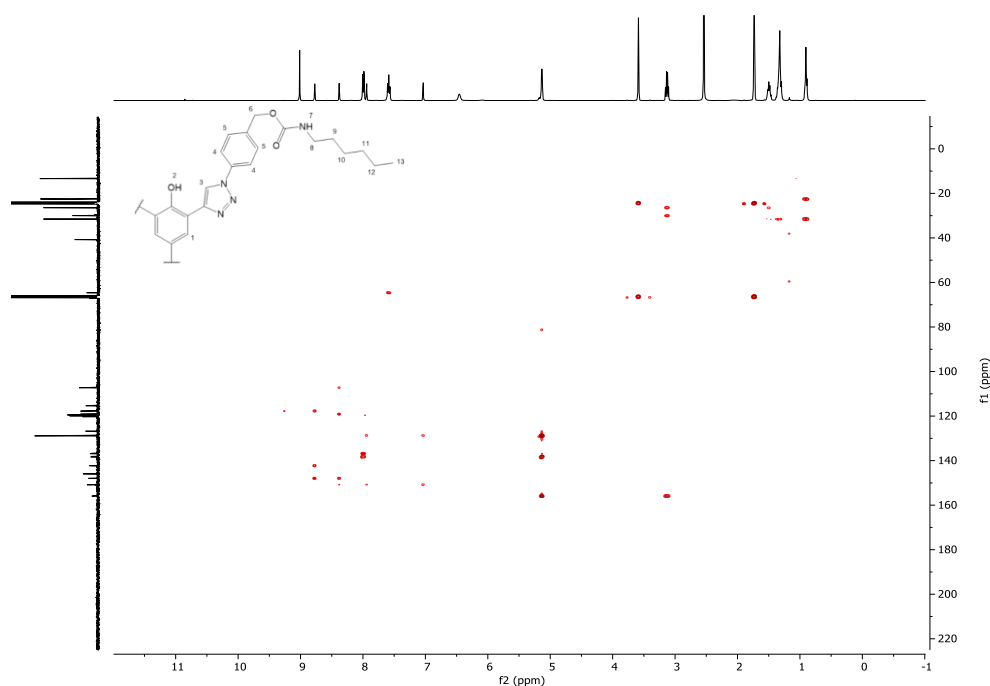
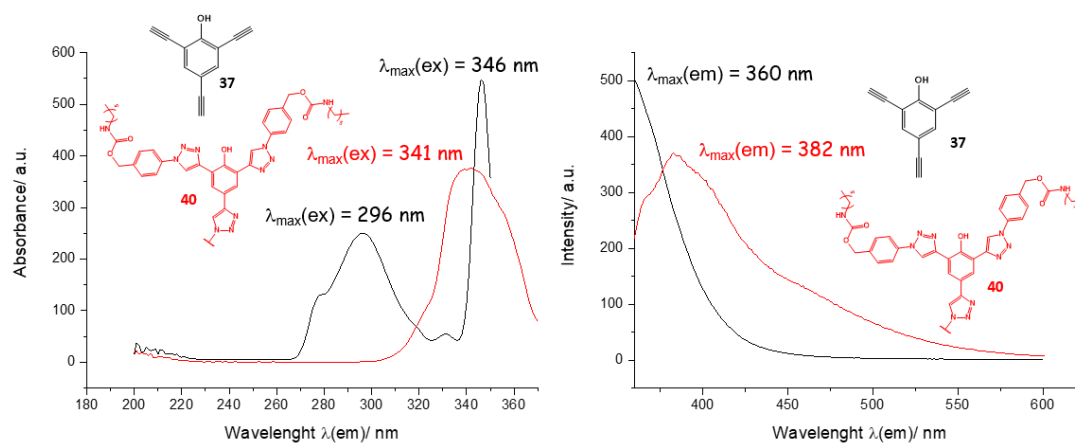
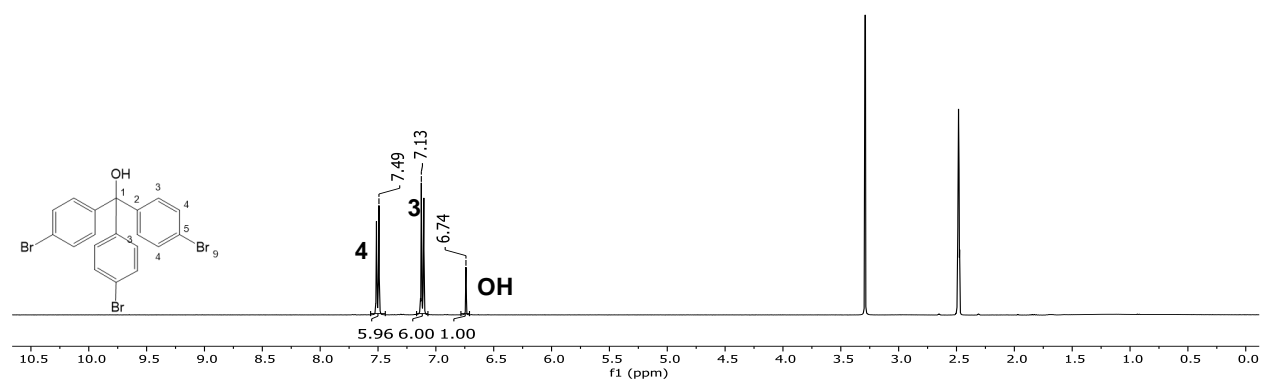


**Figure A 85.**  $^1\text{H}$ -NMR spectrum of **40** in  $\text{THF}-d_8$ .



**Figure A 86.**  $^{13}\text{C}$ -NMR spectrum of **40** in  $\text{THF}-d_8$ .

Figure A 87. H-H COSY-NMR spectrum of **40** in THF- $d_8$ .Figure A 88. gHSQCAD-NMR spectrum of **40** in THF- $d_8$ .

Figure A 89. gHMBCAD-NMR spectrum of **40** in THF-*d*<sub>8</sub>.Figure A 90. Optical properties of the trivalent fluorogenic system. (A) UV-spectrum of **37** (black) and **40** (red) in THF. (B) Fluorescence spectrum of **37** (black) and **40** (red) in THF after excitation at  $\lambda_{ex} \cong 341$  nm.Figure A 91. <sup>1</sup>H-NMR spectrum of **41** in DMSO-*d*<sub>6</sub>.

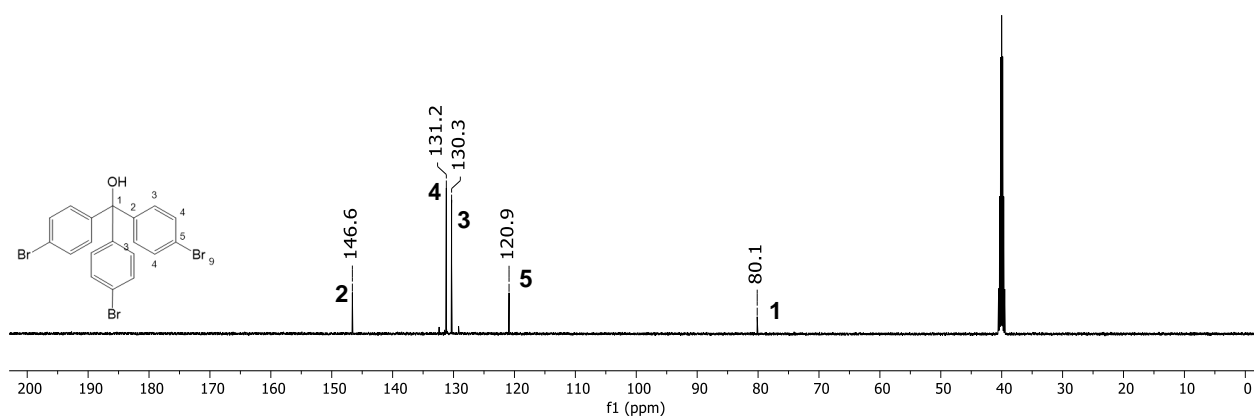


Figure A 92.  $^{13}\text{C}$ -NMR spectrum of **41** in  $\text{DMSO}-d_6$ .

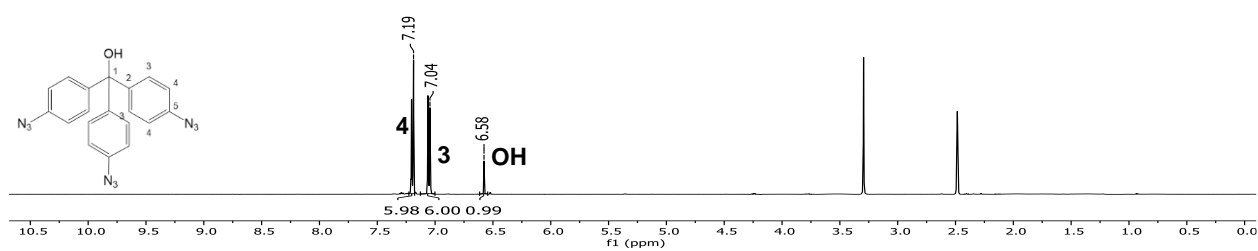


Figure A 93.  $^1\text{H}$ -NMR spectrum of **42** in  $\text{DMSO}-d_6$ .

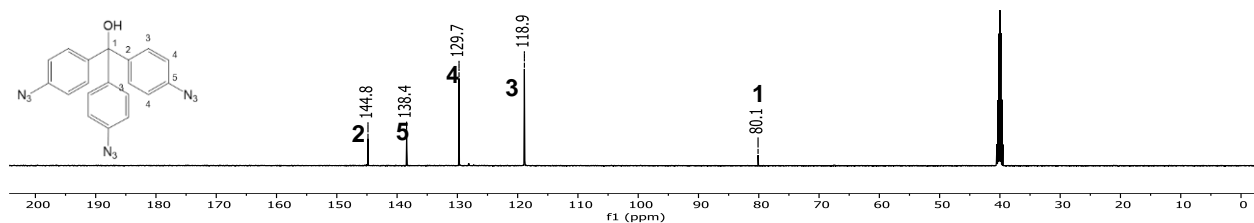


Figure A 94.  $^{13}\text{C}$ -NMR spectrum of **42** in  $\text{DMSO}-d_6$ .

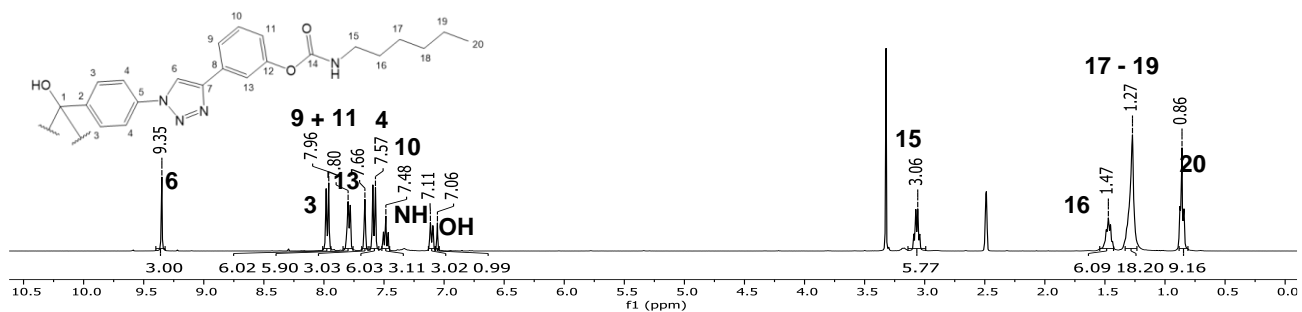
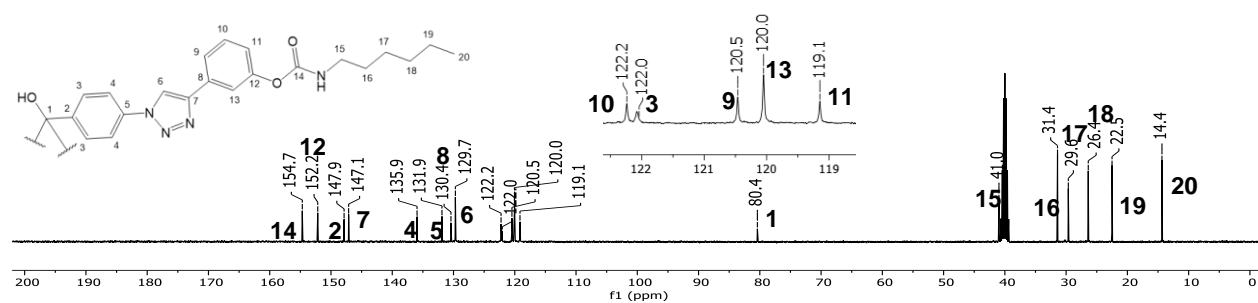
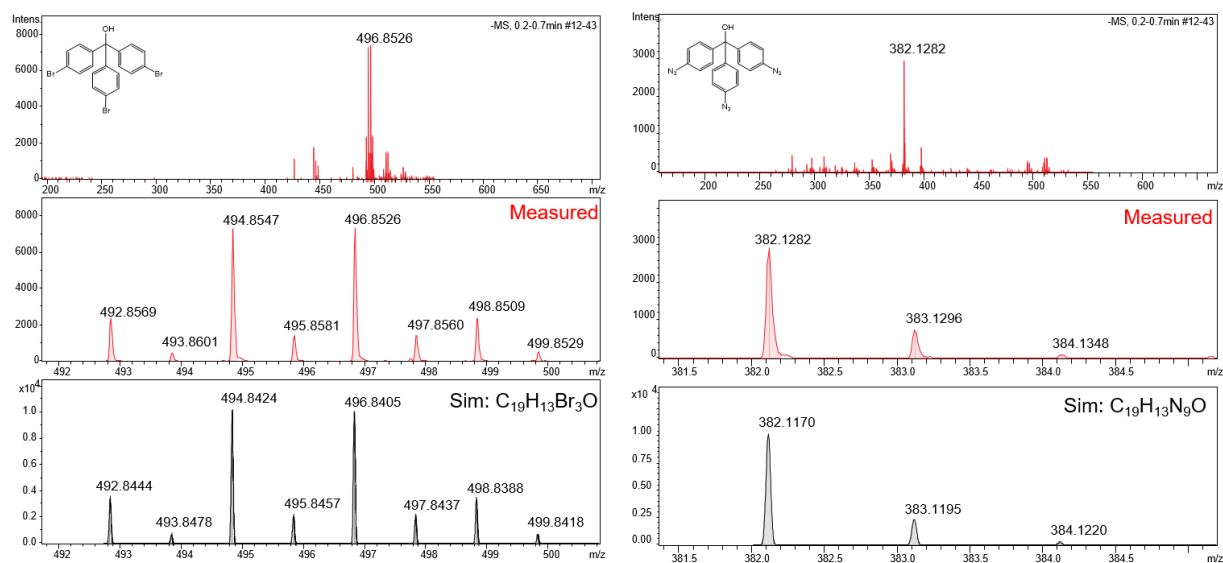
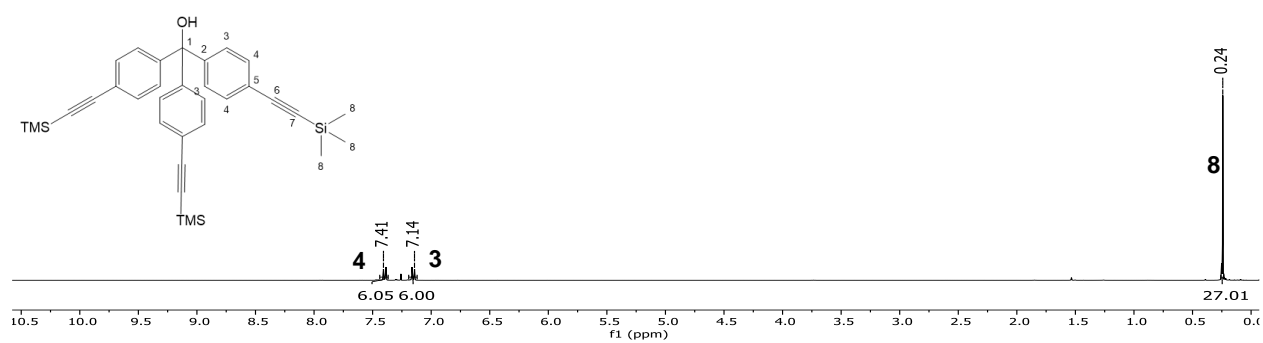
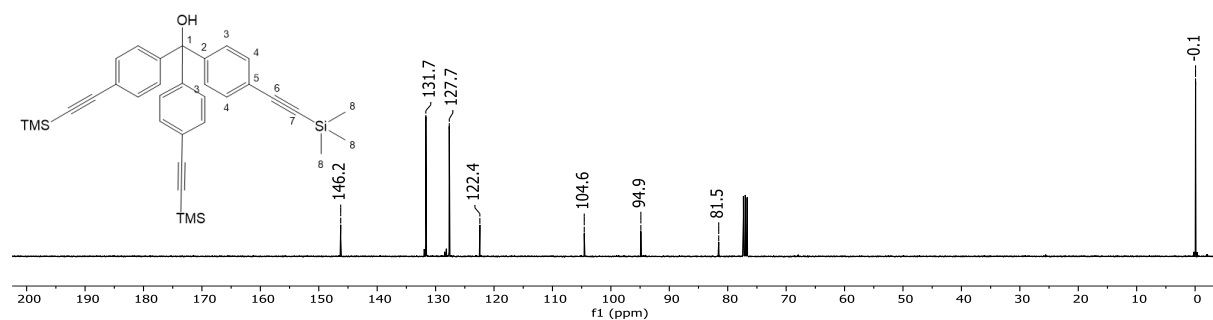
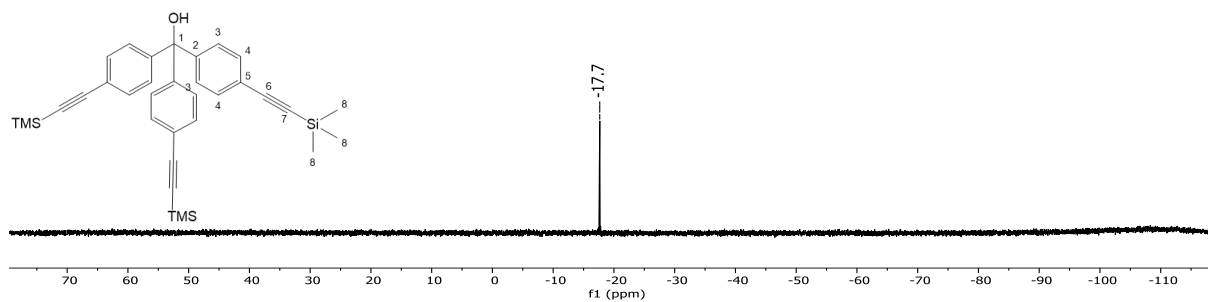
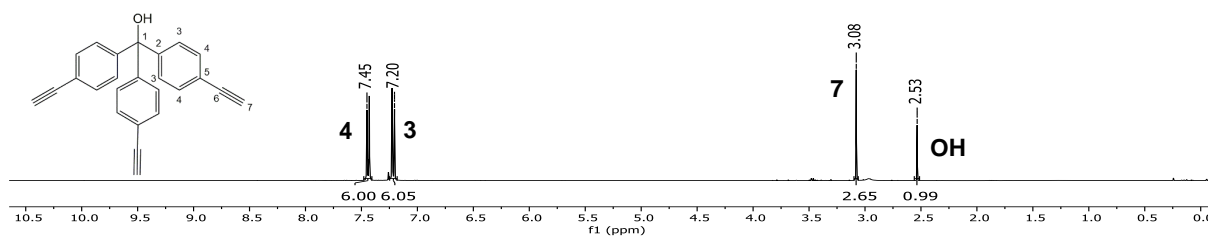
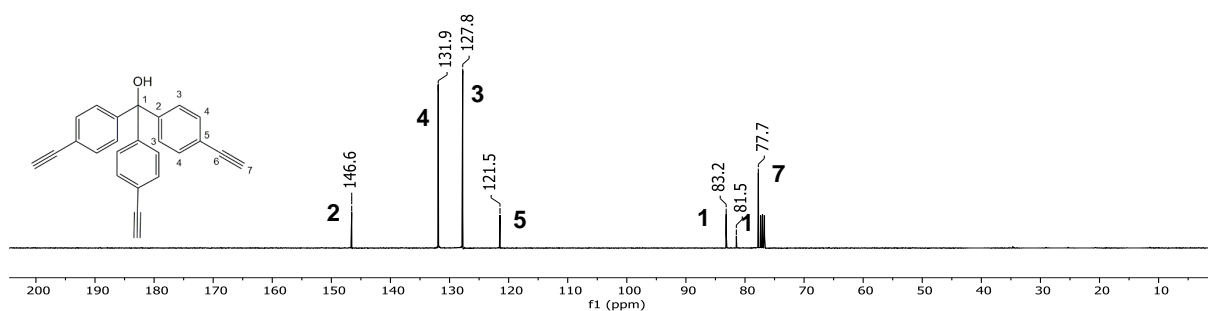
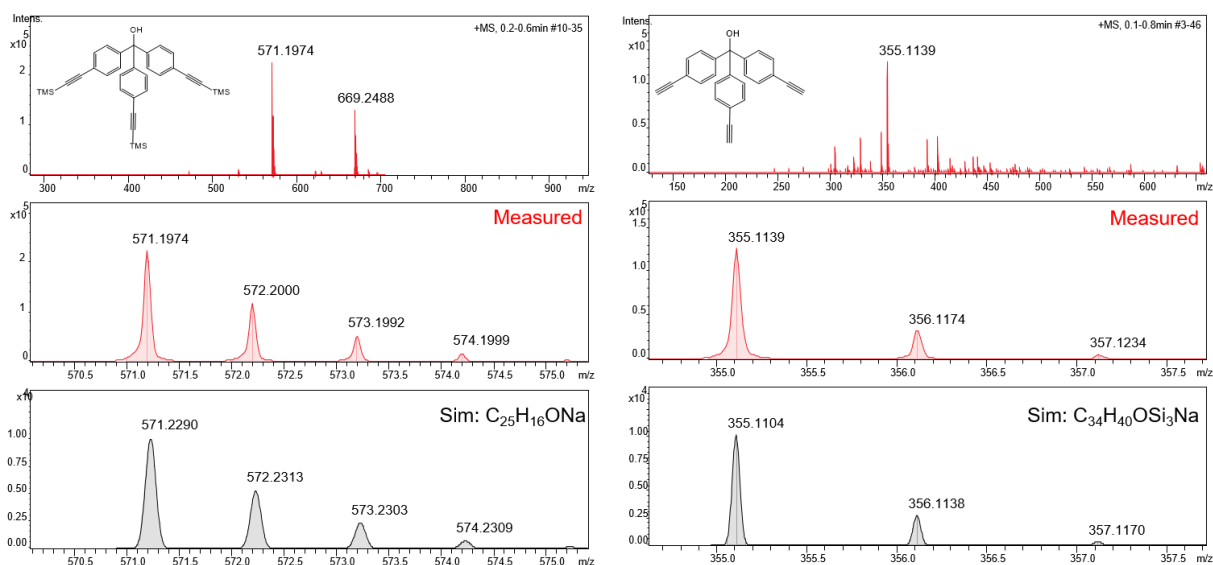


Figure A 95.  $^1\text{H}$ -NMR spectrum of **44** in  $\text{DMSO}-d_6$ .

Figure A 96.  $^1\text{H}$ -NMR spectrum of **44** in  $\text{DMSO}-d_6$ .Figure A 97. ESI-TOF-MS spectrum of **41** and **42**.Figure A 98.  $^1\text{H}$ -NMR spectrum of **45** in  $\text{CDCl}_3$ .Figure A 99.  $^{13}\text{C}$ -NMR spectrum of **45** in  $\text{CDCl}_3$ .

Figure A 100.  $^{29}\text{Si}$ -NMR spectrum of **45** in  $\text{CDCl}_3$ .Figure A 101.  $^1\text{H}$ -NMR spectrum of **46** in  $\text{CDCl}_3$ .Figure A 102.  $^{13}\text{C}$ -NMR spectrum of **46** in  $\text{CDCl}_3$ .Figure A 103. ESI-TOF-MS spectrum of **45** and **46**.

## 8. Curriculum Vitae

### Michel Biewend

Geburtsdatum / -ort: 24.06.1990 / Beckendorf-Neindorf

Familienstand: Ledig

Staatsangehörigkeit: Deutsch

04/2020 – heute

#### **Produktentwickler R&D**

SCS Automotive GmbH & Co. KG, Bitterfeld-Wolfen

11/2016 – 04/2020

#### **Wissenschaftlicher Mitarbeiter/ Promotionsstudium**

Martin-Luther-Universität Halle-Wittenberg, Halle/Saale  
Abteilung: Makromolekulare Chemie

10/2014 – 10/2016

#### **Masterstudium Chemie**

Martin-Luther-Universität Halle-Wittenberg, Halle/Saale  
Lehrstuhl: Makromolekulare Chemie

Thesis-Thema: Synthese und Charakterisierung  
mechanochemisch aktivierbarer Kupfer(I) Bis(NHC)-Komplexe

- *Abschluss: Master of Science (1,3)*

10/2011 – 09/2014

#### **Bachelorstudium Chemie**

Martin-Luther-Universität Halle-Wittenberg, Halle/Saale  
Lehrstuhl: Organische Chemie

Thesis-Thema: Synthese eines Harmonin Analogons

- *Abschluss: Bachelor of Science (1,5)*

08/2008 – 06/2011

#### **Ausbildung zum Chemikanten**

Ligrana GmbH Eilsleben

- *Abschluss: Staatlich anerkannter Chemikant (gut)*

08/2002 – 07/2008

#### **Gymnasium**

Gymnasium Oschersleben, Oschersleben

- *Abschluss: Allgemeine Hochschulreife (2,8)*

Halle (Saale), den 27.01.2021

---

Michel Biewend

## 9. Publikationen

Michael, P.; Biewend, M.; Binder, W. H. Mechanochemical Activation of Fluorogenic CuAAC “Click” Reactions for Stress-Sensing Applications. *Macromolecular Rapid Communications* **2018**, *39*, 1800376.

Biewend, M.; Neumann, S.; Michael, P.; Binder, W. H. Synthesis of polymer-linked copper(i) bis(N-heterocyclic carbene) complexes of linear and chain extended architecture. *Polymer Chemistry* **2019**, *10*, 1078-1088.

Neumann, S.; Biewend, M.; Rana, S.; Binder, W. H. The CuAAC: Principles, Homogeneous and Heterogeneous Catalysts, and Novel Developments and Applications. *Macromolecular Rapid Communications* **2020**, *41*, 1900359.

Biewend, M.; Michael, P.; Binder, W. H. Detection of stress in polymers: mechanochemical activation of CuAAC click reactions in poly(urethane) networks. *Soft Matter* **2020**, *16*, 1137-1141.

Halle (Saale), den 27.01.2021

---

Michel Biewend

## 10. Eigenständigkeitserklärung

Hiermit erkläre ich an Eides statt, dass ich die vorliegende Arbeit selbstständig und ohne fremde Hilfe verfasst habe. Andere als die angegebenen Quellen und Hilfsmittel wurden nicht benutzt und die den benutzten Werken wörtlich oder inhaltlich entnommenen Stellen wurden als solche kenntlich gemacht.

Außerdem erkläre ich, dass ich die vorliegende Dissertation an keiner anderen wissenschaftlichen Einrichtung zur Erlangung eines akademischen Grades eingereicht zu haben.

Halle (Saale), den 27.01.2021

---

Michel Biewend